Non-Markovian Open Quantum Many-Body System Dynamics

vorgelegt von
M. Sc.
Regina Anna Finsterhölzl
ORCID: 0000-0002-0899-4957

an der Fakultät II - Mathematik und Naturwissenschaften
der Technischen Universität Berlin
zur Erlangung des akademischen Grades

Doktor der Naturwissenschaften
Dr.rer.nat.

genehmigte Dissertation

Promotionsausschuss:

Vorsitzende: Prof. Dr. Birgit Kanngießer
Gutachter: Prof. Dr. Andreas Knorr
Gutachter: PD Dr. Uwe Bandelow

Tag der wissenschaftlichen Aussprache: 17.12.2020

Berlin 2021

Danksagung

Als erstes möchte ich mich bei Prof. Dr. Andreas Knorr bedanken, dass er diese Arbeit betreut und mich als wissenschaftliche Mitarbeiterin und Doktorandin in seine Arbeitsgruppe aufgenommen hat. Das Forschen und Lernen in dieser Arbeitsgruppe hat mir sehr viel Freude bereitet und mich um eine Vielzahl spannender Einblicke in die theoretische Physik von quantenmechanischen Vielteilchensystemen, der Quantenoptik und der theoretischen Festkörperphysik bereichert. Ich habe mich dabei immer bestens und vertrauensvoll unterstützt gefühlt - dafür möchte ich mich ganz herzlich bedanken.
Ebenso geht mein Dank an PD Dr. Uwe Bandelow für die Übernahme der Begutachtung dieser Dissertation und für sein Interesse an meiner Arbeit - herzlichen Dank!
Auch bei Prof. Dr. Birgit Kanngießer bedanke ich mich ausdrücklich für die Übernahme der Rolle der Vorsitzenden bei der Verteidigung dieser Arbeit.
Ganz herzlich geht mein Dank auch an Dr. Alexander Carmele: dafür, dass er die Begleitung dieser Arbeit übernommen und mir spannende Themen zur Bearbeitung anvertraut hat, dafür, dass er immer ansprechbar war und mich mit viel Engagement und motivierender Begeisterung für die Physik bei meinen Fragen und der Entwicklung meiner Forschung begleitet hat, und dafür, dass er mich darin unterstützt hat, eine physikalische Intuition aufzubauen und ihr zu folgen.
Ich möchte auch den weiteren Mitglieder der Arbeitsgruppe Danke sagen, für die gemeinsamen Mittagessen, die Diskussionsrunden und die tolle Stimmung in dieser AG. Gerade an Kisa Barkemeyer, Oliver Kästle, Manuel Katzer und Willy Knorr geht ein großes Dankeschön für die gemeinsamen Kaffeerunden, die gute Zusammenarbeit und ihre Unterstützung.
All dies hat die vergangenen zwei Jahre für mich zu einer lehrreichen, spannenden und wertvollen Zeit gemacht.

Abstract

The study of open quantum systems forms one of the main problems of modern physics. This thesis aims at contributing to this field, and focuses on the investigation of non-Markovian dynamics of open quantum systems. Here, as a special case, quantum many-body systems provide for a rich field of research. With the ability to control them being of essential importance for the development of quantum technologies, the characterization of their dynamical properties has also drawn a lot of interest lately.
One of the main methodological tasks in the study of open quantum systems is to reduce the infinite degrees of freedom of the total system. In order to achieve this, the thesis makes use of the tensor network method matrix product states and combines it with the picture of the quantum stochastic Schrödinger equation. However, when computing the dynamics of many-body systems of system size N, even the reduced system dynamics scale with 2^N, making larger system sizes difficult to access. Therefore, especially when computing non-Markovian time-dynamics where the information backflow from the reservoir has to be taken into account, efficiently constructed algorithms are required. This thesis proposes these type of algorithms and demonstrates their application. They enable an access to larger system sizes, thus making it possible to investigate non-equilibrium steady-states of quantum many-body systems in a non-Markovian interaction for system sizes up to $N = 30$.
This thesis consists of three parts. The first part provides an introduction to the theory of open quantum systems and to the methodology for modeling them. The second part examines many-body system-reservoir interaction in the non-Markovian regime by investigating the case of fully coherent self-feedback. It uses the one-dimensional Heisenberg spin-1/2 chain as a paradigmatic and recently intensely studied many-body system. It is demonstrated that this gives rise to new conditions for the feedback phase and to highly non-trivial states within the system as well as to the possibility of partially characterizing the system non-invasively and storing excitation within it. Next, a novel approach to the boundary-driven Heisenberg chain is presented, where the chain is exposed to a coherent

driving field, thus enabling a comparison to the well-studied incoherently driven model. The third part demonstrates the use of an external pump to control the feedback phase of a Λ-type three-level system, where the external pump pulse is shown to be a new control parameter. The thesis concludes with the proposition to enhance the indistinguishability of two photons by feedback control.

Zusammenfassung

Die Untersuchung offener Quantensysteme ist eines der Hauptprobleme der modernen Physik. Diese Dissertation möchte einen Beitrag zu diesem Gebiet leisten und konzentriert sich auf die Untersuchung der nicht-Markovschen Dynamik offener Quantensysteme. Hier bieten Quanten-Vielteilchensysteme als Sonderfall ein reichhaltiges Forschungsfeld, und da ihre Kontrolle für die Entwicklung von Quantentechnologien von wesentlicher Bedeutung ist, hat in letzter Zeit auch die Charakterisierung ihrer dynamischen Eigenschaften großes Interesse geweckt. Die Ergebnisse dieser Arbeit sind für dieses Gebiet von besonderer Relevanz. Eine der wichtigsten methodischen Aufgaben bei der Untersuchung offener Quantensysteme ist die Reduzierung der großen Zahl von Freiheitsgraden des Gesamtsystems. Um dies zu erreichen, wird in dieser Arbeit die Tensornetzwerkmethode matrix product states verwendet und mit dem Bild der quantenstochastischen Schrödingergleichung kombiniert. Bei der Berechnung der Dynamik von Vielteilchensystemen skaliert jedoch selbst die reduzierte Systemdynamik mit 2^N, so dass größere Systemgrößen schwer zugänglich sind. Daher sind insbesondere bei der Berechnung der nicht-Markovschen Zeitdynamik, bei der der Informationsrückfluss aus dem Reservoir berücksichtigt werden muss, effizient konstruierte Algorithmen erforderlich. In dieser Arbeit werden solche Algorithmen vorgeschlagen und ihre Anwendung demonstriert. Sie ermöglichen einen Zugang zu größeren Systemgrößen und damit die Untersuchung von Nichtgleichgewichts-Zuständen von Quanten-Vielteilchen-Systemen in einer nicht-Markovschen Wechselwirkung für Systemgrößen bis zu $N = 30$.
Diese Arbeit besteht aus drei Teilen. Der erste Teil bietet eine Einführung in die Theorie der offenen Quantensysteme und in die Methodik zu deren Modellierung. Der zweite Teil untersucht die Interaktion zwischen Vielkörper-System und Reservoir im nicht-Markovschen Regime, indem er den Fall eines vollständig kohärenten Selbst-Feedbacks in den Blick nimmt. Er verwendet die eindimensionale Heisenberg-Spin-1/2-Kette als paradigmatisches und in der jüngsten Literatur intensiv untersuchtes quantenmechanisches Vielkörper-System. Es wird gezeigt, dass sich daraus neue Bedingungen für die

Feedback-Phase und nicht-triviale Nichtgleichgewichts-Zustände innerhalb des Systems ergeben sowie die Möglichkeit, das System nicht-invasiv zu charakterisieren und Anregung darin zu speichern. Im Anschluss daran wird ein neuartiger Ansatz für die randgetriebene Heisenberg-Kette vorgestellt, bei dem die Kette mit kohärent Feld getrieben wird, wodurch ein Vergleich mit dem häufig untersuchten inkohärent getriebenen Modell möglich wird. Im dritten Teil wird die Verwendung eines externen Pumpfelds zur Steuerung der Rückkopplungsphase eines Λ-Typ Dreiniveausystems gezeigt, wobei sich der externe Pumpimpuls als neuer Steuerparameter erweist. Die Arbeit schließt mit dem Vorschlag, die Ununterscheidbarkeit von zwei Photonen durch kohärente Feedbackkontrolle zu verbessern.

Contents

III Single-emitter system-reservoir interaction

1.

Introduction

1.1 Motivation

Studying open quantum systems ranges among the most important topics of current physical research. An open quantum system is generally described as a microscopic region exhibiting quantum coherence, which is coupled to an external environment [1, 2, 3, 4], where the interaction leads to dissipation and decoherence. Recently, rapid improvements in the ability to control quantum coherence of single particles have been made that are of fundamental importance for the storage and manipulation of quantum information [5]. Here, capturing the effect of the couplings of these systems to their environment is of increasing importance, leading to growing attention for open quantum systems in a broad range of fields of physics. Here, in solid state physics, for instance trapped atoms [6, 7], molecules and ions [8, 9] have been studied, and the transport properties of quantum dots or other mesoscopic devices has been explored [10]. In quantum optics, examples include the investigation of photon modes in cavities [11] or impurities coupled to photonic crystals [12]. See [14, 15, 16, 10] for latest reviews on these topics.
In order to capture the flow of information between system and environment, an important approach is the Markovian approximation. Here, it is assumed that the environment recovers so quickly from the interaction with the system that the information backflow may be neglected [1]. However, due to rapid technological advances in the possibilities of observing and controlling quantum systems on more precise levels, new scenarios continuously emerge where this approximation no longer captures the dynamics adequately, as the information backflow from the environment is found to play a crucial role in the dynamics [17, 18, 19, 15, 6, 7]. By investigating the effects of a structured, non-Markovian reservoir on quantum systems, the work presented in this thesis contributes to this research field. Also, efficient but accurate descriptions of these systems are needed, and

the thesis at hand provides for such a tool.
As a special case of open quantum systems, strongly interacting many-body systems also have drawn increasing interest recently. In particular, quantum spin chains are a paradigm to study quantum many-body physics out-of-equilibrium and their properties when interacting with an environment are currently intensely studies, for instance quantum phase transitions [20, 21, 22, 23, 24, 25], quantum transport properties [26, 27, 28, 29, 30, 31, 32, 33, 34] and entanglement structures [35, 36]. Among quantum spin chains, the Heisenberg spin-1/2 chain [37] is of particular importance. It may be solved analytically [38, 39] and offers a theoretical model to explain experiments in the area of strongly-correlated many-body physics [40, 41, 42, 43, 44]. In the thesis at hand, this paradigmatic model is investigated in different setups.
The observation and control of quantum coherence on a microscopic level of single particles has experienced rapid advance during the past years and has been realized in many different physical systems [45, 8, 46] with the aim to store and manipulate quantum information [5, 47, 48, 49]. Thus, it has become increasingly important to characterize the influence of a structured environment on these systems [15, 14, 50]. While a main goal is to reduce the destruction of quantum coherence within the microscopic system, the last years have also witnessed success in the use of a controlled coupling to the environment as a means to enhance coherence or to bring desired quantum states into being [16, 51, 52]. Here, coherent feedback control already successfully uses the back-action on the quantum state by the coupling to the environment for manipulating quantum states on the level of single particles [53, 54, 55] with important applications in the field of quantum information processing [56, 57, 58]. In particular, feedback control has been successfully used to predict and generate population trapping in different setups [59, 60] of fundamental importance for applications such as quantum memory, which relies on the storage and release of qubits on demand [61, 49, 62, 63, 64].
An application of fundamental importance in the area of quantum many-body physics is the realization and improvement of quantum simulators, where a controlled manipulation of a many-body system is used to engineer it to a desired state [65]. With this, a range of technological applications has been simulated using spin chains as a model, for instance CNOT gates made of superconducting quantum interference devices [66], quantum batteries [67] or new implementations of transistors [68].
Here, atomic and molecular systems - cold atomic and molecular gases and trapped ions - are currently among the leading platforms [50, 69] and have been intensively used to study many-body physics [40, 41, 42, 43, 44]. This makes the extension of the methods from quantum optics onto many-body systems of high interest. By applying self-feedback on a paradigmatic model for a quantum many-body system, a method developed in a atom-molecular-optics and cavity-QED is used with the aim to contribute to the growing possibilities of control over dissipative processes in quantum many-body systems, and to the development of tools to prepare interesting and important states within them. Here, going beyond the single excitation regime [70] provides for promising effects such as anomalous population trapping [71] and is also investigated in this thesis.
In the theory of open quantum systems, one of the methodological tasks is to avoid

the integration of the entire system which usually consists of large number of degrees of freedom. A broad range of techniques has been developed for this purpose, among them master equations - in particular the Lindblad–Kossakowski form [72], quantum Langevin equations [73], the input-output formalism using the Heisenberg representation [74] or continuous measurement theory [2]. Another widely used approach is the quantum trajectories method [14, 3, 75, 76], which time-evolves pure states and captures the coupling to the environment with stochastic quantum jumps.
However, in the case of a quantum many-body system, the reduced Hilbert space grows exponentially with the number of particles involved, often making analytical solutions difficult and numerical approaches very demanding, which imposes strong limits on the size of the studied system. Clearly, to access larger system sizes, approximative methods are needed which allow for an efficient reduction of the exponentially growing Hilbert space, and this thesis aims at providing this kind of tool.
To this end, a powerful combination of two methods is used. The quantum stochastic Schrödinger equation (QSSE) [77, 78, 79] is employed where similar to the master equation approach, the system state vector is evolved in time, while its interaction with the environment is encoded in its dependence on an additional noise with certain statistical properties. This approach is combined with a powerful numerical tensor network method called matrix product states (MPS), which makes an efficient reduction of the Hilbert space possible by truncating the eigenvalues of the decomposed state vector. While this combination has been successfully applied on open few-level systems [80], its application is extended onto many-body systems in this thesis, and efficient ways to structure the MPS-architecture especially in the numerically demanding case of non-Markovian interaction are presented.

1.2 Structure of the thesis

This thesis consists of three parts. The first part, Sec. I, describes the theoretical and methodological background for the research employed. Here, Sec. 2, provides an overview of the recent developments in the field of open quantum systems and describes theoretical concepts of fundamental importance for it. Sec. 2.2 derives the quantum stochastic Schrödinger equation (QSSE) [77, 78, 79] which captures the system-reservoir interaction with a stochastic, time-stroboscopic description. Using it as a numerical basis enables the computation of non-Markovian interaction. Afterwards, in Sec. 2.3, the derivation of the quantum optical master equation as an important tool to describe Markovian effects is presented, which serves as a benchmark model throughout this thesis. This is followed by an introduction to the framework of MPS in Sec. 3.1, which is used for numerical simulations throughout this thesis. The part concludes with an introduction to quantum feedback control in Sec. 4, where dominant approaches and effects are reviewed.
The second part, Sec. II, is dedicated to quantum many-body system-reservoir interaction. It presents investigations of multi-excitation dynamics of open quantum many-body systems, and is organized as follows: after a brief introduction to many-body spin physics, cf. Sec. 5, a method originally developed in a cavity-QED context and well studied for

few-level emitter is extended on a many-body system, cf. Sec. 6. This is done by applying quantum coherent feedback control on a Heisenberg quantum spin chain with nearest-neighbor interaction. Thus, the setup is changed from a spatial driving to a temporal-driving scheme: Loss and driving take place at the same site but include two different points in time separated by the roundtrip-time τ. It is demonstrated that this gives rise to new conditions for the feedback phase and with this to highly non-trivial states within the system as well as to the possibility of partially characterizing the system non-invasively and store excitation within it. Following this, a novel approach to the boundary-driven Heisenberg chain is presented, cf. Sec. 7, a setup which is intensely studied in the Markovian regime in recent literature. In the setup in the present thesis, the chain is exposed to a coherent driving field on one end while coupled dissipatively to a reservoir on its other side, enabling for a comparison of coherent and incoherent driving.
The third part, Sec. III, few-level systems are exposed to self-feedback with the aim to further investigate the influence of the phase and to establish methods of controlling it. Here, Sec. 8 demonstrates the possibilities of a microwave pump field used as an additional control parameter to disentangle the intertwined feedback parameter and thus to provide for further application methods. This is followed by presenting the aim to enhance the visibility of two photons with coherent feedback control in Sec. 9.
The thesis concludes with a summary of the main results and an outlook of further work and open questions in Sec. 10.

Part I.

Theory and methodology

2.

The theory of open quantum systems

Studying open quantum systems ranges among the most important topics of current physical research. Recently, rapid improvements in the ability to control quantum coherence of single particles have been made, while these developments are of fundamental importance for the storage and manipulation of quantum information [5]. With this, capturing the effect of the couplings of these systems to their environment is of increasing importance, leading to growing attention for open quantum systems in a broad range of fields of physics. Here, in solid state physics, for instance trapped atoms [6, 7], molecules and ions [8, 9] have been studied, and the transport properties of quantum dots or other mesoscopic devices has been explored [10]. In quantum optics, examples include the investigation of photon modes in cavities [11] or impurities coupled to photonic crystals [12]. See [14, 15, 16, 10] for latest reviews on these topics.
An open quantum system is generally described with a microscopic region $\mathcal{S}$ exhibiting quantum coherence, which is coupled to an external environment $\mathcal{R}$ [1, 2, 3, 4], where the interaction leads to dissipation and decoherence. The total Hamiltonian $H_{\text{tot}}(t)$ reads

$$H_{\text{tot}}(t) = H_{\text{sys}}(t) + H_{\text{res}}(t) + H_{\text{int}}(t), \tag{2.1}$$

where $H_{\text{sys}}(t)$ describing the dynamics of the closed subsystem $\mathcal{S}$, $H_{\text{res}}(t)$ denotes the free Hamiltonian of the environment $\mathcal{R}$ and $H_{\text{int}}(t)$ represents the interaction between both parts. Thus, the open quantum system represents a subsystem of the combined total system $\mathcal{S} + \mathcal{R}$, where the latter is usually assumed to be closed, meaning that its dynamics evolve unitary and are described through a (time dependent) Hamiltonian $H_{\text{tot}}(t)$ - this will be the case throughout this thesis.
The interaction dynamics results in subsystem-environment correlations which induces state changes of the subsystem. As a consequence, the state of the subsystem alone can

no longer be described by unitary, Hamiltonian dynamics. Its dynamics - resulting from the total unitary evolution of both subsystem and environment - are commonly called reduced system dynamics [1].
In all cases investigated in this thesis, the environment will consist of an electromagnetic field with its modes forming a continuum - thus, it contains an infinite number of degrees of freedom, which in many cases may be described as an environment consisting of bosonic, independent harmonic oscillators. Due to its infinite degrees of freedom, the environment is referred to as a reservoir in this thesis, as it is commonly the case. Note that from now on, the subsystem $\mathcal{S}$ will be referred to as the system, as it is its dynamics which is of central interest.
Due to this very large number of degrees of freedom, one of the main methodological tasks in the theory of open quantum systems is to avoid the integration of the entire system, as this would require to solve an infinite hierarchy of coupled equations of motion. However, as in most cases, the interest lies on the quantities related to the dynamics of the reduced system, and thus a number of approximation techniques and analytical methods for the description of its dynamics are concerned with gaining a simpler description of the reduced Hilbert space describing the dynamics of some reduced system observables. To this end, one way is to trace out the environment and evolve the reduced density matrix of the system $\rho_s(t)$. Here, master equations provide a way to compute this evolution -

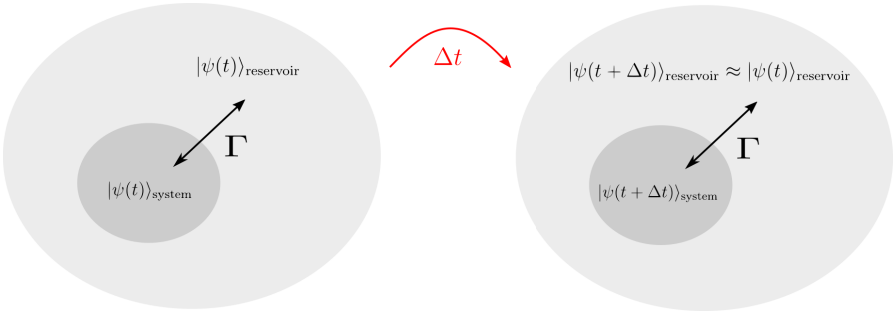

Figure 2.1: Sketch of an open quantum system with Markovian type of interaction. The total system consists of a microscopic region $|\psi(t)\rangle_{\text{sys}}$ which couples to its surrounding environment or reservoir $|\psi(t)\rangle_{\text{res}}$ with a coupling strength Γ. During time evolution for one time step Δt, the Markov approximation requires that the reservoir recovers instantly from the interaction and relaxes again into its previous state, thus $|\psi(t+\Delta t)\rangle_{\text{res}} = |\psi(t)\rangle_{\text{res}}$.

in particular the Lindblad-Kossakowski form which may be applied for systems where the Markov approximation holds [72]. Other important methods are for instance quantum Langevin equations [73], the input-output formalism using the Heisenberg representation [74], continuous measurement theory [2] or the quantum stochastic Schrödinger equation (QSSE). Instead of tracing out the reservoir's degrees of freedom, the approach in the latter case remains in the Schrödinger picture and uses a time discrete basis which includes the interaction with the reservoir at one time step with a stochastic, time-stroboscopic

description [81, 77, 80].
Another widely used approach is the quantum trajectories method [14, 3, 75, 76]. Instead of propagating the density matrix, it relies on solving a Schrödinger equation under the use of a non-Hermitian effective Hamiltonian for the time-evolution of the reduced system, while the incoherent coupling to the bath is simulated by applying quantum jumps at random times and then averaging over many of the obtained trajectories [15].
With regard to the applied approximations, two important scenarios have to be differed, namely that of Markovian and non-Markovian type of interaction between system and reservoir. In the first case, the interaction may be described as a Markov process, meaning that in order to determine the future state of the total system, the knowledge only of its present state is needed - past states do not have to be taken into account [82]. In order for this approximation to be valid, the separation of timescales between system and reservoir is required, meaning that the the frequency scale of the system is much smaller than the one of the reservoir dynamics and the one induced by the system-reservoir coupling, resulting in an instant recovery of the reservoir from the interaction with the system. It thus holds for the correlation time $\tau_{\mathrm{corr,res}}$ of the reservoir that $\tau_{\mathrm{corr,res}} \to 0$. This is illustrated in Fig. 2.1. In this limit, only very few parameters of the reservoir remain of importance for the dynamics of the reduced system.
In many cases, however, the large separation of timescales between system and reservoir does not hold - thus, the past interaction between system and reservoir influences the present state of the reservoir. Fig. 2.2 illustrates this process. This results in non-

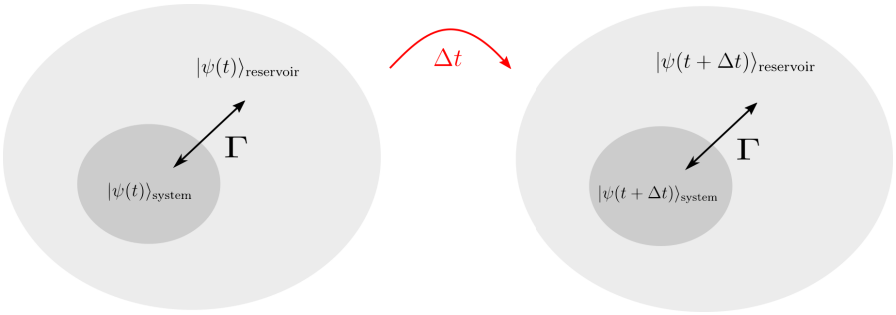

Figure 2.2: Sketch of an open quantum system with non-Markovian type of interaction. The total system consists of a microscopic region $|\psi(t)\rangle_{\mathrm{sys}}$ which couples to its surrounding environment or reservoir $|\psi(t)\rangle_{\mathrm{res}}$ with a coupling strength Γ. Contrary to the Markovian case, the state of the reservoir at the time $t + \Delta t$ remains influenced by the interaction with the system which has occured during the time step Δt, thus $|\psi(t + \Delta t)\rangle_{\mathrm{res}} \neq |\psi(t)\rangle_{\mathrm{res}}$.

Markovian effects which occur in a broad range of contexts, for instance in quantum optics, solid state physics, quantum chemistry and many more [6, 7, 13, 11, 12] - see [15] for an excellent review on the topic.
In this thesis, both Markovian as well as non-Markovian scenarios will be considered. For modeling their dynamics numerically, matrix product states as a state-of-the-art method

will be employed and to this end, Sec. 3.1 provides an introduction to this framework. Two important theoretical models - the formulation of the Lindblad-Kossakowski master-equation and of the quantum stochastic Schrödinger equation (QSSE) - will be derived in this chapter.
Three approximations are being made for both methods: the weak coupling limit, the Markov approximation and the rotating wave approximation. The weak-coupling limit assumes that the coupling between system and reservoir is sufficiently small so that the influence on the reservoir density matrix ρ_{res} may be neglected. This means it may be treated as constant and thus, the total density operator may be written as:

$$\rho_{\text{tot}}(t) = \rho_{\text{sys}}(t) \otimes \rho_{\text{res}}. \tag{2.2}$$

The Markov approximation states that the time evolution of present state of the system only depends on its present and not on its own past. The assumption behind this approximation is that the excitations created in the reservoir during the interaction decay so quickly that the information backflow on the system cannot be resolved on the time scales considered for the simulation of the system's time evolution. Thus, the separation of timescales explained above is a necessary condition for this approximation, which results in a vanishing correlation time of the reservoir.
The rotating wave approximation consists of neglecting the fast rotating terms in the interaction Hamiltonian. In order for this approximation to hold, the weak-coupling limit is required. Additionally, the narrow-bandwidth approximation must hold, meaning that the system couples mainly to the reservoir at a small band of frequencies around its resonance frequency. Due to its importance for the computations in this thesis, its derivation is now demonstrated for the paradigmatic case of a single-electron atom in interaction with an electromagnetic field.

2.1 Atom-field interaction Hamiltonian in full quantization

The total Hamiltonian for the interaction of a two-level atom at the position $\mathbf{r}$ with an electromagnetic field $\mathbf{E}$ reads as

$$H = H_{\text{el}} + H_{\text{res}} - e\,\mathbf{r} \cdot \mathbf{E}, \tag{2.3}$$

with H_{el} and H_{res} describing the free energies of respectively the atom and the field with

$$H_{\text{el}} = \sum_i \hbar\omega_i \sigma_{ii} \tag{2.4}$$

and

$$H_{\text{res}} = \sum_k \hbar\omega_k \big(b_k^\dagger b_k + \frac{1}{2}\big) \tag{2.5}$$

with σ_{ij} the atom transition operator and $b_k^{(\dagger)}$ the creation and destruction operator of a photon with the energy $\hbar\omega_k$ and e the charge of the electron [83]. Note that it is

in dipole approximation where the field is assumed to be uniform over the atom which implies the assumption that the atom couples to the reservoir predominantly at a small band of frequencies around its transition energy $\hbar\omega_0$.
Inserting the expressions $e\mathbf{r} = \sum_{i,j} \xi_{ij}\sigma_{ij}$ with $\xi_{ij} = e\langle i|\,\mathbf{r}\,|j\rangle$ denoting the electric dipole transition element and $E = \sum_k \hat{\epsilon_k}\mathcal{E}_k(b_k + b_k^\dagger)$ into Eq. (2.3), omitting the zero-point energy and describing a two-level atom with the ground level $|1\rangle$ and the excited level $|2\rangle$, from what it follows that $\hat{\xi} = \hat{\xi_{12}} = \hat{\xi_{21}}$, it is obtained:

$$H = \sum_k \hbar\omega_k b_k^\dagger b_k + E_1\sigma_{11} + E_2\sigma_{22} + \hbar\sum_k \kappa_k(\sigma^+ + \sigma^-)(b_k + b_k^\dagger). \tag{2.6}$$

with $\kappa_k = -\frac{\xi\cdot\hat{\epsilon}_k\mathcal{E}_k}{\hbar}$ the coupling constant and the atomic transition operators $\sigma^+ = |2\rangle\langle 1|$ and $\sigma^- = |1\rangle\langle 2|$.
Note that $\mathcal{E}_k = (\hbar\nu_k/2\epsilon_0 V)^{\frac{1}{2}}$, where for simplicity the polarization basis is assumed to be linear and the polarization unit vectors to be real. In the following step, the ground level energy of the atom will be set to zero, thus $E_1\sigma_{11} \equiv 0$, while the energy of the atom excited state is described by its resonance frequency ω_0, $E_2 = \hbar\omega_0$.
Next, Eq. (2.6) is transformed into the interaction picture. This means that it is transformed into the rotating frame defined by its freely evolving part. Therefore, the unitary transformation with the following properties is applied. The system dynamics obeys the Schrödinger equation:

$$i\hbar\frac{\mathrm{d}}{\mathrm{dt}}|\psi\rangle = H|\psi\rangle\,. \tag{2.7}$$

where i is the imaginary unit, $\hbar$ the reduced Planck constant and $|\psi\rangle$ the wave vector describing the combined system-reservoir dynamics. Let U be a unitary transformation U with the property $U^\dagger U = I$ where I is the unitary operator. With this, Eq. (2.7) may be written as:

$$i\hbar U\frac{\mathrm{d}}{\mathrm{dt}}U^\dagger U|\psi\rangle = UHU^\dagger U|\psi\rangle\,. \tag{2.8}$$

Defining the wave function in the interaction picture as $U|\psi\rangle = |\psi\rangle_I$ and regrouping Eq. (2.8) yields

$$i\hbar\frac{\mathrm{d}}{\mathrm{dt}}|\psi\rangle_I = H_I|\psi\rangle_I \tag{2.9}$$

with

$$H_I = UHU^\dagger - iU\frac{\mathrm{d}}{\mathrm{dt}}U^\dagger \tag{2.10}$$

In order to transform into the rotating frame of the freely evolving part, the unitary operator U is defined as:

$$U = \exp\left[\frac{i}{\hbar}t\Big(\sum_k \hbar\omega_k b_k^\dagger b_k + \hbar\omega_0\sigma_{22}\Big)\right] \tag{2.11}$$

With this transformation, Eq. (2.6) reads as

$$H = \hbar\sum_k \kappa_k(\sigma^+ e^{-i\omega_0 t}b_k e^{i\omega_k t} + \sigma^+ e^{-i\omega_0 t}b_k^\dagger e^{-i\omega_k t} + \sigma^- e^{i\omega_0 t}b_k e^{i\omega_k t} + \sigma^- e^{i\omega_0 t}b_k^\dagger e^{-i\omega_k t}). \tag{2.12}$$

In the weak coupling limit for the timescale of the dynamics being much slower than the one of the coupling dynamics, thus $\omega_0 \ll \kappa_k$, the fast oscillating terms in Eq. (2.12) may be neglected, as they average out in the integration. This approximation is called the rotating wave approximation and is valid in many cases in quantum optics, and it will be used in this thesis.
Transforming Eq. (2.6) back into the Schrödinger picture thus yields the Hamiltonian for the atom-field interaction in the rotating wave approximation:

$$H = \sum_k \hbar\omega_k \left(b_k^\dagger b_k\right) + E_2\sigma_{22} + \hbar\sum_k \kappa_k(\sigma^+ b_k + \sigma^- b_k^\dagger). \tag{2.13}$$

2.2 System-reservoir interaction in the Schrödinger picture: the quantum stochastic Schrödinger equation

In order to derive the quantum stochastic differential equations for an quantum mechanical wave function [81, 77, 80], a standard model of an open quantum system in quantum optics is considered: a system where only a single transition of the frequency ω_0 is relevant for the coupling, interacting with a reservoir which consists of bosonic harmonic oscillators, which may for instance represent an electromagnetic field. The total Hamiltonian H_{tot} consists of the system, reservoir and interaction parts. It reads:

$$H_{\text{tot}} = H_{\text{sys}} + H_{\text{res}} + H_{\text{int}}, \tag{2.14}$$

with the Hamiltonian of the free evolution of the electromagnetic field defined as

$$H_{\text{res}} = \sum_k \hbar\omega_k b_k^\dagger b_k. \tag{2.15}$$

Here, $b_k^{(\dagger)}$ creates/annihilates a bosonic excitation, where the index k represents an abbreviation for the wave vector $\mathbf{k}$ and the polarization λ of the respective field mode, thus $k \equiv \{\mathbf{k}, \lambda\}$. They obey the canonical commutation relations:

$$[b_k, b_{k'}^\dagger] = \delta_{k,k'}. \tag{2.16}$$

The reservoir is assumed to be in a vacuum state initially. For H_{sys}, no further specifications are being made except for the fact that it must be exactly solvable and defined by its eigenfunctions and eigenvalues. It may for instance describe the free evolution of a two-level or few-level system or of an harmonic oscillator.
Note that for simplicity, only one reservoir is assumed; however the derivation is easily extended to the generalization of many reservoirs in interaction with a many-body system.
The interaction part describes a linear system-field coupling in rotating wave approximation as derived in Sec. 2.1:

$$H_{int} = \hbar\sum_k \left(\kappa_k b_k^\dagger c^- + \text{h.c.}\right) \tag{2.17}$$

Here, c is a system operator whose free evolution is assumed to be governed by the resonance frequency ω_0, and κ_k is the coupling constant. Therefore, the system operator must satisfy the following commutation relation:

$$[H^0_{\text{syst}}, c] = -\hbar\omega_0 c. \tag{2.18}$$

Next, Eq. (2.14) is transformed into the interaction picture. This means that it is transformed into the rotating frame defined by its freely evolving part. As the system obeys the Schrödinger equation, cf. Eq. (2.7), a unitary transformation as defined in Eq. (2.8) - Eq. (2.10) in the previous section is applied. To this end, the unitary operator U_1 is defined as:

$$U_1 = \exp\left[\frac{i}{\hbar}t\Big(H_{\text{sys}} + \sum_k \hbar\omega_k b_k^\dagger b_k\Big)\right] \tag{2.19}$$

This yields the transformed Hamiltonian $H_{\text{int,I}}(t)$, where the free energies have canceled out:

$$H_{\text{int,I}}(t) = \hbar\sum_k \left(\kappa_k c^\dagger b_k e^{-i(\omega_k-\omega_0)t} + \text{h.c.}\right) \tag{2.20}$$

2.2.1 Time-dependent reservoir operators

Next, time-dependent reservoir operators $b^{(\dagger)}(t)$ are defined with

$$b(t) = \sum_k \kappa_k c^\dagger b_k e^{-i(\omega_k-\omega_0)t}. \tag{2.21}$$

Their commutation relation may be derived using the commutation relations in Eq. (2.16):

$$[b(t), b^\dagger(t')] = \gamma(t-t') \tag{2.22}$$

with

$$\gamma(t-t') = \sum_{|\omega_k-\omega_0|<\theta} |\kappa_k|^2 e^{-i(\omega_k-\omega_0)(t-t')} \to \int_{\omega_0-\theta}^{\omega_0+\theta} d\omega g(\omega)|\kappa(\omega)|^2 e^{-i(\omega-\omega_0)(t-t')} \tag{2.23}$$

where in the last step, the reservoir is described as a continuum of modes and density of states. Also, the narrow-bandwidth approximation is assumed to hold, thus only modes whose frequencies are within a small range defined by θ around the resonance frequency ω_0 have to be included. Note that with $k \equiv \{\mathbf{k}, \lambda\}$ there may be a number of different k corresponding to the same frequency ω_k, thus $|\kappa(\omega_k)|^2$ corresponds to the average value of $|\kappa_k|^2$ for all k with $\omega_k = \omega$.
Next, the Markov approximation is made, hence it is assumed that the time scale of the system is much slower than the coupling dynamics, thus it holds $|t-t'| \gg \frac{1}{\theta}$.
Also, a smooth coupling between system and field is assumed, meaning that within this narrow bandwidth, the coupling $g(\omega_k)|\kappa(\omega_k)|^2$ varies only very little, thus $g(\omega_k)|\kappa(\omega_k)|^2 \equiv$

g_0. The last assumption is also called the white noise approximation, as it allows to extend the integral in Eq. (2.23) over the entire frequency space. With this, the definition of the reservoir operator reads as:

$$b(t) = \int_{-\infty}^{+\infty} d\omega \, b(\omega) e^{-i(\omega-\omega_0)t} \tag{2.24}$$

with the commutation relations

$$[b(t), b^\dagger(t')] = \delta(t-t')\pi g_0^2 e^{i\omega_0(t-t')} \tag{2.25}$$

which means that for different times t, t', they commute. Thus, the operator in Eq. (2.24) includes the entire system-reservoir interaction, where the parameter t must be interpreted as the time at which the initial incoming field will interact with the system [77]. With this, the transformed Hamiltonian in Eq. (2.20) simplifies to

$$H_{\text{int,I}}(t) = i\hbar g_0 \left(c^\dagger b(t) + c b^\dagger(t) \right). \tag{2.26}$$

The interest lies in solving the dynamics of the open system. The time evolution of the combined system is governed by the Schrödinger equation in Eq. (2.7). Integrating it formally yields:

$$|\psi(t)\rangle = U(t, t_0) \, |\psi(t_0)\rangle \tag{2.27}$$

with the time evolution operator $U(t, t_0)$ defined as:

$$U(t, t_0) = \hat{T} \exp\left(-\frac{i}{\hbar} \int_{t_0}^{t} H'(t') dt' \right). \tag{2.28}$$

where $\hat{T}$ represents the time ordering. In order to include the system and the reservoir in the ansatz for the wave function, it is defined as:

$$\begin{aligned} |\psi(t)\rangle &= |(\psi_{\text{sys}} \otimes \psi_{\text{res}})(t)\rangle \\ &= \lim_{k \to d_n} \sum_{i_s=0,1} \sum_{n_0,\ldots,n_k=0}^{\infty} c_{i_s,n_0,\ldots,n_k}(t) \, |i_s, n_0, \ldots, n_k\rangle \,, \end{aligned} \tag{2.29}$$

where the states $|i_s = 0\rangle$, $|i_s = 1\rangle$ denote the ground level and excited state of the system and the $\{|n_k\rangle\}$ denotes the Fock states of the bosonic reservoir, thus n_k denotes the number of excitations in the kth mode. Note that with $\lim_{k\to\infty}$, the reservoir is described by a mode continuum.

Due to the infinite number of degrees of freedom of the reservoir, inserting Eq. (2.29) into Eq. (2.27) results in an infinite number of differential equations for the time dependent coefficients $c_{i_s,n_0,\ldots,n_k}(t)$, making it very difficult to solve. Until now, its definition in Eq. (2.24) is only an abbreviation for the integral over the mode continuum with infinite modes k - the infinite degrees of freedom of the reservoir modes still need to be reduced. This is done by treating the operators $b(t)^{(\dagger)}$ as stochastic elements and introducing a

time-discrete basis, as will be demonstrated in the following.
As the aim is to solve the Schrödinger equation, the start for the derivation is the time evolution for $|\psi(t)\rangle$ in Eq. (2.27), where Eq. (2.28) defines the time evolution operator. Note that here, the time ordering has to be preserved.
The corresponding Hamiltonian $H_{\mathrm{int,I}}$ has been derived in Eq. (2.26). Expanding it to second order reads as, which $|\psi(t)\rangle_{\mathrm{I}} = U^{\dagger}|\psi(t)\rangle$ where $|\psi(t)\rangle$ has been defined in Eq. (2.29):

$$|\psi(t)\rangle_{\mathrm{I}} = \left(I - \frac{i}{\hbar}\int_{t_0}^{t} \mathrm{d}t' H(t')_{\mathrm{I}}\right)|\psi(t_0)\rangle_{\mathrm{I}} - \frac{1}{\hbar^2}\int_{t_0}^{t}\mathrm{d}t' H(t')_{\mathrm{I}}\int_{t_0}^{t'}\mathrm{d}t'' H(t'')_{\mathrm{I}}|\psi(t_0)\rangle_{\mathrm{I}} \quad (2.30)$$

The reservoir is assumed to be in the vacuum state initially, thus $|\psi(t_0)\rangle = |\psi(t_0)\rangle_{\mathrm{sys}} \otimes |\mathrm{vac}\rangle$. Note that for reasons of simplicity, the subscript I will be dropped in the following. Note that the separation of timescales is assumed, which implies the weak-coupling limit: the electromagnetic coupling is sufficiently weak so that for a time interval Δt the dynamics of the reservoir is much quicker than the one induced by the interaction. Also note that from now on, the time will be discretized, thus $t \to \Delta t$.
Inserting the transformed Hamiltonian in Eq. (2.26) into Eq. (2.30) and taking into account that the reservoir is in a vacuum state initially, which implies that $b(t)|\psi(t_0)\rangle_{\mathrm{res}} = 0$, the third term in Eq. (2.30) reads as:

$$\int_{t_0}^{\Delta t} dt' \int_{t_0}^{t'} dt''\Big(- g_0^2 c^{\dagger}cb(t')b^{\dagger}(t'') + g_0^2 ccb^{\dagger}(t')b^{\dagger}(t'')\Big)|\psi(t_0)\rangle\,. \quad (2.31)$$

Using the commutation relations in Eq. (2.25) and the initial conditions of the reservoir, the following relationship holds:

$$c^{\dagger}cb(t')b^{\dagger}(t'')|\psi(t_0)\rangle = \delta(t'-t'')e^{i\omega_0(t-t')}|\psi(t_0)\rangle\,. \quad (2.32)$$

With this, the second term in Eq. (2.31) may be written as:

$$\int_{t_0}^{\Delta t} dt' \int_{t_0}^{t'} dt'' - g_0^2 c^{\dagger}c\,\delta(t'-t'')e^{i\omega_0(t-t')} = -2\pi c^{\dagger}c\,g_0^2\Delta t\frac{1}{2}. \quad (2.33)$$

Note that it is proportional to Δt. Applying the condition $b(t)|\psi(t_0)\rangle_{\mathrm{res}} = 0$ also for the second term in Eq. (2.30), Eq. (2.30) now reads as:

$$\begin{aligned}|\psi(\Delta t)\rangle = \Big(1 - \Gamma c^{\dagger}c\,\Delta t\frac{1}{2}\Big)|\psi(0)\rangle + \int_{t_0}^{\Delta t} dt' g_0 cb^{\dagger}(t')|\psi(t_0)\rangle \\ + \int_{t_0}^{\Delta t} dt' \int_{t_0}^{t'} dt'' g_0^2 ccb^{\dagger}(t')b^{\dagger}(t'')|\psi(t_0)\rangle\,, \end{aligned} \quad (2.34)$$

where $\Gamma \equiv 2\pi g_0^2$ has been defined.
Note that the first term contains the no-photon processes, the second term one-photon processes and the third term two-photon processes.

Next, coarse graining in time is introduced [81]: the time step is chosen so that it holds $\Gamma\Delta t$ is sufficiently small to assume that during one time step, the maximum of one photon may be created or destroyed. Calculating the photon probabilities of the single terms in Eq. (2.34) by taking the average over the initial system vector with $\langle O\rangle_0 = \langle\psi(0)|\, O\,|\psi(0)\rangle$, with O an operator, yields $P_0(\Delta t) = 1 - \langle cc^\dagger\rangle\Gamma\Delta t$ for the first term in Eq. (2.34), $P_1(\Delta t) = \langle cc^\dagger\rangle\Gamma\Delta t$ for the second and $P_2(\Delta t) = \frac{1}{2}\Gamma^2\langle ccc^\dagger c^\dagger\rangle\Delta t^2$. Thus, for a Δt sufficiently small, the two-photon term in Eq. (2.34) may be neglected.

2.2.2 Transformation to a time discrete basis

The next step is to introduce time discrete quantum noise operators, which - for reasons that become clear further below - are also called quantum Ito increment. They include the full interaction with the reservoir at one time increment from t_k to t_{k+1}, where equidistant time steps $\Delta t = t_{k+1} - t_k$ are assumed:

$$\Delta B^{(\dagger)}(t_k) = \frac{1}{\sqrt{\Gamma}}\int_{t_k}^{t_{k+1}} dt' b^{(\dagger)}(t') \tag{2.35}$$

Thus, the operator in Eq. (2.35) represents a quantum noise increment during one time step.
Up to the factor Δt, the noise operators obey bosonic commutation relations, as may be shown for equidistant time steps using Eq. (2.25):

$$[\Delta B(t_k), \Delta B^\dagger(t_j)] = \int_{t_k}^{t_{k+1}} dt \int_{t_j}^{t_{j+1}} dt' \delta(t - t') = \Delta t \delta_{kj}. \tag{2.36}$$

Thus, the $\{\Delta B^{(\dagger)}(t_k)\}$ form an orthogonal set of operators which may be interpreted as annihilation or creation operator for reservoir excitations during the respective time interval. Note that the time interval Δt should be chosen smaller than the system timescales but larger than the bandwidth of the reservoir modes around the resonance frequency. By normalization to a factor $\sqrt{\Delta t}$, a set of orthonormal basis states is obtained:

$$|i_p\rangle = \frac{(\Delta B^\dagger(t_k))^{i_p}}{\sqrt{i_p!\Delta t^{i_p}}}\,|\mathrm{vac}\rangle\,, \tag{2.37}$$

where i_p, p integer, denotes the number of excitations present in the Fock state of the kth time interval. With this, a basis transformation from the frequency representation of the radiation field in the ansatz in Eq. (2.29) to a time representation may be conducted, where the state of the reservoir during each time step is represented by its own Hilbert space $\mathcal{H}_p$. Thus, the total Hilbert space of this new representation reads

$$\mathcal{H} = \mathcal{H}_s \otimes \sum_{p=-\infty}^{+\infty} \mathcal{H}_p, \tag{2.38}$$

where $\mathcal{H}_s$ is the system Hilbert space. The ansatz for the wave function now reads as:

$$|\psi(t)\rangle = \sum_{i_s,\{i_p\}} c_{i_s,i_1,\ldots,i_{N_T}}(t)\,|i_s, i_1, \ldots, i_{N_T}\rangle\,. \tag{2.39}$$

As the $\Delta B^{(\dagger)}(t_k)$ only act on the kth interval, time evolving the state up to the time $k\Delta t$ will not affect the Hilbert space for later times - and it will thus remain in the vacuum state. Note that the dimensions of each subspace are reduced by assuming that Δt is sufficiently small so that the maximum of one excitation may be created during one time step.

2.2.3 Quantum stochastic integration

The operator in Eq. (2.35) is a stochastic description due to the lack of information about the precise mode of interaction with the system. Their increments are defined as:

$$dB(t) = B(t+dt) - B(t) \tag{2.40}$$

and

$$dB^\dagger(t) = B^\dagger(t+dt) - B^\dagger(t) \tag{2.41}$$

As explained above, the field is assumed to be in the vacuum state. With this, the increments may be characterized as follows:

$$\langle dB^{(\dagger)}(t)\rangle = \mathrm{tr}_{\mathrm{res}}\Big(dB^{(\dagger)}(t)\rho(t)\Big) = \sum_{k_i=0}^{\infty} \langle k_i = 0|\,\Delta B^{(\dagger)}(t_k)\rho(t)\,|k_i = 0\rangle = 0 \tag{2.42}$$

and

$$\langle dB(t)dB^\dagger(t')\rangle = dt\delta(t-t') \tag{2.43}$$

Due to these two properties - the mean in Eq. (2.42) and the variance in Eq. (2.43) - the quantum noise increments (Eq. (2.35)) are the quantum mechanical, non-commutative analogues of the classical Wiener process.
In order to integrate the noise increments, a specific form of a quantum stochastic integration has to be considered: The Ito integration. Its form reads:

$$\int_0^t f(s)dB(s) = \lim_{n\to\infty} \sum_{i=0}^{n} f(t_i)[B(t_{i+1}) - B(t_i)], \tag{2.44}$$

where $f(t)$ is an operator values quantity which only depends on $B(s)$ for $s < t$, which means that the function $f(t_i)$ is independent of the stochastic increment $[B(t_{i+1}) - B(t_i)]$. For quantum stochastic integrals of the Ito form, the conventional calculus $d\big[B(t)B^\dagger(t)\big] = dB(t)B^\dagger(t) + B(t)dB^\dagger(t)$ for the differential $d\big[B(t)B^\dagger(t)\big]$ has to be replaced by the following form [84]:

$$d\big[B(t)B^\dagger(t)\big] = dB(t)B^\dagger(t) + B(t)dB^\dagger(t) + dB(t)dB^\dagger(t). \tag{2.45}$$

By using this calculus in Eq. (2.45), the Lindblad master equation may be derived from the quantum stochastic Schrödinger equation, which will be demonstrated in Sec. 2.3.

2.2.4 The quantum stochastic Schrödinger equation

With the time discretized Hilbert space and the quantum Ito increments, the QSSE may now be derived. Writing Eq. (2.34) as a differential equation and inserting the Ito-increments ΔB, $\Delta B^\dagger$ defined in Eq. (2.35) into it yields the equation for the first time step:

$$\begin{aligned}\Delta\,|\psi(t_0)\rangle &\equiv |\psi(t_0+\Delta t)\rangle - |\psi(t_0)\rangle \\ &= \Big(-c^\dagger c\,\Gamma\frac{\Delta t}{2} + \sqrt{\Gamma}g_0 c\Delta B^\dagger(0)\Big)\,|\psi(t_0)\rangle \end{aligned} \tag{2.46}$$

This description may be generalized to the kth time interval, as it only affects the Hilbert space for the kth time interval: evolution up to a time t does not affect the Hilbert spaces for times later than t, thus the Hilbert spaces for $t_i > t_k$ remain in the vacuum state. The whole time interval T may be decomposed into a direct product of the subspaces representing one time interval. Also, the derivation of Eq. (2.46) required that $|\psi(0)\rangle$ is in the vacuum state for the operators $\Delta B(0), \Delta B^\dagger(0)$. As the Ito increments for one time step commute with these of the previous one, $|\psi(k\Delta t)\rangle$ is vacuum state for $\Delta B(k+1\Delta t), \Delta B^\dagger(k+1\Delta t)$. Thus, Eq. (2.46) may be generalized to the kth time step. In the limit of $\Delta t \leq \frac{1}{\theta}$, thus that the strength of the interaction becomes very weak, the change within every time step may be assumed to be sufficiently small, and Eq. (2.46) may be written as:

$$d\,|\psi(t)\rangle = \Big(-c^\dagger c\,\Gamma\frac{dt}{2} + \sqrt{\Gamma}g_0 c dB^\dagger(t)\Big)\,|\psi(t)\rangle\,. \tag{2.47}$$

As the increments $dB(t)$ represent the future state of the reservoir, they are independent of the present state of $|\psi(t)\rangle$, thus the integral resulting from Eq. (2.47) will be of Ito kind.

Eq. (2.47) represents the quantum stochastic Schrödinger equation in the interaction picture. Transforming it back into the Schrödinger picture using the unitary transformation for the time-independent system Hamiltonian $U = \exp\left(\frac{i}{\hbar}H_{\text{sys}}t\right)$ yields:

$$d\,|\psi(t)\rangle = \Big(-\frac{i}{\hbar}H_{\text{eff}}\,dt + \sqrt{\Gamma}\,c\,dB^\dagger(t)\Big)\,|\psi(t)\rangle \tag{2.48}$$

with the non-Hermitian operator

$$H_{\text{eff}} = H_{\text{sys}} - i\hbar\frac{1}{2}c^\dagger c\,\Gamma \tag{2.49}$$

The term $dB^\dagger(t)$ represents the the incoming radiation field in the immediate future. This implies that this field is not yet affected by the system. The second term in Eq. (2.49) may be interpreted as a self-field created by the system which damps the radiation by reacting on the system itself [77].

Also note that Eq. (2.48) formally resembles the classical Langevin equation which describes the motion of a particle in liquid or gas with a fluctuating, stochastic force describing Gaussian white noise and also implies the separation of timescales.

Due to the linear nature of the QSSE, it is possible to solve it explicitly in some cases. Examples include the decay of a single-photon cavity mode or of a two-level atom. Also, the inclusion of several independent reservoirs or the interaction with a heat bath, thus of a reservoir in thermodynamic equilibrium with a temperature above zero, may be derived - see [81] for details. However, this is not the topic of this thesis, as here, the QSSE picture will be used for modeling open quantum system dynamics numerically. Its implementation will be explained in the following section.

2.2.5 Numerical solutions using the QSSE picture

For the numerical model, time-discretized Hilbert space of the QSSE picture serves as a basis. Thus, the wave function is also expressed in this basis and reads

$$|\psi(t)\rangle = \sum_{i_s,\{i_p\}} c_{i_s,i_1,\ldots,i_{N_T}}(t)\,|i_s, i_1, \ldots, i_{N_T}\rangle\,. \tag{2.50}$$

as introduced in Section2.2.2.
Due to this basis transformation, the time evolution operator in in Eq. (2.28) may also be discretized, which may be seen as follows:

$$\begin{aligned} U(t,t_0) &= \hat{T}\exp\left(-i\sum_{n=0}^{n_T}\int_{(n-1)\Delta t}^{n\Delta t} H'(t')dt'\right) \\ &= \hat{T}\exp\left(-i\sum_{n=0}^{n_T} H_n(t_n)\right) \end{aligned} \tag{2.51}$$

with $H_n(t_n) = \int_{(n-1)\Delta t}^{n\Delta t} H'(t')dt'$ With this, the time evolution is now expressed with a stroboscopic map, which reads for the kth time step:

$$|\psi(t_{k+1})\rangle = \exp\left(-i\int_{k\Delta t}^{(k+1)\Delta t} H'(t')dt'\right)|\psi(t_k)\rangle \otimes |i_{k+1}=0\rangle \tag{2.52}$$

with the assumption that in the initial state, system and reservoir are uncorrelated. Due to this stroboscopic time evolution, the time ordering $\hat{T}$ may be dropped.
With this, the time evolution may be computed numerically by repeated application of the time evolution operator on the wave vector $|\psi(t_k)\rangle$ which has to be updated after every time step.

2.3 System-reservoir interaction in the density matrix picture: The quantum optical master equation

In order in order to investigate the dynamics of the reduced system where the partial trace over the reservoir is taken, the statistical operator or density matrix $\rho(t)$ is introduced. It is defined as

$$\rho(t) = \sum_i p_i\,|\psi(t)\rangle_i\,\langle\psi(t)|_i\,, \tag{2.53}$$

where the $\{|\psi\rangle_i\}$ form a complete set of eigenstates with eigenvalues p_i, and the normalization condition $\mathrm{Tr}\,\rho = \sum_i p_i = 1$. With this, incoherently mixed states may be expressed as a weighted sum over pure states. The equation of motion for the density matrix is called the Liouville-von-Neumann equation, which is of the form:

$$\frac{\mathrm{d}}{\mathrm{dt}}\rho(t) = -i[H(t), \rho(t))], \tag{2.54}$$

with $H(t)$ the Hamiltonian of the system. Eq. (2.54) may also be written in a form analogous to the classical Liouville equation.

$$\frac{d}{dt}\rho(t) = \mathcal{L}(t)\rho(t), \tag{2.55}$$

where $\mathcal{L}$ is the so called Liouville operator, which is an operator containing a mapping rule with another operator, $\mathcal{L}[\cdot] \equiv -i[H(t), \cdot]$. For that reason, $\mathcal{L}$ is called a super-operator. Provided $\mathcal{L}$ is time independent, the formal solution to 2.55 is given by

$$\rho(t) = e^{\mathcal{L}(t-t_0)}\rho(t_0). \tag{2.56}$$

When dealing with reduced systems, their quantum dynamics may generally no longer be represented in terms of a unitary time evolution. Its dynamics may instead be formulated by an appropriate equation of motion for its density matrix, a quantum master equation. Various types of these equation have been derived for different types of system dynamics. Here, the quantum optical master equation for Markovian type of interaction between system and reservoir will be derived, as it is used throughout this thesis. It may be derived directly from the quantum stochastic Schrödinger equation, cf. Eq. (2.48).
To this end, the start is Eq. (2.14), where the system Hamiltonian H_{sys} may now contain additional terms to the free system evolution, for instance a coherent driving term; however, for simplicity, it is assumed to be time-independent. Transformed into the interaction picture using the unitary operator defined in Eq. (2.19), it reads as:

$$H_{\mathrm{I}}(t) = H_{\mathrm{I,sys}} + g_0 \int d\omega \left(c^\dagger b(\omega) e^{-i(\omega-\omega_0)t} + \mathrm{h.c.} \right) \tag{2.57}$$

with $H_{\mathrm{I,sys}}$ the system Hamiltonian in the interaction picture. Note that a frequency-independent coupling constant g_0 is assumed.
Expanding the equation of motion for $|\psi(t)\rangle$ to second order as defined in Eq. (2.30), applying $b(t)\,|\psi(t)\rangle_{\mathrm{res}} = 0$ and the commutation relations in Eq. (2.25), neglecting the two-photon term and introducing time discretization yields:

$$\begin{aligned} |\psi(\Delta t)\rangle = & \\ &= \left(1 - c^\dagger c\, g_0^2 \Delta t \frac{1}{2}\right) |\psi(t_0)\rangle + \int_{t_0}^{\Delta t} dt' g_0 c b^\dagger(t')\,|\psi(t_0)\rangle \\ &+ \int_{t_0}^{\Delta t} dt' \int_{t_0}^{t'} dt'' \left(H_{\mathrm{sys}}^2 + H_{\mathrm{sys}}\, g_0\, b^\dagger(t'') c + g_0\, b^\dagger(t'') c\, H_{\mathrm{sys}} \right) |\psi(t_0)\rangle\,. \end{aligned} \tag{2.58}$$

Note that the Markov approximation has been applied by putting $|\psi(t'')\rangle = |\psi(t_0)\rangle$ in the last line of Eq. (2.58), as it has been explained in Sec. 2.2.
For the first term in the second line, it holds that

$$\int_0^{\Delta t} dt' \int_0^{t'} dt'' H_{\text{sys}} = H_{\text{sys}} \frac{1}{2} (\Delta t)^2 \to 0, \tag{2.59}$$

thus it is of order $(\Delta t)^2$ and may be neglected.
Writing Eq. (2.58) as a differential equation generalized for the kth time step, plugging in the Ito-increments $\Delta B^{(\dagger)}$ and putting $\Delta t \to dt$ yields:

$$d\,|\psi(t)\rangle = \Big(-\frac{i}{\hbar} H_{\text{eff}}\, dt + \sqrt{\Gamma} g_0\, c\, dB^\dagger(t) + H_{\text{sys}} c d\bar{B}_1 + d\bar{B}_2 c H_{\text{sys}} \Big)\, |\psi(t)\rangle\,. \tag{2.60}$$

with

$$H_{\text{eff}} = H_{\text{sys}} - i\hbar\Gamma c^\dagger c \frac{1}{2}, \tag{2.61}$$

$$d\bar{B}_1 = \int_0^{dt} dt' \int_0^{t'} dt''\, g_0 b^\dagger(\omega) e^{i(\omega-\omega_0)t'}, \tag{2.62}$$

and

$$d\bar{B}_2 = \int_0^{dt} dt' \int_0^{t'} dt'' g_0\, b^\dagger(\omega) e^{i(\omega-\omega_0)t'}. \tag{2.63}$$

In the following, the differential equation for $d\rho(t) = d(|\psi(t)\rangle\langle\psi(t)|)$ will be derived. Using the Ito-calculus defined in Eq. (2.45), the formal rule reads as:

$$d\rho(t) = d(|\psi(t)\rangle\langle\psi(t)| = (d\,|\psi(t)\rangle)\langle\psi(t)| + |\psi(t)\rangle(d\,\langle\psi(t)|) + (d\,|\psi(t)\rangle)(d\,\langle\psi(t)|). \tag{2.64}$$

As the interest lies on the dynamical quantities of the system, the degrees of freedom will be reduced by calculating the reduced density matrix $\rho_s(t)$. It is obtained by taking the partial trace $tr_R\rho(t) \equiv \sum_{\{i_p\}} \langle\{i_p\}|\,\rho(t)\,|\{i_p\}\rangle$ over the reservoir:

$$\rho_s(t) \equiv tr_{\text{R}}(\rho(t)) = tr_{\text{R}}(|\psi(t)\rangle\langle\psi(t)|), \tag{2.65}$$

Next, the Born approximation is made, thus the large separation of time scales holds with the system dynamics governed by much larger frequencies than the one of the reservoir. With this, the ansatz

$$|\psi(t)\rangle = |\psi(t)\rangle_{\text{sys}} \otimes |\psi\rangle_{\text{res}} \tag{2.66}$$

is used, where the reservoir is assumed to be in the vacuum state $|\psi\rangle_{\text{res}} = |\text{vac}\rangle$.
Thus, the differential is calculated as

$$\begin{aligned} tr_{\text{R}}(d\rho(t)) &= tr_{\text{R}}\big[d(|\psi(t)\rangle\langle\psi(t)|)\big] \\ &= tr_{\text{R}}\big[(d\,|\psi(t)\rangle)\langle\psi(t)|\,\big] + tr_{\text{R}}\big[\,|\psi(t)\rangle(d\,\langle\psi(t)|)\big] + tr_{\text{R}}\big[(d\,|\psi(t)\rangle)(d\,\langle\psi(t)|)\big] \\ &= \langle\text{vac}|\, d(|\psi(t)\rangle)\langle\psi(t)|_{\text{sys}} + |\psi(t)\rangle_{\text{sys}}\, d(\langle\psi(t)|)\,|\text{vac}\rangle + tr_{\text{R}}\big[(d\,|\psi(t)\rangle)(d\,\langle\psi(t)|)\big]. \end{aligned} \tag{2.67}$$

where in the last step, the vacuum state of the reservoir, $|\psi\rangle_{\text{res}} \equiv |\text{vac}\rangle$ has been exploited. Plugging Eq. (2.60) into Eq. (2.67), inserting $|\psi(t)\rangle = |\psi(t)\rangle_{\text{sys}} \otimes |\psi(t)\rangle_{\text{res}} = |\psi(t)\rangle_{\text{sys}} \otimes |\text{vac}\rangle$ and using $\langle\text{vac}| b^\dagger(t) = 0$, we arrive at

$$tr_{\text{R}}(d\rho(t)) = -\frac{i}{\hbar}dt\big[H_{\text{eff}}\rho(t)_{\text{sys}} - \rho(t)_{\text{sys}}H_{\text{eff}}\big] + tr_{\text{R}}\big[(d\,|\psi(t)\rangle)(d\,\langle\psi(t)|)\big] \tag{2.68}$$

with $\rho(t)_{\text{sys}} = |\psi(t)\rangle_{\text{sys}}\langle\psi(t)|_{\text{sys}}$ the system density matrix.
Next, Eq. (2.60) is inserted into the last term in Eq. (2.68). This results in Eq. (11.2),cf. Sec. 11.1 in the appendix. As only summands of of the order of Δt have to be taken into account, the terms in Eq. (11.2) are analyzed by making use of the cyclic property of the trace and of the weak coupling limit. This is also demonstrated in Sec. 11.1. With this, Eq. (11.2) reduces to:

$$tr_{\text{R}}\Big[(d\,|\psi(t)\rangle)(d\,\langle\psi(t)|)\Big] = \Gamma dt c\rho(t)_{\text{sys}}c^\dagger, \tag{2.69}$$

Inserting Eq. (2.69) and (2.61) into Eq. (2.68) yields:

$$\begin{aligned} d\rho_{\text{sys}}(t) &= -\frac{i}{\hbar}dt\big[H_{\text{eff}}\rho(t)_{\text{sys}} - \rho(t)_{\text{sys}}H_{\text{eff}}\big] + \Gamma dt c\rho(t)_{\text{sys}}c^\dagger \\ &= \Big(-\frac{i}{\hbar}H_{\text{sys}}\rho(t)_{\text{sys}} + \Gamma\frac{1}{2}c^\dagger c\rho(t)_{\text{sys}} + \frac{i}{\hbar}\rho(t)_{\text{sys}}H_{\text{sys}} - \Gamma\frac{1}{2}\rho(t)_{\text{sys}}c^\dagger c + \Gamma c\rho(t)_{\text{sys}}c^\dagger\Big)dt. \end{aligned} \tag{2.70}$$

Dividing Eq. (2.70) by dt yields the Lindblad master equation:

$$\dot{\rho}(t)_{\text{sys}} = -\frac{i}{\hbar}\Big[H(t)_{\text{sys}}, \rho(t)_{\text{sys}}\Big] + \Gamma D[c]\rho(t)_{\text{sys}} \tag{2.71}$$

with $\Gamma \equiv 2\pi g_0^2$ and the Lindblad dissipator

$$D[c]\rho(t)_{\text{sys}} = c\rho(t)_{\text{sys}}c^\dagger - \frac{1}{2}\Big\{c^\dagger c, \rho(t)_{\text{sys}}\Big\} \tag{2.72}$$

and the anti-commutator

$$\Big\{c^\dagger c, \rho(t)_{\text{sys}}\Big\} = c^\dagger c\rho(t)_{\text{sys}} - \rho(t)_{\text{sys}}c^\dagger c. \tag{2.73}$$

3.

Modeling open quantum system dynamics

In the theory of open quantum systems, among the most important methodological tasks is to avoid the integration of the entire system which usually consists of large number of degrees of freedom. To this end, various approaches exist. Importantly, master equations provide a way to compute this evolution - in particular the Lindblad-Kossakowski form which may be applied for systems where the Markov approximation holds [72] and has been presented for the quantum optical case in Sec. 2.3. Other approaches include quantum Langevin equations [73], the input-output formalism using the Heisenberg representation [74] or continuous measurement theory [2].
However, when dealing with quantum many-body systems, all these formalisms face a fundamental challenge, which is the large dimension of the Hilbert space: The reduced Hilbert space grows exponentially with the number of particles involved, often making analytical solutions difficult and numerical approaches very demanding. Consider, for instance, one single particle with spin-1/2, which may either be in state spin-up $|s = 1/2\rangle \equiv |0\rangle$ or in the state spin-down $|s = -1/2\rangle \equiv |1\rangle$: the dimension d of the local Hilbert space is $d = 2$. If two particles are considered, obviously it holds that $d = 2 \cdot 2 = 4$. Thus, for N particles, $d = 2^N$, which means that even for moderate numbers as $N = 100$ it is of the rather large dimension $d \approx 1,27 \cdot 10^{30}$. If the state is described as a mixed state in the density matrix picture, as it is necessary for describing open quantum systems, its dimension grows even faster with $d = 2^{2N} = 4^N$.
Thus, full solutions of the equations of motion become very demanding. For instance, solving the full set of differential equations of the reduced density matrix within the master equation framework generally limits the system size to $N \approx 10$ where N counts the number of qubits of the many-body system.
Clearly, in order to access larger system sizes, approximative methods are needed which allow for an efficient reduction of the exponentially growing Hilbert space.

It is the aim of this thesis to work with approximative methods converging to the full solution in the limit of finely tuned approximation parameters. Here, the tensor network method matrix product states (MPS) provides a powerful tool which this thesis makes use of. It is based on the decomposition of the complex coefficient of the wave function into a set of tensors with the truncated quantity being the entanglement within the system. This chapter provides an introduction to the form of matrix product states, demonstrates how to write an arbitrary pure state in the form of an MPS, explains the truncation method, the form and application of operators and the time evolution of an MPS.

3.1 Time evolution with matrix product states (MPS)

Algorithms based on the description of the wave vector as a matrix product state (MPS) have firmly established themselves as an important tool for the numerical treatment of quantum physical systems [85, 86, 87] [1]. They have been used as a convenient and useful class of quantum states already for analytical studies, see for instance [94]. Examples include the study of the Affleck-Kennedy-Lieb-Tasaki (AKLT) state and more general of finitely correlated states [95], which have consequently been used for analytical variational methods, for instance on Heisenberg antiferromagnets [96]. The start of the use of MPS as a numerical tool took place in the context of the density matrix renormalization group (DMRG) technique [85]. The latter was invented in the early 1990s [97, 87] as a powerful numerical tool mainly for the calculation of ground states in one-dimensional systems with open boundary conditions [98]. Its algorithm is based on an iterative increase of the Hilbert space taken into account, the minimization of the energy using variational methods, and an efficient truncation which keeps only the eigenvectors associated to the largest eigenvalues. Today, DMRG methods combined with MPS are a standard tool for modeling one-dimensional systems [99, 100, 101, 89, 102, 85].
Initially, DRMG was limited to ground state calculations, but soon, efficient methods for a description of a time evolution have been developed, the most important ones being the time-dependent density matrix renormalization group (tDRMG) [103, 104], the time-evolving block decimation (TEBD) [105, 106] and the time evolution of the MPS state (tMPS) [85]- see [86] for an excellent review. Although these methods differ in some aspects, all of them are based on the powerful combination of an efficient application of the operators and a valid truncation of the Hilbert space. Currently, these methods are state of the art in the investigation of one-dimensional systems, and their use for two- or three-dimensional systems is being explored. Apart from time-evolution, DMRG-applications have been extended to the use of periodic boundary conditions, the investigation of infinite systems, or single-site DMRG. For an excellent overview, see [85].
Central to these algorithms is the expansion of the state vector coefficient into a product of tensors using the singular value decomposition. In this form, the entanglement between

[1] For detailed introductions to matrix-product states see [88, 89, 90, 91, 92, 93]. See also the tensor network library website *https://itensor.org/*, upon whose open source algorithm the numerical work of this thesis builds.

the subsystems is accessible in form of the singular values which allows for a valid truncation of the Hilbert space by setting those below a certain threshold to zero. The three main algorithms TEBD, tDMRG and tMPS mathematically perform the same operation, which is the application of a time-evolution operator $U(t,t_0) = \hat{T}\exp\left(-i\int_{t_0}^{t} H'(t')dt'\right)$ on a state $|\psi(t)\rangle$, which is described by the time-dependent Schrödinger equation. Here, where H denotes the Hamilton operator of the system, i is the imaginary unit, $\hbar$ the reduced Planck's constant, and t the time. Thus, all of them numerically solve the equation

$$|\psi(t+\Delta t)\rangle = U(t+\Delta t,t)\,|\psi(t)\rangle\,. \tag{3.1}$$

All three algorithms express the state as an MPS and approximate - that is, truncate - it essentially along the same lines, as will be explained in detail in this section. However, there is one difference in the algorithms which concerns the way the MPS is compressed, thus truncated: TEBD and tDRMG evolve and truncate one single site after the other with one or several sweeps through the chain or network, while tMPS first evolves all bonds in time and truncates the entire state by truncation the dimensions of all matrices d^2D to D. Thus, tDMRG and TEBD perform an iterativ variationally compression, which may have the advantage of a numerically less costly time evolution. However, tMPS has the advantage that it is the cleaner and more precise approach, as here, for each time step, the time evolution is done before the truncation is performed [85]. For this reason, this thesis employs tMPS for the time evolution.

Also, all methods go beyond the reach of exact diagonalization by solving Eq. (3.1) making use of sparse matrix exponentials. Here, one can further diffentiate two important approaches for the numerical approximation [86]. In the first, the action of $U(\Delta t)$ is approximated, which is done by a time-dependent variational principle based on the Lanczos formalism [107], as it is done by the global [108, 109] or local [110] Krylov method and by the time-dependent variational principle [111, 112]. In this approach, the operator itself is not directly calculated. the second approach approximates the operator itself [106, 103, 104, 113, 114]. Here, tDRMG, TEBD and tMPS all make use of the Suzuki-Trotter-decomposition [115, 116], which has its origin in quantum field theory and the setting up of path integrals [117]. Another recently proposed method [118] uses a generalized form of the Euler approximation for the matrix exponential.

Despite the fact that tMPS has been developed for the application on pure states only, it has been successfully applied on incoherent dynamics of mixed states - first, for unitary time evolution of quantum states with finite temperatures. Here, the mixed state purified with a duplicate of itself evolved along the imaginary axis [119].

Since roughly ten years, these methods have been extended to non-unitary time evolution [120]. The method for finite temperature evolutions has been extended to the simulation of dissipation [114, 119], and in a parallel development, a method has been proposed where the density operator is written as a super-state and evolved by tDMRG in Liouville space [121]. This method has been applied analytical [122, 123] as well as to numerical time evolution of Markovian open many-body systems described in the density matrix picture [124, 125, 126, 127, 128, 129, 130] and recently even on few-level systems with non-Markovian [131] dynamics. However, the scaling of the Hilbert space with 4^N

- instead of 2^N in Schrödinger space - again imposes a strong disadvantage for larger system sizes. Additionally, the readout of expectation values is limited [121].
For all coherent dynamics with pure states, however, the more efficient Schrödinger picture allows for the full access of expectation values and may be applied on systems with Markovian as well as non-Markovian dynamics, which has already successfully been demonstrated for open few-level systems [80, 132, 71, 133]. For this reason, the picture of the quantum stochastic Schrödinger equation serves as a numerical basis.

3.2 The MPS form and the Schmidt decomposition

An arbitrary pure state of a quantum system can be written as an linear superposition of all basis states. Let $|i_1\rangle, |i_2\rangle \dots |i_N\rangle$ be a basis with N basis vectors of an N-dimensional Hilbert space. Then a state $|\psi\rangle$ within this Hilbert space may be written as

$$|\psi\rangle = \sum_{i_1}^{d_1} \sum_{i_2}^{d_2} \cdots \sum_{i_N}^{d_N} c_{i_1 i_2 \dots i_N} |i_1\rangle \otimes |i_2\rangle \otimes \cdots \otimes |i_N\rangle . \tag{3.2}$$

Here, $\otimes$ denotes the tensor product, $c_{i_1 i_2 \dots i_N}$ are the coefficients with $c_{i_1 i_2 \dots i_N} \in \mathbf{C}$ and $d_1, d_2, \dots d_N$ are the dimensions of each basis vector. For reasons of simplicity, the tensor product symbol will be omitted in the following, resulting in the representation

$$|\psi\rangle = \sum_{i_1 \dots i_N} c_{i_1 \dots i_N} |i_1 \dots i_N\rangle . \tag{3.3}$$

The sum is taken over all possible combinations of the basis states, which means that for the dimension d of $|\psi\rangle$ it holds that $d = d_1 d_2 \dots d_N$. Let the basis $\{|i_k\rangle\}$ be the local Hilbert spaces of a spin chain with N sites, thus $k \in (1 \dots N)$, with $d_1 = d_2 = \cdots = d_N = 2$, while the two possible states are $i_k = |\frac{1}{2}\rangle = |\uparrow\rangle$, for instance for spin up, and $i_k = |-\frac{1}{2}\rangle = |\downarrow\rangle$ for spin down. It holds that $d = 2^N$, which means that the Hilbert space grows exponentially with each site added to the system. In order to describe larger quantum systems numerically, a valid physical approximation for such systems is needed, which is given by transforming the state into a matrix product state and using this form to find a valid approximation.
The key idea of the MPS form is that complex coefficient tensor $c_{i_1 i_2 \dots i_N}$ may be written as a product of matrices A:

$$c_{i_1 i_2 \dots i_N} = A^{i_1} A^{i_2} \dots A^{i_N},$$

so that the state $|\psi\rangle$ can be written as:

$$|\psi\rangle = \sum_{i_1 \dots i_N} A^{i_1} A^{i_2} \dots A^{i_N} \; |i_1\, i_2 \dots i_N\rangle , \tag{3.4}$$

Thus, the description of the state is expanded, as this form may at first glance seem as the more complicated one. However, this representation is very useful because of two

of its features: Firstly, it contains a more local description of the state, as each matrix contains the coefficients for one site; and secondly, as will be shown in the following, it makes the entanglement of each subspace with the respective other subspaces accessible as a physical quantity which can then be used in order to make valid approximations of the physical system.
In order to rewrite the complex coefficient tensor $c_{i_1 i_2 \ldots i_N}$, the singular value decomposition (SVD) is needed. It states that an arbitrary, rectangular matrix A with $A \in \mathbf{C}^{m \times n}$ can be written in the following form:

$$A = USV^T,$$

with $U \in \mathbf{C}^{m \times \min(m,n)}$, $V^T \in \mathbf{C}^{\min(m,n) \times n}$ and $S \in \mathbf{C}^{\min(m,n) \times \min(m,n)}$.
Additional properties are that U has orthonormal columns (left singular vectors), i.e. $U^T U = I$ and V^T has orthonormal rows (right singular vectors), i.e. $V^T V = I$. Here, I indicates the identity matrix in the respective dimensions. S is a diagonal matrix with non-negative entries s_i, $i \in (1, \ldots, \min(m,n))$, the singular values. By convention the singular values are sorted descending resulting in $s_1 > s_2 > \cdots > s_k$, where $k \leq \min(m,n)$ and for all s_i with $i \in (k+1, \ldots, k + \min(m,n))$ it holds that $s_i = 0$.
In order to visualize operations with the MPS form later in this section, a more intuitive, graphical representation in the form of block diagrams is now being introduced. Let $|\psi\rangle = c_{i_1,i_2} |i_1, i_2\rangle$ be an arbitrary quantum state described with Eq. (3.3), while the local Hilbert space is defined by i_1, i_2 - this may for instance describe the state of two coupled two-level system. Using the SVD, the coefficient matrix c_{i_1,i_2} may now be decomposed according to $c_{i_1,i_2} = USV^T$, where $U = U_{i_1,\alpha}$, $V = V_{\alpha,i_2}$ and $S = S_{\alpha\alpha}$. Thus, U gets the index of the first basis state, while V the one of the second, and the index α connects the matrices.
In order to simplify these expressions for larger quantum systems, the block diagram depiction is introduced in Fig. 3.1. The key idea is to represent each tensor with a block, whose shape indicates its properties, while the indexes are represented by labeled lines. Tensors carrying the same index may be connected by these lines, which indicates a summation over this index. Vertical lines represent the physical indexes which are also called site indexes, while horizontal lines indicate the link indexes.
Also, the SVD is the basis for the Schmidt decomposition, which states the following: If $|\psi\rangle$ is a pure state of a composite quantum system of the subsystems A and B with the dimensions N_A, N_B respectively, then there exist orthonormal states $|i\rangle_A$, $|i\rangle_B$ for both systems such that

$$|\psi\rangle = \sum_i^r \lambda_i |i\rangle_A |i\rangle_B . \tag{3.5}$$

For the λ_i - the so called Schmidt-coefficients - it holds that $\lambda_i \in \mathbf{R}^+$ and $\sum_i \lambda_i = 1$. r denotes the so called Schmidt rank, which in quantum information theory is a measure for the entanglement between the states on the two subspaces, and it holds that $r = 1$ for product states and $r > 1$ for entangled quantum states [134].
The Schmidt decomposition and the SVD may be used to express the entanglement of

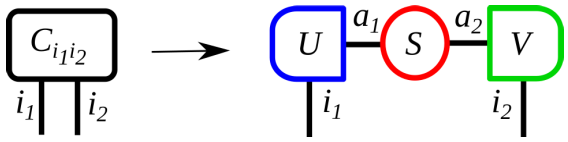

Figure 3.1: Block diagram of the singular value decomposition of a pure quantum state in the Hilbert space i_1, i_2. The black box represents the coefficient matrix c_{i_1,i_2} which is being decomposed into a left orthogonal (blue box), right-orthogonal (green box) and diagonal (red circle) matrix. The horizontal lines labeled with a_1, a_2 are called bond indexes, which connect the matrices with its neighbors. Thus, the number of lines connected to one circle indicates the number of indexes of the matrix. If two circles are connected by a line, the matrices share the same index and may be multiplied by summing over it.

the state between the two subsystems as well as to provide a valid approximation for numerical simulation of the evolution of the state. This can be seen as follows: The pure quantum state $|\psi\rangle$ in Eq. (3.5) can always be expressed in the following form, where $|j\rangle$ and $|k\rangle$ are orthonormal basis for the subsystems A and B:

$$|\psi\rangle = \sum_{jk} c_{jk} |j\rangle |k\rangle . \tag{3.6}$$

The c_{ij} in Eq. (3.6) are coefficients of a matrix C, thus it holds for the reduced density operators $\rho_A = \mathrm{Tr}_B |\psi\rangle \langle\psi| = C^\dagger C$ and $\rho_B = \mathrm{Tr}_A |\psi\rangle \langle\psi| = CC^\dagger$.
Using the singular value decomposition, C may be decomposed such that

$$\begin{aligned} |\psi\rangle &= \sum_{ijk} u_{ji} s_{ii} v_{ik} |j\rangle |k\rangle & (3.7)\\ &= \sum_{i}^{min(N_A,N_B)} \left(\sum_j u_{ji} |j\rangle \right) s_{ii} \left(\sum_k v_{ik} |k\rangle \right) & (3.8)\\ &= \sum_{i}^{r} \lambda_i |i\rangle_A |i\rangle_B , & (3.9) \end{aligned}$$

which is equal to Eq. (3.5) with $\left(\sum_j u_{ji} |j\rangle\right) \equiv |i_A\rangle$, $s_{ii} \equiv \lambda_i$, $(\sum_k v_{ik} |k\rangle) \equiv |i_B\rangle$ and $r = min(N_A, N_B)$.
The reduced density operators can be expressed with the Schmidt basis in Eq. (3.5) as

eigenvectors and the corresponding eigenvalues as the squares of the Schmidt-coefficients:

$$\rho_B = \sum_i^r \lambda_i^2 \left|i_A\right\rangle \left\langle i_A\right| \tag{3.10}$$

$$\rho_A = \sum_i^r \lambda_i^2 \left|i_B\right\rangle \left\langle i_B\right| \tag{3.11}$$

As a measure for the entanglement between the two subsystems, the von Neumann entropy of entanglement $S(\rho)$ is a useful concept. It is a quantum mechanical measure of uncertainty using the density operator $\rho(t)$ of a system as the probability distribution. It is defined as:

$$S(\rho) \equiv -\operatorname{Tr}(\rho \log_2 \rho) = -\sum_p \lambda_p \log_2 \lambda_p, \tag{3.12}$$

where the λ_p denote the eigenvalues of the density matrix ρ. S is non-negative, zero if and only if the state is pure, and in a d-dimensional Hilbert space it is at most $\log d$ for a completely mixed state I/d [134]. If a composite quantum system $|AB\rangle$ is in an entangled state, the conditional entropy $S_{A|B}$ expresses the remaining lack of knowledge about the state of A, if we know the state of B, and thus is a measure for the entanglement between the states in the subspaces. It is defined as:

$$S_{A|B}(|\psi\rangle) = -\operatorname{Tr}(\rho_A \log_2 \rho_A), \tag{3.13}$$

and thus may be expressed using the Schmidt decomposition in Eq. (3.5) as follows:

$$S_{A|B}(|\psi\rangle) = -\sum_i^r \lambda_i \log_2 \lambda_i. \tag{3.14}$$

3.2.1 Decomposing a quantum state into a matrix product state

Let $|\psi\rangle$ be the arbitrary pure quantum state described by Eq. (3.3), assuming it is normalized. If we assume that $d_1 = d_2 = \ldots d_N$, this state vector is of length d^N. This also holds for its coefficients $c_{i_1 \ldots i_N}$, which may be expressed as a vector of length d^N. Next, this state vector is reshaped into a matrix of the dimensions $d \times d^{N-1}$, which is equal to re-expressing the state in Eq. (3.3) as a tensor product of the two subspaces $|i_1\rangle$ and $|i_2 \ldots i_N\rangle$. With this, the state coefficient vector $c_{i_1 \ldots i_N}$ may also be expressed as a matrix $\bar{C} \in \mathbf{C}^{d \times d^{N-1}}$ for which coefficients it holds $\bar{C}_{i_1,(i_2 \ldots i_N)} = c_{i_1 \ldots i_N}$. Thus the state now looks like

$$|\psi\rangle = \sum_{i_1} \sum_{i_2 \ldots i_N} \bar{C}_{i_1,(i_2 \ldots i_N)} \left|i_1\right\rangle \otimes \left|i_2 \ldots i_N\right\rangle. \tag{3.15}$$

The next step is to perform an SVD of $\bar{C}$:

$$c_{i_1 \ldots i_N} = \bar{C}_{i_1,(i_2 \ldots i_N)} = \sum_{a_1}^{r_1} U_{i_1,a_1} S_{a_1,a_1} (V^\dagger)_{a_1,(i_2 \ldots i_N)}, \tag{3.16}$$

where the rank r_1 is $r_1 \leqslant d$.
Before proceeding with the state decomposition, the physical meaning of the SVD decomposition in step 3.16 is explained briefly: Inserting Eq. (3.16) into 3.15 and defining

$$|a_1\rangle_A = \sum_{i_1} U_{i_1,a_1} |i_1\rangle \tag{3.17}$$

$$|a_1\rangle_B = \sum_{i_2 \ldots i_N} (V^\dagger)_{a_1,(i_2 \ldots i_N)} |i_2 \ldots i_N\rangle \tag{3.18}$$

$$S_{a_1,a_1} = s_{a_1} \tag{3.19}$$

yields the Schmidt decomposition in Eq. (3.9) of $|\psi\rangle$ between the subspaces $|i_1\rangle$ and $|i_2 \ldots i_N\rangle$:

$$|\psi\rangle = \sum_{a_1}^{r_1} s_{a_1} |a_1\rangle_A |a_1\rangle_B . \tag{3.20}$$

This means that the SVD in Eq. (3.16) is equivalent to a Schmidt decomposition of $|\psi\rangle$ between the two subspaces $|i_1\rangle$ and $|i_2 \ldots i_N\rangle$, and that the von Neumann entropy in Eq. (3.14) between these two subsystems can be read of using the Schmidt coefficients on S_{a_1,a_1}.
Going back to Eq. (3.16) and proceeding with the decomposition of the state into an MPS, the next step is the following: First, the matrices $S * V^\dagger$ are contracted. This results in an orthogonal matrix, as the multiplication of the singular value matrix S with either the left-orthogonal matrix U or with the right-orthogonal matrix V does. Now, the matrix U_{i_1,a_1} from Eq. (3.9) is decomposed into d row vectors $A^{i_1}_{a_1} = U_{i_1,a_1}$ of the dimension $1 \times r_1$ - thus, for each of the d values that a_1 may take, one row vector exists. Also, the matrix $S * V^\dagger$ - which is orthogonal - in 3.16 is reshaped into a new matrix $\bar{C}_{(i_1 i_2),(i_3 \ldots i_N)} \in \mathbf{C}^{r_1 d \times d^{L-2}}$. Note that the smaller the Schmidt rank r_1, the smaller are the dimensions of the decomposed matrices. With this, the state looks like:

$$c_{i_1 \ldots i_N} = \sum_{a_1}^{r_1} A^{i_1}_{a_1} \bar{C}_{(a_1 i_2),(i_3 \ldots i_N)}. \tag{3.21}$$

Note that the coefficient i_1 is now stored in $A^{i_1}_{a_1}$ and missing in $\bar{C}_{(a_1 i_2),(i_3 \ldots i_N)}$, and that both matrices are linked with the index a_1. Repeating step 3.16 (the SVD decomposition of $\bar{C}_{(a_1 i_2),(i_3 \ldots i_N)}$) as well as step 3.21 (the reshaping of the resulting matrices) and inserting the results into 3.21 yields

$$c_{i_1 \ldots i_N} = \sum_{a_1}^{r_1} \sum_{a_1}^{r_2} A^{i_1}_{a_1} U_{(a_1 i_2),a_2} S_{a_2,a_2} (V^\dagger)_{a_2,(i_3 \ldots i_N)} \tag{3.22}$$

$$= \sum_{a_1}^{r_1} \sum_{a_1}^{r_2} A^{i_1}_{a_1} A^{i_2}_{a_1,a_2} \bar{C}_{(a_2 i_3),(i_4 \ldots i_N)}, \tag{3.23}$$

where in the last step, the matrix $U_{(a_1 i_2),a_2}$ has been reshaped into two matrices $A^{i_2}_{a_1,a_2}$ of the dimensions $r_1 \times r_2$ - note that the A matrices are not vectors any more, like in

the previous step, as it is linked with two other matrices with the indexes a_1 and a_2. Also, note that the $A^{i_2}_{a_1,a_2}$ contains only one index of the basis, i_2 - thus, for each of the d values that i_2 may take, one matrix exists.
Proceeding like that until $c_{i_1 \dots i_N}$ is completely decomposed yields

$$c_{i_1 \dots i_N} = \sum_{a_1 \dots a_{L-1}} A^{i_1}_{a_1} A^{i_2}_{a_1,a_2} \dots A^{i_{L-1}}_{a_{L-2},a_{L-1}} A^{i_N}_{a_{N-1}} \tag{3.24}$$

$$= A^{i_1} A^{i_2} \dots A^{i_{L-1}} A^{i_N}, \tag{3.25}$$

where in the last step, the sum over the $\{a_i\}$ has been written as matrix multiplications. Note that $A^{i_N}_{a_{N-1}}$ is a set of column vectors. As mentioned above, $A^{i_1}_{a_1}$ is a set of row vectors, thus multiplying all matrices will yield the scalar coefficients $c_{i_1 \dots i_N}$ and the whole state may now be written in the MPS form (3.4):

$$|\psi\rangle = \sum_{i_1 \dots i_N} c_{i_1 \dots i_N} |i_1\, i_2 \dots i_N\rangle = \sum_{i_1 \dots i_N} A^{i_1} A^{i_2} \dots A^{i_N} \; |i_1\, i_2 \dots i_N\rangle \,. \tag{3.26}$$

With this, the decomposed state with all indexes as written in Eq. (3.24) looks like displayed in Fig. 3.2.
If all Schmidt values are non-zero, the A-matrices have their maximal dimensions (from left to right) with $(1 \times d), (d \times d^2), \dots, (d^{\frac{L}{2-1}} \times d^{\frac{L}{2}}), \dots, (d^2 \times d), (d \times 1)$. Thus, only a truncation makes this representation useful for calculations.Thus, a form is needed which minimizes the distance of the original state $|\psi\rangle$ and its approximation $|\tilde{\psi}\rangle$ in Hilbert space, $|| \, |\psi\rangle - |\tilde{\psi}\rangle \, ||$.

3.2.2 Truncation of an MPS

There are two ways to compress the MPS [86, 85] in order to gain such a valid approximation $|\tilde{\psi}\rangle$ of $|\psi\rangle$: One is to reduce the dimension directly by an SVD of the MPS, and the other is a variational ansatz where the MPS-dimensions are reduced by minimizing the distance between the original and the approximative state iteratively - the first one is numerically more costly while the second one strongly depends on the chosen initial state.
Both make use of the same principle, which is that the Schmidt decomposition in Eq. (3.5) of $|\psi\rangle$ can be used to derive such a valid approximation $|\tilde{\psi}\rangle$ of $|\psi\rangle$. This becomes clear as follows. In principle, if a given matrix M is supposed to be approximated with a matrix $\tilde{M}$, it has to fulfill the equation

$$\left\| M - \tilde{M} \right\|_p \approx 0. \tag{3.27}$$

First, making a valid approximation of the coefficient matrix C of $|\psi\rangle$ in Eq. (3.6) with the coefficient matrix $\tilde{C}$ of $|\tilde{\psi}\rangle$ is equal to making a valid approximation of the state $|\psi\rangle$, because it holds that the 2-norm of $|\psi\rangle$ is equal to the Frobenius norm $\|\cdot\|_F$ of coefficient matrix C in Eq. (3.6):

$$\| |\psi\rangle \|_2^2 = \sum_{i,j} |c_{ij}|^2 = \|C\|_F^2 \tag{3.28}$$

Such an approximation can be gained from the Schmidt decomposition of C, making use of the so called low rank approximation of the Frobenius norm. It states that the best approximation in the Frobenius norm to a rectangular matrix $M \in \mathbf{C}^{m\times n}$ (with $M = USV^T$) which is of rank r and with $S = \mathrm{diag}\,(s_1, s_2, \ldots, s_r)$, $s_1 > s_2 > \cdots > s_r$, is given by a matrix $\tilde{M}$ with rank $\tilde{r} < r$ with $\tilde{M} = U\tilde{S}V^T$, where $\tilde{S} = \mathrm{diag}\,(s_1, s_2, \ldots, s_{\tilde{r}}, 0, \ldots)$ with $s_1 > s_2 > \cdots > s_{\tilde{r}}$ and the remaining singular values s_i for $i \in (\tilde{r}, \tilde{r}+1, \ldots \tilde{r} + (r - \tilde{r}))$ set to zero [135].
This means that C can be approximated by making a singular value decomposition and cutting of the smallest singular values. This will result in lowering the column dimensions of U and the row dimensions of V^T, which may improve the numerical efficiency enormously. Looking at Eq. (3.19) and (3.20), it can be seen that one way of reducing the dimensions of these matrices is to cut of the smallest eigenvalues from the spectrum of the singular value matrices S_{a_k} during the decomposition procedure, which is exactly the approximation given by Eq. (3.28) discussed above. The key idea is that by cutting of the smallest eigenvalues, the part of information about the entanglement of our system which is least important for its description is lost. If only the the maximum of D singular values is kept during each decomposition step, the dimensions of the MPS are reduced to dN matrices with the dimensions $D \times D$ each at the most. The upper bound for the error made with this approximation $|\tilde{\psi}\rangle$ is given by:

$$\left\| |\psi\rangle - |\tilde{\psi}\rangle \right\|_2^2 \leqslant 2 \sum_i^N \epsilon_i(D). \tag{3.29}$$

The $\epsilon_i(D)$ denote the truncation error caused by the truncation of the singular value matrix during the ith step of the decomposition. It holds that $\epsilon_i(D) = \sum_j^{(N-D)} s_j^2$, so the error is the sum of the squares of the discarded singular values of the ith singular value matrix. If the discarded singular values are small enough, so will be the error made by the approximation.
Thus, finding a valid approximation $|\tilde{\psi}\rangle$ constitutes in the task of reducing the dimensions of the truncated state as much as possible while at the same time minimizing the loss of information, thus the distance to the un-truncated state.

3.2.3 Form of the MPS

For the decomposition of an arbitrary pure quantum state into a matrix product state, several possibilities exist, thus the form of the MPS is not unique. The decomposition explained in Sec. 3.2.1 above results in the so called left canonical form: An important feature of the A-matrices is that they are left-normalized, which means it holds for $k \in (1 \ldots N)$:

$$\sum_{i_k} A^{i_k\dagger} A^{i_k} = I. \tag{3.30}$$

If an MPS is constructed in this way, it is called left-normalized. This form of the MPS emerges if the decomposition is started from the left side of the indexes, as demonstrated

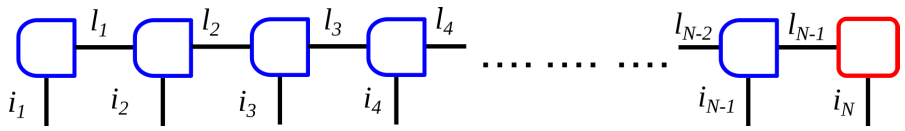

Figure 3.2: Block diagram of a matrix product state in the left canonical form, where the blue boxes represent the left orthogonal tensors and the red box the orthogonality center of the MPS.

in Eq. (3.15) till (3.24) above. The result is depicted in Fig. 3.2. Obviously, one could also start with the decomposition from the right side of the index set in 3.3, which results in an so called right-canonical MPS of the form

$$|\psi\rangle = B^{i_1} B^{i_2} \dots B^{i_N} \; |i_1\, i_2 \dots i_N\rangle \,. \tag{3.31}$$

where all B-matrices are right-normalized with $\sum_{i_k} B^{i_k} B^{i_k\dagger} = 1$ for $l \in (1 \dots N)$. This form is depicted in Fig. 3.3.

From these two representation, two other important ones are easily derived: First, the

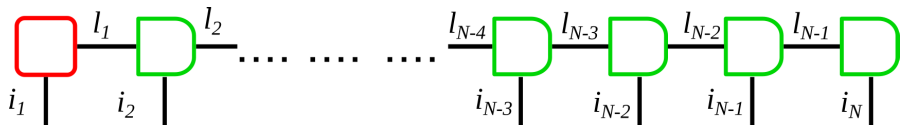

Figure 3.3: Block diagram of a matrix product state in the right canonical form, where the green boxes represent the right orthogonal tensors and the red box the orthogonality center of the MPS.

mixed-canonical form, where the decompositions are started from the left as well as from the right, until the following form results:

$$|\psi\rangle = A^{i_1} \dots A^{i_k} S B^{i_{l+1}} \dots B^{i_N} \; |i_1\, i_2 \dots i_N\rangle \,, \tag{3.32}$$

where S is a singular value matrix, the A-matrices are left-normalized and the B-matrices right-normalized. Defining $|a_l\rangle_A = \sum_{i_1 \dots i_l} (A^{i_1} \dots A^{i_k})_{1,a_l} \, |i_1, \dots, i_l\rangle$ and $|a_l\rangle_B = \sum_{i_{1+1} \dots i_N} (B^{i_{1+1}} \dots B^{i_N})_{a_l,1} \, |i_{l+1}, \dots, i_N\rangle$, this is again the Schmidt decomposition of the state between the l-th and $(l+1)$-th bond with $|\psi\rangle = \sum_{a_l} s_a \, |a_l\rangle_A \, |a_l\rangle_B$. Multiplying S either with its left or right neighbor yields the orthogonality center (OC), whose name is derived from the fact that the all basis states on its left/right are orthonormal. This site is unnormalized, while all tensors to its left are left-normalized and the ones to its right are right-normalized. It is also called active site, as for the calculation of

expectation values, the OC needs to be placed on the respective site in order to exploit the left- and right-normalization of the other lattice tensors, see Sec. 3.4. Fig. 3.4 shows the block diagram notation of this state.
Secondly, the canonical form or Vidal decomposition is explained: here, all singular value matrices are being kept during the decomposition. The mathematical procedure for both decompositions is described very well in [85]. The obvious advantage of this form is that the entanglement between all subspaces is kept accessible at all times.
In order to illustrate the outlined procedure, the decomposition of the W-state into an MPS will be demonstrated in the appendix in Sec. 11.2, which serves as an example of a multipartite entangled quantum state.

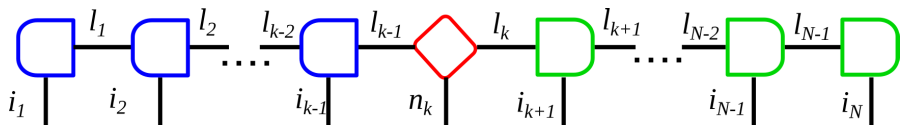

Figure 3.4: Block diagram of a matrix product state in the mixed canonical form, where the green boxes on the right are the right-orthogonal B-matrices and the blue boxes the left-orthogonal A-matrices. The red triangular box represents the singular value matrix S.

3.3 The application of operators

An arbitrary operator O affecting $|\psi\rangle$ expressed in the basis $\{|i_k\rangle\}$ takes the form

$$O = \sum_{\substack{i_1,\ldots,i_N \\ i'_1,\ldots i'_N}} c_{i_1,\ldots,i_N,i'_1,\ldots i'_N} |i_1 \ldots i_N\rangle \langle i'_1 \ldots i'_N| \tag{3.33}$$

The indexes can be rewritten using a compound index (i_k, i'_k), which takes the same role as the index i_k in the decomposition of a state into an MPS. With that, the operator may be decomposed into a matrix product operator (MPO) like

$$O = \sum_{\substack{i_1,\ldots,i_N \\ i'_1,\ldots i'_N}} c_{(i_1,i'_1),\ldots,(i_N,i'_N)} |i_1, \ldots i_N\rangle \langle i'_1 \ldots i'_N| \tag{3.34}$$

$$= \sum_{\substack{i_1,\ldots,i_N \\ i'_1,\ldots i'_N}} W^{i_1 i'_1}_{1,b_1} W^{i_2 i'_2}_{b_1,b_2} \ldots W^{i_N i'_N}_{b_N,1} |i_1, \ldots i_N\rangle \langle i'_1 \ldots i'_N| \tag{3.35}$$

$$= \sum_{\substack{i_1,\ldots,i_N \\ i'_1,\ldots i'_N}} W^{i_1 i'_1} W^{i_2 i'_2} \ldots W^{i_N i'_N} |i_1, \ldots i_N\rangle \langle i'_1 \ldots i'_N| , \tag{3.36}$$

where in the second step the coefficient tensor $c_{(i_1,i'_1),\ldots,(i_N,i'_N)}$ has been decomposed into a matrix product state making use of the same procedure as shown above in Eq. (3.15) - (3.24). Note the important difference to the decomposition of a state $|\psi\rangle$: Now, each W-matrix carries two physical indexes per site. The block diagram notation of an arbitrary operator is shown in Fig. 3.5.
Applying the operator on the state reads as $|\tilde{\psi}\rangle = O\,|\psi\rangle$. Inserting equations 3.35 and 3.24 results in

$$O\,|\psi\rangle = |\tilde{\psi}\rangle = \sum_{\substack{i_1,\ldots,i_N \\ i'_1,\ldots i'_N}} (W^{i_1 i'_1}_{1,b_1} W^{i_2 i'_2}_{b_1,b_2} \ldots W^{i_N i'_N}_{b_N,1})(A^{i'_1}_{1,a_1} A^{i'_2}_{a_1,a_2} \ldots A^{i'_N}_{a_N,1})\,|i_1,\ldots i_N\rangle \quad (3.37)$$

Because operators on different sites commute, it is possible to rearrange the matrices and contract over one of the site indexes. This results in the new MPS $|\tilde{\psi}\rangle$ whose matrices

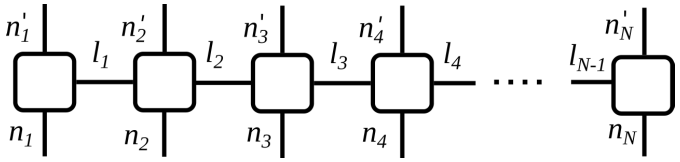

Figure 3.5: Block diagram of an matrix product operator (MPO) which acts on the entire spin chain from site i_1 to i_N. Each solid rectangle represents a W-matrix with two physical site indexes and (apart from the first and the last in the row) two link indexes. The horizontal lines represent the link indexes b_k, $k \in (1,\ldots N-1)$, between the matrices, while the vertical lines represent the physical indexes i_k and i'_k.

now have two new compound indexes $(b_{k-1}, a_{k-1}), (b_k, a_k)$:

$$|\tilde{\psi}\rangle = \sum_{\substack{i_1,\ldots,i_N \\ i'_1,\ldots i'_N}} (W^{i_1 i'_1}_{1,b_1} A^{i'_1}_{1,a_1})(W^{i_2 i'_2}_{b_1,b_2} A^{i'_2}_{a_1,a_2}) \ldots (W^{i_N i'_N}_{b_N,1} A^{i'_N}_{a_N,1})\,|i_1,\ldots i_N\rangle \quad (3.38)$$

$$= \sum_{i_1,\ldots,i_N} N^{i_1}_{(1,1),(b_1,a_1)} N^{i_2}_{(b_2,a_2),(b_3,a_3)} \ldots N^{i_N}_{(b_{N-1},a_{N-1}),(1,1)}\,|i_1,\ldots i_N\rangle \quad (3.39)$$

$$= \sum_{i_1,\ldots,i_N} N^{i_1} \ldots N^{i_N}\,|i_1,\ldots i_N\rangle \quad (3.40)$$

Note that with the introduction of the new compound indexes, the bond dimensions have grow in size, with the dimensions of the new MPS $|\tilde{\psi}\rangle$ being the product of the dimensions of $|\psi\rangle$ and O. If the MPS would not be truncated after each step, this would lead to an exponential increase in its size.
The block diagram of this procedure is shown in Fig. 3.6.

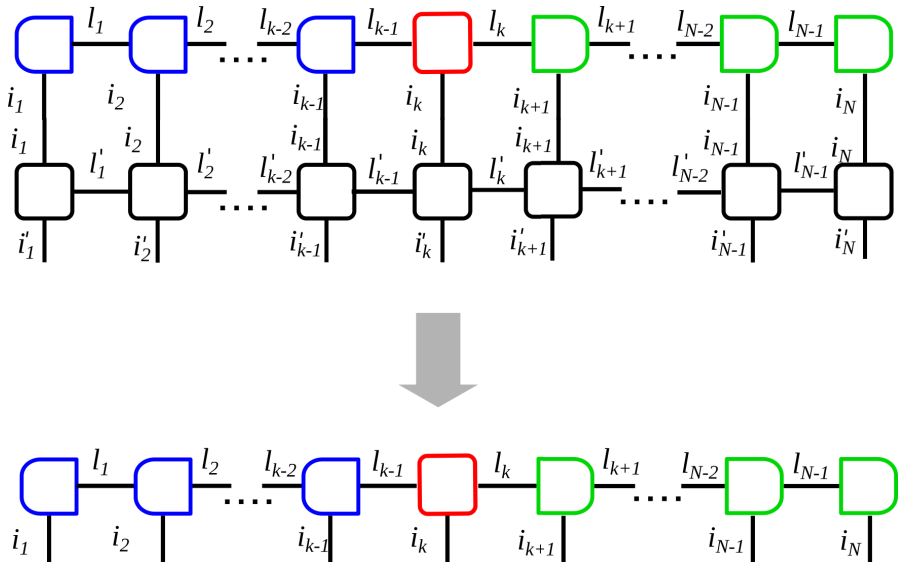

Figure 3.6: The application an MPO on an MPS. The first line shows the application of the operator before the contraction over the physical indexes i'_k. In the second line, this contraction and the re-labeling of the indices has been performed, resulting in a new MPS.

3.4 Calculation of expectation values

Another important step is the calculation of a one-site expectation value from a state in the form of an MPS. First, consider an arbitrary one-site operator $O^{[k]}$ effecting site k. It takes the form

$$O^{[k]} = \sum_{i_k, i'_k} c_{i_k, i'_k} |i_k\rangle \langle i'_k| \tag{3.41}$$

and its application on $|\psi\rangle$ reads $|\tilde{\psi}\rangle = O^{[k]} |\psi\rangle$, while the expectation value $M_{O^{[k]}}$ is calculated with $M_{O^{[k]}} = \langle\psi| O^{[k]} |\psi\rangle$. If $O^{[k]}$ is written as an matrix product operator in the full Hilbert space of $|\psi\rangle$, all the W-matrices will be the identity I, except for the site k. Thus, the operator takes the following form, where $O^{i_l i'_l} = I^{i_l, i'_l}$ for all $l \in 1, \ldots, N$ except for k, and $O^{i_k i'_k} = c_{i_k, i'_k}$:

$$O^{[k]} = \sum_{\mathbf{i},\mathbf{i'}} O^{i_1 i'_1} \ldots O^{i_k i'_k} \ldots O^{i_N i'_N} |i_1, \ldots i_N\rangle \langle i'_1 \ldots i'_N| \tag{3.42}$$

With that, the operator takes the form of an MPO affecting the entire chain, as show in Fig. 3.5. The numerically least expensive way for calculating $M_{O^{[k]}} = \langle\psi| O^{[k]} |\psi\rangle$ is

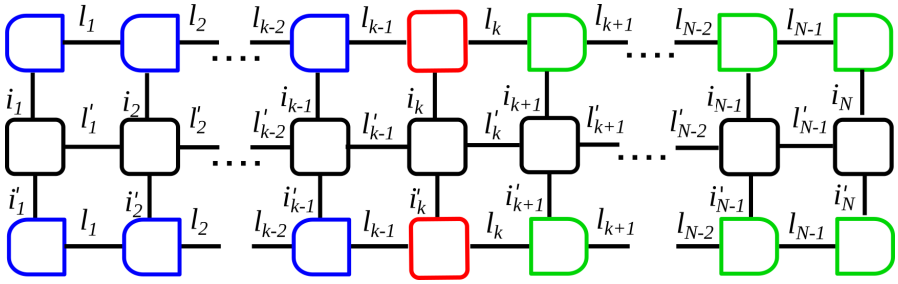

Figure 3.7: Block diagram of the full calculation of an expectation value $\langle\psi| O^{[k]} |\psi\rangle$ of the Observable $O^{[k]}$ acting on site k. The black boxes in the middle represent the matrix product operator, while the colored boxes on the lower line represent $|\psi\rangle$ and the ones in the upper line $\langle\psi|$. Note that the MPS is in the mixed canonical form with the orthogonality center on site k, which is represented by the red box shape.

to write $|\psi\rangle$ in the mixed canonical form with the singular value matrix S between site $k-1$ and k, and contract S into the matrix B_k. This way, all matrices on the left side of site k are left-normalized and the ones on the right are right-normalized. Thus, it holds:

$$M_{O^{[k]}} = \langle\psi| O^{[k]} |\psi\rangle \tag{3.43}$$

$$= \sum_{\mathbf{i},\mathbf{i'}} (A^{i_1 *} \ldots A^{i_N *})(O^{i_1 i'_1} \ldots O^{i_N i'_N})(A^{i'_1} \ldots A^{i'_N}). \tag{3.44}$$

$$\tag{3.45}$$

The block diagram to this equation is shown in Fig. 3.7. The sum over the indexes evaluate to 1 for each site except for site k, as for all matrices left of site k it holds that $A^{i_l\dagger}A^{i_l} = I$ and $O^{i_l} = I$, and on the right side of site k it holds that $A^{i_l}A^{i_l\dagger} = I$ and $O^{i_l} = I$. Thus, contracting the network over all these bonds results in the unitary matrix I and the only calculation to perform is analytically expressed as

$$\langle\psi|\, O^{[k]}\, |\psi\rangle = \sum_{i_k, i'_k} O^{i_k i'_k} A^{i_k\dagger} A^{i_k}. \tag{3.46}$$

The corresponding block diagram is shown in Fig. 3.8. If a two-site correlation function

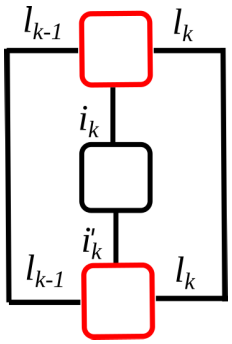

Figure 3.8: Block diagram of the same expectation value $\langle\psi|\, O^{[k]}\, |\psi\rangle$ as shown in Fig. 3.7 above, where the contraction over the left- and right-normalized matrices has already been done, yielding the identity on both sides. The remaining block diagram stands for the analytical expression that remains to be evaluated numerically, which is $\langle\psi|\, O^{[k]}\, |\psi\rangle = \sum_{i_k, i'_k} O^{i_k i'_k} A^{i_k\dagger} A^{i_k}$.

is supposed to be evaluated, the contraction will have to be performed over all sites in between, or the two bins have to be brought next to each other beforehand. This is explained in more detail in Sec. 8.2.2.

3.5 The Suzuki-Trotter decomposition

In order to set up operators for many-body systems within the MPS framework, an approximation of matrix exponential for $U^{\text{exact}}(\Delta t) = e^{iH\Delta t}$ is needed. An efficient form for this is given with the Suzuki-Trotter decomposition [115, 116].
Consider an Hamiltonian modeling a quantum mechanical many-body system, for instance the Hamilton operator H of the isotropic Heisenberg chain consisting of N sites:

$$H = J \sum_{i}^{N-1} \frac{1}{2} \left(s_i^+ s_{i+1}^- + s_i^- s_{i+1}^+ \right) + s_i^z s_{i+1}^z \tag{3.47}$$

It may be written as a sum over local Hamiltonians $h_i = \frac{1}{2}\left(s_i^+ s_{i+1}^- + s_i^- s_{i+1}^+\right) + s_i^z s_{i+1}^z$, which describe the interaction between site i and $i+1$:

$$H = \sum_{i=1}^{N-1} h_i \tag{3.48}$$

and thus the time evolution operator which acts on the system looks like

$$U(\Delta t) = e^{-\frac{i}{\hbar}\left(\sum_{i=1}^{N-1} h_i\right)\Delta t} \tag{3.49}$$

In order to avoid the exponential expansion of the Hilbert space with 2^N, the time evolution operator in 3.49 needs to be split into a product of local operators with the dimension $2^2 = 4$ [85, 86].
It is possible to split the sum in Eq. (3.48) into two parts: H_e containing all even i and H_o all odd i, so that it holds

$$H_e = \sum_{i=1}^{(N-1)/2} h_{2i}, \tag{3.50}$$

$$H_o = \sum_{i=1}^{(N-1)/2} h_{2i-1} \tag{3.51}$$

$$H = H_e + H_o \tag{3.52}$$

and thus

$$U(\Delta t) = e^{-\frac{i}{\hbar}(H_o + H_e)\Delta t} \tag{3.53}$$

As the local operators h_i do not commute, $[h_i, h_{i+1}] \neq 0$, writing the exponential in 3.53 as a product will produce an error. It will now be shown that this error is of $\mathcal{O}(\Delta t^2)$, $\mathcal{O}(\Delta t^3)$ or $\mathcal{O}(\Delta t^5)$ - depending on the chosen approximation method - and thus sufficiently small.
A Taylor expansion of 3.53 yields

$$\begin{aligned} e^{-\frac{i}{\hbar}(H_o+H_e)\Delta t} &= 1 + (H_o + H_e)\,\Delta t + \frac{1}{2}\left((H_o + H_e)\,\Delta t\right)^2 + \dots \\ &= 1 + H_o\Delta t + H_e\Delta t + \frac{1}{2}H_oH_e\Delta t^2 + \frac{1}{2}H_eH_o\Delta t^2 + \frac{1}{2}H_e^2\Delta t^2 + \frac{1}{2}H_o^2\Delta t^2 \dots, \end{aligned} \tag{3.54}$$

while a Taylor expansion of $e^{-\frac{i}{\hbar}H_o\Delta t}e^{-\frac{i}{\hbar}H_e\Delta t}$ yields

$$\begin{aligned} e^{-\frac{i}{\hbar}H_o\Delta t}e^{-\frac{i}{\hbar}H_e\Delta t} &= \left(1 + H_o\Delta t + \frac{1}{2}H_o^2\Delta t^2 \dots\right)\left(1 + H_e\Delta t + \frac{1}{2}H_e^2\Delta t^2 \dots\right) \\ &= 1 + H_o\Delta t + \frac{1}{2}H_o^2\Delta t^2 + H_e\Delta t + H_oH_e\Delta t^2 + \frac{1}{2}H_e^2\Delta t^2 + \dots \end{aligned} \tag{3.55}$$

Subtracting both expansions yields

$$e^{-\frac{i}{\hbar}(H_o+H_e)\Delta t} - e^{-\frac{i}{\hbar}H_o\Delta t}e^{-\frac{i}{\hbar}H_e\Delta t} = \frac{1}{2}\Delta t^2(H_eH_o - H_oH_e) + \dots, \tag{3.56}$$

Inserting 3.56 into 3.53 gives the error for approximating $U(\Delta t)$ by assuming that $[H_o, H_e] = 0$:

$$\begin{aligned} U(\Delta t) &= e^{-\frac{i}{\hbar}(H_o+H_e)\Delta t} \\ &= e^{-\frac{i}{\hbar}H_o\Delta t}e^{-\frac{i}{\hbar}H_e\Delta t} + \frac{1}{2}\Delta t^2(H_eH_o - H_oH_e) + \dots \end{aligned} \tag{3.57}$$

and thus

$$\begin{aligned} U(\Delta t) &= e^{-\frac{i}{\hbar}H_o\Delta t}e^{-\frac{i}{\hbar}H_e\Delta t} + \mathcal{O}(\Delta t^2) \\ &= U^{\mathrm{ST1}}(\Delta t) + \mathcal{O}(\Delta t^2). \end{aligned} \tag{3.58}$$

Eq. (3.58) is called a Suzuki-Trotter decomposition of first order. By symmetrizing, one can show that

$$\begin{aligned} U(\Delta t) &= e^{-\frac{i}{2\hbar}H_e\Delta t}e^{-\frac{i}{\hbar}H_o\Delta t}e^{-\frac{i}{2\hbar}H_e\Delta t} + \mathcal{O}(\Delta t^3) \\ &= U^{\mathrm{ST2}}(\Delta t) + \mathcal{O}(\Delta t^3) \end{aligned} \tag{3.59}$$

In the decomposition 3.59, the accuracy is of higher order in Δt than in 3.58, and it is called a Suzuki-Trotter decomposition of second order. In the same manner, one can derive a formula for an approximation with accuracy of forth order:

$$U(\Delta t) = U^{\mathrm{SZ2}}(\tau_1)U^{\mathrm{SZ2}}(\tau_1)U^{\mathrm{SZ2}}(\tau_2)U^{\mathrm{SZ2}}(\tau_1)U^{\mathrm{SZ2}}(\tau_1) + \mathcal{O}(\Delta t^5) \tag{3.60}$$

with

$$\tau_1 = \tau_2 = \frac{1}{4 - 4^{1/3}}\tau \tag{3.61}$$

$$\tau_2 = (1 - 4\tau_1)\tau \tag{3.62}$$

The error which is made per time step using this approximation is of $\mathcal{O}(\Delta t^5)$.
Generalizing this, for any Hamiltonian H with internally commuting parts $H_\alpha = \sum_{k=1}^{N_\alpha} h_\alpha^k$ where the h_α^k may be diagonalized and commute with each other, one may write

$$U^{\mathrm{ST1}}(\Delta t) = \Pi_{\alpha=1}^{N_H} e^{-iH_\alpha\Delta t} \tag{3.63}$$

for the first order decomposition and

$$U^{\mathrm{ST2}}(\Delta t) = \Pi_{\alpha=1}^{N_H} e^{-iH_\alpha\frac{\Delta t}{2}}\Pi_{\alpha=N_H}^{1} e^{-iH_\alpha\frac{\Delta t}{2}} \tag{3.64}$$

for the second order decomposition. While the error per time step decreases with higher order evolutions, the number of exponentials which need to be set up for one time step increases strongly. Thus, it may be the more efficient choice to reduce the step size Δt instead of increasing the order of the decomposition [86].

4.

Quantum coherent self-feedback

4.1 Introduction to feedback control

Feedback control is well established in modern physical control theory. Its aim is the manipulation of the dynamics of physical systems. The principle setup is that a control system - the controller - is provided with information about the evolution of the system that is to be controlled - the plant. The controller then feeds this information back into the plant in real time in order to achieve an objective, that is to influence its trajectory in a desired way. This may be for instance for the trajectory to follow one precise evolution, or to reach a certain state at a given time, or to reduce the effects of noise or errors on the evolution - using a certain feedback protocol in order to achieve this. As this feedback protocol begins and terminates at the plant, this form of control is also called closed-loop control [136, 137, 138].
In the quantum regime, feedback control is investigated since the 1980s and is nowadays an important method in various physical settings. Two different approaches exist. In all forms of measurement-based feedback control, the protocol involves explicit measurements made on the system, thus it relies on obtaining classical information about the state in a loop containing classical input and output from and to the quantum system [138, 139, 140, 141, 142, 143, 144, 145, 55, 146]. These protocols have been experimentally realized in a broad range of different setups, for instance for adaptive phase estimation [147, 148, 149] or for controlling a single-photon state [150].
In contrast to that, coherent feedback relies on measurement-free control processes and couples the state of the plant and that of the controller by traveling wave fields [151, 152, 3] or, more generally, by unitary interactions [153, 154, 155]. It was first proposed in [151] as an all-optical form of feedback control, and later in its general form presented in [153]. In this form, the controller is a quantum system which obtains quantum information via

unitary interactions from the plant and uses this information to control it. Thus, the control mechanism is fully quantum mechanical.
Coherent feedback has the strong advantage of relying on quantum state preserving interactions, while in the case of measurement-based feedback, coherence is destroyed by repeated measurements, for which additionally a strong amplification and processing of the signal on larger timescales is usually necessary.
Quantum coherent feedback successfully generates a variety of effects such as noise-reduction [156, 157], optical squeezing [158], quantum error correction [159, 160] and entanglement control [161]. It has recently been used to generate nonclassical optical states [162]. It has also been successfully implemented in experimental setups [163, 164, 165, 154, 166, 165, 167, 168].
Important applications lie in the field of quantum information processing [56, 57, 58]. In particular, feedback control has been successfully used to predict and generate population trapping in different setups, which will be discussed in the following. Here, an application of fundamental importance is the field of quantum memory, which relies on the storage and release of qubits on demand [61, 49, 62, 63, 64]. One specific form of feedback control is time-delayed self-feedback. Here, the external control force is replaced by a repeated interaction of the system with former states of itself. In classical physics, it has been studied theoretically as well as experimentally for instance in the field of laser optics [169, 170, 171] or dynamical systems and chaos control [172, 173, 174, 175, 176, 177]. The Pyragas form [172, 173] of the classical differential equations reads

$$\dot{x}(t) = f(x) + \kappa(y(t-\tau) - y(t)), \tag{4.1}$$

with $x(t)$ the state vector, $f(x)$ the equations of motion, $y(t)$ the output signal and τ the delay time. κ constitutes the control force which vanishes in case of $y(t) = y(t-\tau)$, for instance in case of the stabilization of an instable periodic system or when a steady state is reached. In the quantum regime, the enabling mechanism is often based on the interaction of the system with a structured continuum with multi-mode degrees of freedom [178, 179, 180, 181, 182]. In this thesis, the reservoir will be described with a structured bosonic continuum [80, 133].
In the last decade, self-feedback has been intensely studied for single or coupled few-level systems, with the aim to manipulate distinct system degrees of freedom. Its coherent and non-Markovian nature introduces quantum interferences into the dynamics of these systems and allows for the amplification of two-photon processes [132, 80], enhanced entanglement and non-classical photon statistics [183], dimerization [184, 185] and a stabilization of quantum coherence due to interference effects between incoming and outgoing probability waves [186, 70, 187, 188]. Together with the formation of dark states and subsequently emerging population trapping [133, 71], Rabi oscillations in the single-excitation regime have been predicted [187].

4.2 Population trapping

In this thesis, the self-feedback mechanism is employed by placing the system under investigation in a semi-infinite waveguide. The closed end of the waveguide acts as a mirror which is assumed to be perfectly reflecting. Thus, the system is subjected to a time-delayed, coherent self-feedback, which is based on the interaction of the system with a structured continuum : part of the excitation emitted from the system will be reflected by the mirror and subsequently interact with the system again after the delay time τ. A schematic setup is sketched in Fig. 4.1.

This mechanism provides a measurement-free, state preserving coherent form of quan-

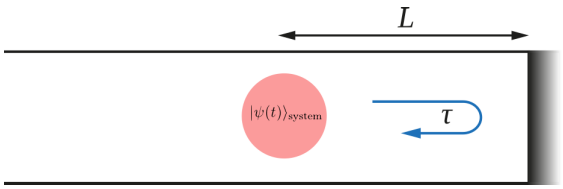

Figure 4.1: Sketch of an quantum system placed in a semi-infinite waveguide where the closed side is of length L and the end consists of mirror. Part of the emitted excitation will then be reflected and interact with the system again, driving it by its own past.

tum feedback control which provides for a method to manipulate system degrees of freedom. It is mainly studied in atom-molecular-optics and cavity-QED [189, 187, 60, 190, 191, 80, 181, 192, 193, 180, 194, 195, 178, 196, 197, 179].
Placing a two-level system (TLS) in this waveguide serves as a brief introductory example in order to discuss the properties of quantum feedback, and provides for an important benchmark for the numerical method with tMPS. It describes the system dynamics in the single-excitation regime, thus the quantum feedback mechanism is of linear nature. This model is well investigated analytically [189, 192, 198, 186, 70, 187], and has also been realized experimentally as a single atom decaying in front of a mirror [199].
The Hamiltonian reads (with $\hbar \equiv 1$):

$$H = \omega_0 \sigma^+ \sigma^- + \int d\omega \omega b^\dagger(\omega) b(\omega) + \int d\omega \left(G_{fb}(\omega) b^\dagger(\omega) \sigma^- + \text{h.c.} \right) \tag{4.2}$$

The first term models the free evolution of the two-level system, where ω_0 is the resonance frequency of the TLS and $\sigma^+ = \sigma^x + i\sigma^y$ and $\sigma^- = \sigma^x - i\sigma^y$ are the creation and destruction operators for an fermionic excitation in the two-level system, respectively.
The second term represents the free evolution of the bosonic mode continuum to which the two-level system is coupled. Here, $b^{(\dagger)}(\omega)$ annihilates (creates) a bosonic excitation of energy ω.

The last term represents the interaction of the two-level emitter with the bosonic reservoir which offers a unitary description of decay and feedback effects. Here, the frequency dependent coupling $G_{fb}(\omega)$ models the feedback interaction and is defined as:

$$G_{fb}(\omega) = g_0 \sin\left(\frac{\omega L}{c_0}\right) = i\sqrt{\frac{\Gamma}{2\pi}}\left(e^{-i\omega\tau/2} - e^{i\omega\tau/2}\right). \tag{4.3}$$

Eq. (4.3) represents the sinusoidal, frequency-dependent system-reservoir coupling in order to model a semi-infinite waveguide, where L is the length of the closed side of the waveguide, c_0 the phase velocity in the waveguide, $\tau = 2L/c_0$ the feedback delay time - which is the round-trip time between the emission of a signal from the two-level emitter into the waveguide and its re-absorption from the reservoir after its reflection at the mirror - and $g_0 = \sqrt{\Gamma/2\pi}$ the coupling constant with the coupling rate Γ. Initializing the bosonic continuum in the vacuum state $|\psi(t_0)\rangle_{\text{res}} = |\{0\}_k\rangle$ with $b_k |\psi(t_0)\rangle_{\text{res}} = 0$ and assuming an initially excited emitter, that is $c_e(t_0) = 1$, $c_g(t_0) = 0$, the total system dynamics is described in the single excitation regime: The electronic as well as the photonic degrees of freedom are restricted to a single excitation, which may be located either in the atom or in the reservoir. With this, the ansatz for the wave function reads

$$|\psi(t)\rangle = c_e(t)\,|1, \{0\}_\omega\rangle + \int d\omega c_g^\omega(t)\,|0, \{1\}_\omega\rangle\,, \tag{4.4}$$

with $|c_e(t)|^2 + \int d\omega |c_g^\omega(t)| = 1$. Here, $c_e(t)$ denotes the complex coefficient with the atomic state excited and the bosonic continuum in the vacuum state, while $c_g^\omega(t)$ is the complex coefficient where the atom is in its ground state and the excitation in the reservoir.
The system obeys the Schrödinger equation, and the equations of motion for the state of the system are derived in order to study its time-evolution under feedback. To this end, a unitary transformation into the interaction picture is applied where the Hamiltonian in Eq. (4.2) is transformed into the rotating frame defined by its freely evolving part using

$$U_1 = \exp\left[it\Big(\omega_0\sigma^+\sigma^- + \int d\omega\omega b^\dagger(\omega)b(\omega)\Big)\right] \tag{4.5}$$

This yields the transformed Hamiltonian $H'(t)$:

$$H'(t) = \int d\omega \left(G_{fb}(\omega)\sigma^+ b(\omega) e^{-i(\omega-\omega_s)t} + \text{h.c.}\right) \tag{4.6}$$

Note that for a frequency-independent coupling constant $G_{fb(\omega)} = g_0$ instead of $G_{fb}(\omega)$, the time dependent solution for $|\psi(t)\rangle$ in Eq. (4.4) under the evolution of the Schrödinger equation would describe the spontaneous decay of a two-level emitter in a fully quantized field, which may be solved with Wigner-Weisskopf approximation yielding the exponential decay in time of the emitter with the solution

$$|c_e(t)|^2 = e^{-2\Gamma t} \tag{4.7}$$

and thus with the the radiative lifetime $\frac{1}{\Gamma}$.
With the frequency dependent coupling, however, the equation reads

$$\partial_t c_e(t) = -i \int d\omega G_{fb}(\omega) e^{-i(\omega-\omega_0)t} c_g^\omega(t) \tag{4.8}$$

$$\partial_t c_g^\omega(t) = -iG_{fb}(\omega) e^{i(\omega-\omega_e)t} c_e(t). \tag{4.9}$$

Next, Eq. (4.9) is formally integrated and plugged into Eq. (4.8). This yields the dynamics for the excited state

$$\partial_t c_e(t) = \Gamma \left(\Theta(t-\tau) c_e(t-\tau) e^{i\phi} - c_e(t) \right), \tag{4.10}$$

where the feedback phase $\phi = \omega_0 \tau$ has been introduced. Note that the first term in Eq. (4.10) only contributes for $t \geq \tau$, while the sign of this contribution is influenced by $e^{i\phi}$: For $\phi = 2n\pi$, $n \in \mathbf{N}_0$, $e^{i\phi} = 1$ which yields a solution for $\partial_t c_e(t) = 0$ with a finite $c_e(t)$. This is the case of a fully constructive feedback phase. For the case of $\phi = (2n+1)\pi$, $n \in \mathbf{N}_0$, $e^{i\phi} = -1$, which results in the enhanced decay of the emitter.
Comparing Eq. (4.10) with the equation of motion for classical time-delayed feedback control in Eq. (4.1), clearly the feedback phase is crucial when extending the classical Pyragas control to the quantum regime. Eq. (4.10) may be solved using a Laplace transformation. The result reads

$$c_e(t) = \sum_{n=0}^{\infty} (\Gamma e^{i\phi})^n \frac{1}{n!} (t-n\tau)^n e^{-\Gamma(t-n\tau)} \theta(t-n\tau). \tag{4.11}$$

Eq. (4.11) is in plugged into Eq. (4.9) in order to obtain a solution for the relaxation dynamics of the emitter. Formally integrating and setting $c_g^\omega(0) = 0$ yields

$$c_g^\omega(t) = -iG_{fb}(\omega) \int_0^t dt e^{i(\omega-\omega_0)t} \sum_{n=0}^{\infty} \frac{\left(\Gamma e^{i\omega_e \tau}\right)^n}{n!} (t-n\tau)^n e^{-\Gamma(t-n\tau)} \Theta(t-n\tau) \tag{4.12}$$

Here, the conservation of probability is checked for the 0th τ- interval by verifying

$$\int_0^\infty d\omega \left| c_g^\omega(t \leq \tau) \right|^2 + \left| c_e(t \leq \tau) \right|^2 \stackrel{!}{=} 1 \tag{4.13}$$

for $n = 0$ in Eq. (4.11) and (4.12). Again, it it is assumed that $t \to \infty$ so that $c_e(t \to \infty) = 0$. Equations (4.11)-(4.12) fully describe the dynamics of $|\psi(t)\rangle$ in Eq. (4.4) under the Schrödinger equation with the Hamiltonian given in Eq. (4.2).
In order to discuss the dynamics of a two-level emitter under feedback, the occupation density of the excited level $|c_e(t)|^2 = \langle \sigma^{11} \rangle$ is calculated from Eq. (4.11) for the first two τ-intervals, that is for $n \in 0, 1$. The result reads, with $\Gamma_\tau = \Gamma e^{i\phi}$:

$$\begin{aligned} |c_e(t)|^2 &= \langle \sigma^{11} \rangle \\ &= e^{-\Gamma t} \Big\{ 1 + \Theta(t-\tau) \Big[e^{\Gamma\tau} \big(\Gamma_\tau t - \Gamma_\tau \tau \big) \Big] \Big\} \end{aligned} \tag{4.14}$$

Eq. (4.14) shows the dependence of the solution on the interval τ. The first term depicts the time trace of the excitation density for the 0th τ-interval. During this interval, the emitter does not interact with its own past yet, and thus decays exponentially into the vacuum reservoir according to the corresponding Wigner-Weisskopf solution in Eq. (4.7). The second term in Eq. (4.14) describes the evolution during the first τ-interval, where the first re-absorbance of the emitted signal occurs.
In the case of a short delay time $\Gamma\tau \ll 1$, the feedback phase ϕ - the phase between emission and re-absorption - matters, which is included in the second last term in Eq. (4.14). Its choice may either slow down or speed up the decay process compared to its free decay. Here, for the case of a fully constructive feedback phase $\phi = 2n\pi$, $n \in \mathbf{N}$, a non-trivial solution for the long-time steady-state is obtained, where $c_e(t \to \infty) = \text{const}$ and $c_e(t \to \infty) > 0$. During the 0th τ-interval, the initial excitation first dissipates partially into the reservoir. In the 1st τ-interval, this process is stopped by the interaction with the feedback signal. In the following τ-intervals, after a convergence time, the system-reservoir interaction reaches a steady-state and dynamically traps the remaining excitation within it. This process is referred to as population trapping or atom-photon bound state [59]: Without any external disturbances, the excitation probability within the system remains constant for $t \to \infty$.
Note that the condition for trapping to occur only depends on the choice of the feedback phase ϕ, not on the delay time τ - the choice of the latter only influences the trapped excited density. For all cases where $\phi \neq 2n\pi$, the system will eventually decay, thus $c_e(t \to \infty) = 0$. For the case of $\phi = (2n+1)\pi$, the destructive feedback phase, the decay process is most strongly enhanced.
Both cases are depicted in the appendix in Sec. 11.3.2 in Fig. 11.1 - 11.2. These plots also serve as a benchmark for the numerical implementation of coherent self-feedback using tMPS (black dotted lines), demonstrating the accordance of the algorithm with the analytical solution. The derivation of the computational basis is given in the appendix in Sec. 11.3.1. This benchmark will serve as a starting point for the applications of quantum feedback control presented in the following.

Part II.

Quantum many-body system-reservoir interaction

5.

Quantum spin physics

5.1 Introduction to spin physics

This thesis is concerned with one-dimensional spin system as paradigmatic models for many-body systems. A spin system consists of two or more particles which have a magnetic moment $\boldsymbol{\mu}$. In most cases electrons are the cause of magnetism, so they may be considered to represent these particles. For their magnetic moment $\boldsymbol{\mu}$ it holds:

$$\boldsymbol{\mu} = \boldsymbol{\mu}_l + \boldsymbol{\mu}_s = \frac{\beta}{\hbar}\left(\mathbf{l} + g_s\mathbf{s}\right) \tag{5.1}$$

where $\mathbf{l}$ is the operator for the orbital angular momentum, $\mathbf{s}$ the operator for the spin angular momentum and $\beta = \frac{e\hbar}{2m}$ is the Bohr magneton, which is the elementary unit of the magnetic moment. g is the gyromagentic factor which indicates the proportionality of the entire magnetic moment $\boldsymbol{\mu}$ to the classical explainable part $\boldsymbol{\mu}_l$. Here, for electrons it holds that $g_s \approx 2$. For reasons of simplicity, the part of the magnetic moment which is due to the orbital angular momentum $\mathbf{l}$ caused by the movement of the electron will not be considered here. Also, only the exchange interaction will be considered here, while the weak magnetic interaction will be neglected. The exchange interaction is due to the Pauli principle for indistinguishable particles, thus quantum mechanical in its origin and due to the Coulomb forces between the electrons [200, 201].
The spin may be interpreted as the intrinsic angular momentum carried by elementary particles, and is a fundamental property of them. For its operator $\mathbf{s} = (s_x, s_y, s_z)$, the general properties for angular momentum operators hold. Thus, the following commutator rules apply:

$$[s_i, s_j] = i\hbar\epsilon_{ijk}s_k \tag{5.2}$$

$$[\mathbf{s}^2, s_z] = 0, \tag{5.3}$$

where $\mathbf{s}^2 = (s_x)^2 + (s_y)^2 + (s_z)^2$ and ϵ_{ijk} denotes the Levi-Civita-Tensor which is defined

$$\epsilon_{ijk} = \begin{cases} 1 & \text{if } (i,j,k) \text{ is an even permutation of } (x,y,z) \\ -1 & \text{if } (i,j,k) \text{ is an uneven permutation of } (x,y,z) \\ 0 & \text{if } i = j \text{ or } i = k \text{ or } j = k. \end{cases} \tag{5.4}$$

Note that the z-component in equ. (5.3) is chosen by convention to have the same eigenbasis as $\mathbf{s}^2$. Note that $\mathbf{s}$ has the following eigenvalue equations:

$$\mathbf{s}^2 \left|l, m\right\rangle = l(l+1)\hbar^2 \left|l, m\right\rangle \tag{5.5}$$

$$s_z \left|l, m\right\rangle = m\hbar \left|l, m\right\rangle \tag{5.6}$$

and $|l, m\rangle$ are the corresponding eigenstates of $\mathbf{s}$ and s_z, where l may be an integer or half-integer. Bosons carry integer spin, fermions half-integer spin. For electrons, it holds that $l = \frac{1}{2}$. The quantum number m takes the values $m \in \{-l, -l+1, \ldots, l\} =$, so for electrons it holds that $m \pm \frac{1}{2}$. The three components of $\mathbf{s}$ are defined with the Pauli-matrices σ_i, $i \in (x, y, z)$, according to

$$s_i = \frac{\hbar}{2}\sigma_i, \tag{5.7}$$

with

$$\sigma_x = \begin{pmatrix} 0 & 1 \\ 1 & 0 \end{pmatrix}, \quad \sigma_y = \begin{pmatrix} 0 & -i \\ i & 0 \end{pmatrix}, \quad \sigma_z = \begin{pmatrix} 1 & 0 \\ 0 & -1 \end{pmatrix}, \tag{5.8}$$

and

$$\sigma_i^2 = I \quad \text{and} \quad \sigma_i\sigma_j = -\sigma_j\sigma_i \quad \text{for } i \neq j. \tag{5.9}$$

The Pauli spin matrices obey to the following commutator rule:

$$[\sigma_i, \sigma_j] = 2i\epsilon_{ijk}\sigma_k. \tag{5.10}$$

When choosing a respective basis, the spin part of the wave function of an electron has the following two eigenstates, which form an orthonormal system and are defined by the values the z-component of the spin may take:

$$|l = \frac{1}{2}, m = +\frac{1}{2}\rangle = |+\frac{1}{2}\rangle \equiv |\uparrow\rangle \equiv \begin{pmatrix} 1 \\ 0 \end{pmatrix} \tag{5.11}$$

$$|l = \frac{1}{2}, m = -\frac{1}{2}\rangle = |-\frac{1}{2}\rangle \equiv |\downarrow\rangle \equiv \begin{pmatrix} 0 \\ 1 \end{pmatrix} \tag{5.12}$$

The eigenstate $|\uparrow\rangle$ is called spin-up and corresponds to the spin being parallel to the z-axis, while $|\downarrow\rangle$ is called spin-down with the spin being anti-parallel to the z-axis.

Two more operators need to be introduced: The ascending operator s_+ and the descending operator s_- which are defined with

$$s_+ \equiv s_x + is_y \tag{5.13}$$
$$s_- \equiv s_x - is_y \tag{5.14}$$

and have the following effect on the eigenstates:

$$s_+ |\uparrow\rangle = 0, \quad s_+ |\downarrow\rangle = |\uparrow\rangle \tag{5.15}$$
$$s_- |\uparrow\rangle = |\downarrow\rangle, \quad s_- |\downarrow\rangle = 0 \tag{5.16}$$

Thus, the ascending operator s_+ flips a spin-down state to a spin-up state, and the descending operator flips a spin-up state to a spin-down state [200].

5.2 The Heisenberg chain and the Bethe ansatz

Different models exist for the interaction in systems of spins, corresponding to the fact that the exchange interaction may take many different forms. This thesis considers the paradigmatic example of the Heisenberg chain, whose physical properties will be sketched briefly in the following. [202, 200, 201].
The Heisenberg model expresses an exchange interaction between two spins. For the isotropic case the Hamiltonian reads

$$H = J\,\mathbf{s}_1 \cdot \mathbf{s}_2, \tag{5.17}$$

where J is the coupling constant and marks the preferred direction and strength of the interaction. If $J < 0$, the interacting spins will minimize their energy - and thus produce the strongest microscopic magnetic moment μ_i - when aligned parallel, which will, on a large scale, result in a ferromagnet with a large total magnetic moment $\mu_{\text{total}} = \sum_i \mu_i$. The energy of the ground state is $E = NJS^2 = \frac{1}{4}NJ$. If $J > 0$, the spins will prefer antiparallel alignment and thus μ_{total} will vanish. The corresponding ground state energy is $E = -NJS^2 = -\frac{1}{4}NJ$.
If a system of N coupled spins is considered, one important question is with how many other spins each single spin interacts. Here, the Heisenberg model for a chain with interaction only with the nearest neighbour will be introduced, which will be used in this thesis. The Hamiltonian for the isotropic case is

$$H = J \sum_{i=1}^{N-1} \mathbf{s}_i \cdot \mathbf{s}_{i+1} + \sum_{i}^{N} h_i s_i^z \tag{5.18}$$
$$= J \sum_{i=1}^{N-1} \left(s_i^x s_{i+1}^x + s_i^y s_{i+1}^y + s_i^z s_{i+1}^z \right) + \sum_{i}^{N} h_i s_i^z. \tag{5.19}$$

Here, h_i denotes an external magnetic field which interacts with the z-component of the spins and may vary for each single spin. Note that the operator s_i only acts on the i-th site in the chain, and that operators which act on different sites commute, thus

$$[s_i^k, s_j^l] = \delta_{ij} \tag{5.20}$$

for $k, l \in [x, y, z]$.
The Heisenberg model for the one-dimensional spin chain has an exact, analytical solution, which is known as the Bethe-ansatz. Bethe showed its validity for the spin-$\frac{1}{2}$-chain in 1931 [38]. In this thesis, the one-dimensional case is treated numerically, which is why the analytic solutions to this model are briefly explained here. However, not the ground state is of interest in this thesis, but non-equilibrium steady states.
The Hamiltonian in equ. (5.19) can be rewritten using the raising and lowering operator

$$H = J \sum_i^{N-1} \left[\frac{1}{2} \left(s_i^+ s_{i+1}^- + s_i^- s_{i+1}^+ \right) + s_i^z s_{i+1}^z \right] + \sum_i^N h_i s_i^z \tag{5.21}$$

which is shown as:

$$\begin{aligned} s_i^+ s_{i+1}^- &= (s_x + i s_y)(s_x - i s_y) \\ &= s_i^x s_{i+1}^x + s_i^y s_{i+1}^y + i(s_i^y s_{i+1}^x - s_i^y s_{i+1}^x) \end{aligned} \tag{5.22}$$

and

$$s_i^- s_{i+1}^+ = s_i^x s_{i+1}^x + s_i^y s_{i+1}^y - i(s_i^y s_{i+1}^x - s_i^y s_{i+1}^x) \tag{5.23}$$

thus

$$s_i^- s_{i+1}^+ + s_i^+ s_{i+1}^- = 2(s_i^x s_{i+1}^x + s_i^y s_{i+1}^y). \tag{5.24}$$

As for the operator of the total z-component $S_T^z = \sum_l s_l^z$ it holds that $[H, S_T^z] = 0$, an eigenbasis of both H and S_T^z may be chosen. Considering the fully aligned state $|A\rangle$ and setting the $h_i = 0$, i.e. all spins up and $s_T^z = \frac{N}{2}$, the eigenvalue equation of the Heisenberg-Hamiltonian reads:

$$H |A\rangle = \frac{JN}{4} |A\rangle \equiv E_A |A\rangle . \tag{5.25}$$

If $J < 0$, E_A is the energy of the ferromagnetic ground state. For the case $J > 0$, this is the state with the highest energy - it is still an eigenstate, but not the ground state.
Considering states with exactly one deviation on the l-th site $|l\rangle$ from the fully aligned state, the eigenvalue equation becomes

$$H |l\rangle = E_A |l\rangle + J \left(\frac{1}{2} |l-1\rangle + \frac{1}{2} |l+1\rangle - |j\rangle \right) \tag{5.26}$$

It is solved using as ansatz a linear superposition of all possible single-excitation states, thus $|\psi\rangle = \sum_l f_l |l\rangle$. It can be shown that the corresponding eigenstates $|\psi_k\rangle$ are of the

form of plane waves, thus $f_l = c_k e^{ikl}$, $c_k = \text{const}$, and are called spin-waves or magnons. These are of the form

$$|\psi_k\rangle = \frac{1}{\sqrt{N}} \sum_l e^{ikl} |l\rangle \,, \tag{5.27}$$

where $|l\rangle$ is the site of the deviation, and k represents the wave vector with $k = \lambda \frac{2\pi}{N}$, $\lambda \in \mathbf{R}$. The energy ϵ_k of one magnon with the wave vector k is

$$\epsilon_k = |J|(1 - \cos k). \tag{5.28}$$

Considering r deviations from the fully aligned state, the ansatz presented by Bethe [38] for the eigenvalue equation requires that

$$f_{l_1 \dots l_r} = \sum_{p=1}^{M} A_p e^{i(k_1^p l_1 \dots k_r^p l_r)} \tag{5.29}$$

and (5.30)

$$A_p = C \exp \left[\sum_{i=1}^{r} \sum_{j=i+1}^{r} \phi_{ij}^p \right] \tag{5.31}$$

This means that the phase factors A_p are of the form of two-body phase factors ϕ_{ij}^p. Here, $M = r!$ are all possible permutations of the values for k, with k_i^p denoting the i-th k in the p-th permutation. This ansatz yields the following relationship for k and ϕ

$$N k_i = 2\pi \lambda_i + \sum_{j \neq i} \phi_{ij} \tag{5.32}$$

$$2 \cot \frac{\phi_{ij}}{2} = \cot \frac{k_i}{2} - \frac{k_j}{2} \tag{5.33}$$

as well as the solution for the eigenvalue of the energy

$$\epsilon = J \sum_{i=1}^{r} (\cos k_i - 1). \tag{5.34}$$

With these equations, it is possible to exactly calculate the ground state energy of the antiferromagnetic spin chain ($J > 0$). In the classical case, this ground state is a state with the z-component of the total spin $s_z^T = 0$ and half the spins reversed, thus $r = \frac{N}{2}$. The corresponding quantum mechanical state is called the Néel state $|\psi_N\rangle$:

$$|\psi_N\rangle = |{\downarrow}{\uparrow}{\downarrow} \dots {\uparrow}{\downarrow}{\uparrow}\rangle \tag{5.35}$$

However, $|\psi_N\rangle$ is the ground state only for infinite chain length; for finite chain lengths, it is a basis state but not an eigenstate, which is due to finite size effects. For a chain with a finite length of N sites, with equ. (5.34) the eigenvalue of the ground state relative to the energy of the aligned state $E_A = \frac{JN}{4}$ is thus given by $\epsilon = J \sum_{i=1}^{\frac{N}{2}} (\cos k_i - 1)$. For

the limit $N \to \infty$, Hulthen calculated in 1938 ϵ_∞ by solving the equations 5.32-5.34 with the following result [203]:

$$\epsilon_\infty = -JN \ln 2 \tag{5.36}$$

This yields the ground state energy of the antiferromagnetic chain with

$$E = \epsilon_\infty - E_A \tag{5.37}$$

$$= -JN \ln 2 + \frac{JN}{4} \tag{5.38}$$

and thus

$$\frac{E}{JN} \approx -0.443147. \tag{5.39}$$

Using this result, Cloiseaux and Pearson calculated 1962 the energy of antiferromagnetic spin waves [204], i.e. of single or several deviations from the antiferromagnetic ground state - relative to the fully aligned state - with the following result for the energy of a spin wave with the wave vector k :

$$\epsilon = -JN \ln 2 + \frac{J\pi}{2} \sin k. \tag{5.40}$$

The Heisenberg chain may also be considered with an anisotropy in z-direction, that is, an additional coupling strength J_z in z-direction exists. The Hamiltonian thus is

$$H = \sum_{i=1}^{N-1} \frac{J}{2} \left[\left(s_i^+ s_{i+1}^- + s_i^- s_{i+1}^+ \right) + J_z s_i^z s_{i+1}^z \right] + \sum_{i=1}^{N} h_i s_i^z. \tag{5.41}$$

So, obviously, if $J_z = 1$ the model corresponds to the isotropic Heisenberg chain in equ. (5.19). The case $|J_z| < 1$ is called axial regime of anisotropy, the case $J_z > 1$ is called the planar regime. It may also be solved using an extended Bethe ansatz.

6.

Many-body system-reservoir interaction in the non-Markovian regime

6.1 Applying feedback control on a spin chain

The Heisenberg spin-1/2 chain represents a simple model for the interaction of quantum particles [37], and its description plays a prominent role in the search for gaining insight into dynamical behavior of quantum many-body systems, for instance strongly correlated electron systems or for experimentally realizable spin-chain materials [40, 41, 42, 43, 44]. For nearest neighbor interaction, the model is exactly solvable with the Bethe ansatz [38], cf. Sec. 5.2. The dynamical behavior of this system, coupled to magnetic reservoirs at its ends, has drawn a lot of interest in recent research publications [122, 121, 125, 126, 127, 128, 129]. Here, the spin chain driven into a non-equilibrium steady-state (NESS) by coupling it to reservoirs on both ends, which are described with the Lindblad formalism and thus rely on a Markovian approximation. With this, the properties of the chain depending on the the driving strength induced by the external reservoir, on an externally-induced disorder parameter [20, 34, 21] or on the strength of the anisotropy [207, 208, 209] are discussed.
This section goes beyond this approach. It does so by studying the effect of a non-Markovian, structured reservoir on an open Heisenberg chain. To this end, coherent time-delayed feedback control is applied on it. While this model has recently been intensely discussed for few-level emitter [60, 187, 185, 80, 196, 71, 194, 133], cf. Sec. 8, it is extended here to a quantum many-body system. This means that a new kind of boundary-driving is implemented, that is a temporal-driving scheme, in contrast to the spatial scheme discussed above. Now, loss and driving take place vie the interaction of one site with two different points in time. These points are separated by the delay time

τ. Thus, applying self-feedback on a one-dimensional many-body system allows for the investigation of a new paradigm of non-Markovian imposed boundary-driving - complementing the existing measurement-based approaches for controlling a one-dimensional many-body system [210, 211, 212]. Due to its coherent nature, it introduces quantum interferences into the dynamics of the system. In the context of cavity-QED, Rabi oscillations have been predicted in the single excitation regime when applying this control on a two-level emitter placed in a cavity [187]. These cavity-induced Rabi oscillations, however, have been limited to the single-excitation and single-emitter case.
As demonstrated in the following, these this phenomenon of feedback-induced stabilization of Rabi oscillations also occurs in the case of a strongly-correlated many-body system. It will be shown that for certain parameter sets, it is possible to stabilize highly symmetric states within the chain. Also, it is demonstrated that for the isotropic Heisenberg spin chain with nearest neighbor interaction the number of possible trapping conditions is equal to the number of sites in the chain, which proposes a way to control the state of the chain non-invasively.

6.1.1 Model and Setup

Fig. 6.1 depicts a sketch of the model, a Heisenberg spin chain modeled as coupled two level systems with the coupling strength J. Its end is placed in a semi-infinite waveguide and couples with the rate Γ to this reservoir which is assumed to be in the vacuum state initially, cf. Sec. 8. The closed end of the waveguide is of length L and acts as a mirror which feeds back part of the excitation after a delay time $\tau = 2L/c$ [182, 213, 214, 189]. At the open end of the waveguide, a detector time-integrates the emitted signal after this second interaction. The Hamiltonian reads (with $\hbar \equiv 1$):

$$H = \sum_{i=1}^{N} \omega_0 \sigma_i^+ \sigma_i^- + \int d\omega\, \omega b^\dagger(\omega) b(\omega) + \sum_{i=1}^{N-1} J\left(\sigma_i^x \sigma_{i+1}^x + \sigma_i^y \sigma_{i+1}^y + \sigma_i^z \sigma_{i+1}^z\right) + \int d\omega \left(G_{fb}(\omega) b_N^\dagger(\omega) \sigma_N^- + \text{h.c.}\right) \quad (6.1)$$

The first term represents the free evolution of N single spin systems, where ω_0 governs the free evolution of each single site and $\sigma_i^+ = \sigma_i^x + i\sigma_i^y$ and $\sigma_i^- = \sigma_i^x - i\sigma_i^y$ create/annihilate a fermionic excitation in the ith two-level system - this corresponds to a flip of a spin on this site.
The second term models the free evolution of the bosonic mode continuum to which the last site is coupled. Here, $b_N^{(\dagger)}(\omega)$ creates/annihilates a bosonic excitation of energy ω in interaction with the Nth site of the spin chain. The third term models the isotropic Heisenberg spin chain with nearest neighbor interaction, a chain of N single sites and with a three-dimensional nearest neighbor interaction in x, y and z direction, where σ^k, $k \in x, y, z$ represent the Pauli matrices interacting with strength J. The last term represents the interaction of the Nth site of the chain with the bosonic reservoir with

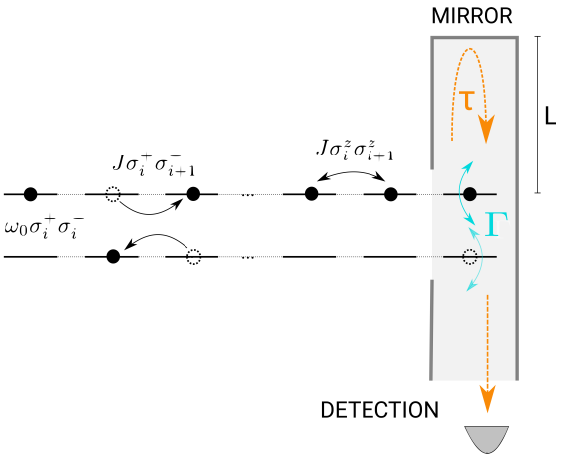

Figure 6.1: Sketch of a Heisenberg spin chain modeled as coupled two level systems with the coupling strength J. Its end is placed in a semi-infinite waveguide and couples with the rate Γ to this reservoir. The closed end of the waveguide is of length L and acts as a mirror which feeds back part of the excitation after a delay time $\tau = 2L/c$. A detector records the emitted signal at the open end of the waveguide for a finite integration time T.

$G_{fb}(\omega)$ defined as:

$$G_{fb}(\omega) = g_0 \sin\left(\frac{\omega L}{c_0}\right) = i\sqrt{\frac{\Gamma}{2\pi}}\left(e^{-i\omega\tau/2} - e^{i\omega\tau/2}\right) \tag{6.2}$$

where L is the length of the closed side of the waveguide, c_0 the phase velocity in the waveguide, $\tau = 2L/c_0$ the delay time and $g_0 = \sqrt{\Gamma/2\pi}$ the coupling constant with the coupling rate Γ. Eq. (6.2) represents the sinusoidal, frequency-dependent system-reservoir coupling in order to model a semi-infinite waveguide, cf. Sec. 4. This frequency-dependent coupling introduces a non-Markovianity into the dynamics. For this reason, the simulation is employed by describing the state of the system and of the reservoir numerically as a matrix product state (MPS), cf. Sec. 3.1. The picture of the quantum stochastic Schrödinger equation (QSSE), cf. Sec. 2.2, serves as a computational basis, in the same manner as for a two-level emitter (Sec. 4). The numerical implementation, however, has to deal with the difficulty inherent to the computation of quantum many-body dynamics: The large Hilbert space required for its description. As explained in Sec. 11.3.1, the swapping technique for the implementation of a non-Markovian time evolution scales with the dimensions of the involved link indices and thus with the entanglement within the MPS. While in case of a few-level emitter, the sub-Hilbert space is usually low in its dimensions, this is not the case for many-body systems, where it generally scales exponentially with the number of sites involved. A convenient MPS architecture will be presented in the following section, but first, the derivation of the time evolution operator is explained.

6.2 Derivation of the time evolution operator

6.2.1 Basis transformation

The start of the derivation is the Hamiltonian in Eq. (6.1), which reads (with $\hbar \equiv 1$):

$$H = \sum_{i=1}^{N} \omega_0 \sigma_i^+ \sigma_i^- + \int d\omega \omega b^\dagger(\omega) b(\omega) + \sum_{i=1}^{N-1} J\Big(\sigma_i^x \sigma_{i+1}^x + \sigma_i^y \sigma_{i+1}^y + \sigma_i^z \sigma_{i+1}^z\Big) + \int d\omega \left(G_{fb}(\omega) b_N^\dagger(\omega) \sigma_N^- + \text{h.c.}\right) \tag{6.3}$$

In a similar manner as in the case of a two-level emitter, this Hamiltonian is transformed into the rotating frame defined by its freely evolving part. The unitary transformation is defined as

$$H' = U_1 H U_1^\dagger - i U_1 \partial_t U_1^\dagger \tag{6.4}$$

where the unitary operator U_1 is defined as:

$$U_1 = \exp\left[it\Big(\sum_{i=0}^{N} \omega_0 \sigma_i^+ \sigma_i^- + \int d\omega \omega b^\dagger(\omega) b(\omega)\Big)\right] \tag{6.5}$$

This yields the transformed Hamiltonian $H'(t)$:

$$H'(t) = \sum_{i=1}^{N-1} J\Big(\sigma_i^x \sigma_{i+1}^x + \sigma_i^y \sigma_{i+1}^y + \sigma_i^z \sigma_{i+1}^z\Big) + \int d\omega \left(G_{fb}(\omega) \sigma_N^+ b_N(\omega) e^{-i(\omega-\omega_0)t} + \text{h.c.}\right) \tag{6.6}$$

Next, the dependency of the delay time τ is shifted into the operators using the unitary transformation

$$U_2 = \exp\left[-i\frac{\tau}{2} \int d\omega \omega b^\dagger(\omega) b(\omega)\right]. \tag{6.7}$$

This yields:

$$H'(t) = \sum_{i=1}^{N-1} J\Big(\sigma_i^x \sigma_{i+1}^x + \sigma_i^y \sigma_{i+1}^y + \sigma_i^z \sigma_{i+1}^z\Big) + i g_0 \int d\omega \left(\sigma_N^+ \big(b_N(\omega) e^{-i(\omega-\omega_0)t} - b_N(\omega) e^{-i(\omega-\omega_0)t} e^{i\omega\tau}\big) + \text{h.c.}\right) \tag{6.8}$$

The next step is to make use of the time dependent reservoir operators $b^{(\dagger)}(t)$, cf. Eq. (2.21), Sec. 2.2,

$$b(t) = \frac{1}{\sqrt{2\pi}} \int d\omega b(\omega) e^{-i(\omega-\omega_0)t} \tag{6.9}$$

which are inserted into Eq. (6.8). This yields the transformed Hamiltonian H'':

$$H''(t) = \sum_{i=1}^{N-1} J\Big(\sigma_i^x\sigma_{i+1}^x + \sigma_i^y\sigma_{i+1}^y + \sigma_i^z\sigma_{i+1}^z\Big) + i\sqrt{\Gamma}\Big(b_N(t) - b_N(t-\tau)e^{i\phi}\Big)\sigma_N^+ - i\sqrt{\Gamma}\Big(b_N^\dagger(t) - b_N^\dagger(t-\tau)e^{-i\phi}\Big)\sigma_N^- \quad (6.10)$$

with the delay time $\tau = \frac{2L}{c_0}$ and the feedback phase $\phi = \omega_0\tau$, which denoted the quantum mechanical phase between the present and feedback signal.
Next, the time discrete quantum noise operators, cf. Sec. 2.2.2, cf. Eq. (2.35),

$$\Delta B^{(\dagger)}(t_k) = \int_{t_k}^{t_{k+1}} dt' b^{(\dagger)}(t') \quad (6.11)$$

are inserted into Eq. (6.10). Note that $B^{(\dagger)}(t_k)$ and $B^{(\dagger)}(t_{k-l})$ only commute for $\Delta t = t_{k+1} - t_k < \tau$.
Discretizing the time evolution operator in this basis, cf. Sec. 2.2.2, yields

$$\begin{aligned} U(t_{k+1}, t_k) &= \\ &= \exp\Bigg[\sum_{i=1}^{N-1} J\Big(\sigma_i^x\sigma_{i+1}^x + \sigma_i^y\sigma_{i+1}^y + \sigma_i^z\sigma_{i+1}^z\Big) \\ &+ \sqrt{\Gamma}\Big(\Delta B_N(t_k) - \Delta B_N(t_{k-l})e^{i\phi}\Big)\sigma_N^+ - \sqrt{\Gamma}\left(\Delta B_N^\dagger(t_k) - \Delta B_N^\dagger(t_{k-l})e^{-i\phi}\right)\sigma_N^-\Bigg] \end{aligned} \quad (6.12)$$

for $k \in [0, N_T - 1]$ as integer of the time steps, where the time evolution operator $\hat{T}$ may be dropped for equidistant time steps $\Delta t = t_{k+1} - t_k$, cf. Sec. 2.2.5. Here, t_k denotes the kth time step, while $t_{k-l} = (k-l)\Delta t$ denotes the time delayed by τ, thus $\tau = l\Delta t$. With this, the QSSE operators defined in Eq. (2.37) may now be used as the basis for the numerical non-Markovian time evolution, while the time evolution is computed as a stroboscopic map, cf. Eq. (2.52).

$$|\psi(t_{k+1})\rangle = \exp\left(-i\int_{k\Delta t}^{(k+1)\Delta t} H'(t')dt'\right)|\psi(t_k)\rangle \otimes |i_{k+1} = 0\rangle\,. \quad (6.13)$$

This will be done using the tensor network method tMPS which has been introduced in Sec. 3.1. The corresponding algorithm based on the Suzuki-Trotter decomposition and on a two-dimensional construction of the wave vector will be explained in the following Sec. 6.3.

6.3 MPS algorithm: Computing quantum feedback on a many-body system

In case of non-Markovian system-reservoir interaction, the information-backflow from the reservoir introduces non-timelocal contributions into the interaction part H_{int}. This

means that the present state of the reservoir is influenced by interactions with the system which have occurred in the past. In terms of the MPS formalism, as a consequence, for calculating the dynamics of the total system, the information backflow from the reservoir of previous time steps needs to be taken into account. To this end, the time bins have to be moved with the swapping technique explained in Sec. 11.3.1 through the MPS during the time evolution, which scales with the dimensions of the involved link indices and thus with the entanglement within the MPS. This constitutes no difficulty in case of a two-level emitter due to the low-dimensional system Hilbert space and due to the favorable scaling of the entanglement in between the time-discretized sub-Hilbert spaces. However, this is generally not the case for the entanglement growth during the time evolution of quantum many-body systems. Here, especially for strongly correlated systems, the Schmidt values strongly grow in number and in size, making larger systems difficult to access numerically. This generates the need to re-structure the algorithm in order to reduce the computational effort. This structure will be presented in the following, but first, the derivation of the time evolution operator is explained.

6.3.1 Setting up the matrix product operator (MPO)

In order to set up the time evolution operator in Eq. (6.12) as a MPO, the Suzuki-Trotter decomposition described in Sec. 3.5 is applied. For this, the time evolution operator in Eq. (6.12) is split into the system and interaction part and written as a sum over local Hamiltonians as explained in Sec. 3.5:

$$U(t_{k+1},t_k) = \exp\left[\Big(\sum_{i=1}^{N-1} h_{i,i+1}\Big)\Delta t\right] = \exp\left[\Big(\sum_{i=1}^{N-1} h^{\mathrm{sys}}_{i,i+1} + h^{\mathrm{int}}_{N,t_k}\Big)\Delta t\right], \tag{6.14}$$

Using this form for the Suzuki-Trotter decomposition, the MPO described with Eq. (6.14) is built iteratively as follows.
First, the operator $h^{\mathrm{sys}}_{i,i+1}$ acting on the sites i,$i+1$ is being set up. Next, the exponential $U(t_{k+1},t_k)^{\mathrm{sys}} = e^{h^{\mathrm{sys}}_{i,i+1}\Delta t}$ is calculated with a Taylor expansion $U(t) = \sum_k^{10} \frac{1}{k!}(h^{\mathrm{sys}}_{i,i+1})^k + \mathcal{O}(\Delta t^{11})$. Following this, the $e^{h^{\mathrm{sys}}_{i,i+1}\Delta t}$ are written into two separated MPO, $U_e(t_{k+1},t_k)$ with even indices, and $U_o(t_{k+1},t_k)$ with odd indices. In case the operator of $h^{\mathrm{sys}}_{N-1,N}$, the interaction part $e^{h^{\mathrm{int}}_{N,t_k}\Delta t}$ is added before the Taylor expansion.
With this procedure, two MPO for even and odd numbers in i are being built separately for the entire chain length. Note that order for both operators to act on the entire chain, the identity operator has to be filled in at the free sites on the end of both operators. Now, each of these two operators acts on each site of the entire chain. The next step is that each local time evolution operator acting on site i and $i+1$ is being decomposed with an SVD, where the singular value matrix S is multiplied into V^T in order to get two matrices, each acting on a single site only:

$$W^{j_i',j_{i+1}'}_{j_i,j_{i+1}} = U^{a_i}_{j_i,j_i'} S^{a_i,a_{i+1}} V^{a_{i+1}}_{j_{i+1},j_{i+1}'} = U^{a_i}_{j_i,j_i'} \bar{V}^{a_i}_{j_{i+1},j_{i+1}'} \equiv W^{a_i}_{j_i,j_i'} W^{a_i}_{j_{i+1},j_{i+1}'} \tag{6.15}$$

This brings U_e and U_o into the form of an MPO. The missing links between each second site can easily be created by the procedure of bringing the MPO into the left, right or mixed canonical form. With this, both operators may now be applied successively on $|\psi\rangle$. However, the numerically least expensive way is to first multiply both operators into one single operator in the MPO representation. This multiplication is performed as a summation over one of the physical indices for each tensor of the MPOs. Afterwards, the MPO may be applied on the MPS as explained in Sec. 3.1.

6.3.2 MPS architecture

To compute the time evolution with tMPS, the state vector is expanded into a MPS. The total wave vector $|\psi\rangle_{\text{tot}}$ consists of the system wave vector $|\psi\rangle_{\text{sys}}$ and the reservoir wave vector $|\psi\rangle_{\text{res}}$:

$$\begin{aligned} |\psi(t)\rangle &= |(\psi_{\text{sys}} \otimes \psi_{\text{res}})(t)\rangle \\ &= \lim_{k\to\infty} \sum_{i_s=0,1} \sum_{n_0,\ldots,n_k=0}^{\infty} c_{i_s,n_0,\ldots,n_k}(t)\, |i_s, n_0, \ldots, n_k\rangle \,. \end{aligned} \tag{6.16}$$

In case of non-Markovian system-reservoir interaction, the information-backflow from the reservoir introduces non-timelocal contributions into the interaction part H_{int}. Translating into the tMPS formalism the fact that the present state of the reservoir is influenced by interactions with the system which have occurred in the past, this implies that for calculating the dynamics of the total system, previous time steps needs to be taken into account during the computation. In order to construct an efficient algorithm for this non-Markovian time evolution, the uncorrelated initial state between system and reservoir is exploited for constructing a two-dimensional MPS-form which enables efficient movement of bins during time-evolution. As the reservoir is in a vacuum state initially and not yet entangled with the spin chain, the wave vector both of system and bath may be expanded separately at the start of the time evolution. In the same manner as demonstrated in Sec. 8.2.2, Eq. (6.16) may be transformed into the time discrete basis defined in Eq. (2.37). It reads as:

$$\begin{aligned} |\psi(t_0)\rangle = &\sum_{\substack{n_1\ldots n_N \\ =0,1}} c_{n_1\ldots n_N}(t_0)\, |n_1 \ldots n_N\rangle \\ &\otimes \sum_{m_1\ldots m_{N_T}} c_{m_1\ldots m_{N_T}}(t_0)\, |m_1 \ldots m_{N_T}\rangle \end{aligned} \tag{6.17}$$

where both complex coefficients are expanded into products of tensors A:

$$c_{n_1\ldots n_N} = A_{n_1} A_{n_2} \ldots A_{n_N} \tag{6.18}$$

$$c_{m_1\ldots k_{N_T}} = A_{m_1} A_{m_2} \ldots A_{m_{N_T}} \tag{6.19}$$

Fig. 6.2 depicts the block diagram of the MPS and the MPO. To preserve the entanglement between the two subspaces during time evolution, they are stuck together at the

Nth chain bin and the kth time bin, where the interaction between the many-body system and the bath occurs. This connection is kept throughout the entire time evolution and thus the entanglement between the two subspaces is preserved. Fig. 6.3 depicts the

(a) MPS (b) MPO

Figure 6.2: Block diagram of MPS and MPO of a Heisenberg spin chain under self-feedback. Figure (a) shows the MPS architecture. It is constructed two-dimensional and consists of two MPS, the first containing the system bins labeled with the site indices n_i and the link indices l_i, and the second containing the reservoir bins labeled with the site indices m_k and the link indices p_k. The two MPS are stuck together at the Nth system bin where the interaction occurs. Figure (b) depicts the corresponding MPO. It affects all system bins, but only the present time bin m_k and relevant time bin describing the past state of the reservoir m_{k-l}.

block diagram algorithm of the algorithm. To compute the kth time step, the Nth chain bin, the kth time bin initialized in a vacuum state and the t_{k-l}th bin containing the feedback signal are contracted. Afterwards, the time-evolution operator $U(t_{k+1}, t_k)$ is applied as explained in Sec. 3.1. With this, the number of swapping operations reduces significantly. The time bin of the past time step only must be moved through the reservoir MPS, where the entanglement is usually well below the one in the chain. In addition, only the Nth chain bin must be moved through the reservoir MPS during time evolution, not the entire chain. After the application of the MPO, the tensors are decomposed and the resulting bins are shifted back to their original position in the chain. With this, the bins of the $(k+1)$th time step may be moved and contracted, and so forth. In order to preserve the entanglement correctly during this process, the position of the orthogonality center has to be moved with the bins, cf. Section. 3.1. It is indicated by the red box in Fig. 6.3.

6.4 The dissipative chain without feedback

First, the dynamics of the dissipative chain without feedback are investigated. In this case, the coupling to the reservoir exhibits a vanishing frequency dependence $G_{fb}(\omega) \equiv 2g_0 = \text{const}$. As only one single spin - the boundary spin - of the chain is subject coupled to the reservoir and thus subject to dissipation, this case is completely equivalent to a Markovian description with the Lindblad formalism. This means that the QSSE evolution

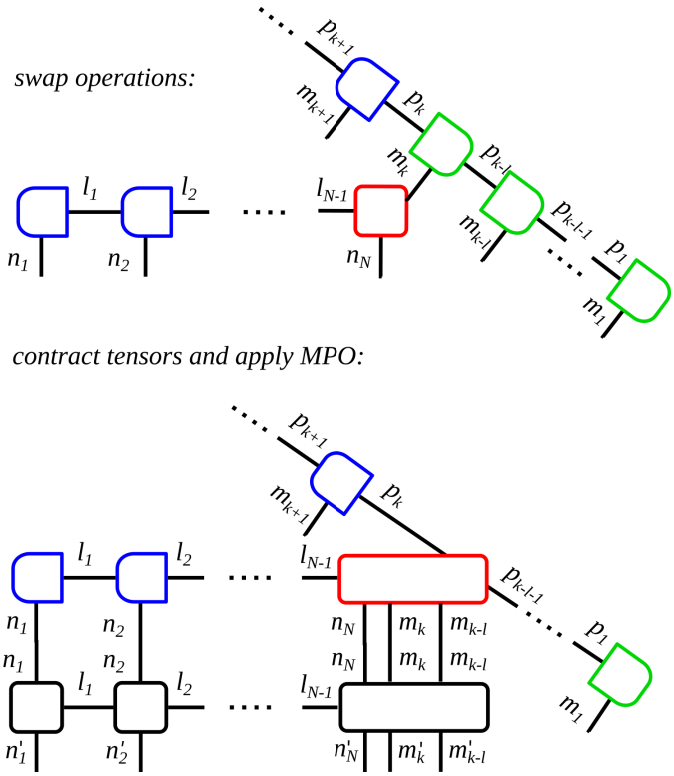

Figure 6.3: Block diagram for the computation of one time step. Blue boxes indicate left-orthogonality of the tensors, while green boxes indicate right-orthogonality and the red box marks the position of the orthogonality center of the MPS. The spin chain MPS and the reservoir MPS are connected at the kth time bin m_k. Also, the past time bin m_{k-l} has been brought next to them with swapping operations. For the application of the MPO, the Nth chain bin, the present and feedback time bin m_k and m_{k-l} are contracted and the chain MPS is multiplied into the MPO. Afterwards, the tensors are decomposed and moved back to their original position in the chain.

models the Lindblad master equation of the form:

$$\frac{\mathrm{d}}{\mathrm{dt}}\rho(t) = -i\,[H_{\mathrm{chain}}, \rho(t)] + \Gamma\mathcal{D}[\sigma_N^-]\rho(t) \tag{6.20}$$

with

$$H_{\mathrm{chain}} = \sum_{i=1}^{N} \omega_0 \sigma_i^+ \sigma_i^- + \sum_{i=1}^{N-1} J\left(\sigma_i^x \sigma_{i+1}^x + \sigma_i^y \sigma_{i+1}^y + \sigma_i^z \sigma_{i+1}^z\right) \tag{6.21}$$

and the Lindblad super-operator $\mathcal{D}[\hat{J}]\rho = \hat{J}\rho\hat{J}^\dagger - \hat{J}^\dagger\hat{J}\rho - \rho\hat{J}^\dagger\hat{J}$, cf. Sec. 2.3.
This equivalence of the time-bin setting without feedback and the dynamics of a Lindblad decay are used to benchmark the algorithm - see Fig. 6.4. Here, the black dotted lines represent the full solution for $|\psi(t)\rangle$ with the Lindblad master Eq. (6.20). The feedback algorithm for the uncoupled last site is also benchmarked using the analytical solution for a single two-level system, cf. Sec. 4.1. In this setting, excitation trapping is not

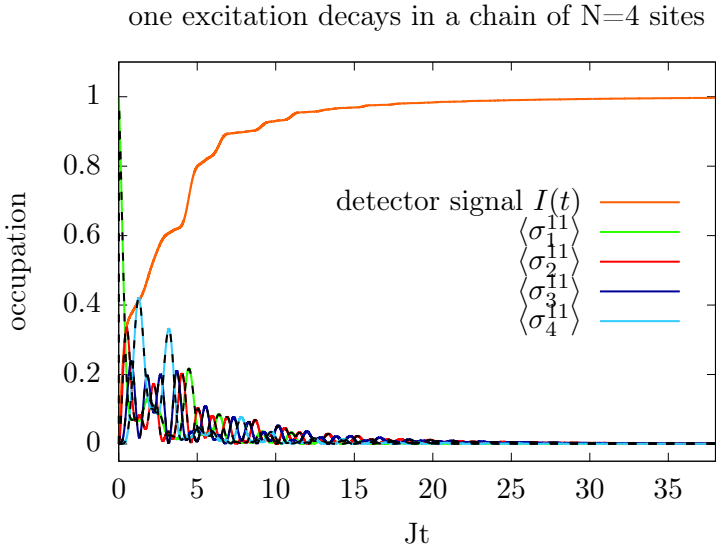

Figure 6.4: Time-dependent occupation densities in a Heisenberg chain of $N = 4$ sites initialized in the $|\downarrow\downarrow\downarrow\uparrow\rangle$ state without feedback. After a transient regime during which the densities oscillate irregularly, the initial excitation is completely lost into the reservoir. Note that each curve is plotted twice demonstrating a benchmark of the tMPS algorithm with a full solution of the equations of motion of the system. The orange line depicts the time-dependent detector signal. It reaches its normalized maximum value after the convergence time T_c, thus $I(t = T_c) = 1$. Parameters for this plot are $\Gamma = 0.24$ and $J = 0.1$.

possible for any initial state or parameter set, which means the excitation stored within the chain is inevitably lost to the reservoir modes. The detector which is placed at

the open end of the waveguide records the time-dependent excitations which leave the feedback loop between the emitter at the end of the quantum chain and the mirror until a finite time T is reached. Thus, the detector signal is formed by the normalized, time-integrated excitation $I(t) = \sum_{t_k=0}^{N_T} \langle \Delta B^\dagger(t_k) \Delta B(t_k) \rangle / \sum_{i=0}^{N} \langle \sigma_i^{11} \rangle_0$. The excitation density within the waveguide at the kth time step $\langle \Delta B^\dagger(t_k) \Delta B(t_k) \rangle$ is summed over until the total integration time $\Delta t N_T$. Additionally, this signal is normalized to the total initial excitation within the system, which is described by $\sum_{i=0}^{N} \langle \sigma_i^{11} \rangle_0$ as the reservoir is in a vacuum state initially. This time-integrated signal serves as a figure of merit. In the case without feedback, it will always reach unity if integrated long enough. In Fig. 6.4, the time evolution of all sites is depicted exemplary for a spin chain of four sites (blue, red and green lines). The system has been initialized in the $|\downarrow\downarrow\downarrow\uparrow\rangle \otimes |\text{vac}\rangle$ state. Additionally, the time dependent detector signal is plotted (orange line), which integrates the dissipated signal during the integration time. Clearly, all sites decay completely into ground state, and the signal at the detector $I(t)$ reaches its normalized maximum value after the convergence time T_c, thus $I(t = T_c) = 1$.
In the given setup, no population trapping or non-trivial steady-states can occur. This is due to the fact that only one site is coupled to the reservoir - if more spins would be coupled dissipatively, this picture would change [71].

6.5 The Heisenberg chain under feedback

6.5.1 Population trapping in a many-body system

Contrary to the Markovian case described in the previous section, when subjecting the chain to coherent self-feedback, population trapping occurs. This means that the initial excitation within the chain first dissipates partially into the environment. This loss of excitation is then stopped by interaction with the feedback signal. This interaction induces quantum interferences which modify the coupling. Consequently, the system-reservoir interaction reaches a steady-state after a convergence time T_c and the remaining excitation within the chain is trapped in it dynamically, cf. Sec. 4.1. From this time on, the detector will not record a signal any longer, and consequently, and longer integration times will not change the detected excitation any more. The conditions for population trapping depend on the two feedback parameters τ and ϕ, cf. Sec. 4. As in the case of the two-level system, cf. Sec. 4, these two parameters are not independent due to their relationship defined by $\phi = \omega_0 \tau$. Fig. 6.5 depicts the dynamics of the occupation densities $\sigma_i^{11} = \sigma_i^+ \sigma_i^-$ of each single site i in the Heisenberg chain of $N = 4$ sites (blue, red and green lines) and the detected excitation leaving the waveguide (orange line). The plot depicts the transient regime as well as the long time limit. During the transient regime, the densities within the chain oscillate irregularly and the detector signal steadily increases. After this, the detector signal saturates as in the case without feedback, however now it remains well below unity. This means that part of the initial excitation remains within the chain, equipartitioned on all sites of the chain. This forms a non-equilibrium steady-state of the chain, where the sum over all excitation in the

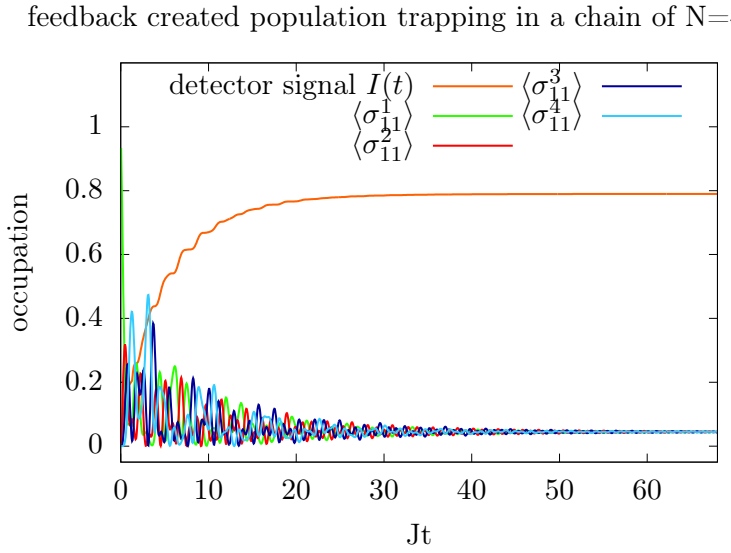

Figure 6.5: Time-dependent occupation densities (blue, red and green lines) in a Heisenberg chain of $N = 4$ sites under self-feedback for the set of feedback parameters $\phi_c = 2\pi$, $\tau_c = 1.25Jt$. The chain has been initialized in the $|\downarrow\downarrow\downarrow\uparrow\rangle$ state. After a transient regime during which the densities oscillate irregularly, the time-dependent detector signal (orange line) saturates, however it remains well below unity. Part of the initial excitation remains within the chain, equipartitioned on all sites, to form a non-equilibrium steady state. Parameters for this plot are $\Gamma = 0.24$ and $J = 0.1$.

chain remains finite and constant, hence the excitation within the chain is conserved:

$$\sum_{i=1}^{N} \langle \sigma_i^{11}(t) \rangle_{\mathrm{tr}} = \mathrm{const}, > 0. \tag{6.22}$$

The same condition holds obviously for a closed chain - however, in the case here, the system is open and dissipative. The initial state of the chain is the $|\downarrow\downarrow\downarrow\uparrow\rangle$ state - only the spin coupled to the reservoir is in excited state, while the remaining spins are in the ground state. As the reservoir is in a vacuum state initially, this means that the system is in the single-excitation regime. However, the results are not limited to the this case but also hold for more excitations, as will be demonstrated further below.

6.5.2 Trapping conditions in the ϕ-τ parameter space

For the case of the many-body system under feedback, the conditions for the trapping to take place differ significantly from the case of a single two-level system. As demonstrated in Sec. 4, a single two-level system coupled within a semi-infinite waveguide only exhibits population trapping at $\phi_{\mathrm{tr}} = \omega_0 \tau = 2\pi n$, $n \in \mathbf{N}^+$, i.e. in the interval $[0, 2\pi)$ only phase allows population trapping. Also, the feedback phase for which trapping occurs ϕ_{tr} does not depend on the delay time τ, thus it holds that $\phi_{\mathrm{tr}}(\tau) = \mathrm{const}$.
In case of a many-body system, this is significantly different. Here, population trapping occurs for a much larger set of trapping parameters ϕ_{tr}, τ_{tr}. The conditions for a two-level system also hold - however, there are other trapping parameter sets where it now holds that the feedback phase ϕ_{tr} depends on the delay time, thus ϕ_{tr}=$\phi_{\mathrm{tr}}(\tau)$. To illustrate this, Fig. 6.6 depicts the survival probability of the excitation in a chain of $N = 2$ sites in the ϕ-τ-plane. It depicts the time integrated detector signal, meaning that darker regions indicate a higher amount of trapped excitation within the system while white regions show that the excitation has been completely lost to the environment. Thus, all special parameter sets ϕ_{tr}, τ_{tr} for which trapping conditions exist are visible as lines in this plane.
Note that the lines broaden out for two reasons: First, for the regions close to the special parameters, $\phi \to \phi_{\mathrm{tr}}$, $\tau \to \tau_{\mathrm{tr}}$ and $\tau\Gamma \gg 1$, no trapping condition exists, however the feedback signal strongly slows down the dissipation into the environment. Also, note that for a fixed integration time T, the areas around the ϕ_{tr}-τ_{tr} lines additionally broaden out with increasing delay time due to the convergence time strongly increasing with increasing τ.
Additionally, in Fig. 6.6, the dependency of the survival probability on τ for a fixed coupling strength Γ becomes visible. The trapped excited density clearly decreases with an increasing delay time. This observation agrees with the behavior of the single two-level system subjected to self-feedback and is due to the fact that the system looses excitation into the reservoir until the first interaction with the feedback signal occurs. This observation also explains that the higher the decay rate Γ, the smaller the survival probability for a fixed τ.

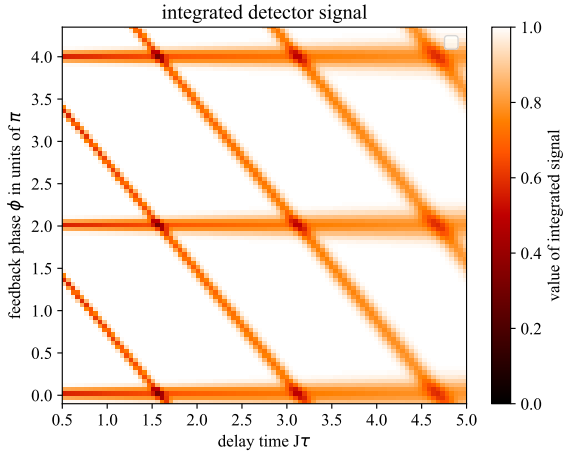

Figure 6.6: Trapping conditions in the ϕ-τ plane for an isotropic Heisenberg chain with nearest neighbor interaction and $N = 2$ sites. The plot depicts the detector signal after a finite integration time T. Darker regions indicate a higher survival probability in the spin chain while white regions show that the excitation has been completely lost into the environment and detected. Broadening of the lines stems from finite calculation times, as mentioned in the main text. The periodic reappearance of the lines is due to the inherent 2π-periodicity of the feedback phase ϕ: Each trapping condition is fulfilled once within every interval of $\phi \in [2\pi n, 2\pi(n+1))$, $n \in \mathbf{N}^+$. Parameters for this plot are $\Gamma = 0.24$, $J = 0.1$.

Coming back to the additional trapping conditions in the many-body system, clearly, in Fig. 6.6 in the interval $[0, 2\pi)$ one more condition for ϕ_{tr} which lead to population trapping exists, and in strong contrast to the single two-level emitter, this conditions depends on τ, thus $\phi_{\mathrm{tr}} = \phi_{\mathrm{tr}}(\tau)$. This dependency of the feedback phase on the delay time is an entirely new phenomenon compared to the well-investigated case of the single two-level system. The many-body system also displays the $\phi = 2n\pi$ trapping condition, equally as the two-level system, which is visible as a horizontal line in Fig. 6.6. Thus, here it holds that $\phi_{\mathrm{tr}}(\tau) = \text{const.}$, ϕ_{tr} does not depend on τ. Due to the inherent periodicity of the phase, each of these additional lines appears once within every interval of $\phi \in [2\pi n, 2\pi(n+1))$, $n \in \mathbf{N}^+$, which means that the lines reappear periodically in the parameter space.
The reason for these additional trapping conditions is the interaction dynamics within the chain which imposes new conditions for the feedback phase ϕ_{tr}, as within the quantum many-body system, more coherent excitation exchange is possible.

Most interestingly, the number of possible population trapping conditions $N_{\phi_{\mathrm{tr}}}$ grows linearly with the number of sites in the chain - despite the complex interactions within the many-body system. If points of degeneracy - hence the points where the lines in Figures 6.6 and 6.7 intersect - are avoided, the number of trapping condition even equals the number of sites in the chain, $N_{\phi_{\mathrm{tr}}} = N$, cf. Fig. 6.8. This implies that the detec-

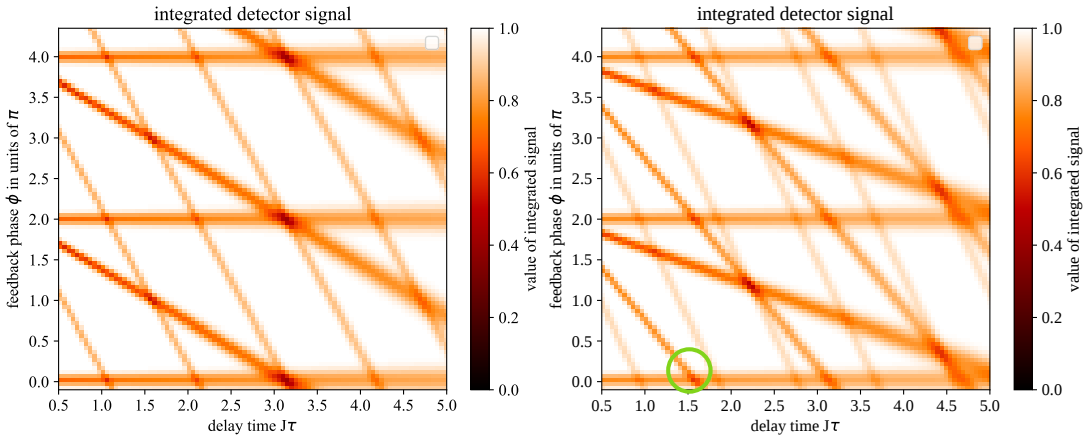

(a) $N = 3$

(b) $N = 4$

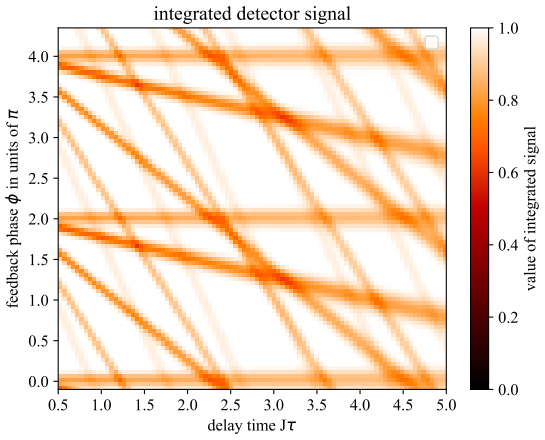

(c) $N = 5$

Figure 6.7: Trapping conditions in the ϕ-τ plane for a Heisenberg chain with different site numbers. Darker regions indicate a higher survival probability in the spin chain while white regions show that the excitation has been completely lost into the environment and detected. Clearly, one additional periodic set of lines appears for each additional site in the chain. Parameters are $J = 0.1$ and $\Gamma = 0.24$.

tor signal provides a means to partially characterize the chain. This linear dependency

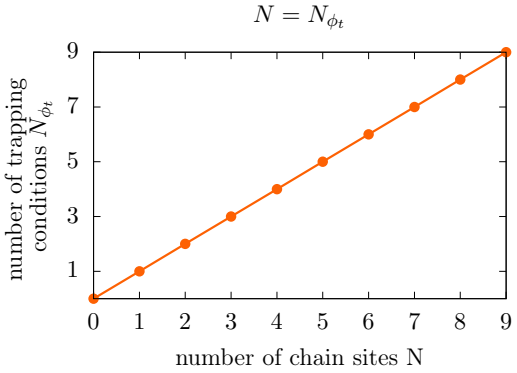

Figure 6.8: Plot of the maximum number of possible trapping conditions for the feedback phase $N_{\phi_{\mathrm{tr}}}$ within one interval $\phi \in [0, 2\pi)$ as a function of the number of sites N in the chain. Strikingly, it holds that $N_{\phi_{\mathrm{tr}}} = N$. Hence, the detector signal provides for a way to partially characterize the chain non-invasively.

may be explained as a resonance effect with traveling excitations within the chain and the waveguide destructively or constructively interfering. Here, the resonance conditions depend on the eigenfrequencies within the chain and thus, the conditions for coherently reinforcing them increase by N for N additional sites within the chain. However, note that the resonance conditions also depend on the eigenvalue degeneracies, and the equality of the trapping conditions and the number of sites, which is true for the isotropic Heisenberg chain, in the chain is not given for all chain types. Investigating chains with less symmetries, shifts and anisotropies reveals that a connections between the degeneracies of the eigenvalues and the number of trapping conditions exists: The lower the degree of degeneracy is, the lower the number of trapping conditions are - further investigations on this relationship are a possible direction of future research.

6.5.3 Relationship to dynamical quantum phase transitions

Also note that these results show features which at first sight might resemble a dynamical quantum phase transition, which is why the relationship to this research field is briefly clarified here. Dynamical quantum phase transitions characterize non-equilibrium quantum systems, and correspond to a qualitative change in the physical behavior of the system characterized by an order parameter (for instance an observable or a correlation function) with this physical quantity becoming nonanalytic as a function of some microscopic control parameter. This nonanalyticity appears as a convergence of a system parameter approaching some limit, most commonly in the limit of large system sizes or long integration times. The current literature on this topic covers closed systems with the focus on transient effects [22, 215, 216, 217, 218, 219, 220], on the long-time limit

[221, 222, 223, 224, 144, 225, 226] or open quantum systems [227, 228, 229, 230, 10].
The results of this study, however, only seemingly exhibit some features related to dynamical quantum phase transitions: Here, the ϕ-τ plane would constitute a parameter space, with ϕ, τ the control parameters. The dynamics of the physical system $|\psi(t)\rangle$ would then be characterized with an order parameter depending on these parameter values, which constitutes the conserved proportion of the initial excitation within the chain in the steady-state:

$$c_{e,\mathrm{tr}}(\phi,\tau) = \sum_{i=1}^{N}\langle\sigma_i^{11}(t)\rangle_{\mathrm{tr}} \Big/ \sum_{i=1}^{N}\langle\sigma_i^{11}\rangle_0, \tag{6.23}$$

which behaves nonanalytical for all parameter sets of ϕ,τ where trapping occurs.
However, in case of this study, this nonanalyticity is not emerging and does not scale with a parameter choice. When trying to relate this kink to a dynamical quantum phase transition, it becomes clear that the kink in $c_{e,\mathrm{tr}}(\phi,\tau)$ occurs independently from the chosen integration time (only its shape converges to a δ-function with $t \to \infty$) and is independent of the limit of large systems (while it depends qualitatively of course on the system size as the values for ϕ,τ where the system traps depend on N).
This kind of parameter dependency often occurs for systems controlled by self-feedback: Effects such as two-photon processes [132, 80], enhancement of entanglement [183] or quantum coherence stabilization [186, 70, 187, 188] achieved with quantum coherent feedback control rely on a specific value of the feedback phase as well as of the delay time. An example from other physical fields of research could for instance be a coherent perfect absorber, where a material becomes perfectly absorbing under specific physical conditions [231, 232].

6.5.4 Characterization of steady states

Investigating the steady-state behavior for different feedback phases and time delays yields that three possibilities exist. First, trivially, in the long-time limit all excitation within the chain is lost to the reservoir. Looking at Figures 6.6 and 6.7 makes clear that this case is the rule, which means that most delay times and phases do not allow a non-trivial steady-state in combination with the quantum spin chain dynamics but will lead to a complete loss of excitation to the environment.
Secondly, all single site occupation densities in the chain are finite and constant. This is the case when a set of parameters ϕ_{tr}, τ_{tr} allows for trapping, which means Eq. (6.22) holds, hence in the non-equilibrium steady state, the excitation within the chain remains finite and constant.
Here, importantly, each trapping line corresponds to one specific steady-state of the chain. One example is depicted in Fig. 6.5, where all single site occupation densities equilibrate out to the same level. Another possibility is that the steady-state densities are finite and constant, but not on the same level. These steady states always are symmetric with respect to the middle of the chain as a axis. If the specific order may reproduce itself for

different N, the parameter set ϕ_c, τ_c for this stability line remains exactly the same. This is explained with the fact that the phase conditions for the site under feedback imposed by the interactions in the chain do not change despite the increasing number of sites. Fig.6.9 depicts this exact overlap for the case of $N = 2$ and $N = 4$. It demonstrates that

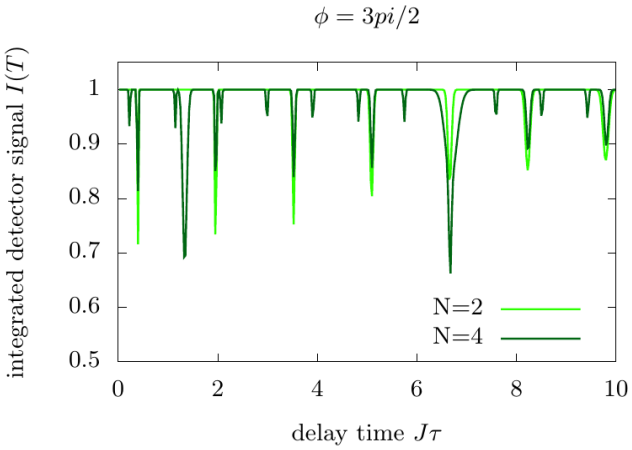

Figure 6.9: Detector signal of a Heisenberg chain of different lengths N in a semi-infinite waveguide as a function of τ, $I(t = T) = I(\tau)$, for a fixed feedback phase $\phi = \frac{2\pi}{3}$. The dips in the curve indicate the trapped steady states where a finite amount of excitation remains within the chain. Due to the inherent 2π-periodicity of the feedback phase, they re-appear with a certain frequency. For $N = 2$, only one frequency occurs, while for $N = 4$, two additional periodic frequencies of these dips appear. Clearly, for one frequency, these dips overlap despite the different site numbers in the chain, indicating that in this case, the exact trapping condition is reproduced.

for a fixed feedback phase $\phi = \text{const}$, trapping is visible as a dip in the strength of the detector signal and occurs with a constant frequency which is due to the 2π-periodicity of the feedback phase, resulting in the fact that one trapping condition reappears once within every interval of $\phi \in [2\pi n, 2\pi(n + 1))$, $n \in \mathbf{N}^+$. or $N = 2$, only one frequency occurs, while for $N = 4$, two additional periodic frequencies of these dips appear. Clearly, for one frequency, these dips overlap despite the different site numbers in the chain, indicating that in this case, the exact trapping condition is reproduced. This allows for a non-invasive characterization of the chain length. If the symmetry with respect to the middle of the chain may not be reproduced, it adapts to the new site number, causing the stability line to shift slightly.
Coming back to the characterization of the trapped steady-states, a third case exists. If a point of degeneracy is chosen for which the system provides two or more population trapping phases, the highly non-trivial steady state of stabilized Rabi oscillations occurs within the chain without any dephasing and dissipation although we simulate an open quantum system. This means the total excitation in the chain remains constant and

finite but the densities oscillate. This highly non-trivial steady state will be discussed in the next section.

6.5.5 Robustness of stabilized Rabi-oscillations

This type of periodic, time-dependent steady-state is created at all points of degeneracy, hence at all intersection points of two or more trapping lines in the parameter space. These steady states differ however in coherence and relative phase shifts between the trapped occupation densities $\langle \sigma_i^{11} \rangle_{\mathrm{tr}}$ at different intersection points. An example of a very regular, time-reversible oscillation pattern is displayed in Fig. 6.10 and appears at a certain intersection which is marked in Fig. 6.7 (b) with a green circle. Note that despite

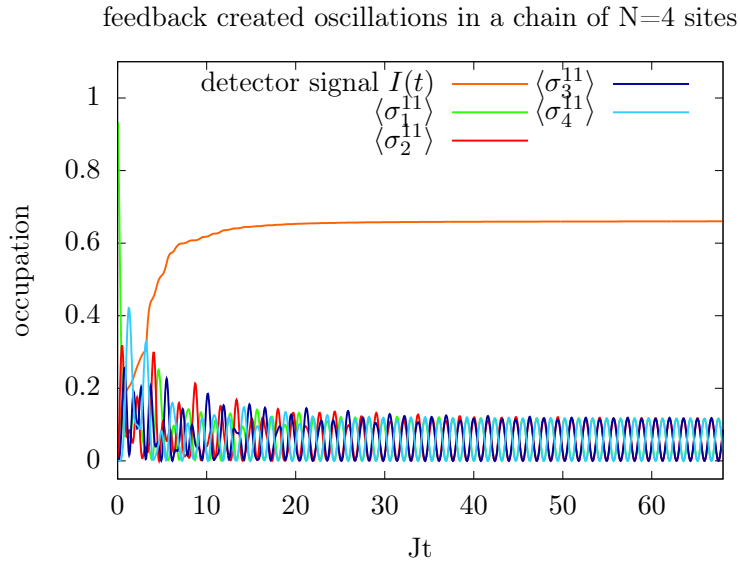

Figure 6.10: Time-dependent occupation densities $\langle \sigma_i^{11}(t) \rangle$ in a Heisenberg chain of 4 sites. Clearly, feedback creates stable Rabi oscillations within the chain where site 2 and 3 as well as 1 and 4 are completely coherent and in phase. Consequently, part of the excitation remains trapped in the chain, clearly visible as the detector signal remains well below $I(T_c) = 1$. As is explained below, these oscillations appear at intersection points of trapping lines in the ϕ-τ plane, where two trapping conditions are fulfilled at the same time. Parameters for this plot are $\Gamma = 0.24$, $J = 0.1$.

this induced, synchronized and regular oscillations, the total excitation within the chain is preserved, thus Eq. (6.22) holds - although the system is open. This holds for different decay strengths Γ and feedback delay times τ, as well as feedback phases ϕ, and is a generic feature of such a system. As visible in Fig. 6.7, the total trapped excited density is maximal at the intersection points, where the oscillations occur.
In Fig. 6.11, the population trapping-induced oscillations within the chain are depicted

for different initial states and number of excitations in the chain. Clearly, the effect is

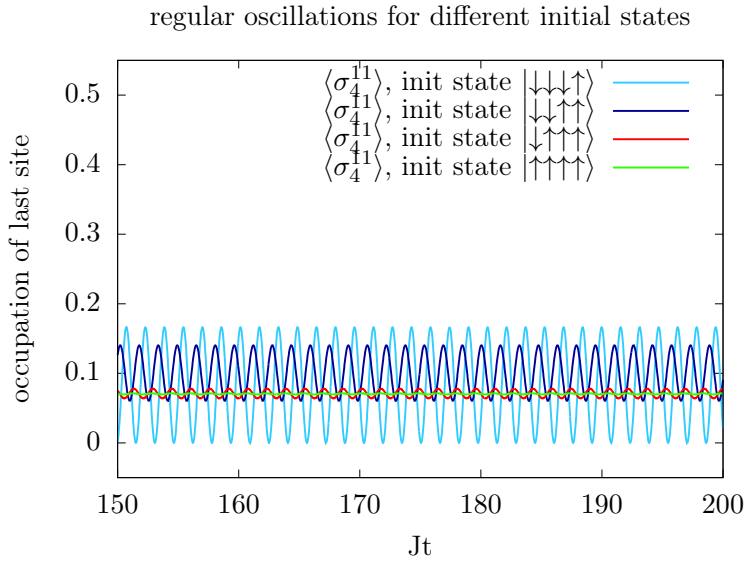

Figure 6.11: Regular oscillations for different initial states and initial numbers of excitations in a chain of $N = 4$ sites. The amplitude decreases with an increasing number of excited states. The oscillations, however, remain regular and periodic. Parameters for this plot are $\Gamma = 0.24$, $J = 0.1$.

not limited to the single-excitation regime, but exists for different excitations and thus is a generic feature of the feedback-driven quantum spin chain.
However, the amplitude of the oscillations is reduced for larger numbers of excitations: it is maximal for a single initial excitation (light blue line) and strongly decreases with an increasing number of initial excitation (e.g. quadruply-excited initial state, green line). This behavior is qualitatively independent of the location of the initial excitation within the chain. The explanation for the dependence of the amplitude on the initial number of excitations lies in the dynamics of the chain up to the first interaction with its own feedback signal. The higher the amplitude of the oscillations occurring in this first time interval $t \in [0, \tau]$ is, the higher the amplitude of the stabilized Rabi oscillations is. This is explained as follows: If the chain is initialized with a single excitation - no matter at which site in the chain - the irregular oscillation of the occupation densities during the initial transient regime has the highest amplitude, as the inversion of the excited site is not slowed down by neighboring excited sites.

These oscillations also persist for much larger systems. Here, with the existing algorithm it is possible to reach system sizes as large as $N = 30$. This is demonstrated in Fig. 6.12, which exemplary shows the oscillation pattern of the last site in the chain for a chain length of $N = 30$.

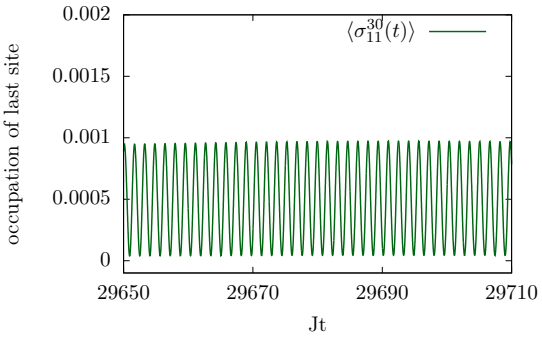

Figure 6.12: Dynamics of the time-dependent occupation density $\langle\sigma_{11}(t)\rangle^{30}$ of the last site in a Heisenberg chain of lengths $N = 30$ under feedback. Clearly, the regular and periodic oscillations persist even for much larger system sizes. Parameters for this plot are $\Gamma = 1.5$, $J = 0.1$.

6.6 Conclusion

In this section, a Heisenberg spin chain with nearest neighbor interaction in non-Markovian interaction with a structured reservoir has been investigated. This reservoir is represented by a semi-infinite waveguide where the closed end serves as a mirror. Thus, part of the excitation emitted from the chain is reflected and fed back into the many-body system. With this, the application of quantum coherent feedback control is extended on a many-body system. It is demonstrated that the many-body interactions give rise to new trapping conditions where the feedback phase ϕ_{tr} depends on the chosen delay time τ_{tr}. Due to the inherent periodicity of the phase, the trapping conditions reappear periodically in the interval $[0, 2\pi)$. Here, it is demonstrated that despite the complex interactions within a quantum many-body system, the number of trapping parameter sets ϕ_{tr}, τ_{tr} within one interval is equal to the number of sites N in the chain. Also, it is shown that each of these parameter set ϕ_{tr}, τ_{tr} may be characterized with a respective steady-state within the chain using the numerical results. Additionally, it is demonstrated that at points in the ϕ-τ plane where several trapping conditions hold at the same time, stable Rabi oscillations occur. These oscillations also persist for much larger systems. Here, it is demonstrated that the proposed algorithm enables the computation of system sizes as large as $N = 30$.

7.

The boundary-driven Heisenberg chain

This part of the thesis at hand aims at the investigation of open quantum many-body systems and their multi-excitation properties in the non-equilibrium steady-state (NESS). In order to do so, it remains with the paradigmatic model of the Heisenberg quantum spin-chain. The dynamical behavior of this system, driven by magnetic reservoirs coupled to its ends, has drawn a lot of interest and brought forth many studies in recent years [122, 121, 125, 126, 127, 128, 129]. Here, the chain is driven into a non-equilibrium steady-state (NESS), and its properties are investigated, depending on the the driving strength via the external reservoir, on an externally-induced disorder parameter [20, 34, 21] or on the strength of the anisotropy [207, 208, 209] are discussed. Next to entanglement growth and energy transport, the most prominent figure of merit in these studies is the quantum spin current through the chain which is induced by the potential difference between the two reservoirs at either end of the chain. A range of non-equilibrium phenomena have been characterized, among them anomalous transport and negative differential conductivity.
Here, the boundary-driving is realized with a full Markovian approximation with respect to the system-reservoir interaction, thus the chain is driven incoherently. Hence, the Markovian approximation of the system-reservoir interaction limits these investigations to incoherent processes of loss and gain. Additionally, the dynamics have to be described in the density matrix picture, making the numerical costs significantly higher and thus larger systems difficult to access.
In this section, a model and an efficient algorithm are presented for studying the steady-state properties of coherently driven many-body systems. In this thesis, the driving is realized with a fully coherent process and described in the Schrödinger picture. With this, the approach presented here goes beyond the dominant Markovian description of decay and loss in these systems. This novel implementation poses most interesting possibilities for the comparison of the out-of-equilibrium properties of many-body systems driven

with different approaches. It proposes an hitherto unexploited scheme in contrast and in complement to the dominant approach of incoherently driven many-body systems.

7.1 Model of the coherently driven chain

The model consists of the open, isotropic Heisenberg spin-chain with nearest-neighbor interaction which has been introduced in the previous section. Contrary to the dominant

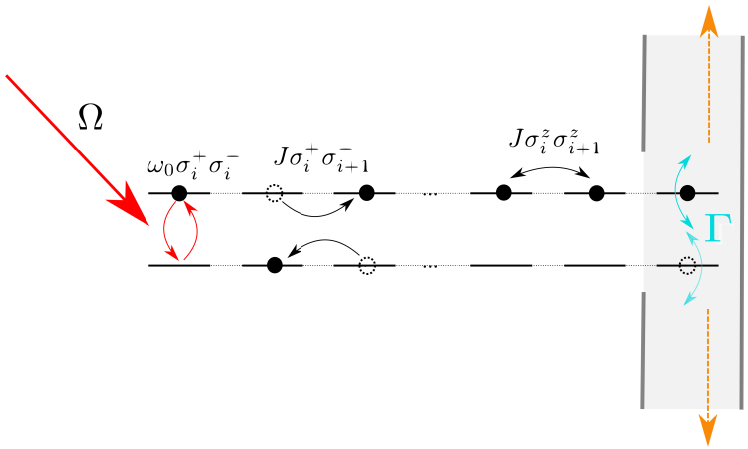

Figure 7.1: Open, isotropic Heisenberg spin-1/2-chain with three-dimensional nearest-neighbor interaction with coupling strength J which is driven out-of-equilibrium. The gain is modeled with a coherent driving via a continuous wave pump field Ω which is applied on the first site of the chain, while the loss is realized with a coherent interaction with a continuous bosonic reservoir which is assumed to be in the vacuum state. This may for instance be represented as an infinite waveguide to which the last site of the chain is coupled with a decay rate Γ.

approach in the research field, here, the gain is modeled with a coherent driving via a continuous wave pump field Ω which is applied on the first site of the chain. The loss is realized with a coherent interaction with a continuous bosonic reservoir which is assumed to be in the vacuum state.

The Hamiltonian thus reads as:

$$H = \sum_{i=1}^{N} \omega_0 \sigma_i^+ \sigma_i^- + \int d\omega\, \omega b^\dagger(\omega) b(\omega) + \sum_{i=1}^{N-1} J\Big(\sigma_i^x \sigma_{i+1}^x + \sigma_i^y \sigma_{i+1}^y + \Delta \sigma_i^z \sigma_{i+1}^z\Big) + \Omega\left(\sigma_1^+ e^{-i\omega_L t} + \sigma_1^- e^{i\omega_L t}\right) + \int d\omega \Big(g_0 b_N^\dagger(\omega) c_N^- + \text{h.c.}\Big) \tag{7.1}$$

The first three terms in Eq. (7.1) are analogous to the model discussed in Sec. 6, cf. Eq. (6.1): The first term models the free evolution of N single spin systems, the second term the free evolution of the bosonic mode continuum to which the last site of the chain is coupled, and the third term describes the Heisenberg spin chain with a three-dimensional nearest-neighbor interaction. If $\Delta \neq 1$, this term models an anisotropic coupling in z-direction. The forth term models the coherent driving via a laser with the continuous wave pump field Ω which is applied on the first site of the chain. A resonant driving is assumed, that is $\omega_l = \omega_0$. Analogous to Eq. (6.1), the last term models the coupling of the last site of the chain to a vacuum reservoir, which may for instance be created by the interaction with an infinite waveguide. Note that this dissipative coupling is completely equivalent to the Markovian description of decay with the Lindblad formalism.

7.2 NESS-properties of the incoherently driven chain

In order to connect this novel setup to the existing research, the NESS-properties of the incoherently driven chain are briefly reviewed in the following, as it is the aim of the approach presented in this thesis to offer a tool for going beyond the dominant Markovian approach.

As the transport properties of the chain are of interest, the reservoir is coupled to the first and the last site of the chain. It is described by two dissipators acting on each site of the chain, $\mathcal{D}[\sigma^+]$ and $\mathcal{D}[\sigma^-]$, where $\mathcal{D}[\sigma^+]$ describes the inscattering of the spin up state $|\uparrow\rangle$ and $\mathcal{D}[\sigma^-]$ describes the inscattering of the state $|\downarrow\rangle$, which may also be described as the outscattering of a spin up state $|\uparrow\rangle$. The four dissipators read as:

$$L_1^{\text{in}} = \sqrt{\Gamma_1^{\text{in}}(1+\mu)}\,\sigma_1^+, \quad L_1^{\text{out}} = \sqrt{\Gamma_1^{\text{out}}(1-\mu)}\,\sigma_1^- \tag{7.2}$$

$$L_N^{\text{in}} = \sqrt{\Gamma_N^{\text{in}}(1-\mu)}\,\sigma_N^+, \quad L_N^{\text{out}} = \sqrt{\Gamma_N^{\text{out}}(1+\mu)}\,\sigma_N^-, \tag{7.3}$$

and the master equation of the open Heisenberg chain reads

$$\begin{aligned}\dot{\rho}(t) &= \mathcal{L}[\rho(t)] \\ &= -\frac{i}{\hbar}[H, \rho(t)] + \mathcal{D}[L_1^{\text{in}}]\rho(t) + \mathcal{D}[L_1^{\text{out}}]\rho(t) + \mathcal{D}[L_N^{\text{in}}]\rho(t) + \mathcal{D}[L_N^{\text{out}}]\rho(t),\end{aligned} \tag{7.4}$$

with $\rho(t)$ the density matrix, $\mathcal{D}[L]\rho$ the Lindblad operator

$$\mathcal{D}[L]\rho = 2L\rho L^\dagger - \Big\{L^\dagger L, \rho\Big\} = 2L\rho L^\dagger - L^\dagger L\rho - \rho L^\dagger L \tag{7.5}$$

and $\mathcal{L}[\rho(t)]$ the Liouville super-operator, cf. Sec. 2.3. The scattering rates Γ are defined using an additional parameter μ with $\mu \in [-1, 1]$, which changes the ratio of the in- and outscattering rate on each side of the chain. Thus, μ models the magnitude of the difference between the two rates, playing the role of an external potential, which induces a spin current through the chain. Due to this potential, the system will never be in a equilibrium state, but will in the long time limit reach a non-equilibrium steady-state $\rho_{\text{NESS}} = \lim_{t\to\infty} e^{\mathcal{L}t}\rho(t_0)$ due to the bias between the two reservoirs.

7.2.1 Spin-transport properties in the non-equilibrium steady-state

The relative current per site $j_k(t)$ serves as a figure of merit for characterizing the transport properties in the non-equilibrium steady state. It may be derived from the continuity equation, where the density of interest is the density of the spin in z-direction σ_z^k. Thus, the continuity equation in one spatial dimension x reads as

$$\partial_t \sigma_z^k + \partial_x j_k = 0.. \tag{7.6}$$

As the current is observed at the lattice points, it is put $\partial_x j_k = \frac{j_k - j_{k-1}}{h}$, and $\partial_t \sigma_z^k$ is calculated using the Heisenberg equation of motion $\frac{d}{dt}\sigma_k^z = -\frac{i}{\hbar}[\sigma_k^z, H] + (\partial_t \sigma_k^z)$, where σ_k^z does not depend explicitly on t. This yields

$$\begin{aligned} j_k &= J(\sigma_k^x \sigma_{k+1}^y - \sigma_k^y \sigma_{k+1}^x), \\ &= 2iJ(\sigma_k^+ \sigma_{k+1}^- - \sigma_k^- \sigma_{k+1}^+). \end{aligned} \tag{7.7}$$

In the steady state, the current will be site independent, thus

$$\langle j(t) \rangle = \frac{1}{N-1} \sum_{k=1}^{N-1} \langle j(t) \rangle_k. \tag{7.8}$$

Another observable of importance is the single site magnetization $M_k(t)$. Note that contrary to the relative current, it is not site-independent. It is defined as:

$$\langle M_k(t) \rangle = \text{Tr}\left(\sigma_z \rho(t)\right), \tag{7.9}$$

As in the NESS, ρ_{NESS} is constant, so will be the expectation value of both figures of merit:

$$\langle j \rangle = \text{Tr}\left(j_k \rho_{\text{NESS}}\right). \tag{7.10}$$

$$\langle M_k \rangle = \text{Tr}\left(\sigma_k \rho_{\text{NESS}}\right). \tag{7.11}$$

Fig. 7.2 (a) depicts the magnetization $\langle M_k \rangle$ of each single site k in a chain with $N = 4$ sites, initialized in the $|\downarrow\uparrow\uparrow\uparrow\rangle$ state. Parameters are set to $\mu = 1$, $J = 0.1$ and all scattering rates to $\Gamma_1^{\text{in}} = \Gamma_1^{\text{out}} = \Gamma_N^{\text{in}} = \Gamma_1^{\text{out}} \equiv \Gamma = 0.01$. Clearly, in the NESS, the spins align along direction of the external reservoir, while this effect is strongest for the edge spins and vanishes for the spins in the middle. Contrary to this behavior, the relative current

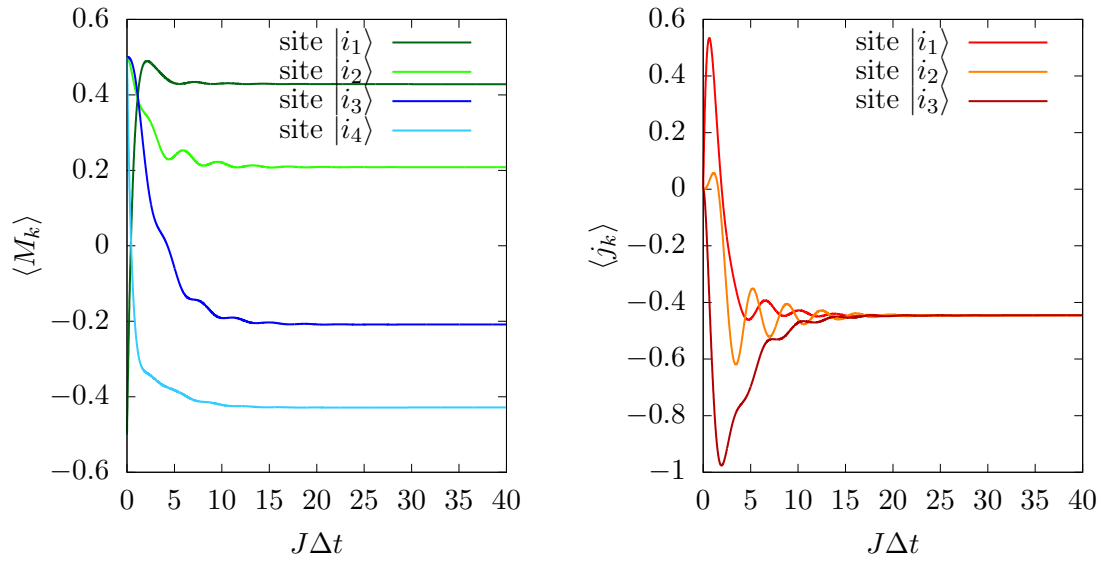

(a) Single site magnetization $\langle M_k \rangle$

(b) Relative current $\langle j_k \rangle$

Figure 7.2: (a) Single site magnetization $\langle M_k \rangle$ of each single site k in a chain with $N = 4$ sites, initialized in the $|\downarrow\uparrow\uparrow\uparrow\rangle$ state. Parameters are set to $\mu = 1$, $J = 0.1$ and all scattering rates to $\Gamma_1^{\text{in}} = \Gamma_1^{\text{out}} = \Gamma_N^{\text{in}} = \Gamma_1^{\text{out}} \equiv \Gamma = 0.01$. Clearly, in the non-equilibrium steady state, the spins align along direction of the external reservoir, while this effect is strongest for the edge spins and vanishes for the spins in the middle. (b) Relative current $\langle j_k \rangle$ of each single site k in the same chain as in (a). Clearly, in the non-equilibrium steady state, all $\langle j_k \rangle$ converge to the same nonzero value induced by the external driving with $\mu \neq 0$. The computation in Fig. 7.2 (a) and (b) has been performed with the tMPS method extended into Liouville-space. The basis transformation and the derivation of the time-evolution operator is explained in the appendix of this thesis, cf. Sec. 11.4.

$\langle j_k \rangle$ of each single site k displayed in Fig. 7.2 (b), clearly converges to the same nonzero value in the NESS which is induced by the external driving with $\mu \neq 0$.
The computation in Fig. 7.2 (a) and (b) has been performed with the tMPS method extended into Liouville-space. The basis transformation and the derivation of the time-evolution operator is explained in the appendix of this thesis, cf. Sec. 11.4.

7.2.2 Transport in the weak driving regime

The spin transport through the chain may generally be described as a diffusive process which is driven by a difference in the density of the magnetic field or spin reservoirs. Hence, it may phenomenologically be characterizes with Fick's first law, which states for the one-dimensional case that the particle current j is proportional to the gradient of the particle density c with a constant of proportionality, the diffusion constant $\mathcal{D}$ [233]:

$$j = -\mathcal{D}\frac{\partial c}{\partial x}. \tag{7.12}$$

If Eq. (7.12) holds, the system is called diffusive. In case of an externally driven spin chain, the spatial density difference is expressed by the difference of the magnetization at both ends of the chain, $\Delta m = \langle m_1 \rangle - \langle m_N \rangle$. As the system is spatially discretized, $\frac{\partial \Delta m}{\partial x}$ may be expressed as

$$\frac{\partial \Delta m}{\partial x} = \frac{\Delta m}{N}. \tag{7.13}$$

Comparing Equations (7.12) and (7.13) makes clear that the characterization of the transport process is expressed with the structure of the diffusion constant $\mathcal{D}$. Here, in case of the diffusive transport, one the one hand, $\mathcal{D}$ is linearly dependent on the magnetization difference on both ends of the chain, $\mathcal{D} \sim \Delta m$. As Δm depends on the potential difference μ of the external driving, one way to characterize a diffusive process is with the relationship $\mathcal{D} \sim \mu$ - if this is the case, this is called the linear regime. On the other hand, if the transport is diffusive, it holds that $\mathcal{D} \sim -\frac{1}{N}$, which is another way of evaluating phenomenologically the diffusive character of the transport [121].
However, the transport may either be faster or slower - superdiffusive or subdiffusive - compared to the diffusive case, or not depend on the system size N at all, in which case the transport is called ballistic. All these cases are called anomalous transport, in contrast to the normal diffusive case. These regimes may be characterized by the following more general dependence, where a scaling exponent $\gamma \in \mathbf{R}$ is introduced:

$$j \sim \frac{1}{N^\gamma}. \tag{7.14}$$

Thus, if $\gamma = 1$, the transport is diffusive. If $\gamma = 0$, the transport is independent of N and thus ballistic. The superdiffusive case is characterized by $0 < \gamma < 1$, which means that the current decreases slower with the system size than in the diffusive case. If $\gamma > 1$, the process is called subdiffusive, where the current decreases faster with the system size than in the diffusive case [234, 124, 32].

Only the fully resonant interaction between the single sites will be discussed here. The weak driving regime is characterized by a small potential difference, $\mu \ll 1$. In this regime, the Heisenberg chain with nearest-neighbor interaction has been demonstrated to be in the linear regime [124, 234, 20]. Here, the transport properties depend strongly on the anisotropy Δ, cf. Eq. (7.1), and depending on it, anomalous transport has been demonstrated. For $\Delta < 1$, the transport is ballistic for any temperature, while it is superdiffusive for $\Delta = 1$ and diffusive for $\Delta > 1$, both for $T \to \infty$ [32].
Note that this picture changes for an interaction with a longer range than nearest neighbor: Here, the ballistic regime may also be reached in the isotropic case, depending on the chain length. For larger system sizes, a transition from a diffusive to a ballistic regime has been demonstrated recently, where the critical chain length for the transition depends on the range of the interaction [34].
Fig. 7.3 plots the relative current j_k over the system size N, with $\Gamma/J = 10$ and weak driving $\mu = 0.1$. The data is fitted with a power law function, and the obtained param-

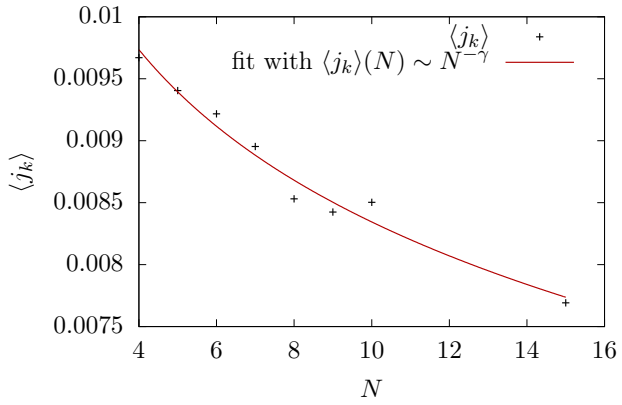

Figure 7.3: Plot of the relative current j_k over the system size N. Parameters are $\Gamma/J = 10$ and $\mu = 0.1$, that it, a weak driving is applied. The data is fitted with a power law function and the parameter $\gamma = 0.02 \pm 0.005$ is obtained. Thus, in accordance with [32], the system displays superdiffusive behavior.

eter is $\gamma = 0.02 \pm 0.005$, indicating superdiffusive behavior in accordance with [32].
Note that obtaining the data is numerically very demanding. The reason for this lies in the growing entanglement within the chain while it evolves in time, and in the disadvantageous scaling of the Liouville space with the number of differential equations growing with 4^N with N the system size. Here, the novel approach presented in this thesis has the strong advantage of describing coherent dynamics which may be done in the QSSE-picture. Thus, the scaling is reduced to 2^N. In the following, an efficent algorithm is presented for this computation.

7.3 Algorithm

The full Hamiltonian H in Eq. (7.1) is transformed into the QSSE-picture as described in Sec. 2.2. The resulting time evolution operator reads:

$$U(t_{k+1}, t_k) = \exp\Big[i\Omega(\sigma_1^+ + \sigma_1^-) + i\sum_{i=1}^{N-1} J\Big(\sigma_i^x\sigma_{i+1}^x + \sigma_i^y\sigma_{i+1}^y + \sigma_i^z\sigma_{i+1}^z\Big) + i\sqrt{\Gamma}\Delta B(t_k)\sigma_N^+ - i\sqrt{\Gamma}\Delta B^\dagger(t_k)\sigma_N^-\Big]. \quad (7.15)$$

Analogous to the case of a many-emitter coupled to a structured reservoir, cf. Sec. 6.4, evolving $|\psi(t)\rangle$ in time using tMPS poses the difficulty of numerically costly swapping processes, cf. Sec. 6.3.2. This thesis thus employs an algorithm which overcomes these limitations and which is optimized for the Markovian type of decay. It operates without swapping the position of the bins. By doing so, it exploits that the future time bins factorize with the system dynamics, and relies on the Markovian approximation from which follows that only the present state of the reservoir matters. Note that for the possibility to include non-Markovian dynamics, the algorithm presented in Sec. 6 may be applied without difficulty, too.
In this case, the MPS contains only the many-body system and the present time step. In order to compute one time step, this time bin is contracted with the last site and the MPO is applied. After the subsequent decomposition, this time bin is not stored in the MPS but dropped, and as a consequence, the information of the state of the bath as well as the entanglement of the state of the bath with the its own past is lost. Next, a new vacuum bin is generated, which may be initialized apart from the many-body system as it is not yet correlated with it. It is contracted with the last site, and continued with the algorithm. Fig. 7.4 depicts the corresponding block diagram.
With this, the computational costly reordering of the bins is avoided, enabling a significant speedup and thus the calculation of the dynamics of larger many-body systems. In order to demonstrate the potential of the proposed algorithm, Fig. 7.5 plots the decay dynamics of the model described with Eq. (7.15) without an external pump field, thus $\Omega = 0$, for a system size as large as $N = 50$.

7.4 Results

As the chain is driven by the pump field on its left end and displays a Lindblad type of decay on its right end, the figure of merit is the spin current through the chain in the NESS, cf. Eq. (7.10), completely equivalent to the case of the incoherently driven chain. In Fig. 7.6, the benchmark of the algorithm with the full solution of the Lindblad master equation is depicted. The plot shows the time dynamics of the spin current between all single sites in a chain with $N = 4$ sites, which has been initialized in the Neel state $|\uparrow\downarrow\uparrow\downarrow\rangle$. In the transient regime, the densities oscillate irregularly and after a convergence time, they equilibrate out a NESS, where the current between all sites takes on the same value. This figure also serves as a benchmark using the full solution for $|\psi(t)\rangle$ with the

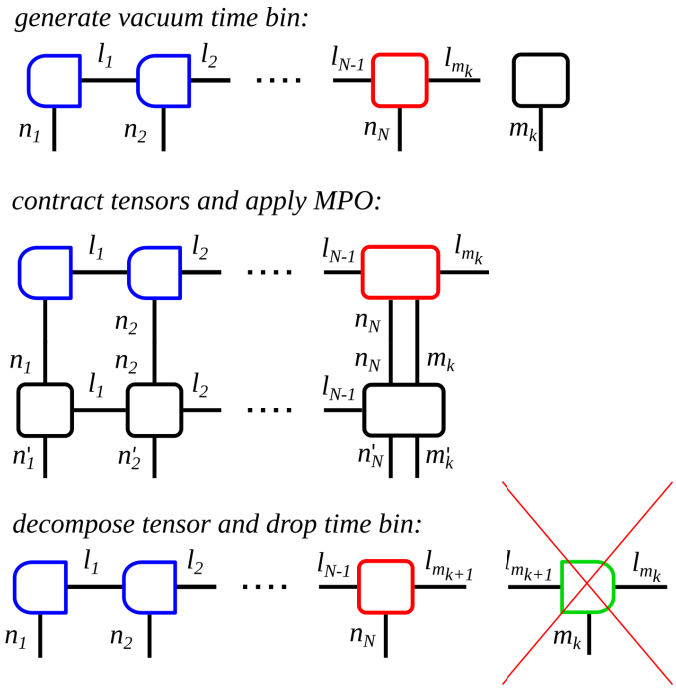

Figure 7.4: Block diagram of an efficient algorithm for a coherently driven quantum spin chain where the last site of the system is subject to dissipation. The diagram demonstrates the calculation of the kth time step. Blue boxes indicate left-orthogonality of the tensors, while green boxes indicate right-orthogonality and the red box marks the position of the orthogonality center of the MPS. The MPS contains only the many-body system and the present time step. In order to compute one time step, this time bin is contracted with the last site and the MPO is applied. After the subsequent decomposition, this time bin is dropped and a new vacuum bin is generated, which may be initialized apart from the many-body system as it is not yet correlated with it. With this, the computational costly reordering of the bins is avoided, enabling a significant speedup and thus the calculation of the dynamics of larger many-body systems.

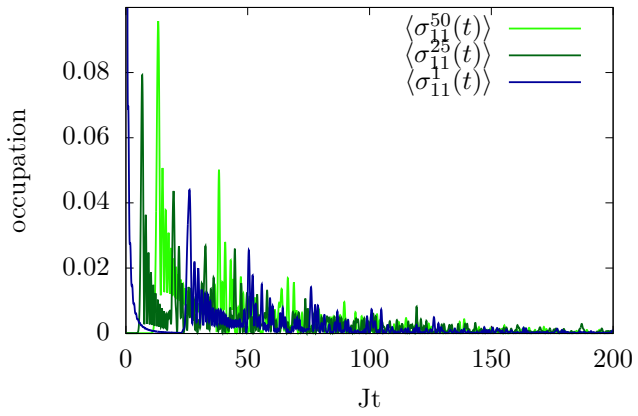

Figure 7.5: Decay dynamics of some selected sites of the model described with Eq. (7.15) without an external pump field, thus $\Omega = 0$, for a system size as large as $N = 50$. This plot serves as a demonstration of the potential of the proposed algorithm.

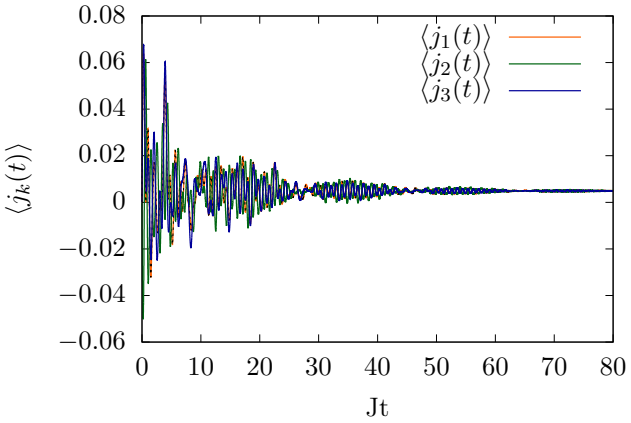

Figure 7.6: Time dynamics of the spin current between all single sites in a chain with $N = 4$ sites in a chain initialized in the Neel state, thus $|\uparrow\downarrow\uparrow\downarrow\rangle$ (green, blue and orange lines). In the transient regime, the densities oscillate irregularly and after a convergence time, they equilibrate out a NESS, where the current between all sites takes on the same value. This figure serves as a benchmark using the full solution for $|\psi(t)\rangle$ with the Lindblad master equation (black dotted lines).

Lindblad master equation (black dotted lines).
In Fig. 7.7, the relative current $\langle\sigma_z\rangle_{\text{rel}}$ through the chain is depicted over the system size N of the chain (black triangles). The data is fitted with a power law function (green line), yielding the value $\gamma = 0.01 \pm 0.0006$. This indicates a superdiffusive behavior.

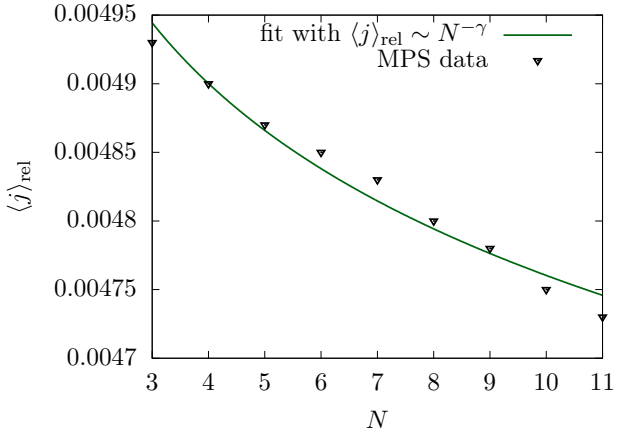

Figure 7.7: Plot of the relative current $\langle \sigma_z \rangle$ over the system size N of the many-body system (black triangles). The data is fitted with a power law function, and the parameter $\gamma = 0.001 \pm 0.3$ is yielded. This indicates a superdiffusive behavior, thus it holds that $\langle \sigma_z \rangle_{\mathrm{rel}} \sim N^{-\gamma}$ with $0 < \gamma < 1$. This is in correspondence with the incoherently driven case depicted in Fig 7.3, where for weak driving regime, these anomalous transport properties have been demonstrated, too.

Interestingly, despite the coherent driving which is applied in this model, this corresponds to the result for an incoherently driven chain modeled with a Lindblad master equation displayed in Fig. 7.3, where the current also displays superdiffusive behavior in the weak driving regime.

7.5 Conclusion

In this section, a novel model for a boundary driven many-body system has been presented, using the example of a Heisenberg spin-chain with nearest-neighbor interaction. Here, the chain is coherently driven with a continuous, resonant pump field applied to the first spin, while the last spin is coupled dissipatively to a vacuum reservoir, and the transport properties of the chain in the non-equilibrium steady state (NESS) are investigated. This novel approach contrasts and complements the dominant model in the research field, where the potential difference is realized with an incoherent driving using a full Markovian approximation by coupling its first and last site to reservoirs which is described with the Lindblad formalism. Due to the coherent time evolution, the dynamics of the pure state of the system may be computed in the tMPS framework in the QSSE-picture. It is shown that for the weak driving regime, the system also displays superdiffusive behavior. This novel implementation poses most interesting possibilities for the comparison of the out-of-equilibrium properties - for instance spin transport properties, entanglement growth or energy transport - of many-body systems driven either coherently or with a full Markovian approximation. Also, it allows for the possibility of investigating driven

many-body systems in non-Markovian interaction with their environment, a setup highly interesting for studying properties of open quantum many-body systems and for future applications in the field of quantum information technologies.

Part III.

Single-emitter system-reservoir interaction

8.

Controlling the feedback phase of a Λ-type three-level system

In the previous part of the thesis at hand, it has been demonstrated that it is possible to dynamically stabilize the excited state density of a many-body system using time-delayed, coherent feedback control. By doing so, trapping parameters arise where the choice of the feedback phase leading to excitation stabilization depends on the delay time. Compared to the case of the two-level system under self-feedback, this is an entirely new phenomenon. This effect immediately leads to the question if further possibilities for stabilization arise if it would be possible to control the feedback phase separately from the delay time.

Adding up to this, the discussed setup has been employed to study the dynamics of few-level emitters in various schemes. Here, enhancement of antibunching or of the two-photon probability [132, 183], or quantum coherence stabilization [186, 70, 187, 188] have been achieved with this approach.

Even though the phase condition for stabilization in these cases does not depend on the choice of the delay time, still, in all these cases, the intrinsic connection between the delay time τ and the feedback phase ϕ which expresses itself as $\phi = \omega_0 \tau$ with ω_0 a system transition frequency does not allow for the delay time τ to be tuned without affecting the feedback phase ϕ. As all the effects reported above rely on a specific value of the feedback phase as well as of the delay time, this intertwining of the two control parameter may well lead to experimental limitations. Furthermore, tuning the two parameters may create the need for major experimental efforts.

In this section, a novel approach to controlling self-feedback induced stabilization processes is presented. In order to tune the phase between the incoming and emitted signal, an external pump field is applied on the system, which induces phase shifts on demand.

As will be demonstrated here for the case of a three-level system (3LS), a resonant microwave pump field leads to an additional way of controlling the system dynamics, using the Rabi-frequency as a new control parameter. These findings increase the application possibilities for coherent quantum feedback [60].

8.1 Model

The model consists of a three-level system (3LS) which is placed in the semi-infinite waveguide introduced in Sec. 4.2. The 3LS consists of a Λ-type system with non-degenerate ground states $|1\rangle$ and $|2\rangle$ and the excited state $|3\rangle$. The system allows for radiative transmission between the excited level and one of the ground states. Between the two non-degenerate ground levels, the 3LS is resonantly pumped with a laser field. Fig. 8.1 shows a sketch of the setup. The Hamiltonian reads (with $\hbar \equiv 1$)

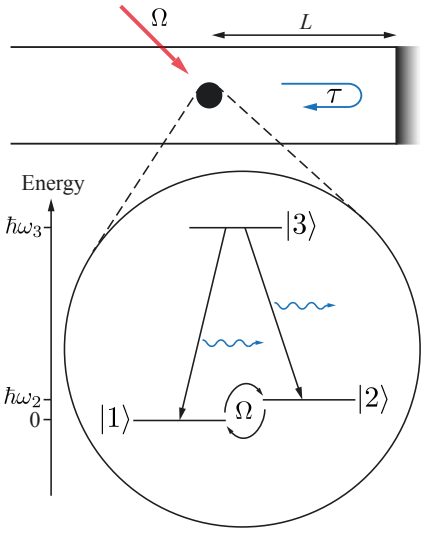

Figure 8.1: Sketch of a three-level system (3LS) placed in a semi-infinite waveguide where the closed end consists of a mirror reflecting the emitted excitation which will subsequently interact with the system after a delay time τ. The 3LS consists of a Λ-type system with non-degenerated ground states $|1\rangle$ and $|2\rangle$ and the excited state $|3\rangle$, with radiative transmission allowed between the excited level $|3\rangle$ and the ground states $|1\rangle$ and $|2\rangle$. Between the two non-degenerate ground levels, the 3LS is resonantly pumped with a laser field.

$$H(t) = \omega_2\sigma_{22} + \omega_3\sigma_{33} + \int d\omega\omega b(\omega)^\dagger b(\omega) + \Omega(t)\cos(\omega_2 t)(\sigma_{12} + \sigma_{21}) + \int d\omega \left[G_{\mathrm{fb}}(\omega)b(\omega)^\dagger(\sigma_{13} + \sigma_{23}) + h.c.\right]. \quad (8.1)$$

The first two terms in Eq. (8.1) describe the free evolution of the 3LS relative to the ground level energy $|1\rangle$. Here, σ_{22}, σ_{33} represent the number operator for the respective level and ω_2, ω_3 represent the transition frequencies. The third term models the free evolution of the bosonic mode continuum to which the three-level system is coupled, where the $b(\omega)^{(\dagger)}$ are the annihilation (creation) operators for a photon in the mode of frequency ω. The forth term models the interaction of the 3LS with the pump field of pump frequency ω_2 which is resonant to the transition between the two non-degenerate ground states, while the amplitude evolves with the Rabi frequency $\Omega(t)$. Here, the σ_{ij}, $i,j = 1,2,3$, are the atomic flip operators and defined as $\sigma_{ij} = |i\rangle\langle j|$, with the commutation relation $[\sigma_{ij}, \sigma_{kl}] = \sigma_{il}\delta_{jk} - \sigma_{kj}\delta_{il}$. The last term models the interaction of the 3LS with the structured reservoir which is assumed to be sinusoidal frequency dependent, cf. Sec. 4.2 and Eq. (4.3). Note that contrary to the case of the two-level presented in Sec. 4.2, excitations on two different levels may now be created or destroyed, annihilating/creating an excitation in the waveguide in this process.
Assuming the case of an umpumped system with $\Omega(t) = 0$, it is possible to derive an analytical solution for the dynamics of the coefficient of level $|3\rangle$, $c_3(t)$. Further assuming the special case of $\omega_2\tau = 2n\pi$, $n \in \mathbf{N}^+$, this solution is identical to the one for a TLS, cf. Eq. (4.10) in Sec. 4.2 [235, 189].
This picture changes, however, in the case of $\Omega(t) \neq 0$ in Eq. (8.1). In the following, the system dynamics will be derived for this case [60].
For this, the Hamiltonian in Eq. (8.1) is transformed into the rotating frame defined by its freely evolving part via

$$U_1 = \exp\left[it\Big(\omega_2\sigma_{22} + \omega_3\sigma_{33} + \int d\omega\omega b(\omega)^\dagger b(\omega)\Big)\right]. \tag{8.2}$$

Together with the rotating-wave approximation, this yields:

$$H'(t) = \frac{\Omega(t)}{2}\left(\sigma_{12} + \sigma_{21}\right) + \int d\omega\left[G_{\mathrm{fb}}(\omega)e^{i\omega t}b(\omega)^\dagger e^{-i\omega_3 t}\left(\sigma_{13} + \sigma_{23}e^{i\omega_2 t}\right) + h.c.\right]. \tag{8.3}$$

Next, in order to gain a suitable basis for the analytical considerations, another unitary transformation is applied, which is defined by the pump field

$$U_2 = \exp\left[it\Big(\frac{\Omega(t)}{2}\left(\sigma_{12} + \sigma_{21}\right)\Big)\right]. \tag{8.4}$$

This yields:

$$\begin{aligned} H''(t) = \int d\omega \Big\{ & G_{\mathrm{fb}}(\omega)e^{i\omega t}b(\omega)^\dagger e^{-i\omega_3 t} \\ & \times \left[\cos\left(\frac{\Omega}{2}t\right)\left(\sigma_{13} + \sigma_{23}e^{i\omega_2 t}\right) \; + i\sin\left(\frac{\Omega}{2}t\right)\left(\sigma_{13}e^{i\omega_2 t} + \sigma_{23}\right)\right] + H.c.\Big\}. \end{aligned} \tag{8.5}$$

The system obeys the Schrödinger equation, while the ansatz for the wave function reads as:

$$|\psi''(t)\rangle = c_3(t)\,|3, \{0\}_\omega\rangle + \int d\omega c_2^\omega(t)\,|2, \{1\}_\omega\rangle + \int d\omega c_1^\omega(t)\,|1, \{1\}_\omega\rangle\,. \tag{8.6}$$

Note that it is in the single excitation limit, analogous to the case of the TLS explained Sec. 4.2. Here, $|3,\{0\}_\omega\rangle$ denotes the excited state of the atom where the reservoir is in the vacuum state, while $|2,\{1\}_\omega\rangle$ and $|1,\{1\}_\omega\rangle$ denote the states where the excitation is located in the mode of frequency ω of the reservoir and the atom is in one of its ground states. The equations of motion for the coefficients may now be derived and read

$$\dot{c}_3(t) = -i\int d\omega G_{\mathrm{fb}}(\omega)e^{-i\omega t}e^{i\omega_3 t}\ \left\{c_2^\omega(t)\left[\cos\left(\frac{\Omega}{2}t\right)e^{-i\omega_2 t} - i\sin\left(\frac{\Omega}{2}t\right)\right]\right.$$
$$\left. + c_1^\omega(t)\left[\cos\left(\frac{\Omega}{2}t\right) - i\sin\left(\frac{\Omega}{2}t\right)e^{-i\omega_2 t}\right]\right\}, \tag{8.7}$$

$$\dot{c}_2^\omega(t) = -iG_{\mathrm{fb}}(\omega)e^{i\omega t}e^{-i\omega_3 t}c_3(t)\ \left[\cos\left(\frac{\Omega}{2}t\right)e^{i\omega_2 t} + i\sin\left(\frac{\Omega}{2}t\right)\right], \tag{8.8}$$

$$\dot{c}_1^\omega(t) = -iG_{\mathrm{fb}}(\omega)e^{i\omega t}e^{-i\omega_3 t}c_3(t)\ \left[\cos\left(\frac{\Omega}{2}t\right) + i\sin\left(\frac{\Omega}{2}t\right)e^{i\omega_2 t}\right]. \tag{8.9}$$

Initially, the emitter is assumed to be in the excited state and the reservoir in the vacuum state, $c_3(t_0) = 1$, $c_2^\omega(t_0) = 0$, $c_1^\omega(t_0) = 0$, analogous to the case of the TLS explained Sec. 4.2. Formally integrating and inserting Equations (8.8) and (8.9) into Eq. (8.7) yields for the dynamics of the excited state coefficient:

$$\dot{c}_3(t) = -2\Gamma c_3(t) + \Gamma e^{i\omega_3\tau}\left[\cos\left(\frac{\Omega}{2}\tau\right)\left(1+e^{-i\omega_2\tau}\right) - i\sin\left(\frac{\Omega}{2}\tau\right)\right.$$
$$\left.\times\left(e^{-i\omega_2 t} + e^{i\omega_2(t-\tau)}\right)\right]c_3(t-\tau)\Theta(t-\tau). \tag{8.10}$$

This equation will be discussed further below. Before doing so, the basis for the computation of the system dynamics using MPS will be derived.

8.2 MPS algorithm

8.2.1 Basis transformation

The start of the derivation is the Hamiltonian given in Eq. (8.1). First, a unitary transformation into the rotating frame of the free energies of the excited level and the reservoir is chosen, thus

$$U = \exp\left[it\Big(\omega_3\sigma_{33} + \int d\omega\omega b(\omega)^\dagger b(\omega)\Big)\right]. \tag{8.11}$$

This yields

$$H''(t) = \omega_2\sigma_{22} + \Omega(t)\cos(\omega_2 t)(\sigma_{12}+\sigma_{21})$$
$$\int d\omega\Big[G_{fb}(\omega)b(\omega)^\dagger b(\omega)e^{i(\omega-\omega_3)t}(\sigma_{13}+\sigma_{23}) + h.c.\Big] \tag{8.12}$$

Next, analogous to Sec. 11.3.1, the τ-dependency is shifted into the operators with the same transformation as applied for the TLS, cf. Eq. (11.15), the definition for the sinusoidal coupling given in Eq. (4.3). The time-dependent bath operators are defined as

$$b_{3\mathrm{LS}}(t) = \frac{1}{\sqrt{2\pi}} \int d\omega b(\omega) e^{-i(\omega-\omega_3)t} \tag{8.13}$$

This yields:

$$\begin{aligned} H''(t) = {} & \omega_2\sigma_{22} + \Omega(t)\cos(\omega_2 t)(\sigma_{12}+\sigma_{21}) \\ & - \Big\{ i\Gamma(\sigma_{13}+\sigma_{23}) \Big[b^\dagger_{3\mathrm{LS}}(t) - b^\dagger_{3\mathrm{LS}}(t-\tau) e^{i\omega_3\tau} \Big] + h.c. \Big\}. \end{aligned} \tag{8.14}$$

The transformed Hamiltonian is inserted into the definition of the time evolution operator

$$U(t,t_0) = \hat{T} \exp\left(-i \int_{t_0}^{t} H''(t')dt' \right) \tag{8.15}$$

and the quantum noise operators are defined

$$\Delta B^{(\dagger)}_{3\mathrm{LS}}(t_k) = \int_{t_k}^{t_{k+1}} dt' b^{(\dagger)}_{3\mathrm{LS}}(t'). \tag{8.16}$$

Note that in this derivation, the fast rotating terms containing $\cos(\omega_2)t$ are kept. Eq. (8.15) has to be solved using the approximation of a constant Rabi frequency during one time interval $t \in [t_{k+1}, t_k]$, thus $\Omega(t) \approx \Omega(t_k)$. With this, the time evolution operator read as:

$$\begin{aligned} U(t_k, t_{k+1}) = \exp\Big[& -i\omega_2\sigma_{22}\Delta t - i\Omega(t_k)(\sigma_{12}+\sigma_{21})[\sin(\omega_2 t_{k+1}) - \sin(\omega_2 t_k)] \\ & -\Gamma(\sigma_{13}+\sigma_{23})[\Delta B^\dagger_{3\mathrm{LS}}(t_k) - e^{-i\omega_3\tau}\Delta B^\dagger_{3\mathrm{LS}}(t_{k-l})] \\ & +\Gamma(\sigma_{31}+\sigma_{32})[\Delta B_{3\mathrm{LS}}(t_k) - e^{i\omega_3\tau}\Delta B_{3\mathrm{LS}}(t_{k-l})] \Big] \end{aligned} \tag{8.17}$$

with which the time evolution of $|\psi(t)\rangle$ may now be computed as explained in Sec. 11.3.1.

8.2.2 Modeling coherent quantum feedback with tMPS

To compute the time evolution with tMPS, as derived in Sec. 2.2, Eq. (8.6) may be transformed into the time discrete basis defined in Eq. (2.37). It thus reads as:

$$|\psi\rangle = \sum_{\substack{n_s=0,1 \\ m_1 \ldots m_{N_T}}} c_{n_s, m_1 \ldots m_{N_T}} \Big(|n_s\rangle \otimes |m_1 \ldots m_{N_T}\rangle \Big), \tag{8.18}$$

where n_s, $n_s \in [0,1,2]$ is the index of the state of the 3LS and the m_k denote the state of the reservoir at the kth time step. The complex coefficients $c_{n_s, m_1 \ldots m_{N_T}}$ are expanded into tensors A:

$$c_{n_s, m_1 \ldots m_{N_T}} = A^{l_{n_s}}_{n_s} A^{l_{n_s}, l_{m_1}}_{m_1} A^{l_{m_1}, l_{m_2}}_{m_2} \ldots A^{l_{m_{N_T-1}}}_{m_{N_T}} \tag{8.19}$$

Throughout all the computations done in this thesis, a time step Δt is chosen small enough as to limit the number of excitations created or annihilated during one time step to one and neglect higher excitation probabilities, cf. Sec. 2.2.2. By convention,

$$|0\rangle \equiv \begin{pmatrix} 1 \\ 0 \end{pmatrix}, \qquad |1\rangle \equiv \begin{pmatrix} 0 \\ 1 \end{pmatrix} \tag{8.20}$$

where $|0\rangle$ describes the vacuum state while $|1\rangle$ describes the fully excited state, either of the the two-level emitter or of the reservoir.
Eq. (8.19) contains the information about the system as well as of the state of the reservoir at every time step. It consist of $N_T + 1$ connected tensors, where $N_T = \frac{T}{\Delta t}$ is the total number of time steps. Thus, the matrix A_{n_s} describes the state of the 3LS, while the matrices A_{m_k} contain the information of the state of the reservoir at one time step. Note that each tensor carries one physical index which is also called site index, and one or several link indices l_{n_i}, l_{m_k}. Fig. 8.2 (a) depicts this decomposition in the form of a block diagram.
Using the form in Eq. (8.19) allows for the preservation of the state of the reservoir at every time step, which is necessary in order to compute the interaction with the feedback signal. Due to the choice of the basis, the Hilbert spaces $\mathcal{H}_k$ describing the reservoir at the time step t_k, cf. Sec. 2.2.2, are entangled, thus the reservoir states $\{|i_k\rangle\}$ do not factorize - writing them in the form of Eq. (8.19) allows to preserve this entanglement. As explained in Sec. 3.2.2, it is this quantity which is truncated during the time evolution of the state, and it is accessible in the above form of $|\psi\rangle$ in Eq. (8.19).
As the time-evolution operator $U(t_{k+1}, t_k)$ in Eq. (11.22) only affects the TLS and the kth as well as the $(k-l)$th time step of the reservoir, it may be kept in the form of a single tensor, cf. Fig. 8.2 (b) for the corresponding block diagram.
During the time evolution, the system bin is moved through the MPS to the right, as will become clear in the following. The first interaction with the feedback signal only occurs after the finite time $\tau = (k-l)\Delta t$, and the waveguide will be in the vacuum state until this time, as it is initialized in it. Thus, the interaction with the vacuum before the time $t = \tau$ has to be included in the algorithm. This is done by enlarging the MPS by placing $(k-l)$ tensors initialized in the vacuum state $|0\rangle$ on the left of the system bin at the start of the time evolution.
To compute the kth time step, the two-level system bin, the kth time bin initialized in a vacuum state and the $(k-l)$th bin of the feedback time step have to be contracted. However, the $(k-l)$th bin is separated from the system bin by the time steps in between. The entanglement in between these subspaces is encoded in the link indices, and in order to preserve it, there are two technical ways within the MPS formalism. The first one would be to contract over the link indices of all the tensors $\sum_{j=k-l}^{k} A_j^{\prime l_{j-1}, l_j}$. This operation would preserve the physical indices j'. Due to this, the dimensions of the resulting tensor depends on the feedback time $\tau = (k-l)\Delta t$ scaling with $2^{(k-l)}$ - thus, for larger τ, providing this storage place quickly becomes numerically too demanding, at least by conventional numerical resources.
The second way is to move the bins through the MPS. Here, in order to preserve the

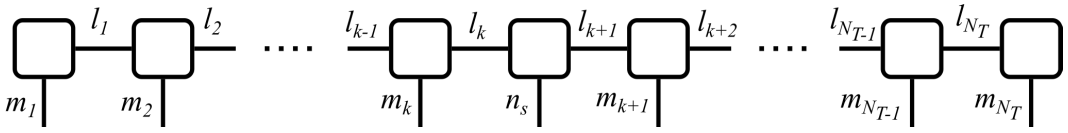

(a) MPS

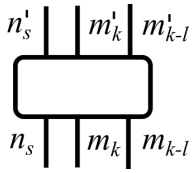

(b) MPO

Figure 8.2: Block diagram of the MPS and the MPO of a few-level under self-feedback. Figure (a) depicts the MPS. Here, n_s labels the site index of the few-level system, while m_k labels the time bins, and $l_1 \dots l_{N_{T-1}}$ label the link indices. The diagram depicts the kth time step, where the system tensor A_{n_s} is placed in between the kth and $(k+1)$th time bin. Figure (b) shows the MPO for the time evolution of the dissipative 3LS system subjected to dissipation. It always affects the emitter, but only the reservoir time bin of the present time step k and of the feedback time step $(k-l)$.

entanglement in between them, the link indices have to be moved with the bin, as they contain the entanglement information, cf. Sec. 3.2. This creates the need to contract the tensor with its respective neighbor and decompose them again, swapping the link indices and the places in the MPS in this procedure. It is illustrated in Fig. 8.3. With this, the tensors may be contracted into each other, and the MPO may be applied according to Eq. (11.24), which means the MPO is multiplied into the MPS as explained in Sec. 3.3. Afterwards, the kth time bin is moved to the left end of the MPS in the same manner as the feedback bin has been moved. With this, all following time steps may be computed accordingly.Fig. 8.3. depicts the corresponding block diagram.
As the swapping technique requires a contraction and re-decomposition of all involved tensors, it scales with the dimensions of the link indices and thus with the entanglement within the MPS: If the entanglement within it strongly grows with time, the Schmidt values grow in number as well as in size, and may not be neglected during the truncation procedure. Subsequently, the number of non-zero entries on the system tensors grows strongly and so does computation effort.
This is generally not the case for the entanglement between different time bins, which makes this algorithm very well suited for computing the time evolution of few-level emitters, where the system part of the MPS is small.

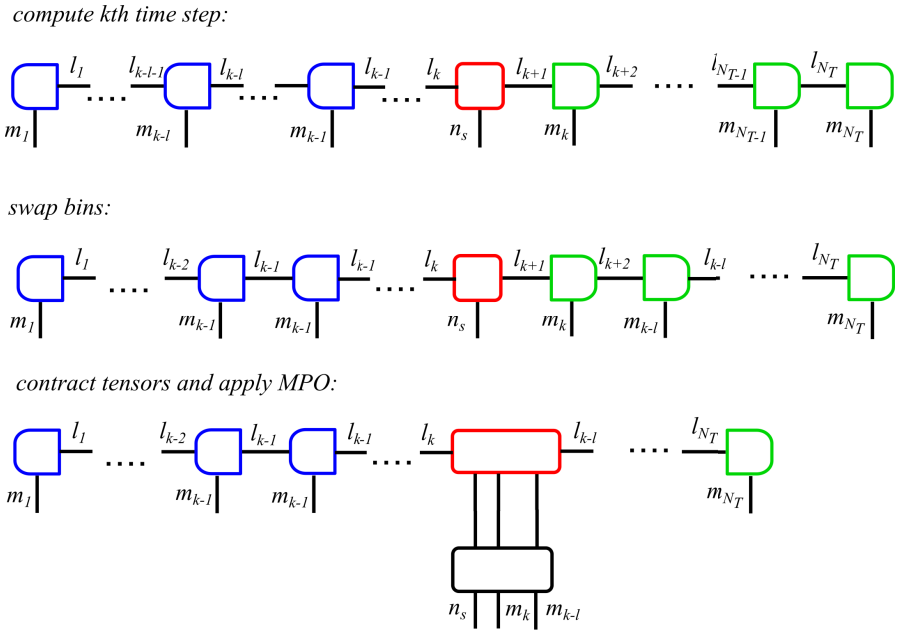

Figure 8.3: Block diagram of the algorithm for computing self-feedback on a single emitter using tMPS demonstrating the computation of the kth time step. First, the feedback time bin is moved through the MPS in order to bring it next to the system bin, a procedure during which the link indices have to be swapped, too. This is illustrated in line 2. Afterwards, the system bin, the present time bin k and the feedback time bin $k - l$ are multiplied into each other over their link indices. Following this, the MPO is applied over the unprimed site indices, which is illustrated in the third line. Afterwards, the tensors are decomposed and the indices unprimed, and the present time bin must be swapped through the MPS to the left of the system, while the feedback time bin has to be brought back to its original position in the same manner.

8.3 Unpumped system

First, the system behavior in the unpumped case, thus $\Omega = 0$ in Eq. (8.1) is discussed. As in the case of the unpumped TLS, population trapping occurs for certain conditions the feedback phase ϕ has to fulfill; however, note that in Eq. (8.1), two phases appear, hence

$$\phi_2 \equiv \omega_2 \tau \tag{8.21}$$

$$\phi_3 \equiv \omega_3 \tau \tag{8.22}$$

For $\Omega = 0$, Eq. (8.1) becomes:

$$\dot{c}_3(t) = -2\Gamma c_3(t) + \Gamma e^{i\omega_3\tau}\left(1 + e^{-i\omega_2\tau}\right) c_3(t-\tau)\Theta(t-\tau). \tag{8.23}$$

If the feedback phase ϕ_2 fulfills the condition $\phi_2 = 2n\pi$ for $n \in \mathbf{N}^+$, Eq. (8.23) again reduces to the equivalent case of the TLS under self-feedback, cf. Eq. (4.10). In this case, if it additionally holds that $\phi_3 = 2n'\pi$, $n' \in \mathbf{N}^+$, the system traps and the remaining excitation is dynamically stabilized. Thus, the delay time τ needs to fulfill the condition

$$\tau = \frac{2\pi n}{\omega_2} = \frac{2\pi n'}{\omega_3}. \tag{8.24}$$

Fig. 8.4 shows the system dynamics for the decaying emitter in the waveguide without an external driving field, that is $\Omega = 0$. It depicts the occupation density of the excited level $\langle\sigma_{33}\rangle$. The system frequencies in the depicted case are $\omega_2/(2\pi) = 0.8\,\mathrm{ps}^{-1}$ and $\omega_3/(2\pi) = 239.3\,\mathrm{ps}^{-1}$, and the dynamics of the excited state density $\langle\sigma_{33}(t)\rangle$ are displayed for various values for the delay time τ.
The solutions shown in Fig. 8.4 have been achieved solving Eq. (8.23) numerically with the tMPS algorithm presented above. Note that each curve is plotted twice, demonstrating the accordance of the tMPS algorithm with the analytical solution which is computed with a program using a Runge-Kutta algorithm of forth order (black dotted lines).
Clearly, the dynamics resemble the case of the TLS: the choice of the delay time - which, as the two parameter are intrinsically intertwined, cf. Eq. (8.22), in turn influences ϕ - either enhances, slows down or stops the decay of the excited state. Also, due to the inherent 2π-periodicity of the feedback phase, stabilization is achieved periodically for different values of τ.
However, the case illustrated in Fig. 8.4 may only be achieved if it holds that $\frac{n}{\omega_2} = \frac{n'}{\omega_3}$. Thus, for certain combination of the transition frequencies, stabilization lies out of experimentally achievable range.

In Fig. 8.5, the same system is depicted, but here for the case of long delay times, $\Gamma\tau \gg 1$. As discussed in Sec. 4.2, the transient part of the decay process displays periodic intervals of decay and re-excitation. After a long transient time lasting more than ten feedback intervals, the delay time $\tau = 10\,\mathrm{ps}$ leads to a stabilization at the value of $\langle\sigma_{33}\rangle = 0.0141$.

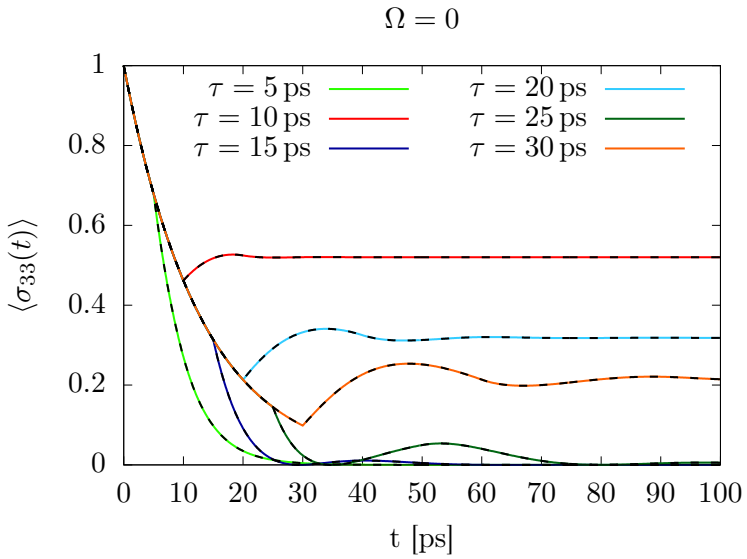

Figure 8.4: Dynamics of the occupation density of the excited level $\langle \sigma_{33} \rangle$ of a decaying 3LS in a semi-infinite waveguide without external driving field, that is $\Omega = 0$, for different delay times τ. The system frequencies in the depicted case are $\omega_2/(2\pi) = 0.8\,\mathrm{ps}^{-1}$ and $\omega_3/(2\pi) = 239.3\,\mathrm{ps}^{-1}$. Clearly, the dynamics resemble the case of the TLS: The choice of the delay time - which, as the two parameter are intrinsically intertwined, cf. Eq. (8.22), in turn influences ϕ - either enhances, slows down or stops the decay of the excited state. Also, due to the inherent 2π-periodicity of the feedback phase, stabilization is achieved periodically for different values of τ. Note that each curve is plotted twice, demonstrating the accordance of the MPS algorithm with the analytical solution (black dotted lines).

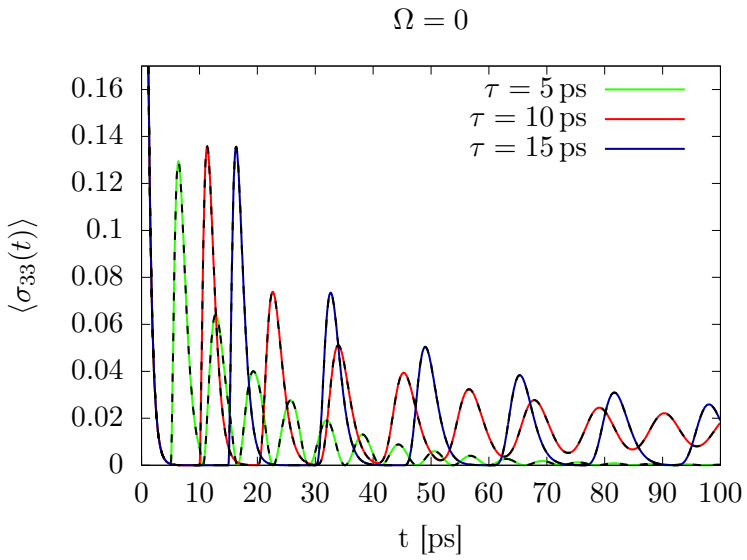

Figure 8.5: Dynamics of the occupation density of the excited level $\langle\sigma_{33}\rangle$ of the same system as depicted in Fig. 8.4 for long delay times, $\Gamma\tau \gg 1$. As discussed in Sec. 4.2, the transient part of the decay process displays periodic intervals of decay and re-excitation. After a long transient time lasting more than 10 feedback intervals, the delay time $\tau = 10\,\mathrm{ps}$ leads to a stabilization at the value of $\langle\sigma_{33}\rangle = 0.0141$.

8.4 Pumped system: Achieving population trapping with a microwave control field

In case of a continuous pump field applied to the system, that is $\Omega \neq 0$, additional parameter sets arise with which population trapping may be achieved. This is the case for the set $\frac{n}{\omega_2} = \frac{n'+1/2}{\omega_3}$, $n, n' \in \mathbf{N}$ - in the unpumped case, for this set the fastest decay is achieved. If, however, a continuous pump field is applied which satisfies $\Omega\tau/2 = \pi$, and additionally the delay time fulfills

$$\tau = \frac{2\pi n}{\omega_2} = \frac{(2n'+1)\pi}{\omega_3}, \tag{8.25}$$

the decay may be stopped completely and the system may be stabilized at a finite excited occupation density.
Fig. 8.6 depicts this stabilization for the same system as displayed in Fig. 8.4. Here, the

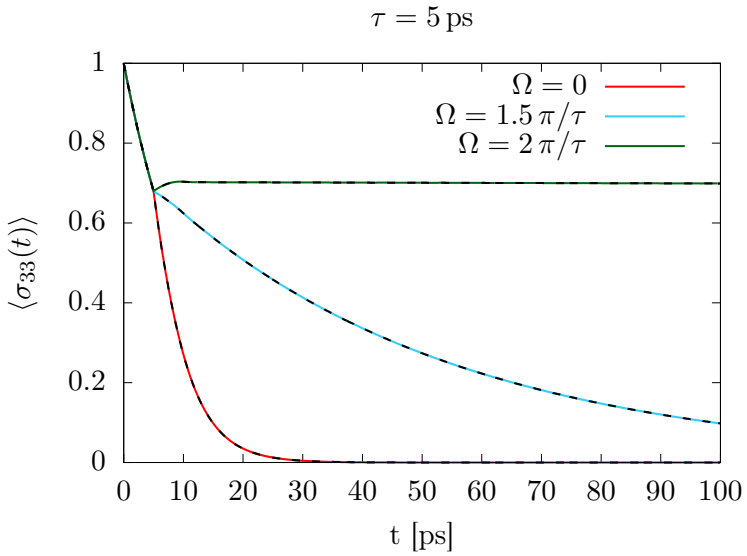

Figure 8.6: Dynamics of the occupation density of the excited level $\langle\sigma_{33}\rangle$ of the same decaying 3LS in a semi-infinite waveguide as depicted in Fig. 8.4 at the delay time $\tau = 5\,\mathrm{ps}$ for different Rabi frequencies Ω of the driving field. Clearly, a finite Rabi frequency slows down the decay process, while a Rabi frequency at the value of $\Omega = 2\pi/\tau$ again induces dynamical population trapping of the system. Note that each curve is plotted twice, demonstrating the accordance of the tMPS algorithm with the analytical solution (black dotted lines). However, for stronger pump fields than depicted here, deviations occur which are due to the approximations made during the basis derivation.

delay time τ is kept fixed at $\tau = 5\,\mathrm{ps}$, and the Rabi frequency of the pump pulse is varied.

Clearly, a finite Rabi frequency slows down the decay process, while a Rabi frequency at the value of $\Omega = 2\pi/\tau$ again induces dynamical population trapping of the system.
Due to the inherent periodicity of the sine and cosine terms in Eq. (8.10), this will be the case for all Rabi frequencies which fulfill the condition

$$\Omega = 2\pi(2n'' + 1)\tau. \tag{8.26}$$

Note that in Fig. 8.6, each curve is plotted twice, and with this, the tMPS algorithm again is proven to produce correct results. However, for stronger pump fields than depicted here, deviations occur which are due to the approximations made during the basis derivation.
Considering the case of long delay times, Fig. 8.7 displays the same system as investigated in Fig. 8.6, but with a faster decay process compared to the delay time, $\Gamma\tau \gg 1$. Strikingly, the pump field $\Omega = 2\pi/\tau$ leads to a much faster stabilization of the system

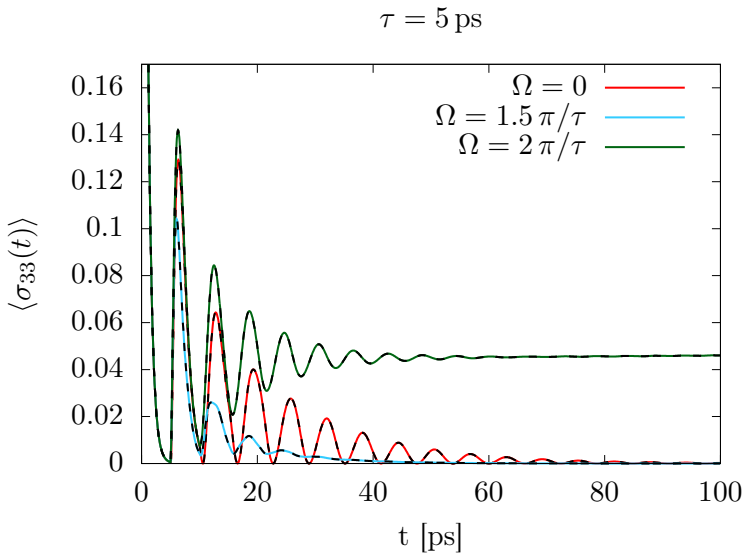

Figure 8.7: Dynamics of the occupation density of the excited level $\langle\sigma_{33}\rangle$ of the same decaying 3LS in a semi-infinite waveguide as depicted in Fig. 8.4 for the case of large $\Gamma\tau \gg 1$. Clearly, the pump field $\Omega = 2\pi/\tau$ leads to a much faster stabilization of the system compared to the unpumped case, cf. Fig. 8.5. Furthermore, the trapped excited density is significantly higher with $\langle\sigma_{33}\rangle = 0.0449$.

compared to the unpumped case, cf. Fig. 8.5. Furthermore, the trapped excited density is significantly higher with $\langle\sigma_{33}\rangle = 0.0449$. Hence, with a control field Ω of microwave light, it is possible to induce a faster stabilization at a higher excited density than in the case the system is solely controlled by tuning the delay time τ.

8.5 Conclusion

In this section, the control of a non-degenerate Λ-type system with coherent self-feedback has been discussed. Here, the novel approach of controlling the system with an external pump field is introduced, which is in resonance with the transition frequency between the two ground levels.
First, the unpumped case is discussed, and it has been demonstrated that stabilization may be achieved at certain delay times. Next, the system behavior with a continuous pump field is investigated. Here, it is shown that the Rabi frequency of the driving field serves as a new control parameter, which gives rise to the possibility of disentangling the two intertwined feedback parameters, the delay time τ and the feedback phase ϕ.
To summarize the results, depending on the properties of the system - the transition frequencies ω_2 and ω_3 - the smallest possible delay time τ may be achieved with or without an external pump field. Assuming that $\omega_2/\omega_3 = n/n'$, $n, n' \in \mathbf{N}$ and the fraction n/n' is irreducible, and if n is even, it is achieved with the external pump field. For odd n, stabilization occurs at smaller τ without an driving field. The example presented here demonstrates the first case, however, for the latter case the additional control parameter may still give rise to stabilization in case experimental limitations do not allow for doing so otherwise. Thus, the results presented here not only broaden the possibilities of feedback control significantly, but also enable a reduction of the transient time and thus a stabilization at higher excited state densities for the investigated system.

9.

Indistinguishable photons with feedback

The Hong-Ou-Mandel effect has been demonstrated in 1987 and describes a method for probing the indistinguishability of two photons. The basic setup is as follows: two photons - which may be emitted by the same or by different sources - interfere at a beam splitter and are transmitted or reflected with probabilities r, t. After passing the beam splitter, the intensity correlation $g^{(2)}(\tau)$ of the two photons is probed as a measure for the indistinguishability. If the two photons are completely identical, they will never be measured at the same time, thus $g^{(2)}(\tau = 0) = 0$, which is the so called Hong-Ou-Mandel dip in the two-photon correlation [236, 237, 238]. This effect has recently been realized experimentally in different settings, for instance taking the influence of dephasing effects into account [239, 240]. As the control of sources emitting indistinguishable photons on demand represents a basis of fundamental importance for quantum communication networks [241, 242, 49, 58], concepts for enhancing the visibility of the two-photon interference are of high interest.
In this chapter, the influence of coherent feedback-control on this effect is investigated. As demonstrated in the previous chapters, time-delayed feedback may enhance or slow down the decay of excited emitters, and hence the question is posed if this effect may be used in order to enhance the visibility $\mathcal{V} = 1 - g^{(2)}$ of photons emitted from photon sources with different properties such as different decay rates.

9.1 The Hong-Ou-Mandel effect

9.1.1 Model

Consider two two-level systems which are excited by a resonant pump pulse of and are placed in front of a beam splitter. During the relaxation process, they will emit photons

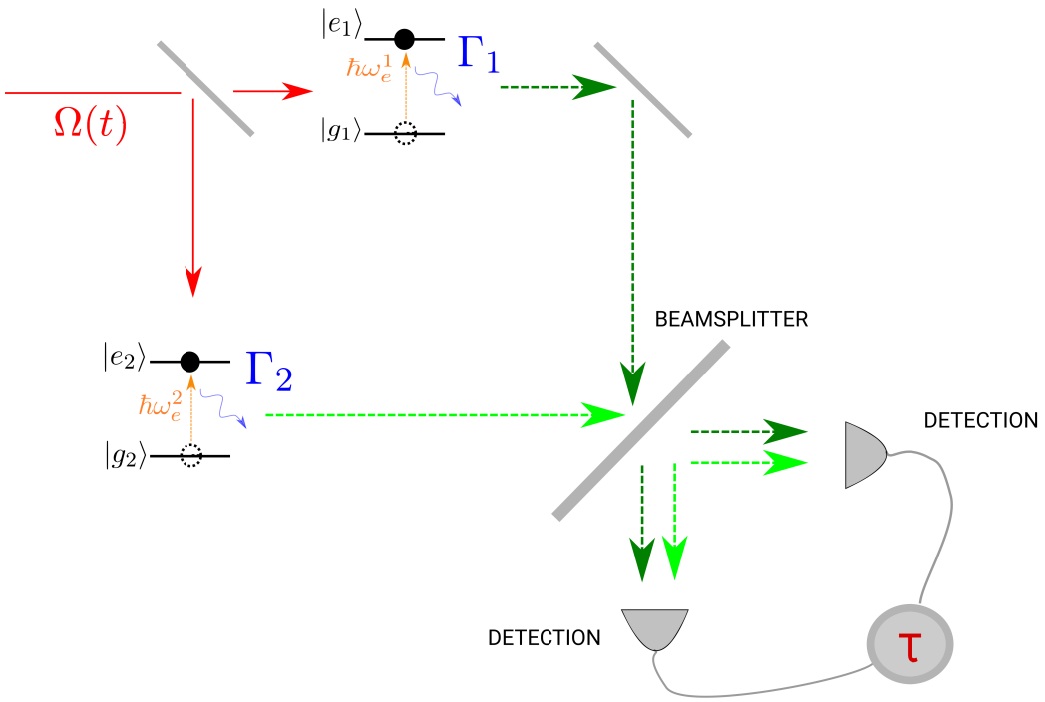

Figure 9.1: Sketch of a Hong-Ou-Mandel type of setup for investigating the two-photon interference. Two two-level systems placed in front of a beam splitter and are excited by a resonant pump pulse. During the relaxation process, they emit photons which interfere at the beam splitter. Behind the beam splitter, two detectors are placed which record the transmitted or reflected photons, while the time difference between the two detection events is denoted by τ.

which will interfere at the beam splitter. Behind it, two detectors are placed which record the transmitted or reflected photons, while the time difference between the two detection events is denoted by τ. Figure 9.1 depicts a sketch of the setup. The emitted photons at the beam splitter are in the modes $a^{(\dagger)}_{in,1}$ and $a^{(\dagger)}_{in,2}$. When passing the beam splitter with the probability t, amplitude and phase remain the same, whereas a reflection with the probability r causes a phase jump of π. This leads to the two output modes behind the beam splitter:

$$a^{(\dagger)}_{out,1} = \frac{1}{\sqrt{2}}\left(\sqrt{t}a^{(\dagger)}_{in,1} + \sqrt{r}a^{(\dagger)}_{in,2}\right) \tag{9.1}$$

$$a^{(\dagger)}_{out,2} = \frac{1}{\sqrt{2}}\left(\sqrt{r}a^{(\dagger)}_{in,1} - \sqrt{t}a^{(\dagger)}_{in,2}\right) \tag{9.2}$$

Note that the commutation relation holds

$$\left[a_{out,1}, a^{\dagger}_{out,2}\right] = 0 \tag{9.3}$$

as well as probability conservation

$$r + t = 1. \tag{9.4}$$

From this, an additional boundary condition for the probabilities is derived which must hold in order to preserve Eq. (9.3) [243, 244]:

$$\sqrt{t}\sqrt{r}^{*} + \sqrt{r}\sqrt{t}^{*} = 0 \tag{9.5}$$

9.1.2 Derivation of the photon wave packet form

The Hamiltonian for the system reads (with $\hbar \equiv 1$):

$$H = \sum_{j=1,2} \omega_e^j \sigma_{ee}^j + \int d\omega_j \omega_j a_\omega^{j\dagger} a_\omega^j + \Omega(t)\left(e^{-i\omega_p t}\sigma_{eg}^j + e^{i\omega_p t}\sigma_{ge}^j\right) + \int d\omega_j g_\omega^j \left(a_\omega^j \sigma_{eg}^j + a_\omega^{j\dagger}\sigma_{ge}^j\right) \tag{9.6}$$

The first term describes the two-level systems with the transition frequency ω_e^j and the number operator σ_{ee}^j, where $j \in [1, 2]$. Note that the energy level of the excited state is considered relative to the ground state. The second term describes the quantized light field by the annihilation and creator operators a_ω^j and $a_\omega^{j\dagger}$ with $\left[a_\omega^i, a_{\omega'}^{j\dagger}\right] = \delta_{ij}\delta_{\omega\omega'}$. The third term denotes the classical excitation field with the amplitude of the pump pulse $\Omega(t)$ and the interaction between the TLS and the light field. The lowering and raising operators of the TLS are denoted by $\sigma_{ik} := |i\rangle\langle k|$, which obey the commutation relations $[\sigma_{ik}, \sigma_{pl}] = \sigma_{il}\delta_{kp} - \sigma_{pk}\delta_{il}$. The pump field is assumed to be in resonance with the transition frequency of the two-level systems, $\omega_p^j = \omega_e^j$. Also, g_j denotes the coupling strength which is assumed to depend only weakly on the frequency, thus $g_\omega^j \approx g_j$.
The equation of motion for the system is the Schrödinger equation

$$i\frac{d}{dt}|\psi(t)\rangle = H(t)|\psi(t)\rangle, \tag{9.7}$$

with the wave function $|\psi\rangle$ describing the two two-level systems and two photons:

$$|\psi\rangle = |\psi_1\rangle \otimes |\psi_2\rangle \tag{9.8}$$

with

$$|\psi_j\rangle = c_g^j(t)\,|g^j, \mathrm{vac}\rangle + c_e^j(t)\,|e^j, \mathrm{vac}\rangle + \int d\omega_j c_g^{\omega_j}(t)\,|g^j, 1_{\omega_j}\rangle + \int d\omega_j c_e^{\omega_j}(t)\,|e^j, 1_{\omega_j}\rangle\,. \tag{9.9}$$

It is assumed that the excitation dynamics caused by the pump pulse is much faster than the emission time scale, which means that the dynamics described by the third term in Eq. (9.6) may be neglected while the two-level systems are assumed to be in the excited state initially. Thus, starting with $c_e(t=0)=1$, $c_g(t=0)=0$ as initial condition, the state vector reads:

$$|\psi_j\rangle = c_e^j(t)\,|e^j, \mathrm{vac}\rangle + \int d\omega_j c_g^{\omega_j}(t)\,|g^j, 1_{\omega_j}\rangle\,. \tag{9.10}$$

In order to obtain a suitable basis, a unitary transformation into the interaction picture is being applied. This results in the time-dependent Hamiltonian $\tilde{H}$ which reads

$$\tilde{H} = \sum_{j=1,2} \left(g_j e^{i(\omega_j - \omega_e^j)t} a_\omega^j \sigma_{ge}^j + h.c. \right) \tag{9.11}$$

Using $c_e(t=0)=1$, $c_g^{\omega_j}(t=0)=0$ as initial condition, the Wigner-Weisskopf problem reads

$$\partial_t c_e^j(t) = -i g_j \int d\omega_j e^{-i(\omega_j - \omega_e^j)t} c_g^{\omega_j}(t) \tag{9.12}$$

$$\partial_t c_g^j(t) = -i g_j e^{i(\omega_j - \omega_e^j)t} c_e^j(t). \tag{9.13}$$

Eq. (9.13) is formally solved with

$$c_g^j(t) = -i g_j \int_0^t dt' e^{i(\omega_j - \omega_e^j)t} c_e^j(t), \tag{9.14}$$

where $c_g^j(0)=0$, and Eq. (9.14) is being plugged into Eq. (9.12) and integrated. This yields a relaxation dynamics for the excited state:

$$c_e^j(t) = e^{-\Gamma_j t}, \tag{9.15}$$

where $c_e^j(0)=1$ and the decay rate is defined as

$$\Gamma_j \equiv g_j^2 \pi. \tag{9.16}$$

Hence, the photon wave packet form in Eq. (9.14) becomes:

$$c_g^j(t) = -i g_j \int_0^t dt' e^{i(\omega_j - \omega_e^j)t} e^{-\Gamma_j t}. \tag{9.17}$$

With this, and with the assumption that $t \to \infty$ so that the TLS has decayed completely to the ground state and $c_e^j(t \to \infty) = 0$, the total wave function now reads:

$$|\psi\rangle = |\psi_1\rangle \otimes |\psi_2\rangle = \left[-ig_1 \int_0^\infty d\omega_1 \int_0^t dt_1 e^{i(\omega_1 - \omega_e^1)t_1} e^{-\Gamma_1 t_1} a_{\omega_1}^\dagger |vac\rangle\right] \otimes \left[-ig_2 \int_0^\infty d\omega_2 \int_0^t dt_2 e^{i(\omega_2 - \omega_e^2)t_2} e^{-\Gamma_2 t_2} a_{\omega_2}^\dagger |vac\rangle\right] \quad (9.18)$$

9.1.3 Calculation of the $g^{(2)}$-function

The visibility $\mathcal{V}$ is expressed via the normalized two-photon correlation [83, 239]:

$$\mathcal{V} = 1 - g^{(2)}. \quad (9.19)$$

The two-photon correlation is defined as:

$$g^{(2)}(t_D, t_D + \tau) = \frac{\langle\psi(t)| E_3^{(-)}(t_D) E_4^{(-)}(t_D + \tau) E_4^{(+)}(t_D + \tau) E_3^{(+)}(t_D) |\psi(t)\rangle}{\langle\psi(t)| E_3^{(-)}(t_D) E_3^{(+)}(t_D) |\psi(t)\rangle \langle\psi(t)| E_4^{(-)}(t_D) E_4^{(+)}(t_D) |\psi(t)\rangle}, \quad (9.20)$$

where the time-dependent electrical field operators are defined with

$$E_k(t)^{(\mp)} = \int d\omega_k e^{\pm i\omega_k t} a_{\omega_k}, \quad (9.21)$$

and t_D denotes the detection time while τ denotes the time difference between the two detection events. Also, $E_3(t)$, $E_4(t)$ denote the two detection modes of the electrical field behind the beam splitter. Let $E_1(t)$, $E_2(t)$ denote the modes of the incoming electrical field. Following the definition in Eq. (9.1) and Eq. (9.2), $E_3(t)$, $E_4(t)$ then read

$$E_3(t)^{(\pm)} = \sqrt{t} E_1(t)^{(\pm)} + \sqrt{r} E_2(t)^{(\pm)} \quad (9.22)$$

$$E_4(t)^{(\pm)} = \sqrt{t} E_1(t)^{(\pm)} - \sqrt{r} E_2(t)^{(\pm)}. \quad (9.23)$$

Hence, Eq. (9.18) may be calculated and reads:

$$E_4^{(+)}(t_D + \tau) E_3^{(+)}(t_D) |\psi(t)\rangle = \left(t E_2(t_D + \tau)^{(+)} E_1(t_D)^{(+)} - r E_1(t_D + \tau)^{(+)} E_2(t_D)^{(+)}\right) |\psi(t)\rangle, \quad (9.24)$$

where all states with two incoming photons in one mode, $|g_j, 2_{\omega_j}\rangle$, are omitted because of the restriction to the single excitation limit. Inserting Eq. (9.18) and 9.21 into 9.24 yields:

$$E_4^{(+)}(t_D + \tau) E_3^{(+)}(t_D) |\psi(t)\rangle = - g_1 g_2 \left(t \int_0^\infty d\omega_2 e^{-i\omega_2(t_D + \tau)} \int_0^\infty d\omega_1 e^{-i\omega_1 t_D} - r \int_0^\infty d\omega_1 e^{-i\omega_1(t_D + \tau)} \int_0^\infty d\omega_2 e^{-i\omega_2 t_D}\right) \int_0^t dt_1 e^{i(\omega_1 - \omega_e^1)t_1} e^{-\Gamma_1 t_1} a_{\omega_1}^\dagger \int_0^t dt_2 e^{i(\omega_2 - \omega_e^2)t_2} e^{-\Gamma_2 t_2} a_{\omega_2}^\dagger |vac\rangle. \quad (9.25)$$

Integrating over the frequencies and the times until the detection event t_D, $t_D+\tau$ yields:

$$E_4^{(+)}(t_D+\tau)E_3^{(+)}(t_D)\,|\psi(t)\rangle = \\ -g_1g_2\pi^2\left(te^{-i\omega_e^1 t_D - i\omega_e^2(t_D+\tau)-\Gamma_1 t_D-\Gamma_2(t_D+\tau)} - re^{-i\omega_e^1(t_D+\tau)-i\omega_e^2 t_D-\Gamma_1(t_D+\tau)-\Gamma_2 t_D}\right). \tag{9.26}$$

With this, the unnormalized two-photon correlation $G^{(2)}(t_D,\tau)$ may be calculated as follows:

$$G^{(2)}(t_D,\tau) = |E_4^{(+)}(t_D+\tau)E_3^{(+)}(t_D)\,|\psi(t)\rangle\,|^2 = \\ g_1^2g_2^2\pi^4e^{-2(\Gamma_1+\Gamma_2)t_D}\left[|r|^2e^{-2\Gamma_1\tau}+|t|^2e^{-2\Gamma_2\tau}-2rt\,\mathrm{Re}\left(e^{i(\omega_1-\omega_2)\tau-(\Gamma_1+\Gamma_2)\tau}\right)\right] \tag{9.27}$$

At this point, the conditions for a perfect beam splitter [244] are plugged in, thus $\sqrt{r}=\sqrt{t}=\frac{1}{2}$. This yields:

$$G^{(2)}(t_D,\tau) = \frac{g_1^2g_2^2\pi^4}{4}e^{-2(\Gamma_1+\Gamma_2)t_D}\left[e^{-2\Gamma_1\tau}+e^{-2\Gamma_2\tau}-2\,\mathrm{Re}\left(e^{i(\omega_1-\omega_2)\tau-(\Gamma_1+\Gamma_2)\tau}\right)\right] \tag{9.28}$$

In order to normalize the two-photon correlation, the population densities of the two output modes are calculated:

$$\langle\psi(t)|\,E_3^{(+)}(t_D)E_3^{(-)}(t_D)\,|\psi(t)\rangle = |E_3^{(+)}(t_D)\,|\psi(t)\rangle\,|^2 = \left|\left(E_1^{(+)}(t_D)+E_2^{(+)}(t_D)\right)|\psi(t)\rangle\right|^2 \\ = -g_1g_2\left(\sqrt{t}\int_0^\infty d\omega_1 e^{-i\omega_1 t_D}a_{\omega_1}+\sqrt{r}\int_0^\infty d\omega_2 e^{-i\omega_2 t_D}a_{\omega_2}\right) \\ \int_0^t dt_1 e^{i(\omega_1-\omega_e^1)t_1}e^{-\Gamma_1 t_1}a_{\omega_1}^\dagger\int_0^t dt_2 e^{i(\omega_2-\omega_e^2)t_2}e^{-\Gamma_2 t_2}a_{\omega_2}^\dagger\,|vac\rangle \\ = t\pi\Gamma_1e^{-2\Gamma_1 t_D}+r\pi\Gamma_2e^{-2\Gamma_2 t_D} \tag{9.29}$$

Integrating over t_d with $t_D\to\infty$ and using $r+t=1$ yields:

$$\langle\psi(t)|\,E_3^{(+)}(t_D)E_3^{(-)}(t_D)\,|\psi(t)\rangle = \frac{\pi}{2} \tag{9.30}$$

Equivalently, it is obtained:

$$\langle\psi(t)|\,E_4^{(+)}(t_D)E_4^{(-)}(t_D)\,|\psi(t)\rangle = \frac{\pi}{2}. \tag{9.31}$$

With this, the normalized time-integrated two-photon correlation reads

$$g^{(2)} = 2\cdot\frac{4}{\pi^2}\int_0^\infty dt_D\int_0^\infty d\tau\,G^{(2)}(t_D,\tau) = \\ \frac{1}{2}\left[1-\frac{4\Gamma_1\Gamma_2}{(\omega_e^1-\omega_e^2)^2+(\Gamma_1+\Gamma_2)^2}\right] = \frac{1}{2}\left[1-U\right], \tag{9.32}$$

where

$$U(\Gamma_1, \Gamma_2, \omega_e^1, \omega_e^2) = \frac{4\Gamma_1\Gamma_2}{(\omega_e^1 - \omega_e^2)^2 + (\Gamma_1 + \Gamma_2)^2} \tag{9.33}$$

denotes the dependency of the two-photon correlation on the different properties of the two two-level systems.

9.1.4 Dependence of the $g^{(2)}$-function on the properties of the wave function

With Eq. (9.32) and (9.33), the dependence of the $g^{(2)}$-function on the properties of the two wave functions is revealed.
If $\Gamma_1 = \Gamma_2 = \Gamma$ and $\omega_e^1 = \omega_e^2 = \omega$, the two emitted photons will be indistinguishable. For this case, it holds that $U = 1$ and thus $g^{(2)} = 0$, or $V = 1$. This is the so called Hong-Ou-Mandel dip in the two-photon-correlation: if the photons are indistinguishable, they will never be measured simultaneously at both detectors.
If, however, the properties of the two emitted wave packets differ, it follows that $U \neq 1$ and thus $g^{(2)} \neq 0$. Consider the case $\omega_e^1 = \omega_e^2 = \omega$, U reads:

$$U(\Gamma_1, \Gamma_2)\Big|_{\omega_e^1 = \omega_e^2} = \frac{4\Gamma_1\Gamma_2}{(\Gamma_1 + \Gamma_2)^2} \tag{9.34}$$

If it additionally holds that $\Gamma_1 = \Gamma$, $\Gamma_2 = \alpha\Gamma$ where $\alpha \in \mathbf{R}^+$, U becomes:

$$U(\alpha)\Big|_{\omega_e^1 = \omega_e^2, \Gamma_1 = \Gamma, \Gamma_2 = \alpha\Gamma} = \frac{4\alpha}{(\alpha + 1)^2} \tag{9.35}$$

Note that for $\alpha \in \mathbf{R}^+$ it holds that $U(\alpha) \in [0, 1]$. Again, for the case $\alpha = 1$, the two wave packets are indistinguishable and thus $g^{(2)} = 0$. For all other cases, $U(\alpha) < 1$ and $U(\alpha) \to 0$ for $\alpha \gg 1$ as well as $\alpha \ll 1$. In this case, the two wave packets differ strongly, and the $g^{(2)}$-function approaches the value of $\frac{1}{2}$.

9.2 The Hong-Ou-Mandel effect with feedback

Having derived the form of the $g^{(2)}$-function without feedback, in this part, the idea is explored to what extend it is possible to enhance the visibility of two different photons using feedback-control.

9.3 Model

The setup is identical to the one described in Sec. 9.1.1. Now, however, one or two of the emitters are subjected to feedback, thus the emission is being fed back into the system by placing each of the photon sources in a semi-infinite waveguide, cf. Sec. 4.2. Fig. 9.2 depicts a sketch of the setup.

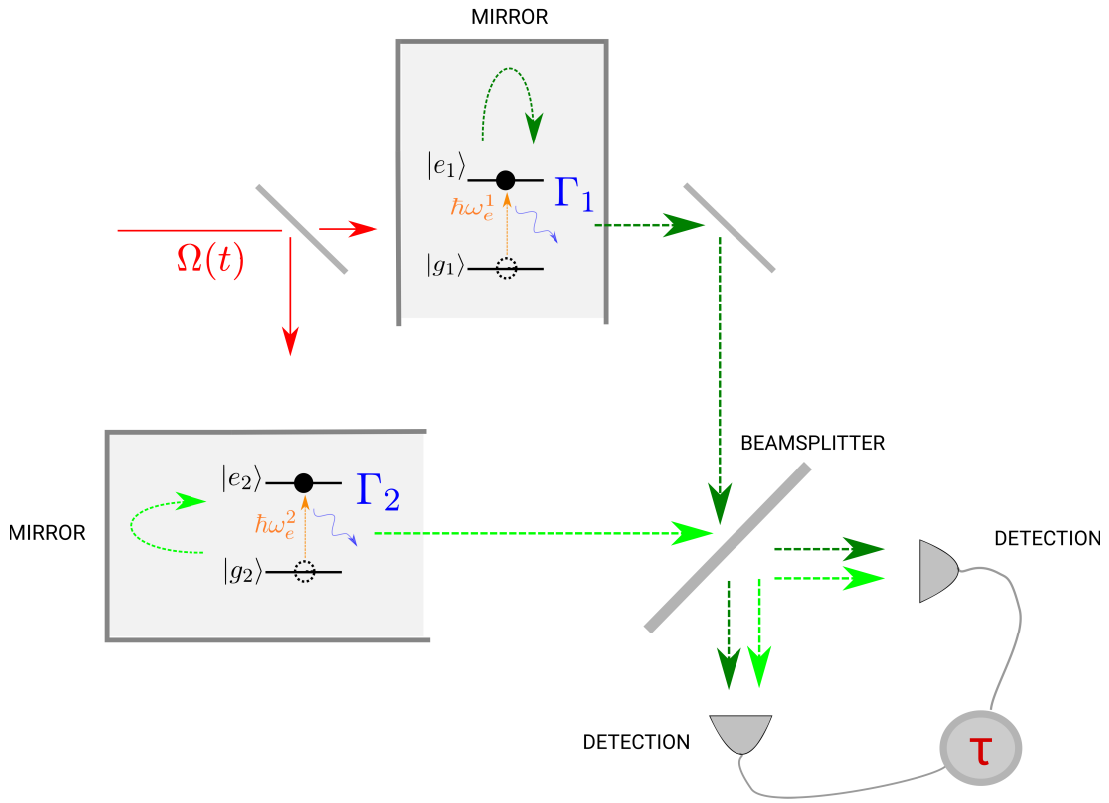

Figure 9.2: Sketch of a Hong-Ou-Mandel type of setup for investigating the two-photon interference where the emitter are now subject to coherent time-delayed feedback control, that is, they are placed in semi-infinite waveguides. Two two-level systems placed in front of a beam splitter and are excited by a resonant pump pulse. During the relaxation process, they emit photons which interfere at the beam splitter. Behind the beam splitter, two detectors are placed which record the transmitted or reflected photons, while the time difference between the two detection events is denoted by τ. However, part of the excitation emitted from the two-level systems will now be reflected by the closed end of the waveguide which serves as a mirror and will interact with the systems again after a feedback delay time $\tilde{\tau}$.

The Hamiltonian for the system remains almost the same as in Eq. (9.6), differing only in the form of the system-reservoir coupling. It thus reads:

$$H = \sum_{j=1,2} \omega_e^j \sigma_{ee}^j + \int d\omega_j \omega_j a_\omega^{j\dagger} a_\omega^j + \Omega(t) \left(e^{-i\omega_p t} \sigma_{eg}^j + e^{i\omega_p t} \sigma_{ge}^j \right) + \int d\omega_j G_{fb}^j(\omega) \left(a_\omega^j \sigma_{eg}^j + a_\omega^{j\dagger} \sigma_{ge}^j \right), \quad (9.36)$$

where the sinusoidal frequency dependent coupling element $G_{fb}^j(\omega)$ with $G_{fb}^j(\omega_j) = g_j \sin\left(\frac{\omega_j L_j}{c_0}\right) = g_j \sin\left(\omega_j \frac{\tilde{\tau}_j}{2}\right)$ as introduced in Eq. (4.3), where L_j is the length of the closed side of the waveguide affecting the jth emitter, c_0 the speed of light in vacuum and $\tilde{\tau}_j = \frac{2L_j}{c_0}$ the resulting delay time of the jth TLS. The equations of motion for the state coefficients now read

$$\partial_t c_{e_j}(t) = -i \int d\omega_j G_{fb}^j(\omega) e^{-i(\omega_j - \omega_e^j)t} c_{g_j}^{\omega_j}(t) \quad (9.37)$$

$$\partial_t c_{g_j}^{\omega_j}(t) = -i G_{fb}^j(\omega) e^{i(\omega_j - \omega_e^j)t} c_{e_j}(t). \quad (9.38)$$

9.3.1 Analytical approach

First, an analytical solution is derived. Here, for simplicity, it is put $\tilde{\tau}_1 = \tilde{\tau}_2 = \tilde{\tau}$. The calculation is demonstrated in the appendix in Sec. 11.4.4. It yields the relaxation dynamics of the emitters:

$$c_{g_j}^{\omega_j}(t) = G_{fb,j}(\omega_j) \sum_{n=0}^{\infty} \frac{\left(\Gamma e^{i\omega_e^j \tau}\right)^n}{n!} \Theta(t - n\tau) e^{-(\Gamma + i(\omega_j - \omega_e^j))(t - n\tau)} \left(\frac{1}{\Gamma + i(\omega_j - \omega_e^j)} (t - n\tau)^n + \sum_{m=1}^{n} \frac{(t - n\tau)^{n-m}}{\left(\Gamma + i(\omega_j - \omega_e^j)\right)^{m+1}} \Pi_{k=0}^{m-1}(n - k) \right) \quad (9.39)$$

Calculating the $g^{(2)}$-function from this solution, however, results in an involved equation even costly when solved numerically, cf. Eq. (11.62) in Sec. 11.4.4. This serves to demonstrate that the the problem formulated with Eq. (9.37) and (9.38) is ideally fitted to be solved with a numerical approach using tMPS.

9.3.2 tMPS-solution: Algorithm and benchmark

The algorithm consists of two two-level emitter under self-feedback and is constructed completely analogous to the derivation in Sec. 11.3.1 and 8.2.2. Here, in a first step, it is assumed that photons emitted by the two different sources differ only in the decay rate Γ_j while the resonance frequency ω_e^j is kept emitter-independent, $\omega_e^1 = \omega_e^2$.

As the state of the reservoir is conserved for each time step, the $g^{(2)}$-function may be calculated straightforward from the obtained MPS by swapping the reservoir bins next to each other as explained in Sec. 8.2.2 and calculating the expectation value according to the procedure explained in Sec. 3.4. With this, the $G^{(2)}(\tau)$-function is calculated for each value of $\tau = j\Delta t$ with $j \in [0, N_T]$, while the $g^{(2)}$-function is obtained with $g^{(2)} = \sum_{j=0}^{N_T} G^{(2)}(j\Delta t)$.
The algorithm is benchmarked using the dependence of the $g^{(2)}$-function on the properties of the wave function, cf. Eq. (9.35) and Eq. (9.32). Thus, it is assumed that it holds for the decay rates that $\Gamma_1 = \Gamma$, $\Gamma_2 = \alpha\Gamma$ where $\alpha \in \mathbf{R}^+$, and the $g^{(2)}$-function is calculated numerically for different α.
Fig. 9.3 depicts the results using Eq. (9.35) and Eq. (9.32) as analytical solution (green line) and comparing it to the numerical computed case (red line). Clearly, the lines are in good accordance, demonstrating the correctness of the employed algorithm.
The plot shows that it holds that $g^{(2)} = 0$ in case of identical decay rates of both emitters, and thus $V = 1$. However, this picture changes if the decay rates differ: Here, with increasing difference, the $g^{(2)}$-function increases and thus the visibility decreases.
Next, both emitter are subject to self-feedback using identical feedback parameters $\phi_1 = \phi_2$, $\tau_1 = \tau_2$. The result is depicted in Fig. 9.3 (blue line). Clearly, for identical decay rates, it holds that $g^{(2)} = 0$, analogous to the case without feedback. For different decay rates, however, the $g^{(2)}$-function yields higher values compared to the case without feedback, thus the visibility decreases.
If only one emitter is influenced by feedback control and the decay rates differ, the visibility decreases by more than one magnitude compared to the case without feedback, for all parameter sets checked numerically. Thus, interestingly, it seems to be the case that for two emitters with the same resonance frequency but with different decay rates, coherent self-feedback may not increase the visibility.
As a next step, the case of detuned emitters will be investigated. Note that the overlap U defined in Eq. (9.33) depends on the detuning $\Delta_{12} \equiv \omega_e^1 - \omega_e^2$ as follows. Consider $\Gamma_1 = \Gamma_2 = 1$, then

$$U(\alpha)\Big|_{\Gamma_1=\Gamma_2=1} = \frac{4}{\Delta_{12}^2 + 4}, \tag{9.40}$$

where again $U = 1$ for $\Delta_{12} = 0$.

9.4 Conclusion

This section investigated the idea of enhancing the indistinguishability of photons radiated by two emitters differing in some properties, for instance in the decay rate or the transition frequency, using coherent time-delayed feedback control. This is done by modeling the intensity correlation of two photons interfering at a beam splitter as a measure for the indistinguishability. The setup is modeled using the tMPS-method and the influence of feedback on the $g^{(2)}$-function is investigated for different feedback parameter sets. However, in case of the sources differing in the decay rate, no enhancement of the

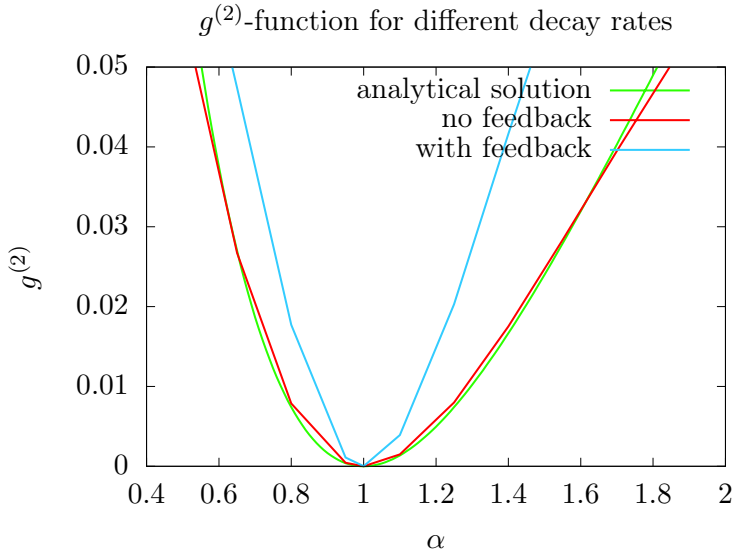

Figure 9.3: Dependence of the $g^{(2)}$-function on the properties of the wave functions of two TLS, where two different decay rates with $\Gamma_1 = \Gamma$ and $\Gamma_2 = \alpha\Gamma$, $\alpha \in \mathbf{R}^+$ are assumed. The green line depicts the analytical solution, cf. Eq. (9.35) and Eq. (9.32).The red line is calculated numerically for different using the tMPS-method and clearly is in good accordance with the analytical solution. The blue line depicts the numerical solution where both emitter are controlled using self-feedback with the same feedback parameters $\phi_1 = \phi_2$, $\tau_1 = \tau_2$. Clearly, for identical decay rates, it holds that $g^{(2)} = 0$, analogous to the case without feedback. For different decay rates, however, the $g^{(2)}$-function yields higher values compared to the case without feedback, thus the visibility decreases.

indistinguishability is achieved. Further work will be to investigate the case of detuned emitters.

10.

Conclusion and outlook

It has been the aim of this thesis to contribute to the research field of many-body systems in non-Markovian interaction with their environment. To this end, in Sec. 6, the one-dimensional Heisenberg spin-1/2 chain is employed as a paradigmatic and recently intensely studied model. With the application of quantum coherent feedback control, a method established for the investigation of single emitter is extended on that model. It is demonstrated that by doing so, it is possible to generate persistent oscillations within the system and thus induce highly non-trivial states which dynamically store excitation within the chain. These oscillations occur at special points in the parameter space and persists for different chain lengths and different initial excitations within the chain. Also, the non-invasive partial characterization of the chain is demonstrated by exploiting on the fact that the different trapping conditions each relate to specific steady states within the chain. Directions of future research on this topic include for instance the investigation of the influence of disorder on the system. Preliminary numerical results for Heisenberg chains with lower symmetries, shifts, and also anisotropies indicate a connection between the eigenvalues of the system and the trapping conditions. Likewise, it would be of high interest to investigate the system dynamics if more sites are coupled to the waveguide.
In Sec. 7, a novel model for a boundary driven many-body system has been presented, also using the model of the Heisenberg spin-chain with nearest-neighbor interaction. Here, the chain is exposed to a coherent, resonant driving field on one end while coupled dissipatively to a reservoir on its other side, and the transport properties of the chain in the non-equilibrium steady state are investigated. This novel approach contrasts and complements the dominant model in the research field, where the potential difference is realized with an incoherent driving using a full Markovian approximation by coupling its first and last site to reservoirs which are described with the Lindblad formalism. It is shown that for the weak driving regime, both driving realizations induce anomalous transport

behavior which is characterized as superdiffusive. This novel implementation poses most interesting possibilities for the comparison of the out-of-equilibrium properties - e.g. spin transport properties, entanglement growth or energy transport - of many-body systems driven either coherently or with a full Markovian approximation. Also, it allows for the possibility of investigating driven many-body systems in non-Markovian interaction with their environment, a setup highly interesting for studying properties of open quantum many-body systems and for future applications in the field of quantum information technologies.

Sec. III was dedicated to single-emitter system-reservoir interaction in the non-Markovian regime by investigating the case of fully coherent self-feedback. In the first part, Sec. 8, the control of a non-degenerate Λ-type system with coherent self-feedback has been discussed. Here, the novel approach of controlling the system with an external pump field has been introduced, with the motivation of further investigating the influence of the feedback phase and establishing methods for controlling it. For the unpumped case, it is demonstrated that stabilization may be achieved at certain delay times. When applying a continuous external field, new trapping conditions arise. It is shown that the Rabi frequency of the driving field serves as a new control parameter, which gives rise to the possibility of disentangling the two intertwined feedback parameters, the delay time τ and the feedback phase ϕ. Depending on the properties of the system - the transition frequencies ω_2 and ω_3 - the smallest possible delay time τ may be achieved with or without an external pump field. Thus, the results presented here not only broaden the possibilities of feedback control significantly, but also enable a reduction of the transient time and thus a stabilization at higher excited state densities for the investigated system. As a direction for future research, further control options using a time-dependent pump pulse might be explored.

In the last chapter, Sec. 9, the influence of time-delayed feedback control on the intensity correlation $g^{(2)}(\tau)$ of two photons interfering at a beamsplitter as a measure for the indistinguishability was investigated. Here, the setup is modeled using tMPS and the influence of feedback on the $g^{(2)}$-function is investigated for different feedback parameter sets. However, in case of the sources differing in the decay rate, no enhancement of the indistinguishability is achieved. Further work includes the study of the case of photon sources also differing in their transition frequencies.

In summary, it can be stated that with these results, the thesis at hand offers a theoretical model to study open quantum systems. It sheds light on topics such as non-equilibrium steady-states, non-Markovianity, properties of many-body systems and coherent feedback control. With this, it contributes to a better understanding of the control of many-body systems as well as of few-level emitter and their applications for quantum simulation and quantum information processing.

11.

Appendix

11.1 Calculations for the derivation of the quantum optical master equation

In Sec. 2.3, the aim is to calculate the following equation:

$$tr_{\mathrm{R}}(d\rho(t)) = -\frac{i}{\hbar}dt\big[H_{\mathrm{eff}}\rho(t)_{\mathrm{sys}} + \rho(t)_{\mathrm{sys}}H_{\mathrm{eff}}\big] + tr_{\mathrm{R}}\big[(d\,|\psi(t)\rangle)(d\,\langle\psi(t)|)\big] \tag{11.1}$$

with $\rho(t)_{\rm sys} = |\psi(t)\rangle_{\rm sys}\,\langle\psi(t)|_{\rm sys}$ the system density matrix.
To this end, Eq. (2.60) is inserted into the last term in Eq. (11.1). This yields

$$
\begin{aligned}
&tr_{\rm R}\Big[(d\,|\psi(t)\rangle)(d\,\langle\psi(t)|)\Big] = \\
&= tr_{\rm R}\Big[\Big(-\frac{i}{\hbar}H_{\rm eff}\,dt + \sqrt{\Gamma}g_0\,c\,dB^\dagger(t) + H_{\rm sys}cd\bar{B}_1 + d\bar{B}_2cH_{\rm sys}\Big)\,|\psi(t)\rangle\,\langle\psi(t)| \\
&\Big(-\frac{i}{\hbar}H_{\rm eff}^\dagger\,dt + \sqrt{\Gamma}g_0c^\dagger dB + d\bar{B}_1^\dagger c^\dagger H_{\rm sys}^\dagger + H_{\rm sys}^\dagger c^\dagger d\bar{B}_2^\dagger\Big)\Big] \\
&= tr_{\rm R}\Big[dtH_{\rm eff}\rho(t)dtH_{\rm eff}^\dagger + \sqrt{\Gamma}g_0dB^\dagger c\rho(t)dtH_{\rm eff}^\dagger \\
&+ H_{\rm sys}cd\bar{B}_1^\dagger\rho(t)dtH_{\rm eff}^\dagger + d\bar{B}_2cH_{\rm sys}\rho(t)dtH_{\rm eff}^\dagger \\
&+ dtH_{\rm eff}\rho(t)\sqrt{\Gamma}g_0c^\dagger dB(t) + \Gamma g_0^2dB^\dagger c\rho(t)c^\dagger dB(t) \\
&+ H_{\rm sys}d\bar{B}_1^\dagger c\rho(t)\sqrt{\Gamma}g_0c^\dagger dB(t) + d\bar{B}_2cH_{\rm sys}\rho(t)\sqrt{\Gamma}g_0c^\dagger dB(t) \\
&+ dtH_{\rm eff}\rho(t)H_{\rm sys}cd\bar{B}_1^\dagger + \sqrt{\Gamma}g_0dB^\dagger c\rho(t)d\bar{B}_1^\dagger c^\dagger H_{\rm sys}^\dagger \\
&+ H_{\rm sys}cd\bar{B}_1^\dagger\rho(t)d\bar{B}_1^\dagger c^\dagger H_{\rm sys}^\dagger + d\bar{B}_2cH_{\rm sys}\rho(t)d\bar{B}_1^\dagger c^\dagger H_{\rm sys}^\dagger \\
&+ dtH_{\rm eff}\rho(t)H_{\rm sys}^\dagger c^\dagger d\bar{B}_2^\dagger + \sqrt{\Gamma}g_0dB^\dagger c\rho(t)H_{\rm sys}^\dagger c^\dagger d\bar{B}_2^\dagger \\
&+ H_{\rm sys}cd\bar{B}_1^\dagger\rho(t)H_{\rm sys}^\dagger c^\dagger d\bar{B}_2^\dagger + d\bar{B}_2cH_{\rm sys}\rho(t)H_{\rm sys}^\dagger c^\dagger d\bar{B}_2^\dagger\Big]
\end{aligned}
\tag{11.2}
$$

As only summands of order of Δt have to be taken into account, the terms in Eq. (11.2) are analyzed by making use of the cyclic property of the trace and of the Born factorization. This yields for instance:

$$
\begin{aligned}
&tr_{\rm R}\big[dB^\dagger c\rho(t)c^\dagger dB(t)\big] \\
&=tr_{\rm R}\big[dB^\dagger c\big(\rho(t)_{\rm sys}\otimes\rho(t)_{\rm res}\big)c^\dagger dB(t)\big] \\
&=tr_{\rm R}\big[\rho(t)_{\rm res}dB(t)dB^\dagger c\rho(t)_{\rm sys}c^\dagger\big] \\
&=tr_{\rm R}\big[\rho(t)_{\rm res}dB(t)dB^\dagger\big]tr_{\rm R}\big[c\rho(t)_{\rm sys}c^\dagger\big] \\
&=tr_{\rm R}\left[\frac{g_0^2}{2\pi}\int_0^{dt}dt'\int d\omega b(\omega)e^{-i(\omega-\omega_0)t'}\int_0^{dt}dt''\int d\omega' b^\dagger(\omega')e^{i(\omega'-\omega_0)t''}\right]c\rho(t)_{\rm sys}c^\dagger \\
&=tr_{\rm R}\left[\frac{g_0^2}{2\pi}\int d\omega\int_0^{dt}dt'\int_0^{dt}dt''e^{-i(\omega-\omega_0)(t'-t'')}\right]c\rho(t)_{\rm sys}c^\dagger \\
&=tr_{\rm R}\left[\frac{g_0^2}{c}\int_0^{dt}dt'\int_0^{dt}dt''e^{-(t'-t'')}\delta(t'-t'')\right]c\rho(t)_{\rm sys}c^\dagger = \frac{g_0^2}{c}dtc\rho(t)_{\rm sys}c^\dagger.
\end{aligned}
\tag{11.3}
$$

where in the second last step, the commutation relations (2.16) and the action on the vacuum reservoir have been exploited.
This term is the only term in Eq. (11.2) which is of order of Δt. All other terms are

neglected as they are of higher order in dt. This is demonstrated exemplary for one term:

$$
\begin{aligned}
&tr_{\mathrm{R}}\Big[d\bar{B}_1^\dagger H_{\mathrm{sys}} c\rho(t) c^\dagger dB(t)\Big] = tr_{\mathrm{R}}\Big[\rho(t)_{\mathrm{res}} dB(t) d\bar{B}_1^\dagger\Big] H_{\mathrm{sys}} c\rho(t)_{\mathrm{sys}} c^\dagger \\
&\quad = tr_{\mathrm{R}}\Big[\rho(t)_{\mathrm{res}} \frac{g_0^2}{2\pi} \int_0^{dt} dt' \int_0^{t'} dt'' \int d\omega' b^\dagger(\omega') e^{i(\omega'-\omega_0)t''} \int_0^{dt} dt' \int d\omega b(\omega) e^{-i(\omega-\omega_0)t'}\Big] H_{\mathrm{sys}} c\rho(t)_{\mathrm{sys}} c^\dagger \\
&\quad = \frac{g_0^2}{c} \int_0^{dt} dt' \int_0^{t'} dt'' = \mathcal{O}(dt^2) \to 0. \qquad (11.4)
\end{aligned}
$$

With this, Eq. (11.2) reduces to:

$$
tr_{\mathrm{R}}\Big[(d\,|\psi(t)\rangle)(d\,\langle\psi(t)|)\Big] = \Gamma dt c\rho(t)_{\mathrm{sys}} c^\dagger. \qquad (11.5)
$$

11.2 The W-state as a matrix product state

In order to give an example for the decomposition of a quantum state, the W-state [5] will now be decomposed into an MPS, which serves as an example of a multipartite entangled quantum state. It takes the form

$$
|W\rangle = \frac{1}{\sqrt{3}} \left(|001\rangle + |010\rangle + |100\rangle\right) \qquad (11.6)
$$

where from now on, the normation factor $\frac{1}{\sqrt{3}}$ will now be omitted for reasons of simplicity. The first step is to reshape the coefficient tensor C_{i_1,i_2,i_3} into a matrix $\bar{C}_{i_1,(i_2,i_3)} \in \mathbf{R}^{2\times 4}$:

$$
\bar{C}_{i_1,(i_2,i_3)} = \begin{pmatrix} 0 & 1 & 1 & 0 \\ 1 & 0 & 0 & 0 \end{pmatrix} \qquad (11.7)
$$

An SVD decomposition of 11.7 yields:

$$
\begin{aligned}
\bar{C} &= U_{a_1}^{i_1} \cdot S_{a1,a2} \cdot (V^T)_{a_2,(i_2,i_3)} \\
&= \begin{pmatrix} 1 & 0 \\ 0 & 1 \end{pmatrix} \cdot \begin{pmatrix} \sqrt{2} & 0 & 0 & 0 \\ 0 & 1 & 0 & 0 \end{pmatrix} \cdot \begin{pmatrix} 0 & \frac{1}{\sqrt{2}} & \frac{1}{\sqrt{2}} & 0 \\ 1 & 0 & 0 & 0 \\ 0 & 0 & 0 & 1 \\ 0 & -\frac{1}{\sqrt{2}} & \frac{1}{\sqrt{2}} & 0 \end{pmatrix}
\end{aligned}
$$

where the third and fourth row in V^T have been added to complete the ONS.
$U_{a_1}^{i_1}$ is decomposed into two row vectors:

$$
A^{i_1=0} = \begin{pmatrix} 1 & 0 \end{pmatrix} \qquad (11.8)
$$

$$
A^{i_1=1} = \begin{pmatrix} 0 & 1 \end{pmatrix} \qquad (11.9)
$$

Next, $S \cdot V^T = \begin{pmatrix} 0 & 1 & 1 & 0 \\ 1 & 0 & 0 & 0 \end{pmatrix}$ is calculated and reshaped:

$$
S \cdot V^T = \bar{C}_{(a_1 i_2),i_3} = \begin{pmatrix} 0 & 1 \\ 1 & 0 \\ 1 & 0 \\ 0 & 0 \end{pmatrix}
$$

An SVD yields:

$$\begin{aligned}\bar{C}_{(a_1,i_2),i_3} &= U_{(a_1,i_2),a_2} \cdot S_{a_2,a_3} \cdot (V^T)_{a_3,i_3} \\ &= \begin{pmatrix} 0 & 1 \\ \frac{1}{\sqrt{2}} & 0 \\ \frac{1}{\sqrt{2}} & 0 \\ 0 & 0 \end{pmatrix} \cdot \begin{pmatrix} \sqrt{2} & 0 \\ 0 & 1 \end{pmatrix} \cdot \begin{pmatrix} 1 & 0 \\ 0 & 1 \end{pmatrix}\end{aligned}$$

Next, $U_{(a_1,i_2),a_2}$ is decomposed into two matrices of the dimensions (2×2):

$$A^{i_2=0}_{a_1,a_2} = \begin{pmatrix} 0 & 1 \\ \frac{1}{\sqrt{2}} & 0 \end{pmatrix} \tag{11.10}$$

$$A^{i_2=1}_{a_1,a_2} = \begin{pmatrix} \frac{1}{\sqrt{2}} & 0 \\ 0 & 0 \end{pmatrix} \tag{11.11}$$

The last step is to calculate

$$\bar{C}_{(a_1 i_2),i_3} = S_{a_2,a_3} \cdot (V^T)_{a_3,i_3} = \begin{pmatrix} \sqrt{2} & 0 \\ 0 & 1 \end{pmatrix}$$

and decompose the result into two column vectors:

$$A^{i_3=0}_{a_3} = \begin{pmatrix} \sqrt{2} \\ 0 \end{pmatrix} \tag{11.12}$$

$$A^{i_3=1}_{a_3} = \begin{pmatrix} 0 \\ 1 \end{pmatrix} \tag{11.13}$$

Putting together equations 11.8 - 11.13, it is finally possible to write the W-state in 11.6 in its full, left-canonical MPS form, which reads as:

$$\begin{aligned}|W\rangle &= |001\rangle + |010\rangle + |100\rangle \\ &= \sum_{i_1,i_2,i_3} A^{i_1} A^{i_2} A^{i_3} \, |i_1\, i_2\, i_3\rangle \\ &= A^{i_1=0} A^{i_2=0} A^{i_3=1} \, |001\rangle + A^{i_1=1} A^{i_2=0} A^{i_3=0} \, |010\rangle + A^{i_1=1} A^{i_2=0} A^{i_3=0} \, |100\rangle\end{aligned}$$

$$\begin{aligned}= \begin{pmatrix} 1 & 0 \end{pmatrix} \begin{pmatrix} 0 & 1 \\ \frac{1}{\sqrt{2}} & 0 \end{pmatrix} \begin{pmatrix} 0 \\ 1 \end{pmatrix} |001\rangle &+ \begin{pmatrix} 1 & 0 \end{pmatrix} \begin{pmatrix} \frac{1}{\sqrt{2}} & 0 \\ 0 & 0 \end{pmatrix} \begin{pmatrix} \sqrt{2} \\ 0 \end{pmatrix} |010\rangle \\ &+ \begin{pmatrix} 1 & 0 \end{pmatrix} \begin{pmatrix} 1 & 0 \\ \frac{1}{\sqrt{2}} & 0 \end{pmatrix} \begin{pmatrix} \sqrt{2} \\ 0 \end{pmatrix} |100\rangle \, .\end{aligned}$$

After this introduction and demonstration of the decompositions in the MPS form, the application of operators on this state will be explained.

11.3 Analytical benchmark of the tMPS code for a two-level emitter

11.3.1 Modeling quantum coherent self-feedback for a two-level emitter with tMPS

The start of the derivation is the Hamiltonian which is already in the rotating frame defined by its freely evolving part and which is given in Eq. (4.2). In order to achieve a facilitating description for the numerical simulation, the full Hamiltonian in Eq. (4.2) has to be transformed to a suitable basis. First, it is transformed into the rotating frame defined by its freely evolving part as demonstrated in Equation-(4.6). It reads:

$$H'(t) = \int d\omega \left(G_{fb}(\omega)\sigma^{+} b(\omega) e^{-i(\omega-\omega_0)t} + \text{h.c.} \right) \tag{11.14}$$

Next, another unitary transformation is applied, in order to shift the dependency of the delay time τ into the operators. This unitary operator U_2 is defined as:

$$U_2 = \exp\left[-i\frac{\tau}{2} \int d\omega \omega b^{\dagger}(\omega) b(\omega) \right] \tag{11.15}$$

This yields:

$$H'(t) = +ig_0 \int d\omega \left(\sigma^{+} \left(b(\omega) e^{-i(\omega-\omega_0)t} - b(\omega) e^{-i(\omega-\omega_0)t} e^{i\omega\tau} \right) + \text{h.c.} \right) \tag{11.16}$$

The time dependent reservoir operators $b^{(\dagger)}(t)$ introduced in Sec. 2.2 in Eq. (2.21) with

$$b(t) = \frac{1}{\sqrt{2\pi}} \int d\omega b(\omega) e^{-i(\omega-\omega_0)t} \tag{11.17}$$

are inserted into Eq. (11.16). As demonstrated in Sec. 2.2 in Eq. (2.25), their commutation relation is proportional to a δ-peak in time space:

$$[b(t), b^{\dagger}(t')] = \delta(t-t')\pi g_0^2 e^{i\omega_0(t-t')}, \tag{11.18}$$

which means that they model white noise, cf. Sec. 2.2.
This yields the transformed Hamiltonian H'':

$$H''(t) = +i\sqrt{\Gamma}\Big(b(t) - b(t-\tau)e^{i\phi} \Big)\sigma^{+} - i\sqrt{\Gamma}\Big(b^{\dagger}(t) - b^{\dagger}(t-\tau)e^{-i\phi} \Big)\sigma^{-} \tag{11.19}$$

with the delay time τ and the feedback phase $\phi = \omega_0\tau$ as introduced in Sec. 4.
The time evolution operator is defined as:

$$U(t, t_0) = \hat{T} \exp\left(-i \int_{t_0}^{t} H''(t')dt' \right). \tag{11.20}$$

As explained in Sec. 2.2.5, $U(t, t_0)$ may discretized in the basis of the time discrete quantum noise operators $\Delta B^{(\dagger)}(t_k)$, which have been introduced in Sec. 2.2.2, cf. Eq. (2.35), and include the interaction with the reservoir at one time step with a stochastic, continuous description

$$\Delta B^{(\dagger)}(t_k) = \int_{t_k}^{t_{k+1}} dt' b^{(\dagger)}(t'). \tag{11.21}$$

They obey canonical commutation relation defined in Eq. (2.36) up to a normalization factor of Δt, but note importantly, that $B^{(\dagger)}(t_k)$ and $B^{(\dagger)}(t_{k-l})$ only commute for $\Delta t = t_{k+1} - t_k < \tau$.
Discretizing Eq. (11.20) in this basis yields the following time evolution operator

$$\begin{aligned} &U(t_{k+1}, t_k) = \\ &\quad = \exp\left[+ \sqrt{\Gamma}\Big(\Delta B(t_k) - \Delta B(t_{k-l}) e^{i\phi}\Big)\sigma^+ - \sqrt{\Gamma}\left(\Delta B^\dagger(t_k) - \Delta B^\dagger(t_{k-l}) e^{-i\phi}\right)\sigma^-\right] \end{aligned} \tag{11.22}$$

for $k \in [0, N_T - 1]$ as integer of the time steps, where the time evolution operator $\hat{T}$ may be dropped for equidistant time steps $\Delta t = t_{k+1} - t_k$, cf. Sec. 2.2.5. Here, t_k denotes the kth time step, while $t_{k-l} = (k-l)\Delta t$ denotes the time delayed by τ, thus $\tau = l\Delta t$. Introducing the normalized basis states, cf. Eq. (2.37) in Sec. 2.2.2, which read as

$$|i_p\rangle = \frac{(\Delta B^\dagger(t_k))^{i_p}}{\sqrt{i_p! \Delta t^{i_p}}} |\text{vac}\rangle\,, \tag{11.23}$$

where i_p, p integer, denotes the number of excitations present in the Fock state of the kth time interval $|i_p\rangle$, the time evolution of $|\psi(t)\rangle$ may now be computed as a stroboscopic map, cf. Sec. 2.2.2:

$$\begin{aligned} |\psi(t_{k+1})\rangle &= \exp\left(-i \int_{k\Delta t}^{(k+1)\Delta t} H'(t') dt'\right) |\psi(t_k)\rangle \otimes |i_{k+1} = 0\rangle \\ &= U(t_{k+1}, t_k) |\psi(t_k)\rangle \otimes |i_{k+1} = 0\rangle \end{aligned} \tag{11.24}$$

This will be done using the tensor network method tMPS which has been introduced in Sec. 3.1. The corresponding construction of the wave vector as well as the algorithm architecture is completely analogous to the case of the Λ-type system and is thus explained in Sec. 8.2.2.

11.3.2 Benchmark plots: computing feedback with tMPS

Note that Figures 11.1-11.2 furthermore serve as benchmarks for the numerical method applied in this thesis, as they also show the solution obtained with the tMPS program described in Sec. 11.3.1 (black dotted lines), demonstrating its full accordance with the analytical solution.

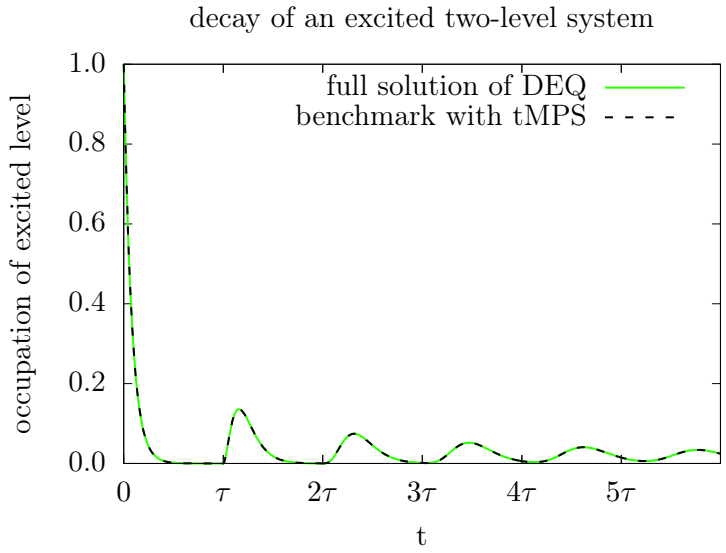

Figure 11.1: Decay of an excited two-level emitter in a semi-infinite waveguide under the influence of self-feedback. The plot depicts the occupation density of the excited level for a long feedback time $\Gamma\tau \gg 1$ over the feedback time intervals, computed from the full solution of the equations of motion, cf. Section 4.1. Clearly, during the 0th τ-interval, the entire excitation dissipates into the reservoir. During the first τ-interval, the first interaction with the feedback signal occurs and a re-absorbance of the emitter of its own past becomes visible, which again decays completely during this period. This process repeats itself during the following τ-intervals, while the amplitude of the excitation decreases, as part of the excitation is lost during each interval. In the limit of long times, this periodic process of emittance and re-absorbance will either lead to a complete decay of the atom and thus to a trivial steady state $c_e(t \to \infty) = 0$ or to a finite excitation within the system. Note that this plot furthermore serve as benchmarks for the numerical method applied in this thesis, as it also shows the solution obtained with the tMPS program described in Sec. 11.3.1 (black dotted lines), demonstrating its full accordance with the analytical solution.

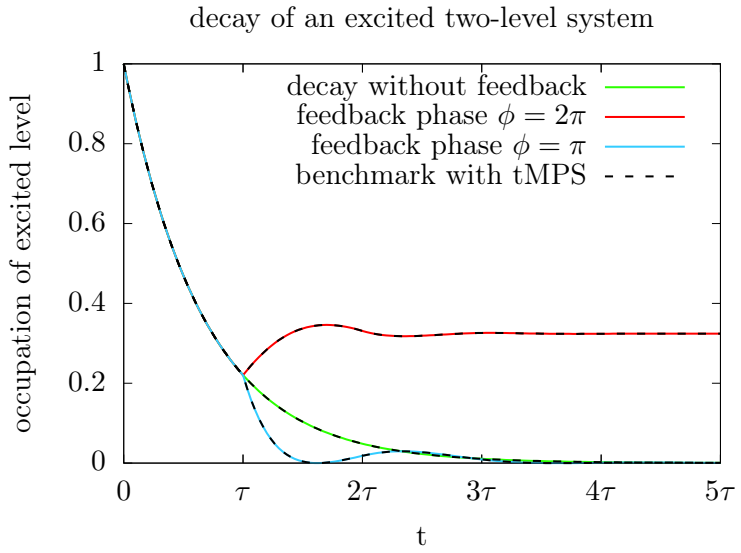

Figure 11.2: Decay of an excited two-level emitter in a semi-infinite waveguide, without feedback (green line) and under the influence of self-feedback (red and blue lines). The plot depicts the occupation density of the excited level for a short feedback time $\Gamma\tau \ll 1$ over the feedback time intervals, computed from the full solution of the equations of motion, cf. Section4.1. In this case, the feedback phase ϕ - the phase between emission and re-absorption - matters, while its choice may either slow down or speed up the decay process. Here, for the case of a fully constructive feedback phase $\phi = 2n\pi$, $n \in \mathbf{N}$, a non-trivial solution for the long-time steady-state is obtained, where $c_e(t \to \infty) = \text{const}$ and $c_e(t \to \infty) > 0$ (red line in Fig. 11.2). During the 0th τ-interval, the initial excitation first dissipates partially into the reservoir. In the 1st τ-interval, this process is stopped by the interaction with the feedback signal. In the following τ-intervals, after a convergence time, the system-reservoir interaction reaches a steady-state and dynamically traps the remaining excitation within the chain. The blue line depicts the case of a destructive feedback phase $\phi = (2n+1)\pi$, which enhances the decay process most strongly. Clearly, compared to the case without feedback (green line), the excitation dissipates quicker into the reservoir. Note that this plot furthermore serves as a benchmark for the numerical method applied in this thesis, as it also shows the solution obtained with the tMPS program described in Sec. 11.3.1 (black dotted lines), demonstrating its full accordance with the analytical solution.

11.4 Modeling system dynamics in Liouville space using MPS

11.4.1 Basis transformation and mapping into Liouville space

This adaption follows two important ideas, recently proposed by [121]. The first one is to treat the density matrix operator $\rho(t)$ not as an operator, but as a pure quantum state, and to use the MPS formalism in order to describe its time evolution: Within the framework of matrix product states, the state and not the operators are evolved in time. In order to do so, the Lindblad superoperator $\mathcal{L}$ has to be written as an time-independent matrix product operator which describes the time evolution of the state of $\rho(t)$.

Secondly, the system is mapped from the carthesian basis $\left\{ \begin{pmatrix} 0 \\ 1 \end{pmatrix}, \begin{pmatrix} 1 \\ 0 \end{pmatrix} \right\}$ to another basis, one which is more convenient for the calculation and description of the matrix product operators in the algorithm and allows for an calculation of expectation values using the MPS framework. This basis consists of the Pauli spin matrices σ_x, σ_y and σ_z, while the forth basis state σ_0 is defined as the identity matrix. Hence the basis is

$$\sigma_0 = \begin{pmatrix} 1 & 0 \\ 0 & 1 \end{pmatrix}, \quad \sigma_1 \equiv \sigma_x = \begin{pmatrix} 0 & 1 \\ 1 & 0 \end{pmatrix}, \quad \sigma_2 \equiv \sigma_y = \begin{pmatrix} 0 & -i \\ i & 0 \end{pmatrix}, \quad \sigma_3 \equiv \sigma_z = \begin{pmatrix} 1 & 0 \\ 0 & -1 \end{pmatrix}. \tag{11.25}$$

Therefore, ρ is element of a 4^n-dimensional Hilbert space, and is now described with:

$$\rho = \sum_{i_1, i_2 \ldots i_N} c_{i_1, i_2 \ldots i_N} (\sigma_{i_1} \otimes \sigma_{i_2} \otimes \cdots \otimes \sigma_{i_N}), \tag{11.26}$$

with $i_k = 1, 2, 3, 4$. Hence, the density operator may be expressed as a state vector $\rho \to |\rho\rangle$ with the following basis

$$\sigma_0 \equiv |0\rangle \equiv \begin{pmatrix} 1 \\ 0 \\ 0 \\ 0 \end{pmatrix} \quad \sigma_x \equiv |1\rangle \equiv \begin{pmatrix} 0 \\ 1 \\ 0 \\ 0 \end{pmatrix} \quad \sigma_y \equiv |2\rangle \equiv \begin{pmatrix} 0 \\ 0 \\ 1 \\ 0 \end{pmatrix} \quad \sigma_z \equiv |3\rangle \equiv \begin{pmatrix} 0 \\ 0 \\ 0 \\ 1 \end{pmatrix} \quad . \tag{11.27}$$

With this, the density operator reads:

$$|\rho\rangle = \sum_{i_1, i_2 \ldots i_N} c_{i_1, i_2 \ldots i_N} \, |\sigma_{i_1} \sigma_{i_2} \ldots \sigma_{i_N}\rangle \, . \tag{11.28}$$

Thus, ρ takes the form of a state vector residing in a 4^n-dimensional Hilbert space and is no longer written as a matrix but as a vector, whose basis is built by matrices. Its coefficient tensor $c_{i_1, i_2 \ldots i_N}$ may be decomposed into $4N$ matrices A_i of the dimensions $A_i \in \mathbf{C}^{4 \times 1}$, cf. Sec. 3.2:

$$|\rho\rangle = \sum_{i_1, i_2 \ldots i_N} A^{i_1} A^{i_2} \ldots A^{i_N} \, |\sigma_{i_1} \sigma_{i_2} \ldots \sigma_{i_N}\rangle \, . \tag{11.29}$$

Analogous to this, the super-operator $\mathcal{L}$ may now be written as an matrix product operator. Its specific form will be derived in Sec. 11.4.3. With this, the time evolution may be performed completely analogous to the evolution of pure states in the Schrödinger picture, cf. Sec. 3.3 and 3.5. Note, however, that in case of $\mathcal{L}$ generating non-unitary transformations - as it will be the case if it describes time-irreversible dynamics using the master equation - within the MPS formalism, the canonical form of the MPS will not be preserved during its application: The MPS is no longer orthonormal after the application of the MPO, which means that the bond values are no longer identical to the Schmidt values and thus, when truncating them, additional information would be lost [105, 120]. In order to avoid this, the MPS has to be re-orthogonalized after the application of the operator, which means each matrix of the chain has to be decomposed and contracted again, bringing it back into the canonical form.

11.4.2 Calculation of expectation values

One of the advantages of the application of the MPS formalism is that the calculation of expectation values within is possible at relatively low computational costs, cf. Section3.4). In order to exploit this, the expectation value of an operator O has to be calculated in the Schrödinger picture with $\langle O\rangle = \langle\psi| O |\psi\rangle$. However, for mixed states in the density matrix picture the trace has to be calculated, thus:

$$\langle O\rangle = \mathrm{Tr}\left(\rho O\right) = \mathrm{Tr}\left(\sum_i p_i \left|\psi_i\right\rangle \left\langle\psi_i\right| O\right) = \sum_i p_i \left\langle\psi_i\right| O \left|\psi_i\right\rangle . \tag{11.30}$$

However, the $\{|\psi_i\rangle\}$ do in principle not factorize, and the entanglement information is contained in the single matrices A_m of the MPS decomposition. Hence, the standard MPS-contraction method, cf. Sec. 3.4, is not to be applied in for the calculation of expectation values in Liouville space.
In this thesis, two different methods for the calculation of expectation values have been developed, which both make use of the MPS formalism, however transforming it into Liouville space.
The first one calculates the exact expectation values by contracting the MPS-decomposition into one single tensor, after which the expectation values may be read off directly. Its computational costs, however, are large and thus, it can only be made use for for small chain lengths and for benchmarking the program. Exploiting the property of the Pauli matrices that

$$\mathrm{Tr}\left(\sigma^x\right) = \mathrm{Tr}\left(\sigma^y\right) = \mathrm{Tr}\left(\sigma^z\right) = 0, \tag{11.31}$$

and the contracted tensor $|\rho\rangle$ is of the form

$$|\rho\rangle = \sum_{i_1 \ldots i_N} c_{i_1 \ldots i_N} \left|\sigma^{i_1} \ldots \sigma^{i_N}\right\rangle , \tag{11.32}$$

with $i_k \in (0,1,2,3)$. Let O be an arbitrary operator acting on $|\rho\rangle$. If mapped into the basis of Pauli matrices, it reads

$$O = \sum_{j_1 \dots j_N} \tilde{c}_{j_1 \dots j_N} |\sigma^{j_1} \dots \sigma^{j_N}\rangle . \tag{11.33}$$

Thus calculating $\langle O \rangle$ is done with

$$\langle O \rangle = \mathrm{Tr}\,(O\rho) = \mathrm{Tr}\left(\sum_{i_1 \dots i_N} c_{i_1 \dots i_N} |\sigma^{i_1} \dots \sigma^{i_N}\rangle \sum_{j_1 \dots j_N} \tilde{c}_{j_1 \dots j_N} |\sigma^{j_1} \dots \sigma^{j_N}\rangle \right) \tag{11.34}$$

$$= \sum_{i_1 \dots i_N} \sum_{j_1 \dots j_N} c_{i_1 \dots i_N} \tilde{c}_{j_1 \dots j_N} \mathrm{Tr}\left(|\sigma^{i_1} \sigma^{j_1} \dots \sigma^{i_N} \sigma^{j_N}\rangle \right) \tag{11.35}$$

$$= \sum_{i_1 \dots i_N} \sum_{j_1 \dots j_N} c_{i_1 \dots i_N} \tilde{c}_{j_1 \dots j_N} \mathrm{Tr}_N\,(\sigma^{i_N} \sigma^{j_N}) \dots \mathrm{Tr}_1\,(\sigma^{i_1} \sigma^{j_1}) \tag{11.36}$$

$$= \begin{cases} 2^N c_{i_1 \dots i_N} \tilde{c}_{j_1 \dots j_N} & \text{if} \quad i_k = j_k \quad \forall k \in (1, \dots, N) \\ 0 & \text{else,} \end{cases} \tag{11.37}$$

where the last condition arises from the fact that if two Pauli matrices are multiplied, it yields the identity matrix only if the matrices are identical, $\sigma_i \sigma_j = \sigma_0$ if and only if $i = j$.

The second way uses the canonical form of the MPS $|\rho\rangle$ and defines MPOs O in Liouville space for each observable $\langle O \rangle$ which makes it possible to use the standard MPS formalism such that it holds $(\langle O \rangle)^2 = \langle \rho | O | \rho \rangle$, but by doing so, sign and phase of the entries of $|\rho\rangle$ are lost during the calculation. This is one important reason for choosing the Pauli matrices as a basis: with that, all coefficients $c_{i_1 \dots i_k}$ are $\in \mathbf{R}$ and calculating $c^2_{i_1 \dots i_k}$ means only the sign of $\langle O \rangle$ is lost. As it preserves the decomposed structure of the MPS, it is much more efficient than the first method.

The definition of the MPO is done as follows: assuming the operator O_k acts on the kth site. First, it is transformed into the basis of the Pauli matrices, thus $O_k \to |O\rangle_k$. As demonstrated in Sec. 3.3, the coefficients of the MPO are defined with

$$\tilde{c}_{(i_1, i_1'), \dots, (i_N, i_N')} = W^{i_1 i_1'} \dots W^{i_k i_k'} \dots W^{i_N i_N'}. \tag{11.38}$$

Now, putting

$$W^{i_l i_l'} = I \tag{11.39}$$

for all $l \neq k$, and

$$W^{i_k i_k'} = |O\rangle_k \langle O|_k \tag{11.40}$$

and calculating $\langle \rho(t) | O | \rho(t) \rangle$ as demonstrated in Sec. 3.3 will read of all needed coefficients squared, thus

$$\langle \rho(t) | O | \rho(t) \rangle = c^2_{i_1=0} \cdot c^2_{i_2=0} \cdot \dots c^2_{i_k=3} \cdot \dots c^2_{i_{N-1}=0} \dots c^2_{i_N=0} \tag{11.41}$$

$$= c^2_{0 \dots 3 \dots 0}, \tag{11.42}$$

and thus

$$\langle M_k \rangle = 2^N \sqrt{\langle \rho(t) | O_k | \rho(t) \rangle}. \tag{11.43}$$

11.4.3 Derivation of the matrix product operator

As explained in Sec. 11.4, the Pauli spin matrices are chosen as a suitable basis for the time-evolution, cf. Eq. (11.27), and the density matrix $\rho(t)$ is mapped into a state vector written in this basis, thus

$$\rho(t) \to |\rho(t)\rangle = |\rho\rangle = \sum_{i_1,i_2 \ldots i_N} c_{i_1,i_2 \ldots i_N} |\sigma_{i_1}\sigma_{i_2} \ldots \sigma_{i_N}\rangle \,. \tag{11.44}$$

The time evolution is given by formally integrating Eq. (7.4), which yields

$$\rho(t) = e^{\mathcal{L}(t-t_0)}\rho(t_0). \tag{11.45}$$

In order to demonstrate its derivation, the super-operator $\mathcal{L}$ is divided into three parts according to

$$\begin{aligned} \dot{\rho} &= \mathcal{L}[\rho] \\ &= \underbrace{-\frac{i}{\hbar}[H,\rho]}_{\mathcal{L}_H} + \underbrace{\mathcal{D}[L_{i_1}^{\text{in}}] + \mathcal{D}[L_{i_1}^{\text{out}}]}_{\mathcal{L}_{B_1}} + \underbrace{\mathcal{D}[L_{i_N}^{\text{in}}] + \mathcal{D}[L_{i_N}^{\text{out}}]}_{\mathcal{L}_{B_N}} . \end{aligned} \tag{11.46}$$

Expressing the fermionic flip operators $\sigma^{+/-}$ with the Pauli spin matrices in order to use the mapping defined in Eq. (11.27) yields for the three terms in Eq. (11.46):

$$\mathcal{L}_{B_1} = \Gamma_1^+ \left(-2c_1 |\sigma_x\rangle_1 - 2c_2 |\sigma_y\rangle_1 - 4c_3 |\sigma_z\rangle_1\right) + \Gamma_1^- 4c_0 |\sigma_z\rangle_1 \,, \tag{11.47}$$

$$\mathcal{L}_{B_N} = \Gamma_N^+ \left(-2c_1 |\sigma_x\rangle_N - 2c_2 |\sigma_y\rangle_N - 4c_3 |\sigma_z\rangle_N\right) + \Gamma_N^- 4c_0 |\sigma_z\rangle_N \,. \tag{11.48}$$

and $\mathcal{L}_H$ given in matrix form, acting on site k,$k+1$:

$$(\mathcal{L}_H)_{(i_k,i_{k+1}),(j_k,j_{k+1})} = (\mathcal{L}_H)_{m,n} = \tag{11.49}$$

$$\begin{pmatrix}
0 & 0 & 0 & 0 & 0 & 0 & 0 & 0 & 0 & 0 & 0 & 0 & 0 & 0 & 0 & 0 \\
0 & 0 & 2h_{k+1} & 0 & 0 & 0 & 0 & 0 & 0 & 0 & 0 & -2J & 0 & 0 & 2\Delta & 0 \\
0 & -2h_{k+1} & 0 & 0 & 0 & 0 & 0 & +2J & 0 & 0 & 0 & 0 & 0 & -2\Delta & 0 & 0 \\
0 & 0 & 0 & 0 & 0 & 0 & -2J & 0 & 0 & +2J & 0 & 0 & 0 & 0 & 0 & 0 \\
0 & 0 & 0 & 0 & 0 & 0 & 0 & 0 & 2h_k & 0 & 0 & +2\Delta & 0 & 0 & -2J & 0 \\
0 & 0 & 0 & 0 & 0 & 0 & 2h_{k+1} & 0 & 0 & 2h_k & 0 & 0 & 0 & 0 & 0 & 0 \\
0 & 0 & 0 & 2J & 0 & -2h_{k+1} & 0 & 0 & 0 & 0 & 0 & 2h_k & 0 & 0 & -2J & 0 \\
0 & 0 & -2J & 0 & 0 & 0 & 0 & 0 & +2D & 0 & 0 & 0 & 2h_k & 0 & 0 & 0 \\
0 & 0 & 0 & 0 & -2h_k & 0 & 0 & +2D & 0 & 0 & 0 & 0 & 0 & 2J & 0 & 0 \\
0 & 0 & 0 & -2J & 0 & -2h_k & 0 & 0 & 0 & 0 & 0 & 2h_{k+1} & 0 & 2J & 0 & 0 \\
0 & 0 & 0 & 0 & 0 & 0 & -2h_k & 0 & 0 & -2h_{k+1} & 0 & 0 & 0 & 0 & 0 & 0 \\
0 & 0 & +2J & 0 & 0 & -2\Delta & 0 & 0 & -2h_k & 0 & 0 & 0 & 0 & 0 & 0 & 0 \\
0 & 0 & 0 & 0 & 0 & 0 & 2J & 0 & 0 & -2J & 0 & 0 & 0 & 0 & 0 & 0 \\
0 & 0 & 2\Delta & 0 & 0 & 0 & 0 & 0 & -2J & 0 & 0 & 0 & 0 & 0 & 0 & 0 \\
0 & 0 & -2\Delta & 0 & 0 & 2J & 0 & 0 & 0 & 0 & 0 & 0 & 0 & 2h_{k+1} & 0 & 0 \\
0 & 0 & 0 & 0 & 0 & 0 & 0 & 0 & 0 & 0 & 0 & 0 & 0 & 0 & 0 & 0
\end{pmatrix}$$

Note that as $\mathcal{L}_H$ acts on two sites simultaneously, the Suzuki-Trotter decomposition has to performed during the setup of the operator, cf. Sec. 3.5 and 6.3.1 for details. With this, $\rho(t)$ may be evolved in time by numerically solving for

$$|\rho(t_{k+1})\rangle = exp[\mathcal{L}]\,|\rho(t_k)\rangle \,. \tag{11.50}$$

11.4.4 Derivation of the photon wave packet form with feedback

The Hamiltonian for the system remains almost the same as in Eq. (9.6), differing only in the form of the system-reservoir coupling. It thus reads:

$$H = \sum_{j=1,2} \hbar\omega_e^j \sigma_{ee}^j + \int d\omega_j \hbar\omega_j a_\omega^{j\dagger} a_\omega^j + \hbar\Omega(t)\left(e^{-i\omega_p t}\sigma_{eg}^j + e^{i\omega_p t}\sigma_{ge}^j\right) + \int d\omega_j \hbar G_{fb}^j(\omega)\left(a_\omega^j \sigma_{eg}^j + a_\omega^{j\dagger}\sigma_{ge}^j\right), \quad (11.51)$$

where the sinusoidal frequency dependent coupling element $G_{fb}^j(\omega)$ with $G_{fb}^j(\omega_j) = g_j \sin\left(\frac{\omega_j L}{c_0}\right) = g_j \sin\left(\omega_j \frac{\tilde{\tau}}{2}\right)$ as introduced in Eq. (4.3), where L_j is the length of the closed side of the waveguide affecting the jth emitter, c_0 the speed of light in vacuum and $\tilde{\tau}_j = \frac{2L}{c_0}$ the resulting delay time of the jth TLS.
Next, the transformation into the interaction picture is applied. With this, and using $c_e(t=0) = 1$, $c_g^{\omega_j}(t=0) = 0$ as initial condition, the Wigner-Weisskopf problem now reads:

$$\partial_t c_{e_j}(t) = -i \int d\omega_j G_{fb}^j(\omega) e^{-i(\omega_j - \omega_e^j)t} c_{g_j}^{\omega_j}(t) \quad (11.52)$$

$$\partial_t c_{g_j}^{\omega_j}(t) = -i G_{fb}^j(\omega) e^{i(\omega_j - \omega_e^j)t} c_{e_j}(t). \quad (11.53)$$

Eq. (11.53) is formally integrated and plugged into Eq. (11.52). This yields the relaxation dynamics for the excited state:

$$\partial_t c_{e_j}(t) = \Gamma\left(c_{e_j}(t-\tilde{\tau}) e^{i\omega_e^j \tilde{\tau}} \Theta(t-\tilde{\tau}) - c_{e_j}(t)\right), \quad (11.54)$$

where $\Gamma \equiv \frac{g_j^2 \pi}{2}$. Eq. (11.54) is solved using a Laplace transformation. The result reads:

$$c_{e_j}(t) = \sum_{n=0}^{\infty} \frac{\left(\Gamma e^{i\omega_e^j \tilde{\tau}}\right)^n}{n!} (t - n\tilde{\tau})^n e^{-\Gamma(t-n\tilde{\tau})} \Theta(t - n\tilde{\tau}) \quad (11.55)$$

Again, we plug the result in Eq. (11.55) into Eq. (9.38) in order to obtain a solution for the relaxation dynamics of the emitter.Formally integrating and putting $c_{g_j}^{\omega_j}(0) = 0$ yields:

$$c_{g_j}^{\omega_j}(t) = -i G_{fb}^j(\omega_j) \int_0^t dt_j e^{i(\omega_j - \omega_e^j)t_j} \sum_{n=0}^{\infty} \frac{\left(\Gamma e^{i\omega_e^j \tilde{\tau}}\right)^n}{n!} (t - n\tilde{\tau})^n e^{-\Gamma(t-n\tilde{\tau})} \Theta(t - n\tilde{\tau}) \quad (11.56)$$

Here, the conservation of probability is being checked for the 0-th $\tilde{\tau}$- interval by verifying

$$\int_0^\infty d\omega \left|c_{g_j}^{\omega_j}(t \le \tilde{\tau})\right|^2 + \left|c_{e_j}(t \le \tilde{\tau})\right|^2 \stackrel{!}{=} 1 \quad (11.57)$$

for $n = 0$ in Eq. (11.55) and 11.56.
Next, it it is assumed that $t \to \infty$ so that $c_e^j(t \to \infty) = 0$. With this, the total wave function reads:

$$\begin{aligned}
&|\psi\rangle = |\psi_1\rangle \otimes |\psi_2\rangle \\
&= -i \int_0^\infty d\omega_1 G_{fb,1}(\omega_1) \int_0^t dt_1 e^{i(\omega_1 - \omega_e^1)t_1} \sum_{n=0}^\infty \frac{\left(\Gamma e^{i\omega_{e_1}\tilde{\tau}}\right)^n}{n!} (t - n\tilde{\tau})^n e^{-\Gamma(t-n\tilde{\tau})} \Theta(t - n\tilde{\tau}) a_{\omega_1}^\dagger |vac\rangle \\
&\otimes - \int_0^\infty d\omega_2 i G_{fb,2}(\omega_2) \int_0^t dt_2 e^{i(\omega_2 - \omega_e^2)t_2} \sum_{n=0}^\infty \frac{\left(\Gamma e^{i\omega_{e_2}\tilde{\tau}}\right)^n}{n!} (t - n\tilde{\tau})^n e^{-\Gamma(t-n\tilde{\tau})} \Theta(t - n\tilde{\tau}) |vac\rangle
\end{aligned} \tag{11.58}$$

The solution to Eq. (4.12) yields the relaxation dynamics of the emitters and is obtained with partial integration. It reads:

$$\begin{aligned}
c_{g_j}^{\omega_j}(t) = G_{fb,j}(\omega_j) \sum_{n=0}^\infty \frac{\left(\Gamma e^{i\omega_e^j \tau}\right)^n}{n!} \Theta(t - n\tau) e^{-(\Gamma + i\left(\omega_j - \omega_e^j\right))(t - n\tau)} \\
\left(\frac{1}{\Gamma + i(\omega_j - \omega_e^j)} (t - n\tau)^n + \sum_{m=1}^n \frac{(t - n\tau)^{n-m}}{\left(\Gamma + i(\omega_j - \omega_e^j)\right)^{m+1}} \Pi_{k=0}^{m-1}(n - k) \right)
\end{aligned} \tag{11.59}$$

Again, it it is assumed that $t \to \infty$ so that $c_e^j(t \to \infty) = 0$. Plugging Eq. (11.59) into Eq. (11.58) yields for the total wave function:

$$\begin{aligned}
|\psi\rangle = &- \int_0^\infty d\omega_1 G_{fb,1}(\omega_1) \sum_{n=0}^\infty \frac{\left(\Gamma e^{i\omega_{e_1}\tau}\right)^n}{n!} \Theta(t_1 - n\tau) e^{-(\Gamma + i\left(\omega_1 - \omega_{e_1}\right))(t_1 - n\tau)} \\
&\left(\frac{1}{\Gamma + i(\omega_j - \omega_{e_1})} (t_1 - n\tau)^n + \sum_{m=1}^n \frac{(t_1 - n\tau)^{n-m}}{(\Gamma + i(\omega_1 - \omega_{e_1}))^{m+1}} \Pi_{k=0}^{m-1}(n - k) \right) \\
&\int_0^\infty d\omega_2 G_{fb,2}(\omega_2) \sum_{n=0}^\infty \frac{\left(\Gamma e^{i\omega_{e_2}\tau}\right)^n}{n!} \Theta(t_2 - n\tau) e^{-(\Gamma + i\left(\omega_2 - \omega_{e_2}\right))(t_2 - n\tau)} \\
&\left(\frac{1}{\Gamma + i(\omega_2 - \omega_{e_2})} (t_2 - n\tau)^n + \sum_{m=1}^n \frac{(t_2 - n\tau)^{n-m}}{(\Gamma + i(\omega_2 - \omega_{e_2}))^{m+1}} \Pi_{k=0}^{m-1}(n - k) \right) a_{\omega_1}^\dagger a_{\omega_2}^\dagger |vac\rangle
\end{aligned} \tag{11.60}$$

With this, the $g^{(2)}$-function with feedback as defined in Eq. (9.18) may be calculated.

11.4.5 Calculation of the $g^{(2)}$-function with feedback

Again, first the ket is evaluated:

$$
\begin{aligned}
&E_4^{(+)}(t_D+\tau)E_3^{(+)}(t_D)\,|\psi(t)\rangle \\
&\quad= \Big(tE_2(t_D+\tau)^{(+)}E_1(t_D)^{(+)} - rE_1(t_D+\tau)^{(+)}E_2(t_D)^{(+)}\Big)\,|\psi(t)\rangle \\
&\quad= -t\int_0^\infty d\omega_2 iG_{fb,2}(\omega_2)e^{-\omega_2(t_D+\tau)}\int_o^\infty d\omega_1 iG_{fb,1}(\omega_1)e^{-\omega_1 t_D} \\
&\qquad\sum_{n=0}^{\infty}\frac{\left(\Gamma e^{i\omega_{e_1}\tilde{\tau}}\right)^n}{n!}\Theta(t_D-n\tilde{\tau})e^{-(\Gamma+i\left(\omega_1-\omega_{e_1}\right))(t_D-n\tilde{\tau})} \\
&\qquad\left(\frac{1}{\Gamma+i(\omega_1-\omega_{e_1})}(t_D-n\tilde{\tau})^n+\sum_{m=1}^{n}\frac{(t_D-n\tilde{\tau})^{n-m}}{(\Gamma+i(\omega_1-\omega_{e_1}))^{m+1}}\Pi_{k=0}^{m-1}(n-k)\right) \\
&\qquad\sum_{n=0}^{\infty}\frac{\left(\Gamma e^{i\omega_{e_2}\tilde{\tau}}\right)^n}{n!}\Theta(t_D+\tau-n\tilde{\tau})e^{-(\Gamma+i\left(\omega_2-\omega_{e_2}\right))(t_D+\tau-n\tilde{\tau})} \\
&\left(\frac{1}{\Gamma+i(\omega_2-\omega_{e_2})}(t_D+\tau-n\tilde{\tau})^n+\sum_{m=1}^{n}\frac{(t_D+\tau-n\tilde{\tau})^{n-m}}{(\Gamma+i(\omega_2-\omega_{e_2}))^{m+1}}\Pi_{k=0}^{m-1}(n-k)\right)|vac\rangle \\
&\qquad+ r\int_o^\infty d\omega_1 iG_{fb,1}(\omega_1)e^{-\omega_1(t_D+\tau)}\int_o^\infty d\omega_2 iG_{fb,2}(\omega_2)e^{-\omega_2 t_D} \\
&\qquad\sum_{n=0}^{\infty}\frac{\left(\Gamma e^{i\omega_{e_1}\tilde{\tau}}\right)^n}{n!}\Theta(t_D+\tau-n\tilde{\tau})e^{-(\Gamma+i\left(\omega_1-\omega_{e_1}\right))(t_D+\tau-n\tilde{\tau})} \\
&\qquad\left(\frac{1}{\Gamma+i(\omega_1-\omega_{e_1})}(t_D+\tau-n\tilde{\tau})^n+\sum_{m=1}^{n}\frac{(t_D+\tau-n\tilde{\tau})^{n-m}}{(\Gamma+i(\omega_1-\omega_{e_1}))^{m+1}}\Pi_{k=0}^{m-1}(n-k)\right) \\
&\qquad\sum_{n=0}^{\infty}\frac{\left(\Gamma e^{i\omega_{e_2}\tilde{\tau}}\right)^n}{n!}\Theta(t_D-n\tilde{\tau})e^{-(\Gamma+i\left(\omega_2-\omega_{e_2}\right))(t_D-n\tilde{\tau})} \\
&\left(\frac{1}{\Gamma+i(\omega_2-\omega_{e_2})}(t_D-n\tilde{\tau})^n+\sum_{m=1}^{n}\frac{(t_D-n\tilde{\tau})^{n-m}}{(\Gamma+i(\omega_2-\omega_{e_2}))^{m+1}}\Pi_{k=0}^{m-1}(n-k)\right)|vac\rangle
\end{aligned}
\tag{11.61}
$$

Plugging the definition for the feedback coupling into Eq. (11.61) yields:

$$
\begin{aligned}
&E_4^{(+)}(t_D+\tau)E_3^{(+)}(t_D)\,|\psi(t)\rangle = \\
&\qquad = \frac{t}{4}\int_o^\infty d\omega_1 \int_o^\infty d\omega_2 \Big(e^{-i\omega_2(t_D-\frac{\tilde\tau}{2}+\tau)}e^{-i\omega_1(t_D-\frac{\tilde\tau}{2})} \\
&\qquad\qquad -e^{-i\omega_2(t_D-\frac{\tilde\tau}{2}+\tau)}e^{-i\omega_1(t_D+\frac{\tilde\tau}{2})} \\
&\qquad\qquad -e^{-i\omega_2(t_D+\frac{\tilde\tau}{2}+\tau)}e^{-i\omega_1(t_D-\frac{\tilde\tau}{2})} \\
&\qquad\qquad +e^{-i\omega_2(t_D+\frac{\tilde\tau}{2}+\tau)}e^{-i\omega_1(t_D+\frac{\tilde\tau}{2})}\Big) \\
&\qquad\qquad \sum_{n=0}^{\infty}\frac{\left(\Gamma e^{i\omega_{e_1}\tilde\tau}\right)^n}{n!}\Theta(t_D-n\tilde\tau)e^{-(\Gamma+i\left(\omega_1-\omega_{e_1}\right))(t_D-n\tilde\tau)} \\
&\qquad\qquad \left(\frac{1}{\Gamma+i(\omega_1-\omega_{e_1})}(t_D-n\tilde\tau)^n+\sum_{m=1}^{n}\frac{(t_D-n\tilde\tau)^{n-m}}{(\Gamma+i(\omega_1-\omega_{e_1}))^{m+1}}\Pi_{k=0}^{m-1}(n-k)\right) \\
&\qquad\qquad \sum_{n=0}^{\infty}\frac{\left(\Gamma e^{i\omega_{e_2}\tilde\tau}\right)^n}{n!}\Theta(t_D+\tau-n\tilde\tau)e^{-(\Gamma+i\left(\omega_2-\omega_{e_2}\right))(t_D+\tau-n\tilde\tau)} \\
&\left(\frac{1}{\Gamma+i(\omega_2-\omega_{e_2})}(t_D+\tau-n\tilde\tau)^n+\sum_{m=1}^{n}\frac{(t_D+\tau-n\tilde\tau)^{n-m}}{(\Gamma+i(\omega_2-\omega_{e_2}))^{m+1}}\Pi_{k=0}^{m-1}(n-k)\right)|vac\rangle \\
&\qquad\qquad -\frac{r}{4}\int_o^\infty d\omega_2 \int_o^\infty d\omega_1 \Big(e^{-i\omega_1(t_D-\frac{\tilde\tau}{2}+\tau)}e^{-i\omega_2(t_D-\frac{\tilde\tau}{2})} \\
&\qquad\qquad -e^{-i\omega_1(t_D-\frac{\tilde\tau}{2}+\tau)}e^{-i\omega_2(t_D+\frac{\tilde\tau}{2})} \\
&\qquad\qquad -e^{-i\omega_1(t_D+\frac{\tilde\tau}{2}+\tau)}e^{-i\omega_2(t_D-\frac{\tilde\tau}{2})} \\
&\qquad\qquad +e^{-i\omega_1(t_D+\frac{\tilde\tau}{2}+\tau)}e^{-i\omega_2(t_D+\frac{\tilde\tau}{2})}\Big) \\
&\qquad\qquad \sum_{n=0}^{\infty}\frac{\left(\Gamma e^{i\omega_{e_1}\tilde\tau}\right)^n}{n!}\Theta(t_D+\tau-n\tilde\tau)e^{-(\Gamma+i\left(\omega_1-\omega_{e_1}\right))(t_D+\tau-n\tilde\tau)} \\
&\qquad\qquad \left(\frac{1}{\Gamma+i(\omega_1-\omega_{e_1})}(t_D+\tau-n\tilde\tau)^n+\sum_{m=1}^{n}\frac{(t_D+\tau-n\tilde\tau)^{n-m}}{(\Gamma+i(\omega_1-\omega_{e_1}))^{m+1}}\Pi_{k=0}^{m-1}(n-k)\right) \\
&\qquad\qquad \sum_{n=0}^{\infty}\frac{\left(\Gamma e^{i\omega_{e_2}\tilde\tau}\right)^n}{n!}\Theta(t_D-n\tilde\tau)e^{-(\Gamma+i\left(\omega_2-\omega_{e_2}\right))(t_D-n\tilde\tau)} \\
&\left(\frac{1}{\Gamma+i(\omega_2-\omega_{e_2})}(t_D-n\tilde\tau)^n+\sum_{m=1}^{n}\frac{(t_D-n\tilde\tau)^{n-m}}{(\Gamma+i(\omega_2-\omega_{e_2}))^{m+1}}\Pi_{k=0}^{m-1}(n-k)\right)|vac\rangle
\end{aligned}
\tag{11.62}
$$

Bibliography

[1] H.-P. Breuer and F. F. Petruccione, *The theory of open quantum systems.* Oxford University Press, 2002.

[2] P. Z. Crispin Gardiner, *Quantum Noise - A Handbook of Markovian and Non-Markovian Quantum Stochastic Methods with Applications to Quantum Optics.* Springer Verlag Berlin, 2002.

[3] H. J. Carmichael, "Quantum trajectory theory for cascaded open systems," *Phys. Rev. Lett.*, vol. 70, pp. 2273–2276, Apr 1993.

[4] U. Weiss, *Quantum Dissipative Systems, Fourth Edition.* World Scientific Publishing Co., 2012.

[5] M. A. Nielsen and I. L. Chuang, *Quantum Computation and Quantum Information.* Cambridge University Press, 2010.

[6] I. de Vega, D. Porras, and J. Ignacio Cirac, "Matter-wave emission in optical lattices: Single particle and collective effects," *Phys. Rev. Lett.*, vol. 101, p. 260404, Dec 2008.

[7] C. Navarrete-Benlloch, I. de Vega, D. Porras, and J. I. Cirac, "Simulating quantum-optical phenomena with cold atoms in optical lattices," *New Journal of Physics*, vol. 13, p. 023024, feb 2011.

[8] H. Häffner, C. Roos, and R. Blatt, "Quantum computing with trapped ions," *Physics Reports*, vol. 469, no. 4, pp. 155 – 203, 2008.

[9] R. Blatt and D. Wineland, "Entangled states of trapped atomic ions," *Nature*, vol. 453, pp. 1008–1015, jun 2008.

[10] I. Rotter and J. P. Bird, "A review of progress in the physics of open quantum systems: theory and experiment," vol. 78, p. 114001, oct 2015.

[11] "Seeing a single photon without destroying it," *Nature*, vol. 400, pp. 239–242, jul 1999.

[12] N. V. Prokof and P. C. E. Stamp, "Giant spins and topological decoherence: a hamiltonian approach," *Journal of Physics: Condensed Matter*, vol. 5, pp. L663–L670, dec 1993.

[13] N. Lambert, Y. N. Chen, Y. C. Cheng, C. M. Li, G. Y. Chen, and F. Nori, "Quantum biology," *Nature Physics*, vol. 9, pp. 10–18, dec 2013.

[14] A. Daley, "Quantum trajectories and open many-body quantum systems," *Adv. Phys.*, vol. 63, 05 2014.

[15] I. de Vega and D. Alonso, "Dynamics of non-markovian open quantum systems," *Rev. Mod. Phys.*, vol. 89, p. 015001, Jan 2017.

[16] C. P. Koch, "Controlling open quantum systems: tools, achievements, and limitations," *J. Condens. Matter Phys.*, vol. 28, p. 213001, may 2016.

[17] U. Weiss and W. Haeffner, "Complex-time path integrals beyond the stationary-phase approximation: Decay of metastable states and quantum statistical metastability," *Phys. Rev. D*, vol. 27, pp. 2916–2927, Jun 1983.

[18] D. Alonso, S. Brouard, and D. Sokolovski, "Quantum decoherence of an anharmonic oscillator monitored by a bose-einstein condensate," *Phys. Rev. A*, vol. 90, p. 032106, Sep 2014.

[19] S. Groeblacher, A. Trubarov, N. Prigge, M. Aspelmeyer, and J. Eisert, "Observation of non-markovian micro-mechanical brownian motion," *Nature communications*, vol. 6, 05 2013.

[20] L. Droenner and A. Carmele, "Boundary-driven heisenberg chain in the long-range interacting regime: Robustness against far-from-equilibrium effects," *Phys. Rev. B*, vol. 96, p. 184421, Nov 2017.

[21] M. Žnidarič, A. Scardicchio, and V. K. Varma, "Diffusive and subdiffusive spin transport in the ergodic phase of a many-body localizable system," *Phys. Rev. Lett.*, vol. 117, p. 040601, Jul 2016.

[22] M. Heyl, A. Polkovnikov, and S. Kehrein, "Dynamical quantum phase transitions in the transverse-field ising model," *Phys. Rev. Lett.*, vol. 110, p. 135704, Mar 2013.

[23] J. Huber, P. Kirton, and P. Rabl, "Non-equilibrium magnetic phases in spin lattices with gain and loss," 2019.

[24] J. Huber and P. Rabl, "Active energy transport and the role of symmetry breaking in microscopic power grids," *Phys. Rev. A*, vol. 100, p. 012129, Jul 2019.

[25] A. Pizzi, A. Nunnenkamp, and J. Knolle, "Bistability and time crystals in long-ranged directed percolation," apr 2020.

[26] B. Bertini, F. Heidrich-Meisner, C. Karrasch, T. Prosen, R. Steinigeweg, and M. Znidaric, "Finite-temperature transport in one-dimensional quantum lattice models," mar 2020.

[27] P. Hauke and L. Tagliacozzo, "Spread of correlations in long-range interacting quantum systems," *Phys. Rev. Lett.*, vol. 111, p. 207202, Nov 2013.

[28] N. Trautmann and P. Hauke, "Trapped-ion quantum simulation of excitation transport: Disordered, noisy, and long-range connected quantum networks," *Phys. Rev. A*, vol. 97, p. 023606, Feb 2018.

[29] T. c. v. Prosen, "Exact nonequilibrium steady state of a strongly driven open xxz chain," *Phys. Rev. Lett.*, vol. 107, p. 137201, Sep 2011.

[30] M. Ljubotina, M. Žnidari, and T. Prosen, "Spin diffusion from an inhomogeneous quench in an integrable system," *Nature Communications*, vol. 8, pp. 1–6, jul 2017.

[31] F. Lange, S. Ejima, T. Shirakawa, S. Yunoki, and H. Fehske, "Spin transport through a spin-$\frac{1}{2}$ xxz chain contacted to fermionic leads," *Phys. Rev. B*, vol. 97, p. 245124, Jun 2018.

[32] M. Žnidarič, "Spin transport in a one-dimensional anisotropic heisenberg model," *Phys. Rev. Lett.*, vol. 106, p. 220601, May 2011.

[33] M. Žnidarič, "Transport in a one-dimensional isotropic heisenberg model at high temperature," *Journal of Statistical Mechanics: Theory and Experiment*, vol. 2011, p. P12008, dec 2011.

[34] M. Katzer, W. Knorr, R. Finsterhölzl, and A. Carmele, "Long-range interaction in an open boundary-driven heisenberg spin lattice: A far-from-equilibrium transition to ballistic transport," *Phys. Rev. B*, vol. 102, p. 125101, Sep 2020.

[35] T. Wang, X. Wang, and Z. Sun, "Entanglement oscillations in open Heisenberg chains," *Physica A: Statistical Mechanics and its Applications*, vol. 383, pp. 316–324, sep 2007.

[36] Y. Z. Wu, J. Ren, and X. F. Jiang, "Dynamics of entanglement in heisenberg chains with asymmetric dzyaloshinskii-moriya interactions," *International Journal of Quantum Information*, vol. 09, no. 02, pp. 751–761, 2011.

[37] W. Heisenberg, "Zur Theorie des Ferromagnetismus," *Zeitschrift für Physik*, vol. 49, pp. 619–636, sep 1928.

[38] H. Bethe, "Zur Theorie der Metalle - I. Eigenwerte und Eigenfunktionen der linearen Atomkette," *Zeitschrift für Physik*, vol. 71, pp. 205–226, mar 1931.

[39] M. Dupont and J. E. Moore, "Universal spin dynamics in infinite-temperature one-dimensional quantum magnets," *Phys. Rev. B*, vol. 101, p. 121106, Mar 2020.

[40] S. Hild, T. Fukuhara, P. Schauß, J. Zeiher, M. Knap, E. Demler, I. Bloch, and C. Gross, "Far-from-equilibrium spin transport in heisenberg quantum magnets," *Phys. Rev. Lett.*, vol. 113, p. 147205, Oct 2014.

[41] Y. Tang, W. Kao, K.-Y. Li, S. Seo, K. Mallayya, M. Rigol, S. Gopalakrishnan, and B. L. Lev, "Thermalization near integrability in a dipolar quantum newton's cradle," *Phys. Rev. X*, vol. 8, p. 021030, May 2018.

[42] T. Langen, S. Erne, R. Geiger, B. Rauer, T. Schweigler, M. Kuhnert, W. Rohringer, I. E. Mazets, T. Gasenzer, and J. Schmiedmayer, "Experimental observation of a generalized gibbs ensemble," *Science*, vol. 348, no. 6231, pp. 207–211, 2015.

[43] T. Kinoshita, T. Wenger, and D. S. Weiss, "A quantum Newton's cradle," *Nature*, vol. 440, pp. 900–903, apr 2006.

[44] C. Maier, T. Brydges, P. Jurcevic, N. Trautmann, C. Hempel, B. P. Lanyon, P. Hauke, R. Blatt, and C. F. Roos, "Environment-assisted quantum transport in a 10-qubit network," *Phys. Rev. Lett.*, vol. 122, p. 050501, Feb 2019.

[45] I. Bloch, "Quantum coherence and entanglement with ultracold atoms in optical lattices," *Nature*, vol. 453, pp. 1016–22, 07 2008.

[46] T. Monz, P. Schindler, J. T. Barreiro, M. Chwalla, D. Nigg, W. A. Coish, M. Harlander, W. Hänsel, M. Hennrich, and R. Blatt, "14-qubit entanglement: Creation and coherence," *Phys. Rev. Lett.*, vol. 106, p. 130506, Mar 2011.

[47] D. D. Awschalom, L. C. Bassett, A. S. Dzurak, E. L. Hu, and J. R. Petta, "Quantum spintronics: Engineering and manipulating atom-like spins in semiconductors," *Science*, vol. 339, no. 6124, pp. 1174–1179, 2013.

[48] M. H. Devoret and R. J. Schoelkopf, "Superconducting circuits for quantum information: An outlook," *Science*, vol. 339, no. 6124, pp. 1169–1174, 2013.

[49] H. Kimble, "The quantum internet," *Nature*, vol. 453, pp. 1023–30, 07 2008.

[50] J. Eisert, M. Friesdorf, and C. Gogolin, "Quantum many-body systems out of equilibrium," *Nature Physics*, vol. 11, pp. 124–130, jan 2015.

[51] R. Blatt and D. Wineland, "Entangled states of trapped atomic ions," *Nature*, vol. 453, pp. 1008–15, 07 2008.

[52] K. Myatt, C. and Q. B., Turchette, "Decoherence of quantum superpositions through coupling to engineered reservoirs," *Nature*, vol. 403, p. 269–273, 12 2000.

[53] H. M. Wiseman and G. J. Milburn, *Quantum Measurement and Control*. Cambridge University Press, 2009.

[54] R. Handel, J. Stockton, and H. Mabuchi, "Modelling and feedback control design for quantum state preparation," *Journal of Optics B: Quantum and Semiclassical Optics*, vol. 7, 09 2005.

[55] C. Sayrin, I. Dotsenko, X. Zhou, B. Peaudecerf, T. Rybarczyk, S. Gleyzes, P. Rouchon, M. Mirrahimi, H. Amini, M. Brune, J. Raimond, and S. Haroche, "Real-time quantum feedback prepares and stabilizes photon number states," *Nature*, vol. 477, pp. 73–7, 09 2011.

[56] D. Dong and I. Petersen, "Quantum control theory and applications: A survey," *Control Theory and Applications, IET*, vol. 4, 10 2009.

[57] J. Dowling and G. Milburn, "Quantum technology: The second quantum revolution," *Philosophical transactions. Series A, Mathematical, physical, and engineering sciences*, vol. 361, pp. 1655–74, 09 2003.

[58] A. Kiraz, M. Atatüre, and A. Imamoğlu, "Quantum-dot single-photon sources: Prospects for applications in linear optics quantum-information processing," *Phys. Rev. A*, vol. 69, p. 032305, Mar 2004.

[59] G. Calajó, Y.-L. L. Fang, H. U. Baranger, and F. Ciccarello, "Exciting a bound state in the continuum through multiphoton scattering plus delayed quantum feedback," *Phys. Rev. Lett.*, vol. 122, p. 073601, Feb 2019.

[60] K. Barkemeyer, R. Finsterhölzl, A. Knorr, and A. Carmele, "Revisiting Quantum Feedback Control: Disentangling the Feedback-Induced Phase from the Corresponding Amplitude," *Advanced Quantum Technologies*, vol. 3, p. 1900078, feb 2020.

[61] S. Chen, Y.-A. Chen, T. Strassel, Z.-S. Yuan, B. Zhao, J. Schmiedmayer, and J.-W. Pan, "Deterministic and storable single-photon source based on a quantum memory," *Phys. Rev. Lett.*, vol. 97, p. 173004, Oct 2006.

[62] A. Lvovsky, B. Sanders, and W. Tittel, "Optical quantum memory," *Nature Photonics*, vol. 3, 02 2010.

[63] E. Saglamyurek, T. Hrushevskyi, A. Rastogi, K. Heshami, and L. LeBlanc, "Coherent storage and manipulation of broadband photons via dynamically controlled autler-townes splitting," *Nature Photonics*, vol. 12, 12 2018.

[64] B. Julsgaard, J. Sherson, J. Cirac, J. Fiurásek, and E. Polzik, "Experimental demonstration of quantum memory for light," *Nature*, vol. 432, pp. 482–6, 12 2004.

[65] J. Cirac and P. Zoller, "Goals and opportunities in quantum simulation," *Nature Physics*, vol. 8, pp. 264–266, 04 2012.

[66] R. Heule, C. Bruder, D. Burgarth, and V. M. Stojanović, "Controlling qubit arrays with anisotropic xxz heisenberg interaction by acting on a single qubit," *The European Physical Journal D*, vol. 63, pp. 41–46, Jun 2011.

[67] T. P. Le, J. Levinsen, K. Modi, M. M. Parish, and F. A. Pollock, "Spin-chain model of a many-body quantum battery," *Phys. Rev. A*, vol. 97, p. 022106, Feb 2018.

[68] O. V. Marchukov, A. G. Volosniev, M. Valiente, D. Petrosyan, and N. T. Zinner, "Quantum spin transistor with a heisenberg spin chain," *Nature Communications*, vol. 7, p. 13070, Oct 2016.

[69] A. Bermudez, T. Schaetz, and M. B. Plenio, "Dissipation-assisted quantum information processing with trapped ions," *Phys. Rev. Lett.*, vol. 110, p. 110502, Mar 2013.

[70] J. Kabuss, F. Katsch, A. Knorr, and A. Carmele, "Unraveling coherent quantum feedback for pyragas control," *J. Opt. Soc. Am. B*, vol. 33, pp. C10–C16, Jul 2016.

[71] A. Carmele, N. Nemet, V. Canela, and S. Parkins, "Pronounced non-markovian features in multiply excited, multiple emitter waveguide qed: Retardation induced anomalous population trapping," *Phys. Rev. Research*, vol. 2, p. 013238, Mar 2020.

[72] G. Lindblad, "On the generators of quantum dynamical semigroups," *Communications in Mathematical Physics*, vol. 48, pp. 119–130, jun 1976.

[73] L. Pollet, "Recent developments in quantum monte carlo simulations with applications for cold gases," *Reports on Progress in Physics*, vol. 75, p. 094501, aug 2012.

[74] H. J. Kimble, M. Dagenais, and L. Mandel, "Photon antibunching in resonance fluorescence," *Phys. Rev. Lett.*, vol. 39, pp. 691–695, Sep 1977.

[75] J. Dalibard, Y. Castin, and K. Mølmer, "Wave-function approach to dissipative processes in quantum optics," *Phys. Rev. Lett.*, vol. 68, pp. 580–583, Feb 1992.

[76] R. Dum, P. Zoller, and H. Ritsch, "Monte carlo simulation of the atomic master equation for spontaneous emission," *Phys. Rev. A*, vol. 45, pp. 4879–4887, Apr 1992.

[77] P. Zoller and C. W. Gardiner, "Quantum Noise in Quantum Optics: the Stochastic Schrödinger Equation," feb 1997.

[78] D. Alonso and I. de Vega, "Multiple-time correlation functions for non-markovian interaction: Beyond the quantum regression theorem," *Phys. Rev. Lett.*, vol. 94, p. 200403, May 2005.

[79] J. Piilo, S. Maniscalco, K. Härkönen, and K.-A. Suominen, "Non-markovian quantum jumps," *Phys. Rev. Lett.*, vol. 100, p. 180402, May 2008.

[80] H. Pichler and P. Zoller, "Photonic circuits with time delays and quantum feedback," *Phys. Rev. Lett.*, vol. 116, p. 093601, Mar 2016.

[81] C. Gardiner and P. Zoller, *The quantum world of ultra-cold atoms and light, Book II: The physics of quantum-optical devices*. Imperial College Press, London, 2015.

[82] C. Gardiner and P. Zoller, *The quantum world of ultra-cold atoms and light, Book I: Foundations of Quantum Optics*. Imperial College Press, London, 2015.

[83] M. O. Scully and M. S. Zubairy, *Quantum optics*. Cambridge University Press, Cambridge, 1997.

[84] C. Gardiner, *Stochastic Methods*. Springer Verlag, Berlin, 2009.

[85] U. Schollwöck, "The density-matrix renormalization group in the age of matrix product states," *Annals of Physics*, vol. 326, pp. 96–192, jan 2011.

[86] S. Paeckel, T. Köhler, A. Swoboda, S. R. Manmana, U. Schollwöck, and C. Hubig, "Time-evolution methods for matrix-product states," *Annals of Physics*, vol. 411, p. 167998, dec 2019.

[87] S. R. White, "Density-matrix algorithms for quantum renormalization groups," *Phys. Rev. B*, vol. 48, pp. 10345–10356, Oct 1993.

[88] R. Orus, "A practical introduction to tensor networks: Matrix product states and projected entangled pair states," *Ann. Phys. New York*, vol. 349, pp. 117 – 158, 2014.

[89] I. P. McCulloch, "From density-matrix renormalization group to matrix product states," *J. Stat. Mech. - Theory E.*, vol. 2007, pp. P10014–P10014, Oct 2007.

[90] P.-G. D. González-Guillén, Carlos E., "Matrix product states, random matrix theory and the principle of maximum entropy," *Comm. Math. Phys.*, vol. 663, p. 677, Jun 2013.

[91] J. J. García-Ripoll, "Time evolution of matrix product states," *New J. Phys.*, vol. 8, pp. 305–305, Dec 2006.

[92] M. M. Wolf, G. Ortiz, F. Verstraete, and J. I. Cirac, "Quantum phase transitions in matrix product systems," *Phys. Rev. Lett.*, vol. 97, p. 110403, Sep 2006.

[93] N. N. Z. L. Garnet Kin-Lic Chan, Anna Keselman and S. R. White, "Matrix product operators, matrix product states, and ab initio density matrix renormalization group algorithms," *J. Chem. Phys.*, vol. 145, p. 014102, Feb 2016.

[94] B. Derrida, M. R. Evans, V. Hakim, and V. Pasquier, "Exact solution of a 1d asymmetric exclusion model using a matrix formulation," *Journal of Physics A: Mathematical and General*, vol. 26, pp. 1493–1517, apr 1993.

[95] M. Fannes, B. Nachtergaele, and R. F. Werner, "Finitely correlated states on quantum spin chains," *Communications in Mathematical Physics*, vol. 144, pp. 443–490, mar 1992.

[96] A. K. Kolezhuk and H.-J. Mikeska, "Finitely correlated generalized spin ladders," *International Journal of Modern Physics B*, vol. 12, no. 23, pp. 2325–2348, 1998.

[97] S. R. White, "Density matrix formulation for quantum renormalization groups," *Phys. Rev. Lett.*, vol. 69, pp. 2863–2866, Nov 1992.

[98] U. Schollwöck, "The density-matrix renormalization group," *Rev. Mod. Phys.*, vol. 77, pp. 259–315, Apr 2005.

[99] S. Rommer and S. Östlund, "Class of ansatz wave functions for one-dimensional spin systems and their relation to the density matrix renormalization group," *Phys. Rev. B*, vol. 55, pp. 2164–2181, Jan 1997.

[100] M. Cozzini, R. Ionicioiu, and P. Zanardi, "Quantum fidelity and quantum phase transitions in matrix product states," *Phys. Rev. B*, vol. 76, p. 104420, Sep 2007.

[101] J. Dukelsky, M. A. Martín-Delgado, T. Nishino, and G. Sierra, "Equivalence of the variational matrix product method and the density matrix renormalization group applied to spin chains," *Europhysics Letters (EPL)*, vol. 43, pp. 457–462, aug 1998.

[102] N. Schuch, M. M. Wolf, F. Verstraete, and J. I. Cirac, "Entropy scaling and simulability by matrix product states," *Phys. Rev. Lett.*, vol. 100, p. 030504, Jan 2008.

[103] S. R. White and A. E. Feiguin, "Real-time evolution using the density matrix renormalization group," *Phys. Rev. Lett.*, vol. 93, p. 076401, Aug 2004.

[104] A. J. Daley, C. Kollath, U. Schollwöck, and G. Vidal, "Time-dependent density-matrix renormalization-group using adaptive effective hilbert spaces," *Journal of Statistical Mechanics: Theory and Experiment*, vol. 2004, p. P04005, apr 2004.

[105] G. Vidal, "Efficient classical simulation of slightly entangled quantum computations," *Phys. Rev. Lett.*, vol. 91, p. 147902, Oct 2003.

[106] G. Vidal, "Efficient simulation of one-dimensional quantum many-body systems," *Phys. Rev. Lett.*, vol. 93, p. 040502, Jul 2004.

[107] C. Lanczos, "An iteration method for the solution of the eigenvalue problem of linear differential and integral operators," *J. Res. Natl. Bur. Stand. B*, vol. 45, pp. 255–282, 1950.

[108] J. J. García-Ripoll, "Time evolution of matrix product states," *New Journal of Physics*, vol. 8, pp. 305–305, dec 2006.

[109] P. E. Dargel, A. Wöllert, A. Honecker, I. P. McCulloch, U. Schollwöck, and T. Pruschke, "Lanczos algorithm with matrix product states for dynamical correlation functions," *Phys. Rev. B*, vol. 85, p. 205119, May 2012.

[110] M. L. Wall and L. D. Carr, "Out-of-equilibrium dynamics with matrix product states," *New Journal of Physics*, vol. 14, p. 125015, dec 2012.

[111] J. Haegeman, J. I. Cirac, T. J. Osborne, I. Pižorn, H. Verschelde, and F. Verstraete, "Time-dependent variational principle for quantum lattices," *Phys. Rev. Lett.*, vol. 107, p. 070601, Aug 2011.

[112] J. Haegeman, C. Lubich, I. Oseledets, B. Vandereycken, and F. Verstraete, "Unifying time evolution and optimization with matrix product states," *Phys. Rev. B*, vol. 94, p. 165116, Oct 2016.

[113] M. Zwolak and G. Vidal, "Mixed-state dynamics in one-dimensional quantum lattice systems: A time-dependent superoperator renormalization algorithm," *Phys. Rev. Lett.*, vol. 93, p. 207205, Nov 2004.

[114] F. Verstraete, J. J. García-Ripoll, and J. I. Cirac, "Matrix product density operators: Simulation of finite-temperature and dissipative systems," *Phys. Rev. Lett.*, vol. 93, p. 207204, Nov 2004.

[115] M. Suzuki, "Relationship between d-Dimensional Quantal Spin Systems and (d+1)-Dimensional Ising Systems: Equivalence, Critical Exponents and Systematic Approximants of the Partition Function and Spin Correlations," *Progress of Theoretical Physics*, vol. 56, pp. 1454–1469, 11 1976.

[116] M. Suzuki, "General theory of fractal path integrals with applications to many-body theories and statistical physics," *Journal of Mathematical Physics*, vol. 32, no. 2, pp. 400–407, 1991.

[117] J. B. Keller and D. W. McLaughlin, "The feynman integral," *The American Mathematical Monthly*, vol. 82, no. 5, pp. 451–465, 1975.

[118] M. P. Zaletel, R. S. K. Mong, C. Karrasch, J. E. Moore, and F. Pollmann, "Time-evolving a matrix product state with long-ranged interactions," *Phys. Rev. B*, vol. 91, p. 165112, Apr 2015.

[119] S. Langer, F. Heidrich-Meisner, J. Gemmer, I. P. McCulloch, and U. Schollwöck, "Real-time study of diffusive and ballistic transport in spin-$\frac{1}{2}$ chains using the adaptive time-dependent density matrix renormalization group method," *Phys. Rev. B*, vol. 79, p. 214409, Jun 2009.

[120] R. Orús and G. Vidal, "Infinite time-evolving block decimation algorithm beyond unitary evolution," *Phys. Rev. B*, vol. 78, p. 155117, Oct 2008.

[121] T. Prosen and M. Žnidarič, "Matrix product simulations of non-equilibrium steady states of quantum spin chains," *Journal of Statistical Mechanics: Theory and Experiment*, vol. 2009, p. P02035, feb 2009.

[122] T. Prosen, "Matrix product solutions of boundary driven quantum chains," *Journal of Physics A Mathematical and Theoretical*, vol. 48, p. 373001, 08 2015.

[123] D. Karevski, V. Popkov, and G. M. Schütz, "Matrix product ansatz for non-equilibrium quantum steady states," in *From Particle Systems to Partial Differential Equations* (P. Gonçalves and A. J. Soares, eds.), (Cham), pp. 221–245, Springer International Publishing, 2017.

[124] G. Benenti, G. Casati, T. Prosen, and D. Rossini, "Negative differential conductivity in far-from-equilibrium quantum spin chains," *EPL (Europhysics Letters)*, vol. 85, p. 37001, feb 2009.

[125] D. Karevski, V. Popkov, and G. M. Schütz, "Exact matrix product solution for the boundary-driven lindblad xxz chain," *Phys. Rev. Lett.*, vol. 110, p. 047201, Jan 2013.

[126] Z. Cai and T. Barthel, "Algebraic versus exponential decoherence in dissipative many-particle systems," *Phys. Rev. Lett.*, vol. 111, p. 150403, Oct 2013.

[127] X. Xu, C. Guo, and D. Poletti, "Interplay of interaction and disorder in the steady state of an open quantum system," *Phys. Rev. B*, vol. 97, p. 140201, Apr 2018.

[128] J. J. Mendoza-Arenas, M. Žnidarič, V. K. Varma, J. Goold, S. R. Clark, and A. Scardicchio, "Asymmetry in energy versus spin transport in certain interacting disordered systems," *Phys. Rev. B*, vol. 99, p. 094435, Mar 2019.

[129] V. Popkov, T. c. v. Prosen, and L. Zadnik, "Inhomogeneous matrix product ansatz and exact steady states of boundary-driven spin chains at large dissipation," *Phys. Rev. E*, vol. 101, p. 042122, Apr 2020.

[130] E. Mascarenhas, H. Flayac, and V. Savona, "Matrix-product-operator approach to the nonequilibrium steady state of driven-dissipative quantum arrays," *Phys. Rev. A*, vol. 92, p. 022116, Aug 2015.

[131] A. Strathearn, P. Kirton, D. Kilda, J. Keeling, and B. W. Lovett, "Efficient non-Markovian quantum dynamics using time-evolving matrix product operators," *Nature Communications*, vol. 9, pp. 1–9, dec 2018.

[132] L. Droenner, N. L. Naumann, E. Schöll, A. Knorr, and A. Carmele, "Quantum pyragas control: Selective control of individual photon probabilities," *Phys. Rev. A*, vol. 99, p. 023840, Feb 2019.

[133] N. Német, A. Carmele, S. Parkins, and A. Knorr, "Comparison between continuous- and discrete-mode coherent feedback for the jaynes-cummings model," *Phys. Rev. A*, vol. 100, p. 023805, Aug 2019.

[134] M. A. Nielson and I. L. Chuang, *Quantum computation and quantum information.* Cambridge University Press, Cambridge, 2010.

[135] I. Markovsky, *Low rank approximation : algorithms, implementation, applications.* Springer Verlag, Berlin, 2012.

[136] J. Zhang, Y.-x. Liu, R. Wu, K. Jacobs, and F. Nori, "Quantum feedback: Theory, experiments, and applications," *Physics Reports*, vol. 679, 07 2014.

[137] A. C. Doherty, S. Habib, K. Jacobs, H. Mabuchi, and S. M. Tan, "Quantum feedback control and classical control theory," *Phys. Rev. A*, vol. 62, p. 012105, Jun 2000.

[138] H. Wiseman and G. Milburn, "Quantum measurement and control," *Quantum Measurement and Control, by Howard M. Wiseman , Gerard J. Milburn, Cambridge, UK: Cambridge University Press, 2009*, 11 2009.

[139] P. Rabl, V. Steixner, and P. Zoller, "Quantum-limited velocity readout and quantum feedback cooling of a trapped ion via electromagnetically induced transparency," *Phys. Rev. A*, vol. 72, p. 043823, Oct 2005.

[140] V. Steixner, P. Rabl, and P. Zoller, "Quantum feedback cooling of a single trapped ion in front of a mirror," *Phys. Rev. A*, vol. 72, p. 043826, oct 2005.

[141] A. Serafini, "Feedback Control in Quantum Optics: An Overview of Experimental Breakthroughs and Areas of Application," *ISRN Optics*, vol. 2012, pp. 1–15, dec 2012.

[142] N. Yamamoto, "Coherent versus Measurement Feedback: Linear Systems Theory for Quantum Information," *Phys. Rev. X*, vol. 4, p. 041029, nov 2014.

[143] K. Jacobs, X. Wang, and H. M. Wiseman, "Coherent feedback that beats all measurement-based feedback protocols," *New J. Phys.*, vol. 16, p. 073036, jul 2014.

[144] J. Zhang, G. Pagano, P. W. Hess, A. Kyprianidis, P. Becker, H. Kaplan, A. V. Gorshkov, Z.-X. Gong, and C. Monroe, "Observation of a many-body dynamical phase transition with a 53-qubit quantum simulator," *Nature*, vol. 551, pp. 601–604, Nov 2017.

[145] V. Sudhir, D. J. Wilson, R. Schilling, H. Schütz, S. A. Fedorov, A. H. Ghadimi, A. Nunnenkamp, and T. J. Kippenberg, "Appearance and Disappearance of Quantum Correlations in Measurement-Based Feedback Control of a Mechanical Oscillator," *Phys. Rev. X*, vol. 7, p. 011001, jan 2017.

[146] X. Zhou, I. Dotsenko, B. Peaudecerf, T. Rybarczyk, C. Sayrin, S. Gleyzes, J. M. Raimond, M. Brune, and S. Haroche, "Field Locked to a Fock State by Quantum Feedback with Single Photon Corrections," *Phys. Rev. Lett.*, vol. 108, p. 243602, jun 2012.

[147] M. A. Armen, J. K. Au, J. K. Stockton, A. C. Doherty, and H. Mabuchi, "Adaptive homodyne measurement of optical phase," *Phys. Rev. Lett.*, vol. 89, p. 133602, Sep 2002.

[148] B. Higgins, D. Berry, S. Bartlett, H. Wiseman, and G. Pryde, "Entanglement-free heisenberg-limited phase estimation," *Nature*, vol. 450, pp. 393–6, 11 2007.

[149] G.-Y. Xiang, B. Higgins, D. Berry, H. Wiseman, and G. Pryde, "Entanglement-enhanced measurement of a completely unknown phase," *Nature Photonics*, vol. 5, 01 2011.

[150] G. G. Gillett, R. B. Dalton, B. P. Lanyon, M. P. Almeida, M. Barbieri, G. J. Pryde, J. L. O'Brien, K. J. Resch, S. D. Bartlett, and A. G. White, "Experimental feedback control of quantum systems using weak measurements," *Phys. Rev. Lett.*, vol. 104, p. 080503, Feb 2010.

[151] H. M. Wiseman and G. J. Milburn, "All-optical versus electro-optical quantum-limited feedback," *Phys. Rev. A*, vol. 49, pp. 4110–4125, May 1994.

[152] C. W. Gardiner, "Driving a quantum system with the output field from another driven quantum system," *Phys. Rev. Lett.*, vol. 70, pp. 2269–2272, Apr 1993.

[153] S. Lloyd, "Coherent quantum feedback," *Phys. Rev. A*, vol. 62, p. 022108, Jul 2000.

[154] R. J. Nelson, Y. Weinstein, D. Cory, and S. Lloyd, "Experimental demonstration of fully coherent quantum feedback," *Phys. Rev. Lett.*, vol. 85, pp. 3045–3048, Oct 2000.

[155] K. Jacobs and X. Wang, "Coherent feedback that beats all measurement-based feedback protocols," *New Journal of Physics*, vol. 16, 11 2012.

[156] S.-B. Xue, R.-B. Wu, W.-M. Zhang, J. Zhang, C.-W. Li, and T.-J. Tarn, "Decoherence suppression via non-markovian coherent feedback control," *Phys. Rev. A*, vol. 86, p. 052304, Nov 2012.

[157] C. Emary and J. Gough, "Coherent feedback control in quantum transport," *Physical Review B*, vol. 90, 07 2014.

[158] J. E. Gough and S. Wildfeuer, "Enhancement of field squeezing using coherent feedback," *Phys. Rev. A*, vol. 80, p. 042107, Oct 2009.

[159] J. Kerckhoff, H. I. Nurdin, D. S. Pavlichin, and H. Mabuchi, "Designing quantum memories with embedded control: Photonic circuits for autonomous quantum error correction," *Phys. Rev. Lett.*, vol. 105, p. 040502, Jul 2010.

[160] J. Kerckhoff, D. Pavlichin, H. Chalabi, and H. Mabuchi, "Design of nanophotonic circuits for autonomous subsystem quantum error correction," *New Journal of Physics - NEW J PHYS*, vol. 13, 02 2011.

[161] Z. Yan, X. Jia, C. Xie, and K. Peng, "Coherent feedback control of multipartite quantum entanglement for optical fields," *Phys. Rev. A*, vol. 84, p. 062304, Dec 2011.

[162] L. Zhongpeng, H. Wang, J. Zhang, Y.-x. Liu, R. Wu, and F. Nori, "Feedback-induced nonlinearity and superconducting on-chip quantum optics," *Physical Review A*, vol. 88, p. 063851, 09 2013.

[163] H. Mabuchi, "Coherent-feedback quantum control with a dynamic compensator," *Phys. Rev. A*, vol. 78, p. 032323, Sep 2008.

[164] S. Iida, M. Yukawa, H. Yonezawa, N. Yamamoto, and A. Furusawa, "Experimental demonstration of coherent feedback control on optical field squeezing," *IEEE Transactions on Automatic Control*, vol. 57, pp. 2045–2050, 03 2011.

[165] J. Kerckhoff and K. W. Lehnert, "Superconducting microwave multivibrator produced by coherent feedback," *Phys. Rev. Lett.*, vol. 109, p. 153602, Oct 2012.

[166] S. Iida, M. Yukawa, H. Yonezawa, N. Yamamoto, and A. Furusawa, "Experimental Demonstration of Coherent Feedback Control on Optical Field Squeezing," *IEEE Trans. Autom. Control*, vol. 57, pp. 2045–2050, aug 2012.

[167] J. Kerckhoff, R. W. Andrews, H. S. Ku, W. F. Kindel, K. Cicak, R. W. Simmonds, and K. W. Lehnert, "Tunable Coupling to a Mechanical Oscillator Circuit Using a Coherent Feedback Network," *Phys. Rev. X*, vol. 3, p. 021013, jun 2013.

[168] M. Hirose and P. Cappellaro, "Coherent feedback control of a single qubit in diamond," *Nature*, vol. 532, pp. 77–80, apr 2016.

[169] R. Lang and K. Kobayashi, "External optical feedback effects on semiconductor injection laser properties," *IEEE Journal of Quantum Electronics*, vol. 16, no. 3, pp. 347–355, 1980.

[170] M. Kantner, S. Yanchuk, and E. Schöll, "Delay-induced patterns in a two-dimensional lattice of coupled oscillators," *Scientific reports*, vol. 5, 01 2014.

[171] M. Wegert, D. Schwochert, E. Schöll, and K. Lüdge, "Integrated quantum-dot laser devices: modulation stability with electro-optic modulator," *Optical and Quantum Electronics*, vol. 46, pp. 1337–1344, 10 2014.

[172] K. Pyragas, "Continuous control of chaos by self-controlling feedback," *Physics Letters A*, vol. 170, no. 6, pp. 421 – 428, 1992.

[173] K. Pyragas and A. Tamaševičius, "Experimental control of chaos by delayed self-controlling feedback," *Physics Letters A*, vol. 180, no. 1, pp. 99 – 102, 1993.

[174] W. Just, T. Bernard, M. Ostheimer, E. Reibold, and H. Benner, "Mechanism of time-delayed feedback control," *Phys. Rev. Lett.*, vol. 78, pp. 203–206, Jan 1997.

[175] B. Fiedler, V. Flunkert, M. Georgi, P. Hövel, and E. Schöll, "Refuting the odd-number limitation of time-delayed feedback control," *Phys. Rev. Lett.*, vol. 98, p. 114101, Mar 2007.

[176] A. Zakharova, N. Semenova, V. Anishchenko, and E. Schöll, "Time-delayed feedback control of coherence resonance chimeras," *Chaos: An Interdisciplinary Journal of Nonlinear Science*, vol. 27, no. 11, p. 114320, 2017.

[177] E. Schöll, P. Hövel, V. Flunkert, and M. A. Dahlem, *Time-Delayed Feedback Control: From Simple Models to Lasers and Neural Systems*, pp. 85–150. Berlin, Heidelberg: Springer Berlin Heidelberg, 2010.

[178] P. W. Milonni and P. L. Knight, "Retardation in the resonant interaction of two identical atoms," *Phys. Rev. A*, vol. 10, pp. 1096–1108, Oct 1974.

[179] G. Alber, "Photon wave packets and spontaneous decay in a cavity," *Phys. Rev. A*, vol. 46, pp. R5338–R5341, Nov 1992.

[180] T. Tufarelli, M. S. Kim, and F. Ciccarello, "Non-markovianity of a quantum emitter in front of a mirror," *Phys. Rev. A*, vol. 90, p. 012113, Jul 2014.

[181] S. M. Hein, F. Schulze, A. Carmele, and A. Knorr, "Optical feedback-enhanced photon entanglement from a biexciton cascade," *Phys. Rev. Lett.*, vol. 113, p. 027401, Jul 2014.

[182] S. Hughes, "Coupled-cavity qed using planar photonic crystals," *Phys. Rev. Lett.*, vol. 98, p. 083603, Feb 2007.

[183] Y. Lu, N. L. Naumann, J. Cerrillo, Q. Zhao, A. Knorr, and A. Carmele, "Intensified antibunching via feedback-induced quantum interference," *Phys. Rev. A*, vol. 95, p. 063840, Jun 2017.

[184] P.-O. Guimond, M. Pletyukhov, H. Pichler, and P. Zoller, "Delayed coherent quantum feedback from a scattering theory and a matrix product state perspective," *Quantum Science and Technology*, vol. 2, p. 044012, sep 2017.

[185] P.-O. Guimond, H. Pichler, A. Rauschenbeutel, and P. Zoller, "Chiral quantum optics with v-level atoms and coherent quantum feedback," *Phys. Rev. A*, vol. 94, p. 033829, Sep 2016.

[186] J. Kabuss, D. O. Krimer, S. Rotter, K. Stannigel, A. Knorr, and A. Carmele, "Analytical study of quantum-feedback-enhanced rabi oscillations," *Phys. Rev. A*, vol. 92, p. 053801, Nov 2015.

[187] A. Carmele, J. Kabuss, F. Schulze, S. Reitzenstein, and A. Knorr, "Single photon delayed feedback: A way to stabilize intrinsic quantum cavity electrodynamics," *Phys. Rev. Lett.*, vol. 110, p. 013601, Jan 2013.

[188] A. Carmele, S. Parkins, and A. Knorr, "Quantum-optical realization of an ornstein-uhlenbeck-type process via simultaneous action of white noise and feedback," *Phys. Rev. A*, vol. 102, p. 033712, Sep 2020.

[189] U. Dorner and P. Zoller, "Laser-driven atoms in half-cavities," *Phys. Rev. A*, vol. 66, p. 023816, Aug 2002.

[190] F. M. Faulstich, M. Kraft, and A. Carmele, "Unraveling mirror properties in time-delayed quantum feedback scenarios," *Journal of Modern Optics*, vol. 65, no. 11, pp. 1323–1331, 2018.

[191] A. L. Grimsmo, "Time-delayed quantum feedback control," *Phys. Rev. Lett.*, vol. 115, p. 060402, Aug 2015.

[192] R. J. Cook and P. W. Milonni, "Quantum theory of an atom near partially reflecting walls," *Phys. Rev. A*, vol. 35, pp. 5081–5087, Jun 1987.

[193] T. Tufarelli, F. Ciccarello, and M. S. Kim, "Dynamics of spontaneous emission in a single-end photonic waveguide," *Phys. Rev. A*, vol. 87, p. 013820, Jan 2013.

[194] N. Német and S. Parkins, "Enhanced optical squeezing from a degenerate parametric amplifier via time-delayed coherent feedback," *Phys. Rev. A*, vol. 94, p. 023809, Aug 2016.

[195] R. Cook, D. I. Schuster, A. N. Cleland, and K. Jacobs, "Input-output theory for superconducting and photonic circuits that contain weak retroreflections and other weak pseudocavities," *Phys. Rev. A*, vol. 98, p. 013801, Jul 2018.

[196] G. Crowder, H. Carmichael, and S. Hughes, "Quantum trajectory theory of few-photon cavity-qed systems with a time-delayed coherent feedback," *Phys. Rev. A*, vol. 101, p. 023807, Feb 2020.

[197] N. Trautmann and G. Alber, "Dissipation-enabled efficient excitation transfer from a single photon to a single quantum emitter," *Phys. Rev. A*, vol. 93, p. 053807, May 2016.

[198] A. Glaetzle, K. Hammerer, A. Daley, R. Blatt, and P. Zoller, "A single trapped atom in front of an oscillating mirror," *Optics Communications*, vol. 283, no. 5, pp. 758 – 765, 2010. Quo vadis Quantum Optics?

[199] G. Hétet, L. Slodička, M. Hennrich, and R. Blatt, "Single atom as a mirror of an optical cavity," *Phys. Rev. Lett.*, vol. 107, p. 133002, Sep 2011.

[200] D. Parkinson, J. B. / Farnell, *An introduction to quantum spin systems. Lecture notes in physics.* Springer Verlag, Berlin, 2010.

[201] V. Ohanyan, *Introduction to quantum spin chains.* Yerevan State University, Armenia, 2009.

[202] H. Niggemann, *Exact ground states for one- and two-dimensional quantum spin systems*. Ph.D. thesis, University of Cologne, 1998.

[203] L. Hulthen, "Über das austauschproblem eines kristalles," vol. 26, pp. 1–105, 10 1938.

[204] J. des Cloizeaux and J. J. Pearson, "Spin-wave spectrum of the antiferromagnetic linear chain," *Phys. Rev.*, vol. 128, pp. 2131–2135, Dec 1962.

[205] E. Wigner, "Über das paulische Äquivalenzverbot," *Z. Phys.*, vol. 47, pp. 631–651, 09 1928.

[206] E. Lieb, T. Schultz, and D. Mattis, "Two soluble models of an antiferromagnetic chain," *Annals of Physics*, vol. 16, pp. 407–466, 12 1961.

[207] C. Karrasch, J. E. Moore, and F. Heidrich-Meisner, "Real-time and real-space spin and energy dynamics in one-dimensional spin-$\frac{1}{2}$ systems induced by local quantum quenches at finite temperatures," *Phys. Rev. B*, vol. 89, p. 075139, Feb 2014.

[208] E. Ilievski, J. De Nardis, M. Medenjak, and T. c. v. Prosen, "Superdiffusion in one-dimensional quantum lattice models," *Phys. Rev. Lett.*, vol. 121, p. 230602, Dec 2018.

[209] M. Medenjak, C. Karrasch, and T. c. v. Prosen, "Lower bounding diffusion constant by the curvature of drude weight," *Phys. Rev. Lett.*, vol. 119, p. 080602, Aug 2017.

[210] C. Altafini, "Feedback control of spin systems," *Quantum Information Processing*, vol. 6, pp. 9–36, feb 2007.

[211] G. Morigi, J. Eschner, C. Cormick, Y. Lin, D. Leibfried, and D. J. Wineland, "Dissipative quantum control of a spin chain," *Phys. Rev. Lett.*, vol. 115, p. 200502, Nov 2015.

[212] K. Tsumura, *Stabilization of quantum spin systems via continuous feedback control*, pp. 109–117. 01 2012.

[213] Y.-L. L. Fang and H. U. Baranger, "Waveguide qed: Power spectra and correlations of two photons scattered off multiple distant qubits and a mirror," *Phys. Rev. A*, vol. 91, p. 053845, May 2015.

[214] G. Calajó, Y.-L. L. Fang, H. U. Baranger, and F. Ciccarello, "Exciting a bound state in the continuum through multiphoton scattering plus delayed quantum feedback," *Phys. Rev. Lett.*, vol. 122, p. 073601, Feb 2019.

[215] N. Flaeschner, D. Vogel, M. Tarnowski, B. Rem, D.-S. Lühmann, M. Heyl, J. Budich, L. Mathey, K. Sengstock, and C. Weitenberg, "Observation of dynamical vortices after quenches in a system with topology," *Nature Physics*, vol. 14, 03 2018.

[216] C. Karrasch and D. Schuricht, "Dynamical phase transitions after quenches in non-integrable models," *Phys. Rev. B*, vol. 87, p. 195104, May 2013.

[217] P. Jurcevic, H. Shen, P. Hauke, C. Maier, T. Brydges, C. Hempel, B. P. Lanyon, M. Heyl, R. Blatt, and C. F. Roos, "Direct observation of dynamical quantum phase transitions in an interacting many-body system," *Phys. Rev. Lett.*, vol. 119, p. 080501, Aug 2017.

[218] M. Heyl, "Scaling and universality at dynamical quantum phase transitions," *Phys. Rev. Lett.*, vol. 115, p. 140602, Oct 2015.

[219] M. Heyl, "Dynamical quantum phase transitions: a review," *Reports on Progress in Physics*, vol. 81, p. 054001, apr 2018.

[220] M. Heyl, "Dynamical quantum phase transitions: A brief survey," *EPL (Europhysics Letters)*, vol. 125, p. 26001, 02 2019.

[221] K. Macieszczak, M. u. u. u. u. Guţă, I. Lesanovsky, and J. P. Garrahan, "Towards a theory of metastability in open quantum dynamics," *Phys. Rev. Lett.*, vol. 116, p. 240404, Jun 2016.

[222] M. Eckstein, M. Kollar, and P. Werner, "Thermalization after an interaction quench in the hubbard model," *Phys. Rev. Lett.*, vol. 103, p. 056403, Jul 2009.

[223] B. Sciolla and G. Biroli, "Quantum quenches, dynamical transitions, and off-equilibrium quantum criticality," *Phys. Rev. B*, vol. 88, p. 201110, Nov 2013.

[224] P. Wang and S. Kehrein, "Phase transitions in the diagonal ensemble of two-band chern insulators," *New Journal of Physics*, vol. 18, p. 053003, may 2016.

[225] P. Pérez-Fernández, P. Cejnar, J. M. Arias, J. Dukelsky, J. E. García-Ramos, and A. Relaño, "Quantum quench influenced by an excited-state phase transition," *Phys. Rev. A*, vol. 83, p. 033802, Mar 2011.

[226] L. F. Santos and F. Pérez-Bernal, "Structure of eigenstates and quench dynamics at an excited-state quantum phase transition," *Phys. Rev. A*, vol. 92, p. 050101, Nov 2015.

[227] S. Diehl, A. Tomadin, A. Micheli, R. Fazio, and P. Zoller, "Dynamical phase transitions and instabilities in open atomic many-body systems," *Phys. Rev. Lett.*, vol. 105, p. 015702, Jul 2010.

[228] J. P. Garrahan and I. Lesanovsky, "Thermodynamics of quantum jump trajectories," *Phys. Rev. Lett.*, vol. 104, p. 160601, Apr 2010.

[229] C. Ates, B. Olmos, J. P. Garrahan, and I. Lesanovsky, "Dynamical phases and intermittency of the dissipative quantum ising model," *Phys. Rev. A*, vol. 85, p. 043620, Apr 2012.

[230] I. Rotter, "Dynamical phase transitions in quantum systems," *Journal of Modern Physics, v.1, 303-311 (2010)*, vol. 01, 05 2010.

[231] Y. D. Chong, L. Ge, H. Cao, and A. D. Stone, "Coherent perfect absorbers: Time-reversed lasers," *Phys. Rev. Lett.*, vol. 105, p. 053901, Jul 2010.

[232] D. G. Baranov, A. Krasnok, T. Shegai, A. Alù, and Y. Chong, "Coherent perfect absorbers: linear control of light with light," *Nature Reviews Materials*, vol. 2, p. 17064, Oct 2017.

[233] P. Hanggi, U. Eckern, T. Dittrich, B. J. Kramer, and G. Schon:, *Quantum transport and dissipation*. Wiley-VCH Verlag, 1998.

[234] G. Benenti, G. Casati, T. c. v. Prosen, D. Rossini, and M. Žnidarič, "Charge and spin transport in strongly correlated one-dimensional quantum systems driven far from equilibrium," *Phys. Rev. B*, vol. 80, p. 035110, Jul 2009.

[235] K. Sinha, P. Meystre, E. A. Goldschmidt, F. K. Fatemi, S. L. Rolston, and P. Solano, "Non-markovian collective emission from macroscopically separated emitters," *Phys. Rev. Lett.*, vol. 124, p. 043603, Jan 2020.

[236] Z. Y. Ou and L. Mandel, "Observation of spatial quantum beating with separated photodetectors," *Phys. Rev. Lett.*, vol. 61, pp. 54–57, Jul 1988.

[237] C. K. Hong, Z. Y. Ou, and L. Mandel, "Measurement of subpicosecond time intervals between two photons by interference," *Phys. Rev. Lett.*, vol. 59, pp. 2044–2046, Nov 1987.

[238] R. Ghosh and L. Mandel, "Observation of nonclassical effects in the interference of two photons," *Phys. Rev. Lett.*, vol. 59, pp. 1903–1905, Oct 1987.

[239] A. Thoma, P. Schnauber, M. Gschrey, M. Seifried, J. Wolters, J.-H. Schulze, A. Strittmatter, S. Rodt, A. Carmele, A. Knorr, T. Heindel, and S. Reitzenstein, "Exploring dephasing of a solid-state quantum emitter via time- and temperature-dependent hong-ou-mandel experiments," *Phys. Rev. Lett.*, vol. 116, p. 033601, Jan 2016.

[240] T. Jonckheere, J. Rech, C. Wahl, and T. Martin, "Electron and hole hong-ou-mandel interferometry," *Phys. Rev. B*, vol. 86, p. 125425, Sep 2012.

[241] P. Kok, W. J. Munro, K. Nemoto, T. C. Ralph, J. P. Dowling, and G. J. Milburn, "Linear optical quantum computing with photonic qubits," *Rev. Mod. Phys.*, vol. 79, pp. 135–174, Jan 2007.

[242] N. Gisin and R. Thew, "Quantum communication," *Nat. Photon.*, vol. 1, 04 2007.

[243] R. Loudon, *The Quantum Theory of Light, 3rd ed. (Oxford Science Publications)*. Oxford University Press, USA, 2000.

[244] Z. Ou, C. Hong, and L. Mandel, "Relation between input and output states for a beam splitter," *Optics Communications*, vol. 63, no. 2, pp. 118 – 122, 1987.